Bangor University

DOCTOR OF PHILOSOPHY

Contemporary sediment dynamics and Holocene evolution of Hamford Water, Essex, England.

Rampling, Paul

Award date:
2000

Awarding institution:
Bangor University

[Link to publication](#)

Contemporary Sediment Dynamics and
Holocene Evolution of
Hamford Water, Essex, England.

A thesis submitted to the University of Wales
for the degree of Doctor of Philosophy

by

Paul Rampling

University of Wales, Bangor
School of Ocean Sciences
Menai Bridge
Gwynedd LL59 5EY

14 December 2000
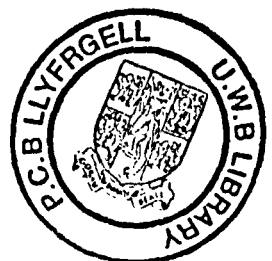
The heart of the marsh beats, ebb-flow,

Creeks like silvery tresses fill, so slow.

She sighs, birds caress her marsh grass skin,

As lifeblood flows along inlets and around isles within.

Her health, once thought so strong but now so frail,

Each silted layer beneath recites its tale.

"Marsh Spirit"
Carol Rampling (1999)

Contemporary Sediment Dynamics and Holocene Evolution of Hamford Water, Essex, England.

Abstract

Contemporary sediment transport, suspended sediment flux, rates of intertidal sedimentation, and Holocene sedimentation history are assessed for Hamford Water, a small meso-tidal inlet and saltmarsh embayment in Essex, UK. Sediment transport rates are calculated using semi-empirical equations; suspended sediment flux is computed by integration of suspended sediment concentration and velocity across the inlet throat; intertidal sedimentation rates are assessed from monitoring of discrete markers on saltmarsh and mudflat; and Holocene sedimentation is estimated from radiocarbon dating of buried organic layers, sampled using a vibrocorer.

Results show a tidal regime typical of ebb-dominated inlets: moderate, ebb-dominant flow (≈ 1 m s^{-1}) in the central ebb channel is matched by similar flood-dominant marginal channel flows. The sediment dynamics are not influenced by any fluvial input; there is negligible fresh water input. The net direction of sediment transport is predominantly ebb-orientated. Coarse sand transport pathways are circulatory and dependent on longshore drift. Sand ($D = 0.25$ mm) enters at the margins and is expelled in the central ebb channel. Negligible sand is transported further landward than the mouth; intertidal sedimentation relies mainly on levels of suspended sediment. Rates of intertidal sedimentation are spatially variable: tidal creek sedimentation is greater than saltmarsh, with a mean rate of 4.2mm yr^{-1}. Buried organic horizons, radiocarbon dated to 600 years BP, are attributed to reclaimed land levels. Holocene sedimentation rates since 4300 years BP, estimated from ^{14}C dating of shell bands, accord with current estimates of sea-level rise of approximately 1 mm y^{-1}.

The role and evolution of the inlet entrance and ebb tidal delta are seen as critical to the evolution of the embayment as a whole. The interaction of the embayment with the adjacent coastal zone considered essential when formulating shoreline management plans. Hamford Water is considered an integral part of the Stour/Orwell/Naze coastal system.

Acknowledgements

This thesis is the culmination of five years work during which time many people from various backgrounds assisted me. Their assistance, be it physical, mental, or moral in some instances, is gratefully acknowledged.

At the top of the list, I am particularly indebted to Mark Dixon (Environment Agency, Ipswich) and the Local Flood Defence Committee without whose initial interest, enthusiasm and financial support, this research would not have materialised. I am equally indebted to my parents for their patient support, both financial and material: without the use of Quay House, its quay, boats, workshop facilities, storage, transport, office and living accommodation, and copious mugs of tea and "bacon butties", this research would not have been undertaken.

I am particularly thankful to my supervisors, Dr. Colin Jago and Dr. James Scourse of the School of Ocean Sciences, Menai Bridge. Their initial enthusiasm for the project and continuous supervision, advice and encouragement throughout this research was invaluable. In addition, thanks must go to Kadir Ishak and Joseph Cheok for many useful hours exchanging ideas and fine-tuning computer programs. I would like to thank and acknowledge Professor John Pethick and Jeremy Lowe, of the University of Cambridge Coastal Research Unit, who provided valuable help and advice on coastal management and geomorphological matters during a year in their employment.

A sincere thanks is also extended to all Menai Bridge staff and students who were, in some way, involved with this research. Chief amongst whom is Alan Neild: his tireless preparation and maintenance of field equipment contributed enormously to the smooth running of field excursions and the successful collection of data. His good humour and cheerfulness during coffee breaks at Craig Mair are memorable. On the technical side, thanks to Gywn Jones and Geriant Williams, and not forgetting all in the workshop for their expert assistance in opening the vibrocorer samples. For assistance with fieldwork: Kadir, Nacho from the Canaries, Lee Cobbold, Donna Kodz and her brother, Dr. Jon Taylor and Mr Fyans (UEA) who helped and advised with vibrocoring, my wife and finally, my Father. I am also grateful to Roy Switsur of the Godwin Radiocarbon Laboratory for the ^{14}C dates and Professor Seed (Menai Bridge) for helping to identify shells used for dating.

Table of Contents

List of Figures

List of Tables

1 Introduction

1.1   Background

This thesis is primarily concerned with physical processes in the coastal zone: in particular the sediment dynamics and Holocene evolution of Hamford Water. The background to the research, however, is centred on the concerns of those entrusted with the management of the coastal zone of East Anglia. Coastal zone management (CZM) is the process which brings together those involved in the development, management and use of the coast (DoE, 1996). The cost-effective management of any coastal zone depends on an understanding of how the zone has developed and responded to conditions in the recent past (Allen, 1993). The intrinsic value of such estuarine environments is dependent, to a large degree, on their physical nature. An understanding of the physical dynamics and evolution of the site is, therefore, necessary in order to manage effectively the physical features of central importance to nature conservation.

Hamford Water is one of East Anglia's estuaries that is the subject of considerable attention regarding nature conservation and coastal management as reflected in extensive statutory protected areas. The majority of current literature dealing with Hamford Water is "grey" literature produced by Local Government Authorities and independent Consulting Companies, for example: Dixon, 1989, Dixon, 1990; HR Wallingford, 1991; Dixon, 1992; Unicomarine, 1992; Posford Duvivier, 1993; WS Atkins Ltd., 1993 and IECS, 1995. (*See* Appendix A for grey literature contact addresses.) Burd (1992) draws on some of this literature in an extensive survey of erosion and vegetation change on Essex and North Kent saltmarshes between 1973 and 1998. Hamford Water is an important site in that investigation; it is particularly important as a saltmarsh habitat and its preservation and protection is afforded much importance. Saltmarsh alone has become an increasingly important part of sea defence worldwide: the greatest significance being its ability to dissipate wave energy to such an extent that very little reaches the landward limit (Brampton, 1992; King and Lester, 1995). However, continuing problems of erosion of East Anglian saltmarsh especially, are resulting in destabilisation of sea defences, requiring increased expenditure on upgrade and maintenance. For example, figures produced by the UK

Environment Agency (EA) in 1993 show that for a saltmarsh fronting a sea wall with a width of 80m, a sea wall of 3m in height is required at a cost of £400 m^{-1}. However, for areas where there is no saltmarsh, the height of wall required is 12m at a cost of £5000/m (NRA, 1992).

In an attempt to combat coastal erosion, the EA has adopted various schemes involving "foreshore recharge", or "replenishment" using dredged sediment from harbours such as Harwich Harbour at the entrance to the Stour and Orwell Rivers. In 1990 a trial was implemented at three sites in Hamford Water: Foulton Hall Point, Stone Point and Horsey Island, the purpose of the trial being to:

"...*assess the use of dredged material from Harwich Harbour for the replenishment of beaches downdrift of Harwich*" (HR Wallingford, 1990).

Although exact quantities and grade of material are not known, between 1993 and 1994 approximately 150,000 m^{-3} of sand and gravel were deposited. An appraisal of the scheme and its effects on this research are discussed at various stages throughout this thesis.

Sheltered coastal environments such as embayments and estuaries are affected by tidal, fluvial and meteorological events that lead to a dynamic state between deposition and erosion. The balance between these two processes varies over cyclic periods such as tidal cycles, seasonal cycles, or over a number of years. Coastal changes are circulatory in space or periodic in time and it is important to discriminate between progressive change and cyclic change (Carter, 1988). For example, erosion of beach sand experienced in winter storms gives way to spring and summer accretion: the net change over a year being difficult to detect. Similarly, the geomorphic response to erosion of one morphological feature may be to aid deposition of another. Pethick (1992) has shown that saltmarsh, for example, acts as a "safety valve" of the intertidal zone; erosion of the marsh surface and edges being a natural response to imposed energy conditions and the response of the intertidal profile is to increase in length. However, a feature of the Essex estuaries is the extent of their sea walls. Over 400 kilometres, representing >80% of the total shoreline, are protected by some form of seawall. Unfortunately, the walls act to restrict any landward movement of saltmarsh and therefore reduce the effectiveness of fronting saltmarsh to dissipate wave energy.

This process by which coastal habitats and natural features are progressively lost or drowned, caught between coastal defences and rising sea-levels is termed "coastal squeeze" (MAFF, 1995).

1.2 Aims and Objectives

The principal aim of this research is to provide a comprehensive appraisal of the sediment dynamics of Hamford Water viewed within a Holocene perspective. Particular emphasis is placed on the hydrodynamics and sediment dynamics of the inlet and embayment and their subsequent influence on spatial and temporal variations of sedimentation and erosion rate. A study of the Holocene evolution enables the evolution of the system prior to extensive anthropogenic impact to be compared with the present day situation. Informed decisions on possible management options require considerable baseline data on the current sedimentary dynamics of the area within a Holocene (last 10,000 years) context (Scourse, 1992).

The aim has been to answer certain pertinent questions relating to the evolution of the site. In particular: what is already known about the site and what are the present-day physical processes? How much Holocene sediment has accumulated within the site and when did that sediment begin to fill the site? What is the rate of sedimentation, and has it varied through time? What are the characteristics of the sediment both spatially and temporally and what is the sediment provenance; what are the current patterns of sediment transport; and, can existing knowledge of the site be used to infer future evolutionary patterns?

The fundamental objective of this investigation is to establish the nature of sediment transport, erosion and deposition in Hamford Water. Of particular interest is the rate of sediment transport (q) through the inlet. The rate of sediment transport is defined as the mass of sediment passing through the inlet entrance per unit time, and is the product of the mass of sediment in the water column over a unit area times the velocity at which the sediment moves (Dyer, 1986). The calculation of q requires a consideration of both the bedload sediment transport rate (q_b), and the suspended sediment transport rate (q_s). The calculation of both q_b and q_s require knowledge of the sediment grain size and the current velocity. It follows that the hydrodynamics and morphology of the inlet

determine the rate of sediment transport through an inlet. However, the long term changing morphology of an inlet and embayment is in turn determined by the residual sediment transport (Dronkers, 1986). The interaction between residual sediment transport and the nature of the tidal cycle are, therefore, a primary control on the morphological evolution of both the embayment and the inlet.

1.3 Specific objectives

The specific objectives of this research are to:

- Determine the tidal dynamics of the inlet and embayment and assess the relative significance of waves, tides and currents in the contemporary sedimentary regime, and the significance and direction of sediment transport pathways in the region;

- Determine the general sediment grain size characteristics and distribution of surficial sediments within the site and discuss the environment of deposition;

- Calculate rates of sediment transport on the basis of semi-empirical formulae that utilise the physical relationships of sediment grain size and current flow data;

- Compute suspended sediment flux from an evaluation of the tidal prism: the instantaneous discharge being obtained by a vertical and lateral integration of the instantaneous velocity and suspended sediment concentration over a cross-section of the inlet throat;

- Determine the contemporary, spatial and temporal patterns of erosion and accretion in the embayment by an historical assessment of maps and charts and by routinely measuring vertical rates of change of saltmarsh and tertiary tidal creeks;

- Estimate rates of sedimentation through the Holocene from downcore evidence by radiocarbon (^{14}C) dating of organic layers, and identify the major controls on these patterns (tectonic subsidence, sea-level change, and sediment supply).

- Discuss the results from a coastal management perspective.

1.4 Methodology

The research method is centred on a thorough understanding of current methods of sediment dynamics, sedimentology and geomorphology, complemented by established techniques of palaeoenvironmental reconstruction.

Data collection methodology is based on the requirement to gather sufficient data, from a combination of boat-deployed current meters and velocity gradient units, to understand the nature of the tidal flow through the inlet. Simultaneous monitoring of current velocity, the nature of the boundary layer and the rate of suspended particulate matter (SPM) will enable some measure of the flux of sediment through the inlet to be obtained. Standard methods of grain size analysis are used to assess the characteristics of the bed sediment for use in calculations of bedload sediment transport. An assessment of vertical rates of change of saltmarsh and tertiary tidal creeks within the embayment, are assessed from routine monitoring of the depth of buried plates and the height of protruding stakes. These can be compared with temporal rates of sediment accretion obtained from downcore evidence estimated from radiocarbon (^{14}C) dating of buried organic layers and marine carbonate bands taken from two vibrocores. Thus, a picture of the contemporary and Holocene history of the inlet and embayment may be obtained.

1.5   Hypotheses

A number of hypotheses largely based on previous research and surveys were established at the outset of this project. Hamford Water is traditionally recognised as a significant sediment sink on the East Anglian coast (McCave, 1987; Clayton *et al.* 1982). However, investigations by Burd (1992) point to an apparent loss of saltmarsh and rapid change of inlet morphology. Recent reports document considerable morphological change, particularly at the entrance (Leeks, 1975; Dixon, 1989; 1990; IECS, 1995) but offer little explanations for the apparent changes occurring. Predicted tidal cycles for the site (Admiralty Tide Tables) show shorter ebb duration than flood, indicative of an ebb-dominant tidal regime and typical of East Anglian rivers. Estimates of relative rates of sea-level change for this region indicate an annual positive trend of between one and two millimetres (Carter, 1988).

Gaps in current knowledge and understanding of the physical processes at work in Hamford Water and the contradictory nature of past reports on the dynamic nature of the site, provide a useful setting in which to test certain hypotheses regarding the physical processes at work in tidal inlets, salt marshes and embayments. The principal hypothesis that forms the target of this study is as follows:

Given the evidence for an apparent deterioration of salt marsh, coupled with an ebb-dominated tidal cycle, the embayment is no longer a significant sediment sink for the southern North Sea.

In addition, it is hypothesised that such a system is likely to have a sediment transport regime made up of a coarse, non-cohesive sediment fraction, and fine cohesive sediment in suspension. The interaction and inter-dependence of the two regimes and their effect on the overall sediment budget being critical to the geomorphic evolution of the system.

1.6   Structure of Thesis

The basic structure of the thesis and the format of each chapter follows a consistent theme: introduction; main text (including methods, presentation of data and data analysis); discussion; summary and conclusion.

- Following this chapter, Chapter 2 (*p.8*) concentrates on the physical setting. The geographical location, morphology, conservation importance and local history are first discussed, followed by an account of the Quaternary geological history and Holocene history of the area.

- Chapter 3 (*p.25*) is a literature review based on the main morphological features of the site: saltmarsh and tidal inlet. It includes a discussion on some fundamentals of sediment transport and the principal methods used for estimating the transport of sediment within tidal inlets. Details of concurrent research adjacent to, and intimately related to Hamford Water is summarised.

- Chapter 4 (*p.48*) concentrates on the hydrodynamics: each principal parameter, relevant to hydrodynamics and sediment transport, is individually dealt with in the following format: data collection, presentation and analysis of results.

- Chapter 5 (*p.119*) is a study of the sediment characteristics and distribution of the surficial sediments and suspended particulate matter contained within the study area. It includes the methods of collection, analysis and environmental interpretation of the results.

- Chapter 6 (*p*.148) is an assessment of the nature of sediment transport through the inlet. SPM flux measurements are computed from an evaluation of the tidal prism and sand transport rates are calculated based on equations utilising the physical relationships of grain size and current flow.

- Chapter 7 (*p*.172) is a study of the contemporary spatial and temporal patterns of erosion and accretion in the embayment. Spatial variations are assessed by reference to published maps and charts of the site and any previous work. Temporal variations are assessed by measuring the vertical rate of change using discrete markers on saltmarsh, in tidal creeks and on mudflats.

- Chapter 8 (*p*.191) is a study of the palaeoenvironmental significance of the Holocene deposits in Hamford Water, and attempts to relate any findings to the pattern of changing sea-level and coastal geomorphology of the East Anglian coast.

- Chapter 9 (*p*.211) is a synthesis of the research, and a discussion on the implications of the results for both coastal geomorphology and also coastal management.

- Chapter 10 (*p*.225) concludes the thesis and outlines areas for future study.

Lists of Figures and Tables are produced at the front of the thesis and a list of References follows the concluding chapter. Contact address for "grey" literature references cited in the text, are included after the reference list at Appendix A along with other appendices.

*An A3, indexed map of the study site is included at the back of the thesis. It is recommended that the reader unfold the map whilst reading the thesis.

2 Physical Setting and Geological History

2.1 Physical Setting

Hamford Water is a small tidal inlet on the north-east Essex coast of England (Figure 2-1). It is bounded to the north by Blackman's Head at the mouth of the estuaries of the Stour and Orwell, and to the south by the cliffs of The Naze (Figure 2-2 and pullout map). The inlet shelters an embayment that opens out into a complex network of creeks, islands, saltmarsh and mudflats some 2,300ha in area. The entrance is partially restricted by an ebb-tidal delta (Pye Sand) and there is a negligible freshwater input, being enclosed to the north, south and west by a small semicircular catchment area (approximately 40 km²) with no significant river. The width of the main entrance channel, Pye Channel, varies in size over a tidal cycle from only 200m wide at extreme low water, to nearly 2-km at high water.

The present shape of Hamford Water has resulted from a long history of reclamation, discussed later in Section 2.4 below. The remaining salt marsh and mudflats are now almost entirely bounded by a sea wall backed by drainage ditches that empty through conduits into the salt marsh. The surrounding land, including Horsey Island, is predominantly agricultural. Old commercial quaysides, most no longer used for commerce, exist at Kirby, Beaumont, Landermere, Walton-on-the-Naze and Oakley Creek. A large explosives manufacturing plant, situated on reclaimed land on Bramble Island, is the only significant industry on the site. The main anthropogenic use of Hamford Water is for recreation including fishing, sailing, windsurfing, water skiing and wildfowling. A large marina, Titchmarsh Marina, is situated on the southern side of Hamford Water and provides berths for approximately 300 small craft and access to numerous moorings that run most of the length of Walton Channel. A few boatyards and a yacht club exist up Foundry Reach, in Walton-on-the-Naze; but apart from a few moorings in Landermere Creek and Kirby Creek, the rest of the area is undisturbed. The basic dimensions of Hamford Water are summarised in Table 2-1.
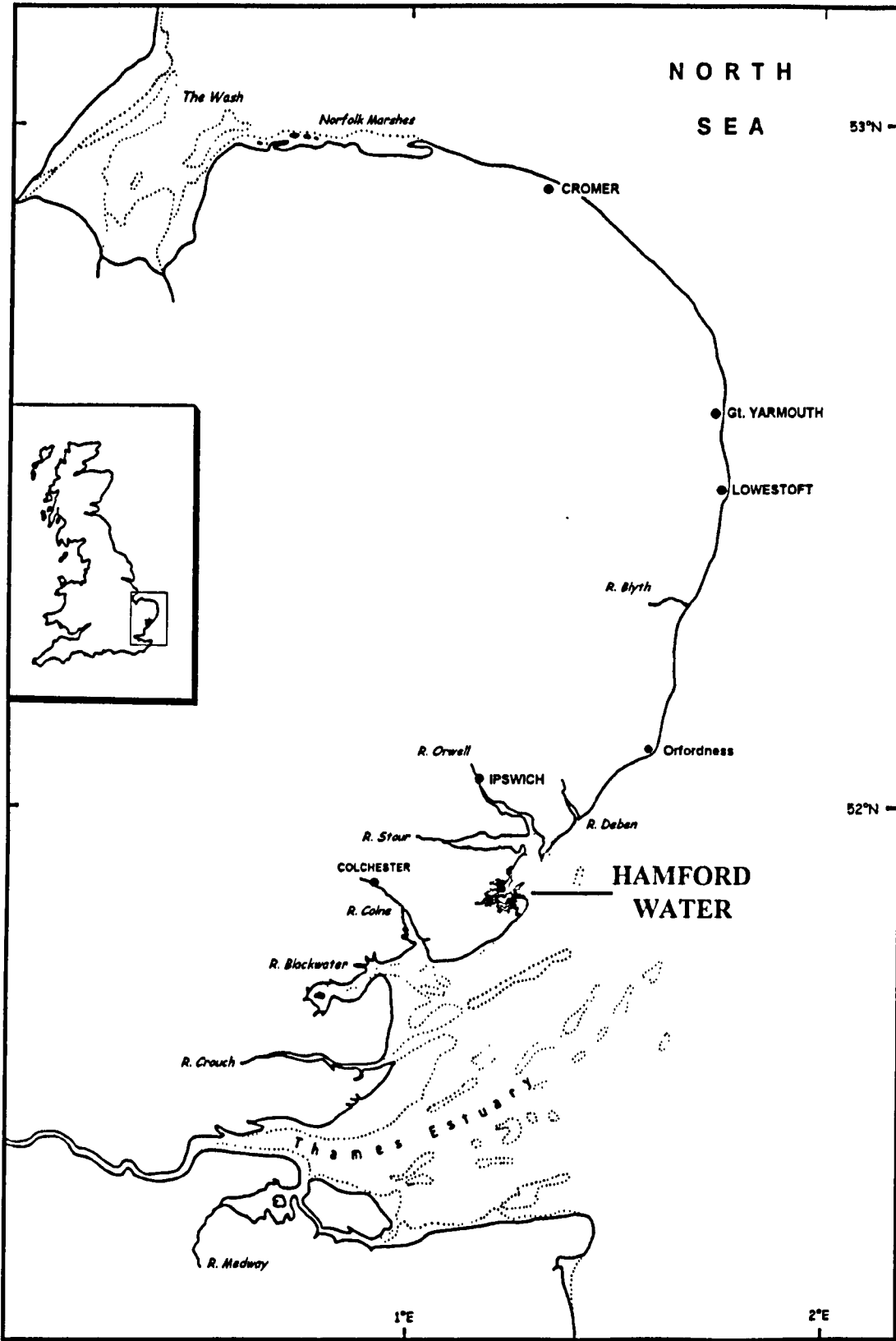
Figure 2-1 – East Anglia showing location of Hamford Water
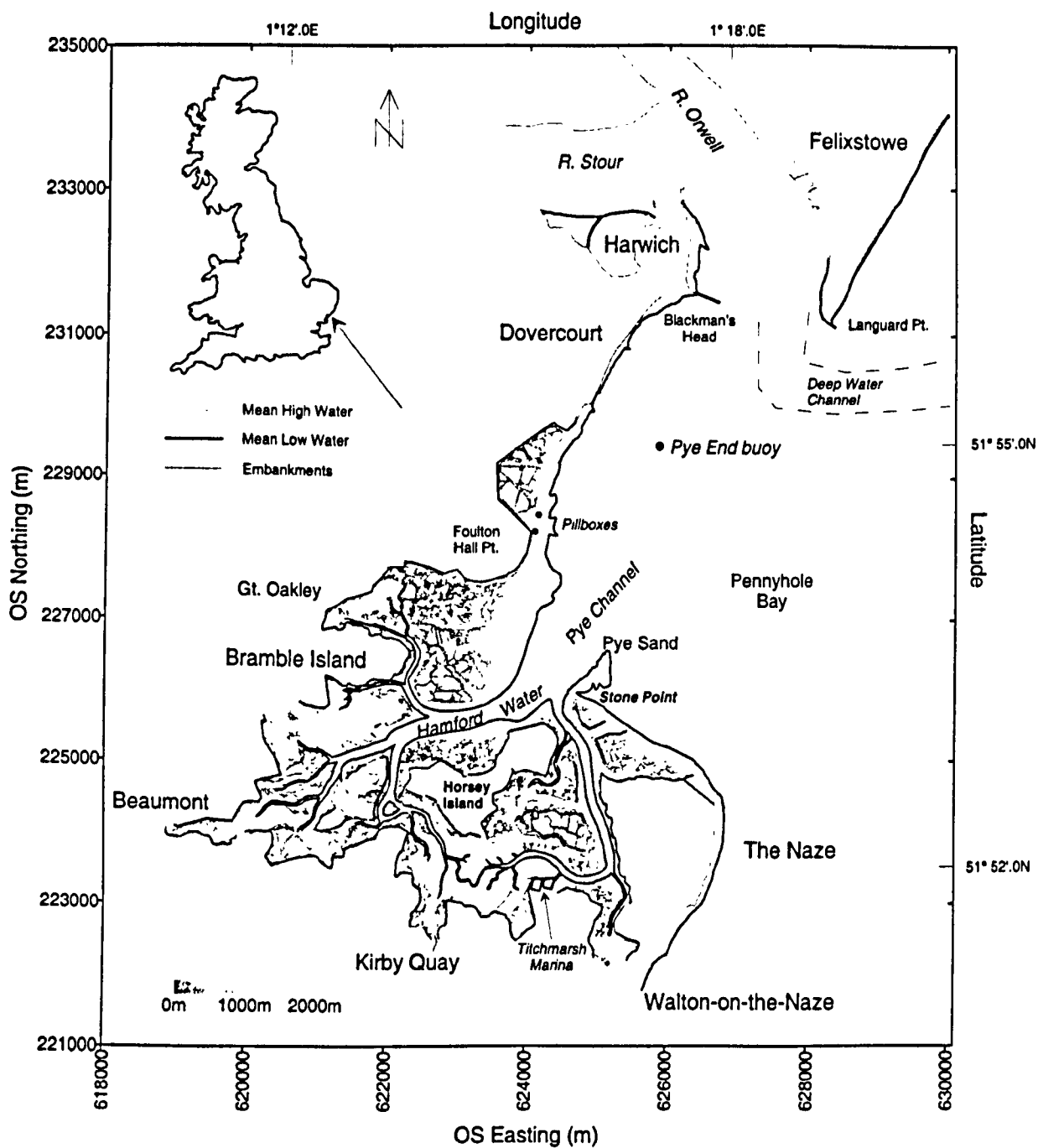
Figure 2-2 – Hamford Water

Table 2-1 – Summary of dimensions of Hamford Water

Shoreline length	54.0 km	Mean tidal range	3.7m

2.2 Conservation Importance

Hamford Water is an important area for nature conservation; almost the entire area is a Site of Special Scientific Interest (SSSI). First notified in 1956 under the National Parks and Access to Countryside Act of 1949 and re-notified in 1987, with minor boundary changes, under Section 28 of the Wildlife and Countryside Act 1981. It was afforded Grade I status in *A Nature Conservation Review*, (Ratcliffe, 1977) — a review of the key sites for nature conservation in Great Britain. The majority of the intertidal mudflats were leased by the Nature Conservancy Council (NCC) [now English Nature] from the Crown Estate Commissioners and declared a National Nature Reserve in 1983, under Section 19 of the National Parks and Access to Countryside Act, 1949. Skipper's Island, and the John Weston Reserve, are Essex Naturalists' Trust Reserves. The whole of Hamford Water has recently been designated, in 1993, as a Wetland of International Importance under the Ramsar Convention of 1971, and a Special Protection Area under EC Directive 79/409 on the Conservation of Natural Habitats and of Wild Flora and Fauna. Hamford Water qualifies for such extensive statutory protection for numerous reasons: As regards fauna, the site regularly supports, in summer, a nationally important breeding population of *Sterna albifrons* (Little Terns) and a nationally important wintering population of *Recurvirostra avosetta* (Avocet). It also supports nationally or internationally important wintering populations of *Branta bernicla bernicla* (Brent Geese); *Limosa limosa* (Black tailed Godwit); *Tringa totanus* (Redshank); *Charadrius hiaticula* (Ringed Plover); *Tadorna tadorna* (Shelduck); *Anas crecca* (Teal); and *Pluvialis squatorola* (Grey Plover). During severe winter weather elsewhere in Europe, Hamford Water can assume even greater national and international importance as wildfowl and waders from many other areas arrive, attracted by the relatively mild climate and abundant food resources available. The intertidal areas support abundant invertebrates, the commonest species being the ragworm *Nereis diversicolor*, the bivalve molluscs *Macoma balthica*, *Scrobicularia plana*, and the gastropod mollusc *Hydrobia ulvae*. There are also *Mytilus edulis* beds and *Ostrea edulis* lays. The site also supports one of the rarest coastal plants in Britain, *Peucedanum officinale* (Hog's Fennel) which is found elsewhere only in Kent (English Nature SPA citation, July 1992).

Finally, the eastern coast of The Naze was notified a SSSI under Section 28 of the Wildlife and Countryside Act 1981, with revisions. The nature conservation importance of this site is the cliff exposure of the Red Crag, which is rich in marine Mollusca and other invertebrate fossils. The site is essential to studies of Pliocene and Pleistocene stratigraphy and is discussed in more detail in Section 2.5 below.

2.3   Geography

In the following description of the present day geography, the seaward limit of Hamford Water is taken to be a line drawn from the northern tip of The Naze to the southern end of Dovercourt (Figure 2-2). Hamford Water can be divided into three main components: subtidal, intertidal mudflats, and saltmarsh.

The **subtidal** area occupies 34% of the total inlet area of 2377ha (Table 2-1 refers). The main Hamford Water Channel flows almost along the centreline of the inlet, measuring 4.5km from its mouth north of Pye Sand to a point 350m north-east of Skipper's Island. The channel has an almost constant width along its entire length, generally varying between 175m and 250m. Maximum depths reach 6.8m close to where it flows into the sea, although the channel shallows considerably to less than 2m near Pye End buoy. In general, however, the channel displays a remarkably constant depth, rarely being shallower than 4m between the confluence of Landermere and Kirby Creeks and Pye Sand.

The Hamford Water channel is fed by two small subtidal creeks at its head; Landermere Creek, which drains the area to the west of Skipper's Island, and Kirby Creek, which drains the area to the South of Skipper's Island and the western half of the Wade. A further channel, Bramble Creek, enters the Hamford Water channel approximately 500m from the confluence of Landermere and Kirby Creeks draining the area of Garnham's Island to the south of Bramble Island.

The other main channel system is Walton Channel, which is subtidal from the eastern side of the Wade, from which it flows to the south and east of Hedge End Island, meeting the Hamford Water channel between Stone Point and the north-eastern side of Horsey Island. Walton Channel also attains a maximum depth of 6.8m between Stone Point and Horsey Island, although this shallows to less than 2m at is confluence with

the Hamford Water channel. The depth of this channel also varies more than the Hamford Water channel, south of the deeper section generally varying between 2.6 and 4m, although towards its head the channel shallows considerably. The main channels of Hamford, Pye and Walton appear to be stable features of the region, possibly relict channels cut into the London clay when sea-level was considerably lower.

The **intertidal mudflat** area of Hamford Water covers 864.4ha, approximately 36% of the total area of the embayment. The largest expanse of mudflat is the Wade to the south of Horsey Island, marking the watershed between Walton Channel to the east, and Hamford Water Channel to the west. This watershed has been artificially modified by the construction of the causeway to Horsey Island reputed to date from Viking times (AD800) (Kodz, *pers. comm.*). Other significant areas of mudflat include Cunnyfur Ooze to the south of Bramble Island, and Bull's Ooze, to the north.

Closer to the mouth of Hamford Water the nature of the intertidal flats change from mud to fine sand over a very sharp boundary. These intertidal areas include Pye Sand, which has a linear extension stretching parallel to the main channel 1500m beyond the main body of the sand, and the wide intertidal area fronting Irlam's Beach. At the northern end of Irlam's Beach, a spit extends normal to the direction of the beach marking the limit of the Hamford Water channel, this being known as Crabknowe Spit. North of Foulton Hall Point the intertidal area begins to narrow towards the sea walls which protect Dovercourt.

Saltmarsh in Hamford Water currently covers 705ha (Burd, 1992), approximately 30% of the total intertidal area of the inlet. This high percentage of saltmarsh is probably the greatest in any of the UK East Coast estuaries (although Hamford water is not technically an estuary), compared with a national average of 14% (Pethick, 1993). The natural development of saltmarsh within Hamford Water has been interrupted by a history of extensive reclamation, and setback (discussed in Section 2.4).

The saltmarsh is conventionally sub-divided into various zones: **pioneer** marsh, **low** marsh, **low-mid** marsh, **mid** marsh, and **upper** marsh. In 1988 (Burd, 1992) the pioneer zone of vegetation occupied 69.4ha and is characterised by *Puccinellia maritima* (common Saltmarsh grass), *Spartina* spp. (Cord grass), *Aster tripolium* (Sea Aster), *Suaeda maritima* (Annual Seablite), *Atriplex portulacoides* (Sea Purslane) and

Salicornia spp. (Glasswort, or pickleweed). The low marsh occupied 57.7ha and included species such as *Atriplex, Puccinellia, Spartina, Salicornia* and *Suaeda*. The largest zone is that of the low-mid marsh, occupying 486.7ha - 69% of the total area of saltmarsh in Hamford Water. This zone is characterised by species such as *Puccinellia, Salicornia, Suaeda, Limonium vulgare* (Common Sea-Lavender), *Aster* and *Atriplex*. The second largest zone is the mid marsh, which represents 12% or 88.1ha of the total area of saltmarsh, and is occupied by *Atriplex, Puccinellia, Spartina* and *Suaeda*. Finally, upper marsh is characterised by *Atriplex, Puccinellia* and *Elytrigia atherica* (Sea Couch) (Burd, 1992).

2.4   Reclaimed marsh

In addition to the three main morphological components described above, Hamford Water's morphology is much influenced by a complex historical battle of reclamation by the landowners surrounding Hamford Water, versus erosion of the low-lying land by the sea. Although reclaiming land from the sea was well established in parts of Essex by the 13th century, the history of reclamation in the Hamford Water area prior to the 17th century is obscure. Gramolt (1960) presents the most comprehensive review of marsh reclamation in East Anglia between the 17th and mid-19th century. The main areas and periods of reclamation applicable to Hamford Water are illustrated in Figure 2-3 and summarised below.

- Reclamation before 1774 but after 1574 – Pewit Island; Horsey Island; land to the east of Beaumont Quay. Area of marsh reclaimed or regained by the sea unknown.

- Reclamation before 1774 – Dovercourt to Bramble Island; Skipper's Island; land to the west of Kirby Creek; land either side of Kirby Quay; land at the northern end of The Naze. Approximately 235 ha reclaimed.

- Reclamation 1774-1799 – none noted by Gramolt in Hamford Water.

- Reclamation 1800-1840 – land north of Bramble Island; land to the south of what is now Titchmarsh Marina; Walton Hall marshes and Stone Point; Landermere and the land to the east; land to the east of Foundry Reach. Approximately 480 ha reclaimed.

- Reclamation after 1840 – Garnham's Island; Hedge End Island. Approximately 1022 ha reclaimed and 633 ha regained by the sea.

- Reclamation for the whole period 1755 ha; area regained by the sea, 648 ha; total 1107 ha of marsh reclaimed from the sea.

Probably the most ambitious reclamation scheme was during the 1860's when it was proposed that the whole of the area south of Horsey Island should be reclaimed. The construction of a seawall was started at the entrance to the Dardanelles creek, the plan being to wall the whole of the west bank of Walton Channel. On the western side of Horsey Island, the area was to be walled from Ambrose Point, across Honey Island and Kirby Creek to the mainland to the south. The works, if successful would have resulted in the whole of the Wade being reclaimed. It is interesting to consider that under the present day philosophy of conserve rather that reclaim, such grand schemes do not conform; however, it was only in the 1980's that the whole of Hamford Water was the focus of a tidal energy feasibility study that would have involved construction of a barrage across the entrance and effectively reclaim the entire area (UKAE, 1984). The consequences of Hamford Water's reclamation history on the geomorphology of the site, and an analysis of saltmarsh loss due to both reclamation and erosion is conducted in Section 7 below.

Figure 2-3 – Main areas of reclamation – Hamford Water (reproduced from Gramolt (1960)).

2.5   Geology

The coastal zone from the Wash to the River Thames consists mainly of soft Quaternary rocks, pre-Holocene tills and Holocene alluvium: variously made up of sand, gravel and mud with some intercalated post-glacial peat. The present day morphology of Hamford Water is much a product of processes active throughout the Quaternary. The Quaternary Period covers the last two million years up to the present day. (The exact duration is subject to many debates with estimates ranging from 1.8 million years to 2.6 million years by different authors.) The Quaternary is conventionally divided into two epochs; the Pleistocene (two million years to ten thousand years ago) and the Holocene (ten thousand years ago to the present day). The conventional division of the Quaternary is into glacials (cold) and interglacials (warm), and further subdivision into stadial and interstadial episodes.

The surface geology of the Hamford Water area, including Walton-on-the-Naze, is described briefly in a geological memoir (Whitaker, 1877); the first edition British Regional Geology: London and Thames Valley (Sherlock, 1935), and the latest edition (Sumbler, 1996). There is no in-print one-inch or 1:50,000 scale geological map covering the area; the most recent map is an old series quarter-inch map. However, the stratigraphy can be reconstructed from a variety of published literature: borehole logs from water supply investigations (Whitaker and Thresh, 1916), Environment Agency [ex-NRA] engineering sea defence work (EA archives, Ipswich), a morphological study (Leeks, 1975), and various works on the geology and evolution of the surrounding area (for example: Markham, 1973; Jermyn, 1974; Funnell and Wilkes, 1976; Boyden, 1979; Leeks, 1979; Dixon, 1979; UKAE, 1984; Allsop and Smith, 1988; Bridgland, 1988; Mathers and Zalasiewicz, 1988; Bridgland *et al.*, 1990; Whiteman, 1992; Whiteman and Rose, 1992; Bridgland *et al.*, 1993). Generally, the stratigraphy of the Hamford Water embayment consists of modern Holocene Alluvium overlying Eocene London Clay, but flanked to the west, north-west and south-east by Red Crag deposits capped by glacial sand and gravel. The geological succession represented in Hamford Water is summarised in Table 2-2 and a simplified map of the geology is illustrated in Figure 2-4.

Third Party material excluded from digitised copy.
Please refer to original text to see this material.

Note on the age of the Red Crag – The placing of the Red Crag in the stratigraphic sequence appears to be subject to a certain degree of controversy. Jones and Keen (1993) discuss the Pliocene-Pleistocene boundary in some detail. Although traditionally considered to be Lower Pleistocene in age (Mitchell, *et al.*, 1973, Dixon, 1979), by international definition the base of the Pleistocene has been placed at 1.81 Ma BP (Aguirre & Passini, 1985; Hilgen, 1991) which places the British Red Crag deposits, correlated by palynological evidence to continental strata of 2.4 Ma (Hunt, 1989), as latest Pliocene (Mathers and Zalasiewicz, 1988; Sumbler, 1996). Allen (1995) states that: "*the Red Crag* [at Walton] *is now classified as Pliocene, but above the Red Crag are Pleistocene deposits*".
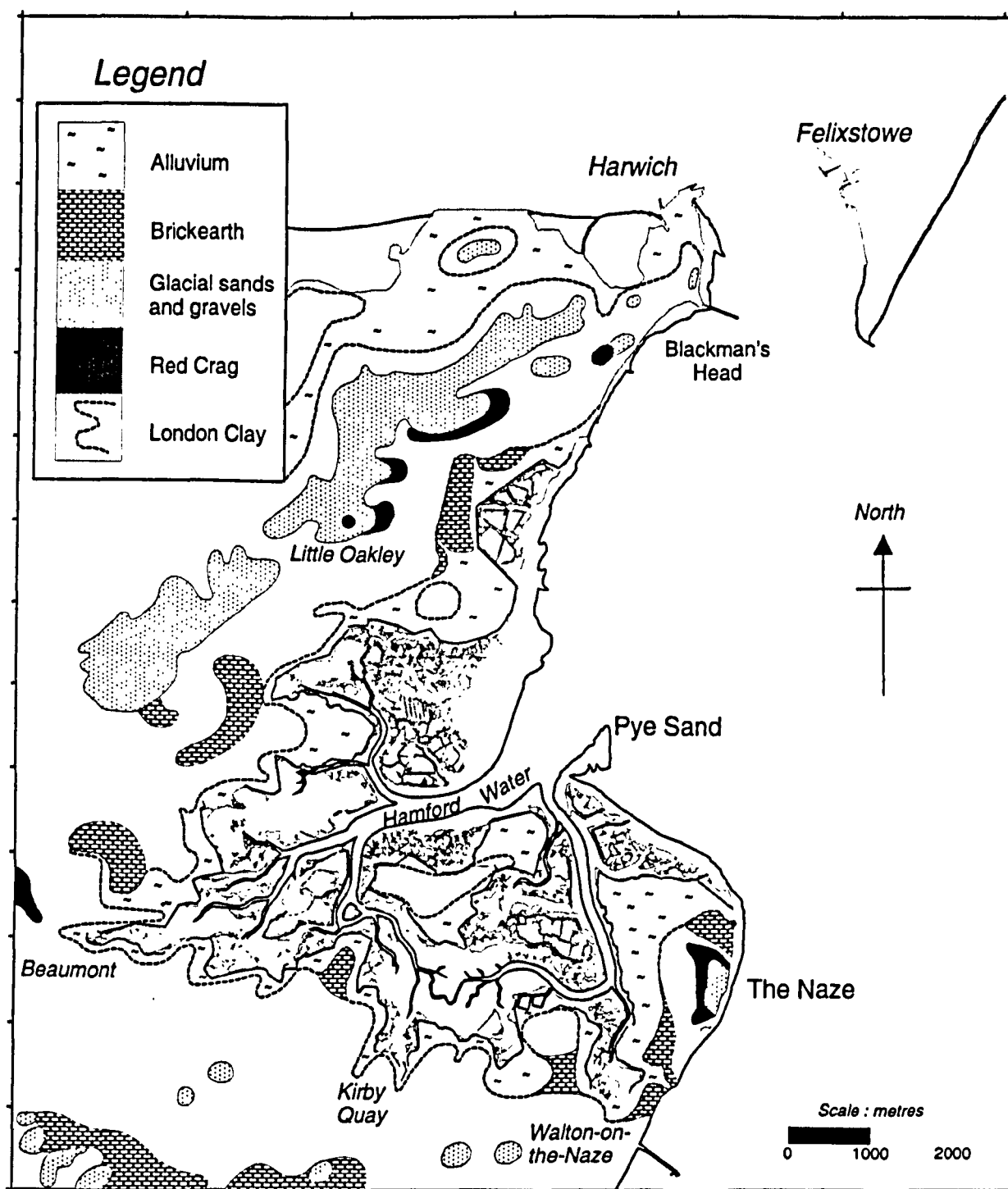
Figure 2-4 – Hamford Water and The Naze – Geological Sketch Map

2.5.1 EOCENE LONDON CLAY

The London Clay makes up the islands of Horsey and Skipper's and outcrops extensively at the foot of the Naze. It is a stiff, dark or bluish-grey clay containing variable amounts of fine-grained silt and weathers to a chocolate-brown colour. Clay minerals present include illite, kaolinite and smectite. Beds of calcareous 'cementstone' concretions such as septaria, about 0.4m thick, occur sporadically, especially at Harwich (Sherlock, 1935; Sumbler, 1996). In addition, two layers of

septaria were reported whilst excavating Titchmarsh marina (John Titchmarsh, *pers. comm. – Eastern Soil Search Ltd. Survey, 1977*). The London clay constitutes the basement rock in Hamford Water and therefore is both the sub-Holocene surface, and the sub-Red Crag surface of the Walton-on-the-Naze deposits discussed in the next section. Dixon (1979) describes the morphology of the surface of the London clay in the context of it being the sub-Red Crag surface, as resulting from pre-depositional marine scouring as investigated by Funnell (1972).

2.5.2   RED CRAG DEPOSITS

The Walton-on-the-Naze Red Crag is part of the Red Crag and Norwich Crag deposits of East Anglia and lie between 13 and 14m above sea-level. The sedimentary facies of the Red Crag are described extensively by Dixon (1979). The deposits at Walton are variably ferruginous, medium- to coarse-grained and relatively poorly sorted sands, which are locally very shelly. Dixon (1979) lists median grain sizes of two samples from the Walton deposits as 700 and 500μm, and a sample from Little Oakley, as 440μm. At the base of the Red Crag deposits at Walton large wave-rolled flints and phosphatic nodules and pebbles are found. The Walton deposits are exposed in cliff section and show large-scale cross-bedding produced by the migration of sand-waves (dunes) in a tidal sea. Current direction is determined by Dixon (1979) as being between 235° and 260°, an east-north-easterly trend. Extensive fossils are found in the Red Crag, including the bivalves: *Astarte obliquata, Cardium parkinsoni, Glycymeris glycymeris* and *Spisula arcuata;* gastropods: *Hinia granularta, Natica multipunctata, Neptunea contraria* and *Nucella tetragona*; and the echinoderm *Echinocyamus pusillus* (Sumbler, 1996).

2.5.3   PLEISTOCENE SANDS AND GRAVELS

The glacial sands and gravels found within and surrounding Hamford Water, including the Naze, owe their origin to the complex pattern of Quaternary climatic fluctuations and associated drainage of the River Thames. Hamford Water may owe much of its origin to the Pleistocene evolution of the Thames, Medway and Rhine drainage systems (Bridgland and D'Olier, 1995)(Figure 2-5). The Pleistocene history of the landscape of Hamford Water, and indeed the majority of the Essex countryside, is dominated by the movement of the Pre-glacial Thames. In Early and early Middle Pleistocene times the

river flowed across the northern half of Essex and due to subsidence of the southern North Sea Basin, uniclinal shifting and diversion by the Anglian ice sheet, has gradually migrated south-eastward to its present position (Bridgland, 1988; Bridgland *et al.*, 1990). Figure 2-5, below, reproduced from Bridgland *et al.* (1990), is a reconstruction of the palaeodrainage of the Tendring Plateau in: a) Oakley Gravel times (pre-Cromerian), b) Cooks Green Gravel times (immediately post Cromerian, and c) Lower Holland Gravel times (early Anglian). The main relevance of former drainage patterns of the Thames and Medway to this study is the possible origin of the form of the Eocene London clay basement deposits in Hamford Water and the presence of possible glacial till. It can be seen from Figure 2-5 that from pre-Cromerian to early Anglian (*c.*650-450*ka*), the Thames and the Medway meandered across the present-day site of Hamford Water. Probably the only significant effect of the proto-Thames-Medway on the present-day shape of Hamford Water is the form of the London Clay surface, which would have been cut into by the river flow resulting in the present undulating form. Later variations in sea-level, especially during the Devensian and the Holocene transgression, would have exploited topographical lows in the London clay, cutting them deeper and contributing to the present-day form of the inlet.

The site also falls within an area of thin loess (Catt, 1978), a fine-grained Quaternary aeolian deposit, often having a high carbonate content, and frequently possessing a distinctive heavy mineral and clay mineral suite (Lowe and Walker, 1984). Almost all the loess was deposited during the later part of the Late Devensian (*c.*14,000 yrs. BP), and often mixed by cryoturbation with subjacent deposits. Most of the deposits in the study area have been affected by the action of fluvial and colluvial processes, and are therefore frequently intermixed with other deposits to form what is referred to in south-east England, as brickearth, so called because of its value to the brick-making industry.

Third Party Material excluded from digitised copy.
Please refer to original text to see this material.

Figure 2-5 – The Pleistocene evolution of the Lower Thames drainage basin (from Bridgland *et al.*1990)

2.5.4   HOLOCENE ALLUVIUM

The Holocene epoch of the last 10,000 years corresponds with the Flandrian Stage of the British Quaternary chronostratigraphy (Sumbler, 1996). In Essex it is characterised by climatic amelioration, rising sea-levels, and a progressive modification of the landscape by man (Lowe and Walker, 1984). Holocene alluvium is predominantly composed of fine silt and clay with coarser seems of sand and gravel recording flood events. The alluvium commonly contains fossils such as molluscs, ostracods, insect remains, mammal bones and teeth, as well as common wood and other plant material including pollen (Hunt, 1989; Sumbler, 1996). Distinct peat beds and lenses also occur locally, particularly in the Lower Thames Valley, although they are not evident in Hamford Water nor in the adjacent estuaries of the Deben, Stour and Orwell. Early Holocene alluvium may also contain Mesolithic artefacts and other archaeological material. For example, Warren (1912) and Warren *et al.* (1936) describe a discovery in 1910, of humanoid remains at The Naze, possibly of Neolithic age, but not certain. The find was located in clay on what is described as a *"peat and occupation level"*. This level is dealt with comprehensively by Zeuner (1958) in which he describes a succession somewhere at Stone Point [he is not specific] that includes a peat layer overlying an occupation layer and underlying an estuarine sequence. The peat is described as being discontinuous and of only a few inches thick and more like a 'peaty marsh-clay'. Leeks (1975) also reports a peat layer exposed on the north shore [presumably near Foulton Hall Point] containing *"carbonised wood and root material"*, although he does not elaborate. The presence of *"peaty clay"* is also reported in NRA borehole records, in an area just west of the Naze, at depths of around 3 metres below Ordnance Datum (OD) (NRA archives, Ipswich). The presence of intercalated layers of peat below salt marsh is significant in that they can be attributed to either ancient land levels formed when the land may have been reclaimed from the sea, or to minor sea-level fluctuations during the Holocene transgression.

In general, the Holocene alluvium deposits of Hamford Water are composed mainly of silt and clay, with occasional seams of sand and gravel deposited during the period from the end of the last glaciation to the present. Towards the entrance the shoreface is capped by ridges of sand and broken shells; the sand is of both alluvial and aeolian origin. The geological map shows that across the entrance to Hamford Water the

London Clay is overlain by Recent clayey alluvium (not shown on Figure 2-4), of an unknown origin and thickness, with sand/shingle banks on the seaward side. It is not certain whether the clayey alluvium at the entrance is Holocene mud or glacial till.

It has been postulated by Robinson (1952) and was discussed in the preliminary report (Annex A), that at the end of the last cold stage (Devensian) the catchment area that now forms Hamford Water was the source of a small river valley, the waters of which drained south-east to join the Stour-Orwell drainage system into the proto-Thames. As sea-level rose throughout the Holocene, the head of the valley eventually flooded and an embayment formed, probably maintained by a barrier island centred on the Naze. The accompanying dune system, resulting from the erosion of soft sediments that make up the Naze, protected the embayment from wave action and allowed the settlement of fine-grained sediments upon which saltmarsh plants colonised, stabilising the fine-grained sediment and forming the present day extensive areas of saltmarsh.

3 Literature Review

3.1 Introduction

The following literature review concentrates on the main subject areas of the thesis and is based on Hamford Water fitting a relevant pre-determined geomorphological classification. Although classification tends to describe rather than explain (Pethick, 1984), a classification allows a comparison to be made with similar systems, thereby enabling a framework of general principles to be established. This, in-turn may enable predictions of certain characteristics of the system to be made (Dyer, 1973).

Hamford Water has been considered as an estuary, in broad terms, under a comprehensive review of British estuaries by Davidson *et al.* (1991). The review adopted a simple two-part classification of estuaries based on their geomorphology and tidal range characteristics and Hamford Water is thus classified as an embayment. An embayment is classified as existing where the line of the coast follows a concave sweep between rocky headlands: in this case between Blackman's Head and the Naze.

This research has adopted a more specific classification: Hamford Water is thus described as a:

"semi-natural, embayment saltmarsh connected to the southern North Sea through a poorly defined, transitional tidal inlet."

This description is drawn together from Hubbard *et al.*(1979), Carter (1988), Goudie (1990) and Allen and Pye (1992). The rationale behind such a protracted description is the embodiment of the two main features of the site: saltmarsh, and tidal inlet. Semi-natural saltmarsh is significantly, and deliberately modified by man, but retains elements of the original salt marsh community. Embayments are, as implied, found in shallow coastal bays, but significant in that the entrance is restricted by a bar and/or headland and that there is a limited freshwater input. A transitional tidal inlet is neither wave- nor tide-dominated and as such has features of both. The significance of the prefix "poorly-defined" is simply that none of the morphological features is particularly well defined. Thus, the main features of Hamford Water are a tidal inlet and an

embayment saltmarsh. These features are reviewed within the context of this research, namely the morphology, hydrodynamics and sediment dynamics.

3.2 Tidal Inlets

3.2.1 DEFINITION

The strict definition of a tidal inlet appears ambiguous: commonly they are associated with breaches that link the open ocean with the coastal environment landward of barrier islands (Davis, 1994). They are therefore found world-wide, particularly in North America and common along the coasts of south and west Australia, The Netherlands, north Germany, the Atlantic coast of south America and parts of the Atlantic coast of Africa (Viles and Spencer, 1995). However, from a more traditional coastal engineering sense, Bruun (1978) includes all connections between the open ocean and a bay, fjord, lagoon or lake, but does not include estuaries *per se*. Thus, a distinguishing feature of an inlet may be the negligible effect of freshwater on the hydrodynamics of the inlet system; and the predominant flow is considered that caused by astronomic tides.

A distinction is also made between the origin of inlets. Bruun (1978) divides these into three main groups: those with a geological origin, those with a hydrological origin, and those with a littoral drift origin. Examples of inlets with a geological origin include San Francisco Bay and the fjords of Norway and Alaska. Those with a hydrological origin include where rivers enter the ocean; and Bruun (1978) cites hydrological inlets as the Schelde, the Mersey, the Nile, the Thames, the Seine and the Hudson, for example; although the distinction between inlet and estuary looses its clarity.

The predominant form of inlets, however, are those with a littoral drift origin and hence the commonly recognised association with barrier islands. A barrier island is an elongated island, mainly sandy, parallel to the coast and separated by a lagoon. They are not attached at the ends and are usually separated by tidal inlets (Goudie, 1985). A tidal inlet is therefore considered to be the relatively narrow connection linking tidal basins to the ocean (Van de Kreeke, 1985, 1990). The term may also be used to include both basin and inlet although within the context of this research inlet and basin are considered separately. Nevertheless, it is emphasised that the two separate components, inlet and basin, are inextricably linked and inter-dependent: a change in

one is linked to changes in the other. The inlet plays an important role in the exchange of water and sediments between basin and ocean and hence maintains important breeding grounds and habitats for marine fauna and flora. They also provide navigable channels and access to sheltered natural harbours and recreational space.

3.2.2 MORPHOLOGY

There are three major components to a tidal inlet: the channel, or inlet throat; the ebb tidal delta; and the flood tidal delta. The ebb and flood tidal deltas consist of accumulations of sand that vary greatly in size and shape and are located at the seaward and landward ends of the inlet channel respectively (Davis, 1994). Morphologically, Hubbard *et al.* (1979) divide inlets into three basic types: wave-dominated, tide-dominated, and transitional (Table 3-1).

Table 3-1 – Morphological variations of tidal inlets

Third Party Material excluded from digitised copy.
Please refer to original text to see this material.

After Hubbard *et al.* (1979) and reproduced from Carter (1988)

Although the above table is compiled from work on inlets on the eastern seaboard of the USA, it is a suitable summary of the main features of all tidal inlet. It does not,

however, reflect the features associated with whether tide-dominated inlets have flood-
or ebb-dominated residual tidal currents.

Ebb-tidal Deltas – The ebb-delta of a tidal inlet is the accumulation of sands seaward of
the inlet and formed by the interaction of tidal- and wave-generated currents (Smith and
FitzGerald, 1994). Numerous authors have documented the morphology, physical
processes and sediment dynamics of typical ebb-tidal deltas (Hayes, 1975, 1979; Hine,
1975; Oertel, 1975; Hubbard, 1977; Finley, 1978; FitzGerald and Nummedal, 1983;
FitzGerald, 1984; Reynolds, 1988; Smith and FitzGerald, 1994). The sediment
dynamics of tidal inlets are discussed in Section 3.2.3 below. The morphological
components of a typical ebb-tidal delta are described by Hayes (1980) and Boothroyd
(1985) and illustrated in Figure 3-1 below. They include a *main ebb channel*, which
shows a dominance of ebb-tidal currents over flood-tidal currents. Flanking the main
ebb channel are *channel-margin linear bars* — levee-like deposits built by the
interaction of tidal currents with wave-generated currents. At the end of the main
channel is a seaward sloping lobe of sand called the *terminal lobe* flanked by broad
sheets of sand called *swash platforms*. Occurring on the swash platforms are isolated
swash bars resulting from the swash action of waves. Between the swash platform and
the updrift and downdrift beaches occur *marginal flood channels* dominated by flood-
tidal currents (Hayes, 1980). The overall morphology of an ebb-tidal delta is a function
of the interaction of tidal currents and waves, and in particular, the occurrence of
time—velocity asymmetry discussed in Section 3.2.5 below.

Third Party material excluded from digitised copy.
Please refer to original text to see this material.

Figure 3-1 – Morphological model of an ebb-tidal delta (after Hayes, 1980).

Flood-tidal Deltas – The morphology and bedforms of flood-tidal deltas is described by Hayes (1980) based on research by Hayes (19690); Hine (1975); and Boothroyd and Hubbard (1975). Typically, the main morphological features of a flood-tidal delta consists of: (a) *Flood ramp* — seaward-facing slope on the sand body over which the main force of the flood current is directed and always covered with flood-orientated sand waves; (b) *Flood Channels* —channels dominated by flood currents that bifurcate off the flood ramp; (c) *Ebb shields* — raised margins around the tidal delta that protect portions of it from modification by ebb currents; (d) *Ebb Spits* — spits formed by ebb-tidal currents; and (e) *Spillover lobes* — lobate bodies of sediment formed by unidirectional currents. Figure 3-2 shows the morphology of an idealised flood-dominant tidal inlet. The dominant morphological feature is a delta-type structure which is affected by considerable sediment recycling between the various sub-aqueous and sub-aerial forms (Carter, 1988).

Third Party material excluded from digitised copy. Please refer to original text to see this material.

Figure 3-2 – Morphology of an idealised flood-tidal delta (after Carter, 1988).

3.2.3   Tidal Inlet Sediment Dynamics

The source of sediment available for transport through an inlet may be a combination of fluvial sediment, sediment supplied by littoral drift, sediment eroded from the embayment, *in situ* sediment from the inlet bed, or re-entrained sediment. The origin of the sediment that makes up the bulk of tidal deltas, that form part of tidal inlets, is viewed by Oertel (1988) as originating from within the inlet throat, as opposed to constituting a sink for littoral transport. He demonstrates that the ebb-delta may result from sediment scouring of the inlet throat and need not rely on long-shore transport of sediment and subsequent flushing out to the delta on the ebb current for its sediment supply. Ebb-dominated inlets can build ebb deltas by excavating the inlet gorge and depositing the sediment at the outer reaches of the ebb jet. Carter (1988), however, likens a tidal inlet (or 'pass') as a "magnet" for sediment. Sediment supplied to an inlet by littoral drift is either stored, or its drift transportation impeded. Thus, the morphological fate of sediment accumulation in a tidal inlet depends on whether sediment is supplied primarily by inlet throat scouring, or by long-shore transport.

The nature of tidal flow through an inlet is dependent upon several factors: inlet and bay geometry; bed roughness characteristics; tidal characteristics, including tidal surges; offshore wave characteristics; sediment movement, and freshwater flow. Any combination of these factors can produce complex situations (Bruun, 1978). Where fresh water is negligible, the dominant characteristic tends to be tidal forcing. If the tidal velocity residual is non-zero, or if the velocity is asymmetric about the mean, the result is a net flood, or ebb sediment transport. An asymmetric tidal velocity may be flood or ebb dominant. Ebb dominance occurs when currents in the ebb direction are stronger but have a shorter duration than the flood. The opposite is true for flood dominance.

In the ebb-deltas studied by Hayes (1980), the maximum ebb currents occur late in the tidal cycle, near low water. This means that when the tide turns, just after low water, there are still strong ebb currents flowing seaward in the main ebb channel. Therefore, as the tide rises, the water seeks the margins of the delta where resistance is least, resulting in marginal flood channels (Figure 3-1). Smith and FitzGerald (1994) present a detailed analysis of current flow and sediment transport patterns at the Essex River

inlet ebb-tidal delta (USA). They found that the inlet throat is increasingly dominated by ebb-tidal currents and seaward sediment transport as tidal range increases from neaps towards springs. A similar trend was found to exist in the marginal flood channels with increasingly stronger flood than ebb-tidal currents with increasing tidal range. The flow patterns experienced on the East Coast of the North America is not mirrored in estuaries and inlets of the North Sea coast of the United Kingdom. A brief inspection of Admiralty Tide Tables shows that the tidal cycles in the North Sea vary from ebb- to flood-dominated; this is discussed in more detail in Section 3.2.5.

3.2.4   SEDIMENT TRANSPORT IN TIDAL INLETS

Tidal flow in a tidal inlet is similar, to some extent, to open channel flow (Mehta, 1978). Departures from simply open channel flow occur due to tidal-induced acceleration and deceleration and the varying effects of waves. Sediment will move when the force of the fluid flowing over it is capable of overcoming both the gravity force acting on the sediment grains and the friction between the grains and the underlying surface. The fluid force is composed of a buoyancy component, acting vertically upward (lift force) and a frictional force between the fluid and the underlying grains (drag force). It follows that fluid flowing over the seabed results in a frictional drag between the fluid and the sediment. Friction imposed by the flow of water against the bed is restricted so that the bottom of the water column moves more slowly than the surface and results in a shearing force, or shear stress (τ_0) at the bed. The layer of water where the effects of friction affect the flow, the boundary layer, will usually occupy the whole water depth in shallow water (Dyer, 1986). The movement of sediment is therefore dependent on the shear stress applied to the bed by the flowing water. When the shear stress exceeds a critical, or threshold value (τ_c), sediment will move along the bed. The initiation of motion is a function of the characteristics of the sediment (density, size, packing, sorting shape, etc.), the fluid (density and viscosity), and the depth average velocity of the fluid (Miller *et al.*, 1977). With increasing shear stress, due to increasing fluid velocity, sediment grains will eventually move into suspension. The mode of sediment transport through an inlet, therefore, may be bedload or suspended load.

The extent to which sediment transport takes place depends on the degree of turbulence and shear in the boundary layer which, in turn are influenced by the velocity of the

current and by the roughness of the seabed. Theoretically, water in direct contact with the bed should be stationary. Above the bed, the fluid velocity should increase with increasing distance until frictional forces are negligible. A velocity gradient, therefore, exists in the boundary layer. The value of shear stress operating at the seabed (τ_0) is directly related to the rate at which the fluid velocity (u) increases with height (z) above the bed according to

$$\tau_0 = \mu \frac{du}{dz}$$

(3:1

where μ, is the molecular viscosity.

Fluid flow can be either laminar or turbulent. In laminar flow, molecular fluid flow streamlines around a sediment grain are smooth. However, most flows in inlets and the sea are turbulent where the fluid flow can be resolved into three component velocities: u, v and w. The u-direction is horizontal, parallel to the flow; the v-direction is horizontal and at $90°$ to the flow, and the w-direction is vertical. These turbulent eddies result in an eddy viscosity (η) of several orders of magnitude greater than molecular viscosity (μ). Turbulent shear stress is therefore greater than laminar shear stress and has been shown experimentally to be proportional to the square of the time-averaged velocity (Dyer, 1986):

$$\tau_0 \propto (\bar{u})^2$$

(3:2

Therefore, for turbulent flow, equation (3:2 becomes:

$$\tau_0 = (\mu + \eta) \frac{d\bar{u}}{dz}$$

(3:3

Shear stress may be converted into shear velocity (u_*), a term that has units of velocity, derived from the shear stress (τ) and the fluid density (ρ):

$$u_* = \sqrt{\frac{\tau_0}{\rho}}$$

(3:4

or,

$$\tau_0 = \rho u_*^2$$

(3:5

In the boundary layer, there are three separate flow states: laminar flow, smooth turbulent flow and rough turbulent flow. As already mentioned, laminar flows rarely occur in nature. Water flowing over a smooth bed (smooth turbulent flow), has a thin layer of water next to the bed ($\approx$mm) where flow is almost laminar, known as the viscous sublayer. Here du/dz is constant and therefore the shear stress (τ_o) is also assumed to be constant with height. Above the viscous sub-layer is a transitional zone to the fully turbulent layer above, in which the velocity profile is logarithmic with height. In rough turbulent flow, the viscous sublayer and the transitional zone are absent. Above the logarithmic layer is an outer layer that comprises most of the boundary layer.

The turbulent logarithmic velocity profile is given by the von-Karman-Prandtl equation (Dyer, 1986):

$$\frac{u}{u_*} = \frac{1}{\kappa} \ln\left(\frac{z}{z_0}\right) \quad (3:6$$

where $u = u(z)$ is the horizontal flow velocity at an elevation z above the bed, z_0 is the virtual origin of the logarithmic profile, and κ is the von Karman constant. Although the value of κ varies with concentration of suspended sediment in the flow, it is generally sufficient to select $\kappa = 0.4$ which corresponds to a sediment free flow in an open channel (Dyer, 1986). With this value of κ and using a logarithm to the base 10 rather than to the base e, Equation (3:6) becomes:

$$\bar{u} = 5.75 u_* \log z - 5.75 u_* \log z_0 \quad (3:7$$

so that a plot of u versus $\log z$ would have a slope of 5.75 u_* and an intercept of $-5.75\ u_* \log z_0$, from which both the shear velocity (u_*) and the roughness length (z_0) may be evaluated (Mehta, 1978).

The shear velocity (u_*) can then be calculated from the velocity profile according to:

$$u_* = \frac{d\bar{u}}{d\log z} \quad (3:8$$

and the bed roughness length (z_0) is calculated from the intercept of the logarithmic profile with the log z axis. The roughness length is important in that it is related to the

sediment grain size on the bed and also to the presence of features such as ripples and dunes; the value of z_0 generally increases as the grain size increases.

The bed shear stress (τ_0) can be calculated from:

$$\tau_0 = \rho\, u_*^2 \qquad\qquad (3:9$$

and has been shown, by experiment, to be proportional to the square of the velocity in the boundary layer, $\tau_0 \propto u^2$.

or, the Quadratic Stress Law:

$$\tau_0 = \rho C_D u^2 \qquad\qquad (3:10$$

where C_D is a drag coefficient. Commonly, current meter measurements are taken at 1.0m above the bed and therefore,

$$\tau_0 = \rho\, C_{100}\, u_{100}^2 \qquad\qquad (3:11$$

or

$$u_*^2 = C_{100}\, u_{100}^2 \qquad\qquad (3:12$$

Therefore C_{100} is related to the roughness length, z_0 by

$$C_{100} = \left[\frac{\kappa}{ln(100/z_0)}\right]^2 \qquad\qquad (3:13$$

Where z_0 is in cm. It is therefore possible to estimate the bed shear stress from near bed velocity measurements (Dyer, 1986).

In reality, there are a number of factors that affect the straight line form of logarithmic velocity profiles. Dyer (1986) lists the main disturbing effects on the form of the profile as: accelerating or decelerating flow; variations in upstream roughness; the presence of bedforms; stratification in the water column due to salinity or suspended sediment; errors in determining the zero datum of the current meter array; and waves. A significant effect in tidal inlets is both accelerating and decelerating flow due to the changing direction of the tidal currents. The shear stress at the bed and also u_* and z_0 can be overestimated for decelerating flow and underestimated for accelerating flow (Figure 3-3). However, in most situations of tidal current flow reversal, the

accelerating and decelerating stages of the tide occur either side of slack high water and slack low water. Currents at these stages of the tide are generally weak and the potential for sediment movement is therefore, low.
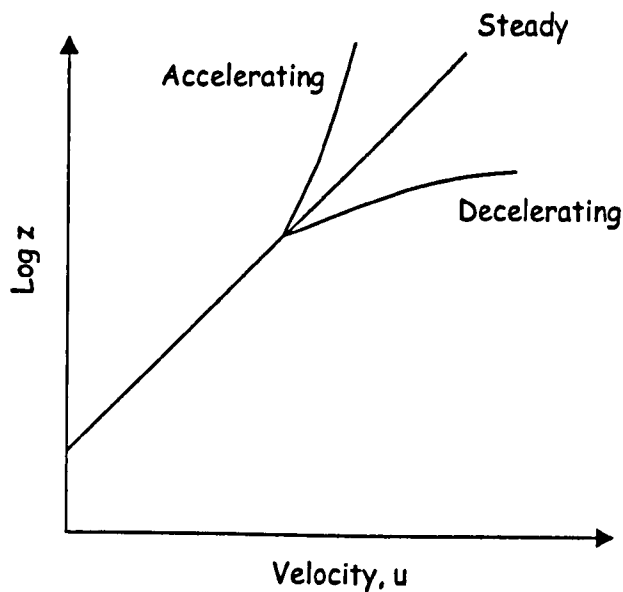
Figure 3-3 – Departures from a theoretical logarithmic velocity profile.

Another significant effect on logarithmic profiles is when the current flow encounters surfaces of different roughness. When bed roughness is increased due to, for example, ripples, a pressure gradient is produced above the ripple which causes added resistance to the flow called form drag. The ability of the flow to move sediment is therefore reduced and not all the shear stress calculated from the logarithmic profile is available to move sediment.

Finally, in addition to the above effects, the theoretical application of the logarithmic velocity profile only assumes flow of a fluid of homogenous density. Since the main reason for studying the form of the velocity profile is to estimate the rate of sediment transport, the very movement of sediment will affect the density of the fluid. Sediment concentration and therefore density of the water decreases away from the bed. Turbulent eddies are less able to move denser fluid upwards so the density gradient reduces the turbulence and in doing so leads to a lower shear stress at the bed (Dyer, 1996; OU, 1989).

3.2.4.1   Sediment Transport Rate

Numerous methods have been used to measure rates of sediment transport: natural sediment tracers (Wang and Murray, 1983; Gao and Collins, 1995), artificial tracers (reviewed by Madsen, 1989), geomorphological change (McCave and Geiser, 1979; Boothroyd, 1985; Harris, 1988), sediment trend analysis (McLaren and Bowles, 1985; Gao and Collins, 1992), direct measurement (Thorne, 1986; Ludwick, 1989; Land *et al.*, 1997), empirical formulae (Thorne *et al.*, 1989), and semi-empirical formulae. Equations for the calculation of sediment transport, either bedload or total load, can be divided into two main groups: those that have a threshold condition and those that do not. These are summarised in Table 3-2 below.

Table 3-2 – Summary of Sediment Transport Equations.

Threshold Condition	*No Threshold*
Yalin, 1963	Rouse, 1938
White, 1970	Einstein, 1950
Sternberg, 1972	Bagnold, 1956, 1963, 1966
Gadd et al., 1978	Engelund and Hansen, 1967
Langhorne, 1981	Ackers and White, 1973
Hardisty, 1983	Van Rijn, 1986
Mahamod, 1989	
Jago & Mahamod, 1999	

(Underlined references used in this thesis)

In tidal inlets, transport rates have also been approximated using a form of Maddock's (1969) equation. This is based on current velocities in which the maximum potential load is proportional to the cube of the velocity (Smith and FitzGerald, 1994):

$$Load = 15.244\,u^3/1600\;(m^3\;s^{-1})\qquad(3:14$$

where u is the maximum velocity (m s^{-1}). The equation has also been used by FitzGerald *et al.*, (1976) and Hubbard *et al.*, (1977). It is, however, only an approximation used where hydraulic data are limited. It was developed for fluvial systems for determining qualitative estimates of sand transport in tidal inlets channels and for comparing transport rates within an ebb-tidal delta system (Smith and FitzGerald, 1994). Use of the equation has also been restricted to inlets on the east

coast of North America. For more comprehensive hydraulic data sets, methods in which the transport rate is expressed as a function of the near-bed shear stress (Dyer, 1986) are commonly adopted and form the basis of sediment transport calculations in this research.

Bagnold (1963) considered that the rate of bedload transport is proportional to the available fluid power

$$q = K\omega / g \qquad (3:15$$

where q is the rate of bedload transport, ω is the fluid power (= τu), and K is an efficiency factor. This can be rewritten as

$$q = \frac{K u_*^3}{g} \qquad (3:16$$

where q is the mass discharge of sediment in g cm^{-1} s^{-1}.

Field measurements show that K is related to the grain size D and to the excess boundary shear stress $(\tau - \tau_t)/\tau_t$.

Gadd et al (1978) developed the following equation based on an extensive data set from Guy *et al.* (1966):

$$q = \beta(u_{100} - u_{100t})^3 \qquad (3:17$$

where β depends on the grain size ($\beta = 7.22 \times 10^{-5}$ where $D = 0.18$mm; $\beta = 1.73 \times 10^{-5}$ when $D = 0.45$mm).

Hardisty (1983) also used Guy *et al.* (1966) data and modified Equation 17 to:

$$q = k_1 (u_{100}^2 - u_{100t}^2)u_{100} \qquad (3:18$$

where $\log k_1 = -5.28 - 1.23 \log D$ (where D is in mm and u in cm s^{-1}).

Both Gadd and Hardisty formulae were calibrated for low flow velocities (<0.55 ms^{-1}) and for conditions of low transport rate (as on the continental shelf). More recently Jago and Mahamod (1999) re-assessed the data of Guy *et al.* (1966) and developed a total load algorithm for sand transport by fast steady currents. The paper is significant

in that the work of Gadd *et al.* (1978) is re-examined and found to contain errors that were repeated by Guy *et al.* (1966) and Hardisty (1983). Jago and Mahamod's (1999) algorithm was calibrated using the data set of Guy *et al.* (1966) and uses both bed and suspended load transports for current velocities of 0.2–1.5 ms^{-1}, and sand grain sizes 190–930μm. Total sand flux is given by:

$$q = k\left[(u_1 - u_{1t})\right]^n \tag{3:19}$$

which is a power function of mean current velocity at 1m above the bed and constrained by a threshold velocity. The exponent n and the entrainment function k are dependent on grain diameter as determined, respectively, by

$$n = 5.028 - 5564D + (3225 \times 10^3)\, D^2 \tag{3:20}$$

and

$$\log_{10} k = -2.465 - 1163D + (2973 \times 10^3)\, D^2 \tag{3:21}$$

A earlier equation is the total load equation of Engelund and Hansen (1967) which was developed for high transport rates in rivers. It expresses transport in terms of a dimensionless sediment discharge (Φ), a friction factor (C$_f$), and a non-dimensional shear stress (θ). The latter is referred to as the Shields entrainment function. The complete formula for total load transport is given by

$$q_t = 0.05\, \rho_s \bar{u}^2 \left[\frac{D}{g(\rho_s - \rho)/\rho}\right]^{0.5} \left[\frac{\tau_0}{(\rho_s - \rho)gd}\right]^{1.5} (g\ cm^{-1}s^{-1}) \tag{3:22}$$

where ρ and ρ_s are the density of the fluid and sediment respectively, g is acceleration due to gravity, τ_0 is bed shear stress, D is mean grain diameter (cm), and $\bar{u}$ is depth average velocity in $cm\ s^{-1}$. The equation is limited in that it is not applicable in plane beds, being more applicable for dune-covered beds. However, it is applicable for grain sizes greater than 150μm and is a popular formula for general use in sediment transport prediction (*see for example* Graf (1971), ASCE (1975), Raudkivi (1976), Heathershaw (1981), Mahamod (1989) and Asghar Ali (1992).

In this research, the formula of Hardisty (1983) is used to assess bedload transport, and the formulae of Engelund and Hansen (1967), and Jago and Mahamod (1999) are used

to assess total load transport. The use of the respective equations and the variables used are described and compared in Section 6 below.

3.2.5   TIDAL INLET EQUILIBRIUM AND STABILITY

The stability of a tidal inlet is considered within the context of whether or not the inlet may attain an equilibrium state after some alteration or disturbance. Such an alteration may be due to a storm event, for example, which may cause a sudden change in the inlet's cross-sectional area due to increased wave action on the ocean side of the inlet. A disturbance may also be due to engineering works such as dredging or the construction of a jetty.

The concept of equilibrium in this sense is applied to open systems in which the quantities of stored energy are adjusted so that input, throughput and output of energy are balanced (Goudie, 1990). Equilibrium is the balance of forces that allows an inlet to exist and is determined by the balance between two opposing mechanisms: input of sediment into the inlet, and removal of sediment by tidal scouring. The time-span for an inlet to reach equilibrium is controlled largely by the availability of sediment. The tidal prism, the volume of water transported into and out of an inlet during a tidal cycle, determines the erosive capacity of the inlet in conjunction with the cross-sectional area. Thus, an inlet will have an equilibrium state if there is sufficient bottom stress to export sediment from the inlet at the same rate that littoral drift, or fluvial mechanisms import it. The inlet can therefore be classified as stable if, after some event which deposits enough sediment into the inlet to change the inlet cross-sectional area, the inlet then increases its velocity to increase erosion and return to the original area. Thus, the cross-sectional area of an inlet fluctuates around a mean value depending on environmental conditions remaining constant (Gao, 1993).

Escoffier (1940) presented an equation for computing the velocity in an inlet when the dimensions of the inlet and the tidal characteristics are known. Escoffier defined a critical velocity; just large enough to transport deposited sand out of the inlet, depending on the grain size of the sediment. His ballpark critical velocity value is 1 m s^{-1}. An inlet can then be characterised as stable or unstable by plotting the average velocity against inlet length and including a horizontal line corresponding to the critical velocity. If the critical velocity intersects the curve in two places (i.e., if the critical

velocity is strictly less than the maximum inlet velocity), the inlet with the larger length parameter will be stable, all others will be unstable. In particular, if the critical velocity is equal to, or greater than the maximum velocity of the inlet, the inlet is unstable and may be closed by the dominant sediment transport into the inlet.

O'Brien (1969) introduced the concept of equilibrium based on an empirical relationship that related the cross-sectional area of the mouth of an inlet, A_c, to the tidal prism, P

$$A_c = cP \qquad (3:23$$

where c is a constant of 6.6×10^{-5} m^{-1}. This relationship implies that an increase in tidal prism will result in an increase in tidal velocity and therefore an increase in the size of the cross-sectional area of the inlet; the converse being true as well. The O'Brien relationship is used extensively for morphodynamic modelling and is even used to explain local sections within an estuary (Dyer, 1997).

It is evident that the morphological evolution of an embayment depends essentially on two processes (Dronkers, 1986; Dyer, 1986). Firstly, the long-term averaged sediment supply, and direction and magnitude of the long-term averaged sediment transport; and secondly, any abrupt changes in the estuarine morphology caused by storms surges or by engineering works. The sediment supply and sediment transport pattern, in turn, depend on several factors: sediment characteristics; wind, waves and swell; current velocity distribution and in particular its variation during a tidal cycle; and, river inflow. Although important in estuaries with significant fresh water input, river flow is considered negligible in Hamford Water. Dronkers' (1986) work was devoted to the analysis of tidal wave deformation in shallow systems with a regular or a complex geometry, and its effect on the residual sediment flux. In conclusion, it was found that the main features of tidal wave distortion for residual sediment transport are, firstly, a difference between the slack water periods before ebb and flood, which affects the residual transport of the fine fraction of the suspended load; and secondly, a difference between the maximum velocity during ebb and flood, which affects the residual transport of the coarse fraction of the suspended load. The effects are different depending on the shape of the tidal basin. In regularly shaped basins (no important width variation with water-level) and in the absence of river inflow, the tidal wave

tends to be distorted such that the maximum flood velocity is greater than the ebb and the slack water period before the ebb is greater than the flood. This distortion is manifest in the inner part of both long and short tidal basins (compared to the tidal wave length). The result is a sediment infilling of such estuaries in periods of low river discharge. Conversely, in irregularly shaped estuaries (meandering and braided channel system, tidal flats) the tidal current variation is influenced by the geometry, within which two types of geometry are distinguished: a) shallow channels and landward decreasing depth with tidal flats below mean sea-level; and b) deep channels throughout with tidal flats above mean sea-level. In the first case the slack water period before ebb will exceed the slack water period before flood and hence a residual import of fine sediment is favoured. In the second case the inverse situation occurs: slack water period before flood exceeds slack water period before ebb and hence a residual export of fine sediment is favoured (Dronkers, 1986).

Tidal asymmetry in estuaries and its effects on sediment transport are discussed by Fitzgerald *et al.* (1976); Boon and Byrne (1981); Aubrey and Speer (1985); Fry and Aubrey (1990); and Pethick (1995) and (1996). Changes in the plan-form of an estuary are paralleled by cross-sectional area and depth changes of the estuarine channels. Pethick (1995) presents a model of the temporal development of an estuarine channel through the Holocene (Figure 3-4).

Third Party material excluded from digitised copy.
Please refer to original text to see this material.

Figure 3-4 – Model of the temporal development of an estuarine channel through the Holocene (from Pethick (1995)).

During Holocene sea-level rise, intertidal mudflats are poorly developed, exhibiting a flood-dominant tidal wave and, therefore, a positive sediment budget. Deposition rates on the intertidal mudflats are high and thus they increase their elevation. As the process continues, however, sediment accretion on the inter-tidal flats produces a defined sub-tidal channel with an increasing relative depth. The result is a cross-section with a deep central channel bounded by high inter-tidal flats and a switch to ebb-asymmetry resulting in a net transport of sediment out of the estuary.

Critical to East Anglian estuaries and inlets is the effect of dredging. Pethick (1995) points out that dredging of the sub-tidal channel can cause over-deepening and in the case of narrow channels dredging can affect the whole cross-section and lead to a flood dominant tide. In broad channels a deeper central channel will cause ebb dominance. This effect can be seen in the Thames estuary where the outer reaches at Southend are flood dominant while the inner reaches at Greenwich are ebb dominant (Pethick, 1995).

3.2.6   CONTEMPORARY ESTUARINE SEDIMENT ACCRETION AND EROSION

The rates of accretion and/or erosion of both saltmarshes and mudflats have been studied by authors for over a century, although most work has concentrated on saltmarshes as opposed to mudflats. In most cases, methods used to study sedimentation look at saltmarsh accretion rates; they are rarely designed to measure erosion since saltmarshes are usually areas of deposition. This is generally the case where a saltmarsh is not affected by man-made structures such as coast defence works. Recently, increasing concern over the rate of loss of saltmarsh has prompted a closer look at erosion rather than accretion. Several studies have looked at seasonal changes in tidal flat elevation, especially the tidal flats that front areas of saltmarsh. Examples include studies by Kestner (1961) in the Wash and other UK sites; Richard (1978) in Long Island, USA; Frostick and McCave (1979) nearby in the Deben estuary, Suffolk, UK; Anderson et al. (1981) Maine, USA; Bale et al. (1985) Tamar Estuary, UK; and Kirby et al. (1993) Strangford Lough, Northern Ireland. Generally, highest accretion is recorded in the summer and lowest in the winter. This is attributed to calmer summer conditions allowing settling of fine sediment which is then enhanced by algal binding. In the winter, wind and wave action increases erosion which, in very cold regions, is then exacerbated by the spring break-up of ice. Frostick and McCave's (1979) work measured the level of mud flats in the Deben estuary and showed accretion rates of approximately 5.0 cm between April and September during algal growth, and erosion of a similar amount during the autumn and winter when algae are dead or absent. Kirby et al. (1993) studied tidal mud flat stability in Ardmillan Bay, Strangford Lough, Northern Ireland over a 22 month period. The observations point to a seasonal waxing and waning of tidal flat elevations and to the controlling influence of wind. Real sediment level changes were detected on several time-scales. Some changes were unsteady, but still following a generally unidirectional trend. On a second time scale a

repeating, yearly, seasonal cycle was detected: winter/spring erosion was frequently matched by summer accretion. Gale-generated waves caused the erosion and, in summer, deposition was enhanced by algal binding. Kirby *et al.* (1993) concluded that episodic wind waves are the main cause of tidal flat instability and that large quantities of sediment are redistributed by these forces. Daborn *et al.* (1993) studied the effects of migratory birds on the stability of intertidal mudflats in the Minas Basin, Nova Scotia. It was found that before birds arrived, sediment cohesion resulted partly from secretion of polysaccharides by benthic diatoms whose production was controlled mainly by a grazing amphipod *Corophium volutator*. After the birds arrived, the behaviour of *Corophium* changed: bioturbation and grazing pressure on the diatoms decreased, and the production of cohesion-inducing carbohydrates increased, resulting in a decrease in bed erodibility.

3.2.7 CONCURRENT STUDIES AFFECTING HAMFORD WATER

Concurrent with this research project was a series of more regional projects being conducted by the Institute of Estuarine and Coastal Studies, University of Hull (IECS) for the Environment Agency and English Nature, involving various geomorphological aspects of the Essex estuaries and coastal zone. In particular IECS (1995) looked at the pattern of sand transport in the Harwich to The Naze bay area including Cork Sand (Figure 3-5), which has a possible influence on the pattern of sand transport in Hamford Water. A summary of the offshore sand transport pathways is as follows (numbers refers to Figure 3-5 and italics are text of IECS (1995) report):

Third Party material excluded from digitised copy.
Please refer to original text to see this material.

Third Party Material excluded from digitised copy.
Please refer to original text to see this material.

Despite its complexity, IECS (1995) have postulated that the entire area between the mouths of Hamford Water and the Stour-Orwell, and Cork Sand appears to follow the basic morphology of inlet mouths which was outlined in a model by Ocrtal (1975) for the US east coast. In this model Cork Sand, Pye Sand and Landguard Point are seen as part of the ebb tide delta of the Stour-Orwell, an estuary whose composite morphology is maintained by a southerly net tidal current and strong onshore wave action. The presence of these ebb-tide deposits provided sufficient shelter to the Hamford Water area to allow the development of tidal mudflat and saltmarsh.

IECS (1995) also postulated that progressive reclamation of saltmarsh has constricted the mouth of Hamford Water, setting up an ebb-dominant tidal regime, which is now causing a net export of sediment from the inlet.

> "*This exported sediment, in part, is being deposited as an ebb delta coincidentally on Pye Sand, which is then available for transport in the circulatory system of the Harwich-Walton Bay.*"

Finally IECS (1995) studied the impact of dredging on the Harwich-Walton Bay area in the light of reports by HR Wallingford (1992a) and Posford Duvivier (1993). The Harwich Approach Channel, which extends for 10 km due east of Landguard Point, was deepened to a depth of 13m following a capital dredging programme which was started in May 1993, involving removal of 8.5Mm^3 of sediment over an 18 month period. The channel was previously maintained at a depth of 11m. A modelling exercise was carried out by HR Wallingford (1992b) to assess any impact of the work. It was found that deepening the channel would reduce peak tidal currents in the channels, presently 1.3m s^{-1}, by less than 0.1m s^{-1}, and maximum bed shear stresses of 2.0N mm^{-2} would be reduced by 0.1-0.3N mm^{-2}. Such reductions are predicted to increase sedimentation in the channel and reduce the present tendency for sand to be transported seawards. The deepening of the channel is also predicted to increase the

one year return period wave (from the North-east) at the entrance to the harbour from 1.1m to 1.4m (Posford Duvivier, 1993; IECS, 1995).

3.2.8   SUMMARY

Hamford Water has been reviewed from the point of view of the site fitting a pre-determined geomorphological classification as a semi-natural, embayment saltmarsh connected to the southern North Sea through a poorly defined, transitional tidal inlet. The morphology of tidal inlets, sediment transport through an inlet and the concept of tidal inlet equilibrium have been reviewed. In addition, sedimentation in the estuarine environment, particularly on saltmarsh and on intertidal mudflats, has been considered. A review of concurrent research has been included since it highlights the importance of the site within a much more regional context.

4 Hydrodynamics

4.1 Introduction

The aim of this chapter is to investigate the hydrodynamic nature of the inlet and its influence on the boundary layer structure, patterns of sediment transport, and the overall mechanisms determining the morphology of the inlet. The chapter is divided into sections in which each parameter is investigated, field methods are described and data are presented and discussed.

In assessing the hydrodynamics and the nature of sediment transport of Hamford Water, the following parameters were considered: waves, tidal wave form, tidal currents, salinity and temperature and boundary layer flow. Recording of these parameters involved several separate deployments:

- **Deployment 1** (April to August 1993) consisted of reconnaissance surveys of tidal currents, boundary layer flow and temperature and salinity profiles. The data were used in the preliminary report (Annex A) and are also used in the following sections on tidal currents (Section 4.4) and salinity and temperature (Section 4.5).

- **Deployment 2** (August 1994) was an anchor station, tidal velocity/CTD profiling deployment that had to be abandoned due to a defective survey vessel and data were not used.

- **Deployment 3** (November – December 1994) was an attempt to expand on boundary layer flow data obtained in Deployment 1 and data were subsequently used (in hindsight) to support Deployments 4 and 5.

- **Deployments 4 and 5** (June 1995) were comprehensive surveys of current velocity, boundary layer flow structure and suspended particulate matter (SPM) on a spring and a neap tide respectively. Deployment locations are illustrated in Figure 4-1; transect line A–B was used for Deployments 4 and 5.
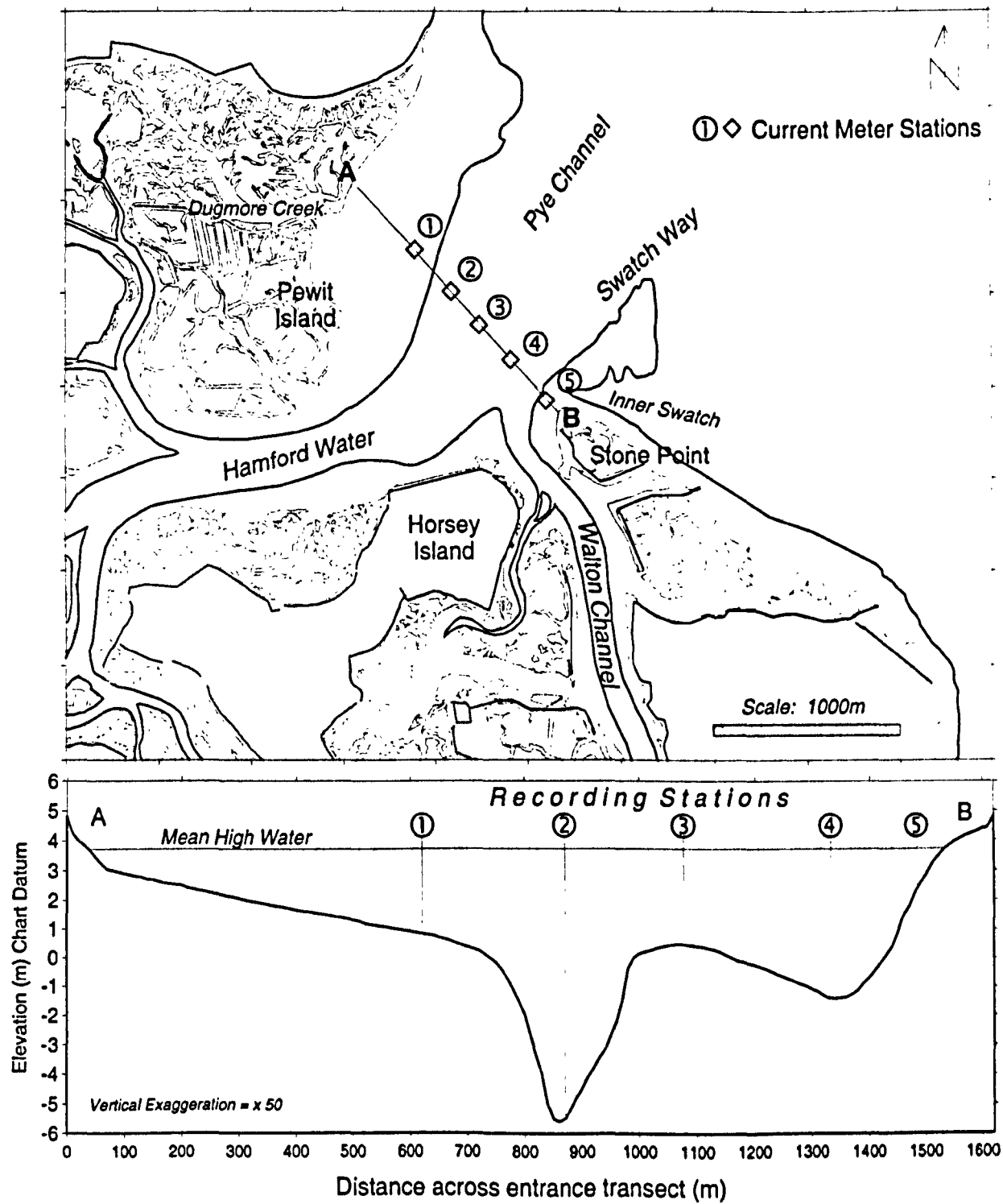
Figure 4-1 – Current Meter Stations and Survey Transect (Line A-B).

4.2 Waves

4.2.1 METHODS

Exclusive wave data were not collected as part of this research; instead, recourse was made to recent wave research by independent private Consultants and UK Government Agencies as part of on-going expansion of Harwich and Felixstowe Harbours at the mouth of the Stour and Orwell. Several hindcasting and modelling exercises were conducted for the area (UKAE, 1984; HR Wallingford, 1992b; WS Atkins, 1993). In addition, although no actual wave data were collected, an assessment of wave conditions, by observation, was made in the Wade and at Stone Point. Data is summarised in Table 4-1 and locations illustrated in Figure 4-2.
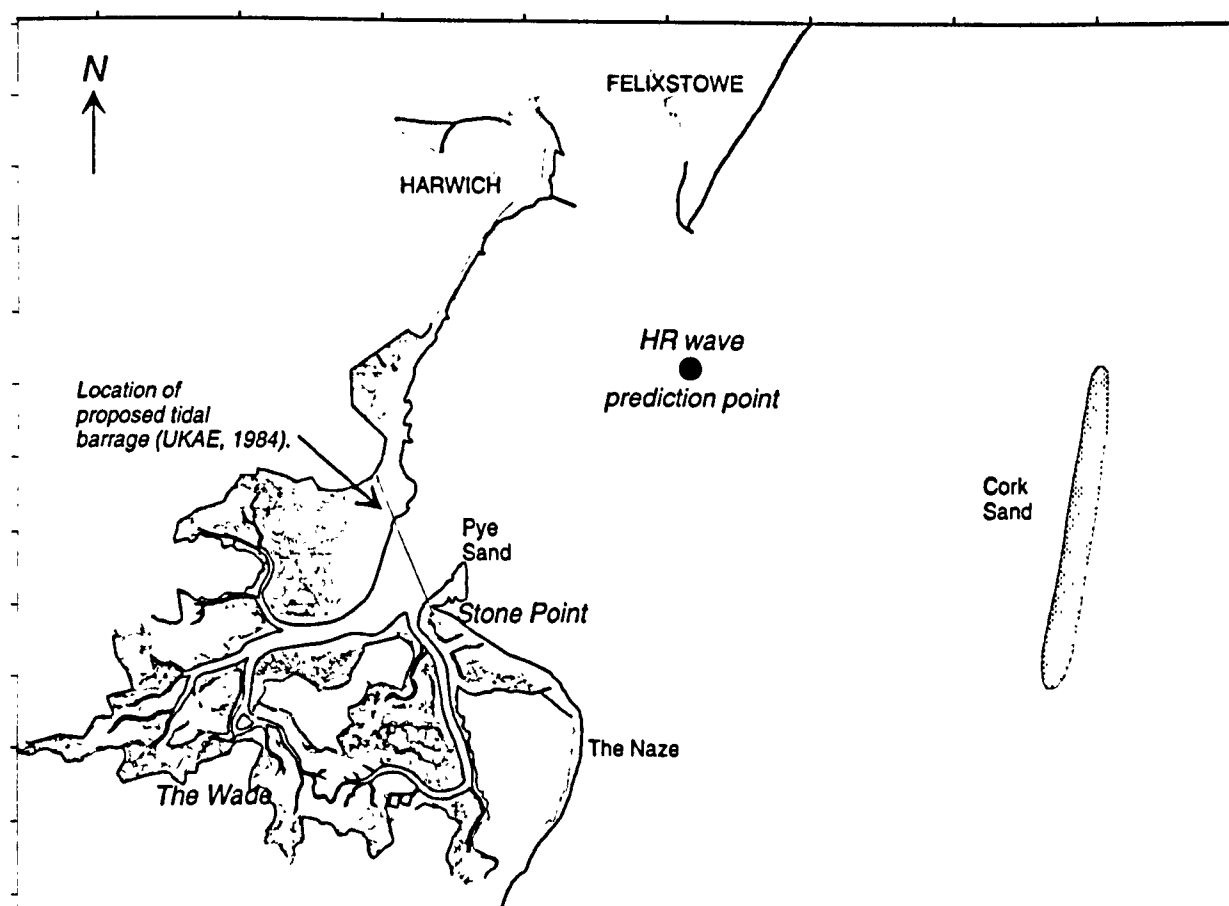
Figure 4-2 – Sites of wave measurements and model predictions.

4.2.2 RESULTS AND DISCUSSION

Previous workers considered various differing wave spectra, ranging from offshore conditions to those present within the Harwich–Walton Bay and Hamford Water. UKAE (1984) calculated significant wave heights (H_s) either side of a proposed tidal barrage spanning the mouth of Hamford Water from Stone Point to the northern

entrance of Bridgedock Creek (Figure 4-2). On the seaward side, UKAE calculated H_s as 3m and on the basin side, 1.5m. However, typical events for which H_s were calculated were not stated.

More recently, both offshore and nearshore wave conditions have been studied by HR Wallingford (1992b, updated in 1997) in continuing studies of the hydrodynamic effect of deepening the main navigation approach channel to Harwich and Felixstowe. The offshore wave climate for Harwich and Walton-on-the-Naze region was hindcast (using HR's program, HINDWAVE) utilising wind data from Gorleston for the period 1973 to 1990 and 1994 to 1996. The predicted offshore results show that the larger waves approach the area from north-easterly directions, due to the long fetch lengths in this direction. It was also predicted that the highest frequency of wave events is from the south-west, but the waves are much smaller (95% with H_s <2m) due to a shorter fetch from this direction.

HR also used a wave refraction model, OUTRAY, to model conditions closer inshore. Wave conditions were found to be mainly from an easterly or south-easterly direction, primarily due to the effects of refraction aligning the waves with the bathymetry offshore from Harwich. The maximum wave expected with a 1-year return period has a H_s of 3.1m and a period of 5.9 seconds, approaching from the east. Using data generated by HR's study, WS Atkins (1993) modelled H_s over the area of the Harwich-Walton Bay. The study highlighted the sheltering effect of Cork Sand as an offshore breakwater to waves from the east and south-east, providing a wave shadow in its lee. The degree of energy dissipation by Cork Sand differs with the angle of the incoming waves due to the differing cross sectional shape of the sand relative to the incident wave; in each of the modelled cases the wave shadow effects stretched almost to the coast (WS Atkins, 1993).

The propagation of waves into Hamford Water itself is most likely to occur when waves approach from between the north and east. Wave conditions for the north shore of Horsey Island and the more open beach sites at Foulton Hall and Pye Sand were modelled by HR Wallingford (1992b) using 70% wind speed for 1, and 50 year return periods. The study used offshore wave conditions for a point approximately 2 km south of Landguard Point (Figure 4-2), these being subjected to modification by

shoaling, refraction and frictional effects. These waves have an H_s for a 'typical' event of 0.9m, while for the 1 year and 50 year return intervals, the H_s is 2.3m and 3.3m respectively. Once transformed to the inshore zone these wave heights are reduced: the H_s at Horsey Island being lower than those for the open beach sites at Foulton Hall and Pye Sands. The resulting wave conditions are shown in Table 4-1.

Table 4-1 – Inshore wave conditions in Hamford Water.

Third Party material excluded from digitised copy. Please refer to original text to see this material.

(Source: HR Wallingford, 1992b)

Further within Hamford Water in areas with short fetches (no more than 2km), in severe conditions, such as were experienced in the floods of 1953 (Grieve, 1959), typical wind speeds of 20 and 30 $m\,s^{-1}$, yield H_s of 0.5m and 0.7m, respectively. However, individual wave crest to trough will reach about 1.9 times the significant height (IOS, Draper *pers comm*). Although rare, such waves within Hamford Water could cause considerable undercutting, collapses of saltmarsh cliffs, and destroy the integrity of saltmarsh vegetation. In practice, in areas such as the Wade, H_s rarely exceeds 0.3m and the tidal window when wave action is most significant, varies depending on whether it is neap or spring tides. On neaps, the saltmarsh is not covered and erosion is predominantly by undercutting of the cliff. On springs the combined effects of undercutting, stripping and flattening of the saltmarsh vegetation can occur. The effect of wave action on deposition and erosion of both mudflat and saltmarsh is considered in more detail in Chapter 7.

4.2.3 SUMMARY

Hamford Water is affected by two different wave regimes: fully-developed open sea waves, and depth-limited internally generated waves within the embayment. The

seaward shores between Stone Point and the Naze, and to some extent from Blackman's Head to Foulton Hall Point, are subject to fully developed offshore waves from the east, north-east and south-east. Within Hamford Water the waves are characterised by short, locally generated waves within the bay increasing to depth-limited moderate waves in Hamford Water Channel. The ability of waves to erode and transport sediment depends to a large extent on the state of the tide and the age of the tidal cycle. Strong onshore winds and neap tides are considered to be the most erosive.

4.3   Tides

4.3.1   METHODS

As with wave data, independent tidal data were not collected for this research. Instead, use was made of Admiralty Tide Tables (ATT) (NP201, Volume 1), Admiralty TIDECALC tidal predication program (NP158 Version 1.1), and Harwich tide-gauge data courtesy of Harwich Haven Authority. ATT and TIDECALC list two Standard Ports: Harwich (No.131), and Walton-on-the-Naze (No.129), and a Secondary Port, Bramble Creek (No.129a)(Figure 4-3). Data for Bramble Creek are based on an Admiralty survey conducted in 1983 using a temporary automatic tide gauge (type unknown). The published data in ATT for Bramble Creek are based on 36 days readings obtained in January and February 1983 (Admiralty, 1983).
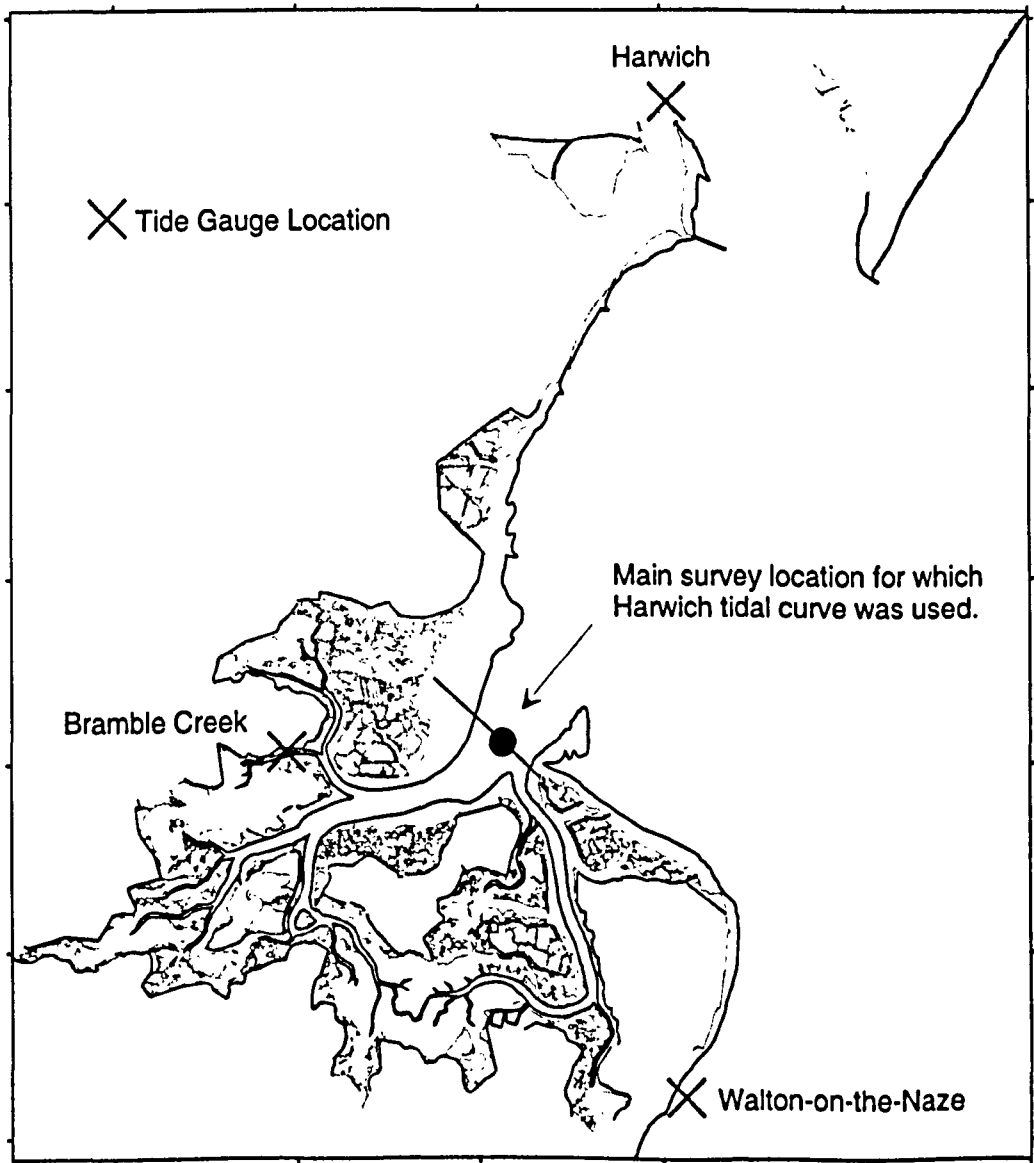
Figure 4-3 – Tide gauge location near Hamford Water.

4.3.2 RESULTS

The tides of Hamford Water are driven by the amphidromic system in the Southern Bight of the North Sea (Pugh, 1987). The mean tidal range varies considerably on the East Anglian coast: north of Hamford Water, as far as Great Yarmouth, it is relatively constant at approximately 2.0m. Southwards, as far as Margate, the range increases from 3.0m to 6.0m (ATT, 1996).
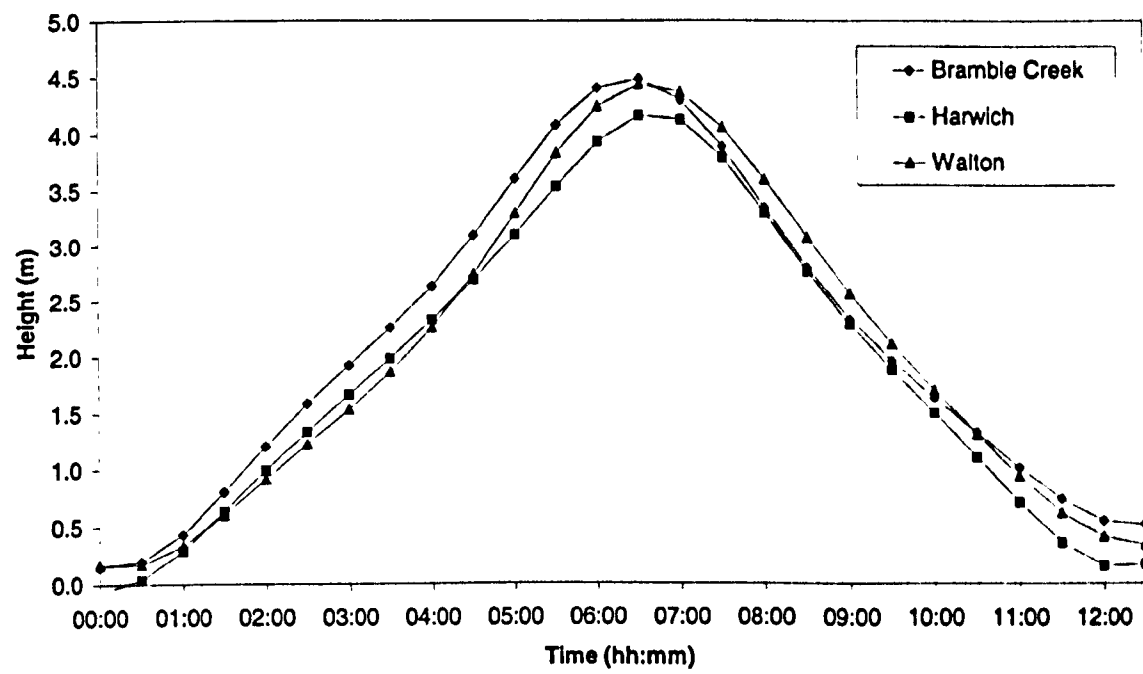
Figure 4-4 – Tidal Stage Curves: Bramble Creek and Harwich (computed using TIDECALC).

Table 4-2 – Tidal asymmetry in Hamford Water and at Harwich

Station	Flood tide duration (Springs)	Ebb tide duration (Springs)	Mean Range (Springs)
Harwich	6.4 hrs	6 hrs	3.6m
Bramble Creek	6.6 hrs	5.6 hrs	4.2m
Walton-on-the-Naze	6.3 hrs	5.9 hrs	3.8m

Hamford Water tides are semi-diurnal with a diurnal inequality amounting to 0.1-0.2m difference on high water spring tides at Bramble Creek. Predicted tidal stage curves for a typical spring tide at Harwich, Bramble Creek and Walton-on-the-Naze are shown in Figure 4-4. The duration of the flood and ebb limbs of the tides at both these locations are shown in Table 4-2. Data obtained from Harwich Harbour Authority for the period of 21 June to 22 June 1995 which coincides with Deployments 4 and 5 at the mouth of

Hamford Water are plotted in Figure 4-5 and Figure 4-6 and illustrate examples of observed versus predicted tidal stage curves for Harwich at the time of both spring and neap surveys. Observed, in this instance, is as recorded by the Harwich tide gauge, and predicted is as calculated from TIDECALC and appears to correlate well for the period of survey.
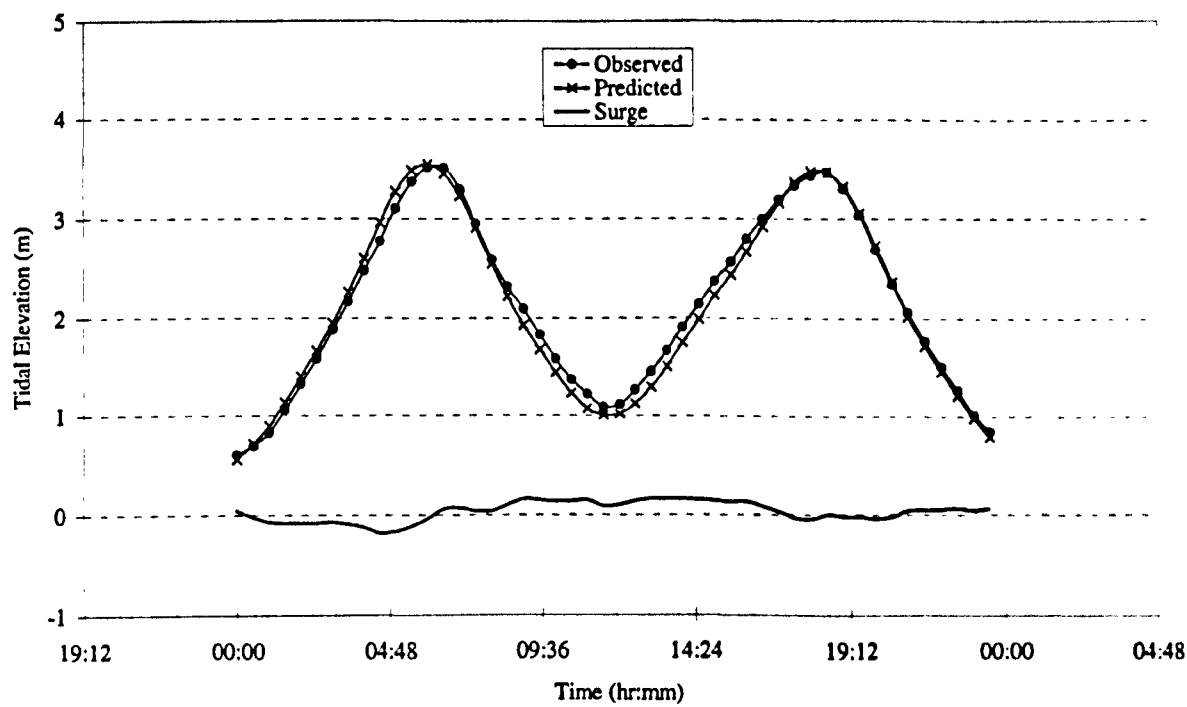
Figure 4-5 – Observed versus predicted tidal curve for Harwich – 21 June 1995.
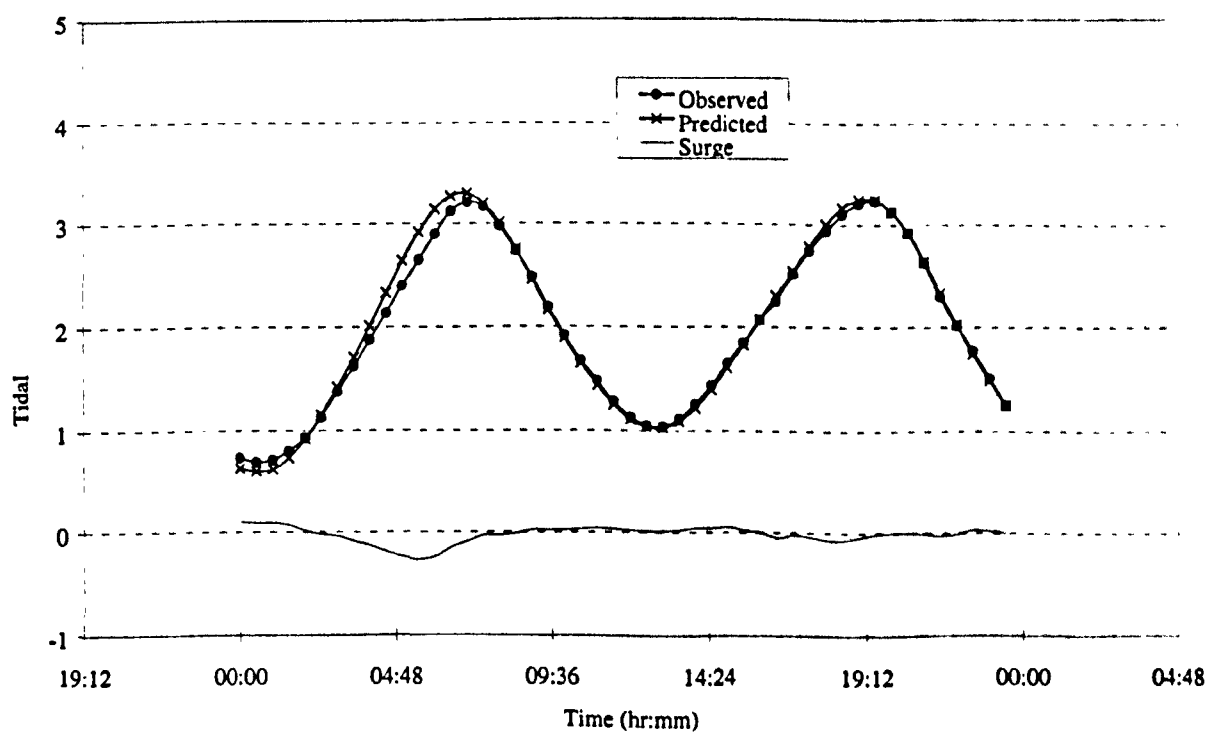
Figure 4-6 – Observed versus predicted tidal curve for Harwich – 22 June 1995.

Although it was not possible to install an independent tide gauge at the mouth of Hamford Water for any of the surveys, it was found that predicted tides for Harwich were a best approximation and were used in all calculations in the inlet throat. The decision to use Harwich was based on a combination of visual observation and recorded times of slack water at current meter stations as discussed in Section 4.4.

4.3.3   DISCUSSION

It is evident from an analysis of predicted tidal data that the predicted ranges at Bramble Creek and Walton-on-the-Naze are greater than Harwich. A comparison of tidal curves for Bramble Creek, Harwich and Walton-on-the-Naze (Figure 4-4) would suggest that Hamford Water is a *hyper*synchronous hydrodynamic system after the classification of Nichols and Briggs (1985), where convergence exceeds friction thereby increasing the tidal range towards the head of an estuary. However, given the short observation period (36 days) from which the Bramble Creek curve was produced, it is possible that the curve is not accurate. The level of such accuracy was not investigated in this survey. The opposite term, *hypo*synchronous is where friction dominates and the tidal range decreases throughout the estuary. It is more likely that convergence is not important and the tidal range should decrease landward (hyposynchronous). According to Dyer (1996), if the intertidal area increases toward the land, then filling that volume of the tidal prism will occur when the cross section area through which the water has to flow is large because of the flooding tide. The ebb, however, occurs through a much smaller area, which leads to an ebb dominant response. This is considered to be characteristic of estuaries and inlets with a large intertidal volume to channel volume ratio together with a small tidal range. Assuming the Bramble Creek curve in Figure 4-4 to be accurate, and in the absence of any other tide data within Hamford Water, there may be areas of both hypersynchronous and hyposynchronous existing within the embayment. Variations in tidal amplitude throughout the site were not investigated in this research.

4.3.4   SUMMARY

The tidal regime in Hamford Water is typical of bays, inlets and estuaries around the UK coast: the tide is semi-diurnal, and classified as mesotidal after Davies (1964) with an average tidal range of 3.8m on springs and 2.3m on neaps. Predicted tidal duration

(to the nearest 5 minutes) of the flood is 6 hours 40 minutes during springs and 6 hours 30 minutes during neaps. Predicted ebb times are 5 hours 40 minutes during springs and 5 hours 50 minutes during neaps. The tidal curve for Bramble Creek would suggest an hypersynchronous hydrodynamics system although it is more likely that the system is hyposynchronous and has an ebb dominant tidal regime.

4.4 Currents

4.4.1 METHODS

An Eulerian sampling method was adopted for the measurement of current velocity utilising two different techniques:

- Anchor Station Profiling: current meters suspended from an anchored boat and used for profiling from the surface to the bottom. This method also involved simultaneous measurement of salinity and temperature discussed in Section 4.5 below.

- Velocity Gradient Unit (VGU): current meters attached to a mast and positioned at fixed distances above the bed in a vertical array. This method also allowed the collection of current data for use in sediment flux calculations and to measure the bed stress for use in sediment transport equations (Chapter 6).

4.4.1.1 Anchor station profiling

In the first instance, the method involved profiling from boats anchored in various channels throughout the site. Either the instrument was lowered and raised by hand, or a winch was used to raise and lower the instrument whilst recording the relevant parameters. In both cases the instrument was first lowered until the bottom was 'felt', then lifted clear at least 0.5m. Data were then recorded at 0.5m intervals from the bottom to the surface. Water depth was simultaneously recorded by the respective instruments and by a hull-mounted echo sounder on the main survey vessel.

The following stations were used for anchor station profiling:

- Walton Channel – 1 spring tide cycle (low water-high water-low water)

- Hamford Water – ½ cycle (high water to low water)

- Pye Channel (also Station 2) – 1 spring and 1 neap cycle

- Swatch (also Station 3) – 1 spring and 1 neap cycle simultaneous with Pye Channel

Errors associated with Eulerian measurement of current velocity are discussed in Appendix C. The error deemed to have a significant effect on results was the effect of yaw around slack water at Station 2 (Pye Channel anchor station). An increase in recorded velocity of 0.4 m s^{-1}, 30 minutes either side of slack water, translated into an additional water flux of 1.08 x 10^6 m^3 over a 60 minute averaging period. The cross-sectional area, over which station 2 was applicable, was 741.5m^2. Although this only amounted to 0.01% of the net water flux on springs, the error was accounted for in subsequent flux calculations (*see* Section 6.2 below).

4.4.1.2 Velocity Gradient Unit

Velocity Gradient Unit (VGU) technical details are contained in Appendix D. The VGU is capable of obtaining lengthy periods of continuous velocity data and hence was used over various periods and in various locations between April 1993 and June 1995. Deployment location details are summarised in Table 4-3 and illustrated in Figure 4-7. The time each VGU covered or uncovered, as represented by the time they started and/or stopped recording, gave a good indication of the time and height. The charted elevation of the base of each VGU was estimated from Admiralty Chart 2695 – Plans on the East Coast of England.

Table 4-3 – VGU Deployment and Data Recovery Status

TS	Observation Period	VGU	Location	Cycles Deployed *	Cycles Recovered	% Data Recovered
1	06 – 22 Apr 1993	1	Stone Point	31	10	32%
2	29 Apr – 07 May 1993	2	Pewit Island	16	11	69%
3	02 – 17 Nov 1994	1	Stone Point	29	29	100%
4	03 – 17 Nov 1994	2	Pye Sand	27	27	100%
5	25 – 29 Nov 1994	1	Horsey Is.	8	3	38%
6	26 Nov – 08 Dec 1994	2	Swatch Way	24	24	100%
7	15 – 22 Jun 1995	1	Dugmore Ck	13	13	100%
8	15 – 22 Jun 1995	2	Pye Sand	13	13	100%
			Totals	161	130	81%

* One cycle equals low water – high water – low water.
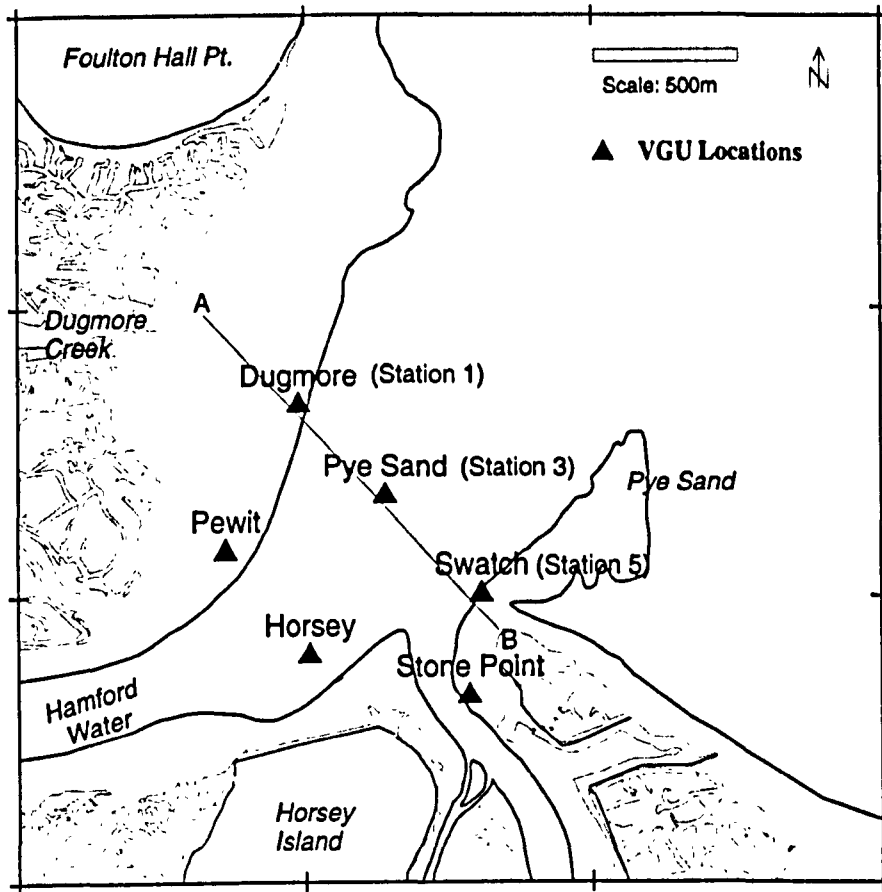
Figure 4-7 – Location map of VGU deployments

The poor recovery record from the first two deployments (TS-1 and TS-2) is attributed to data download problems and obsolete software. They were the final deployments of an earlier logger version which utilised a BBC microcomputer program and required 240V power supply in the field for downloading. TS-1 and TS-2 were consequently not used in any analysis. TS-3 through to TS-8 were obtained using new loggers that only required a laptop computer in the field for downloading. The poor recovery from TS-5 was the result of a logger-to-PC communication incompatibility, which resulted in gapped records. The problem was not solved at the time and the deployment was terminated.

4.4.2   RESULTS

4.4.2.1   Anchor Stations

Results from current velocity monitoring are presented in the following forms: surface and bottom velocity variations, mean velocity profiles, inlet cross-sectional velocity plots, and velocity-time distribution plots. The convention of plotting flood values as

negative and ebb values as positive after Dyer (1979), is adopted whenever possible throughout the thesis.
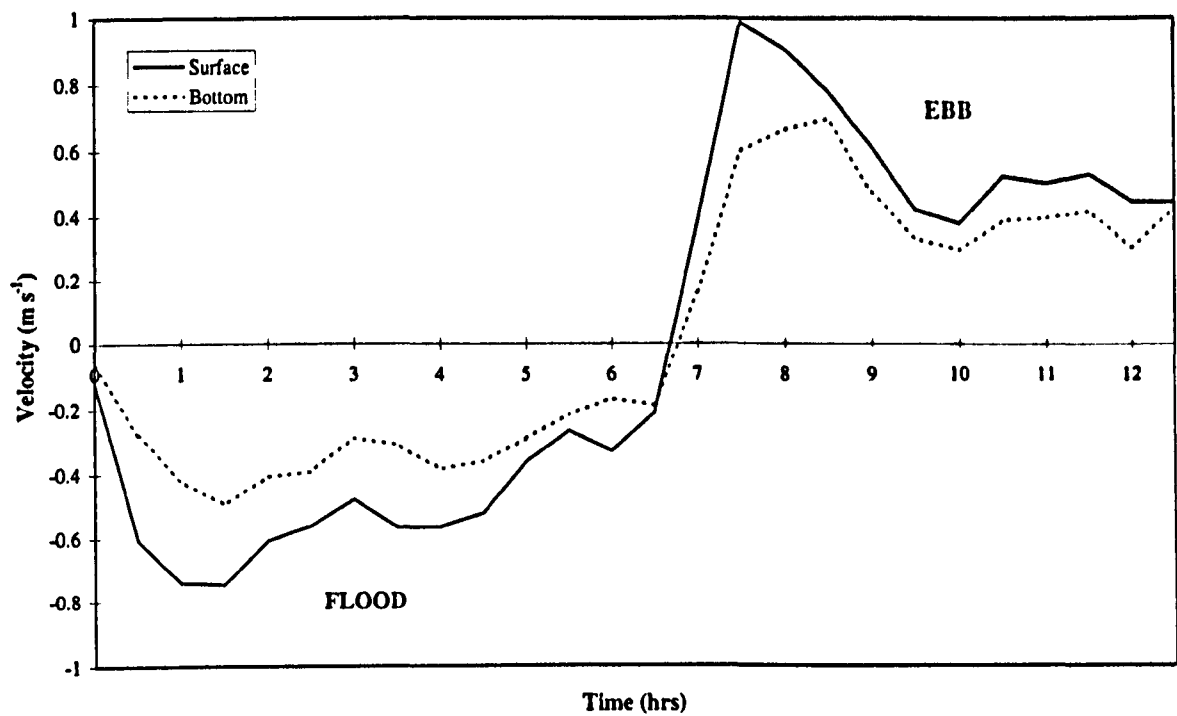
Figure 4-8 – Velocity variations during a spring tide in Pye Channel (Station 2).
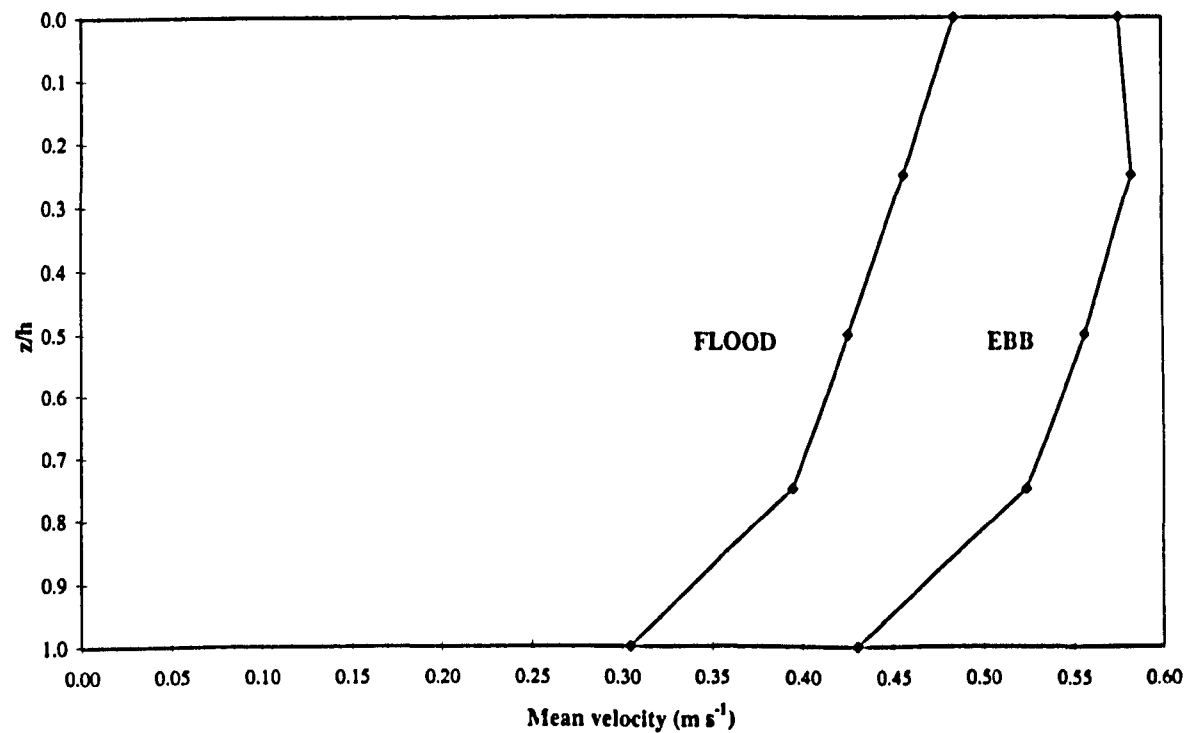
Figure 4-9 – Mean spring flood and ebb current-velocity profiles – Pye Channel (Range = 3.5m).

Data collected in Pye Channel during a single spring tidal cycle show ebb velocities consistently greater than the flood (Figure 4-8 and Figure 4-9). Surface ebb velocities peak at 0.99m s^{-1} compared with a flood peak of 0.75m s^{-1}. Bottom ebb velocities peak

at 0.7 m s^{-1} compared with 0.49m s^{-1} during the flood. The mean ebb velocity profile is consistently greater than the flood over all depths. Velocities increase uniformly towards the surface although there is a slight shear below the surface on the ebb.
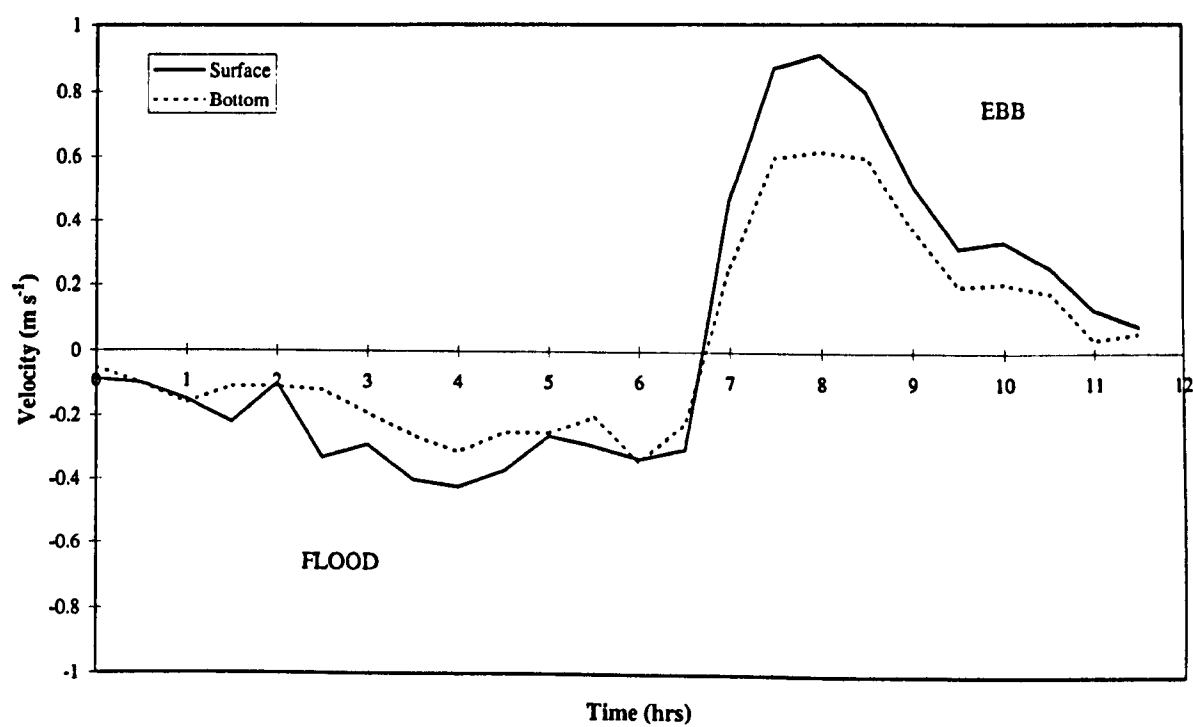
Figure 4-10 – Velocity variations during a spring tide in the Swatch Way (Station 4).
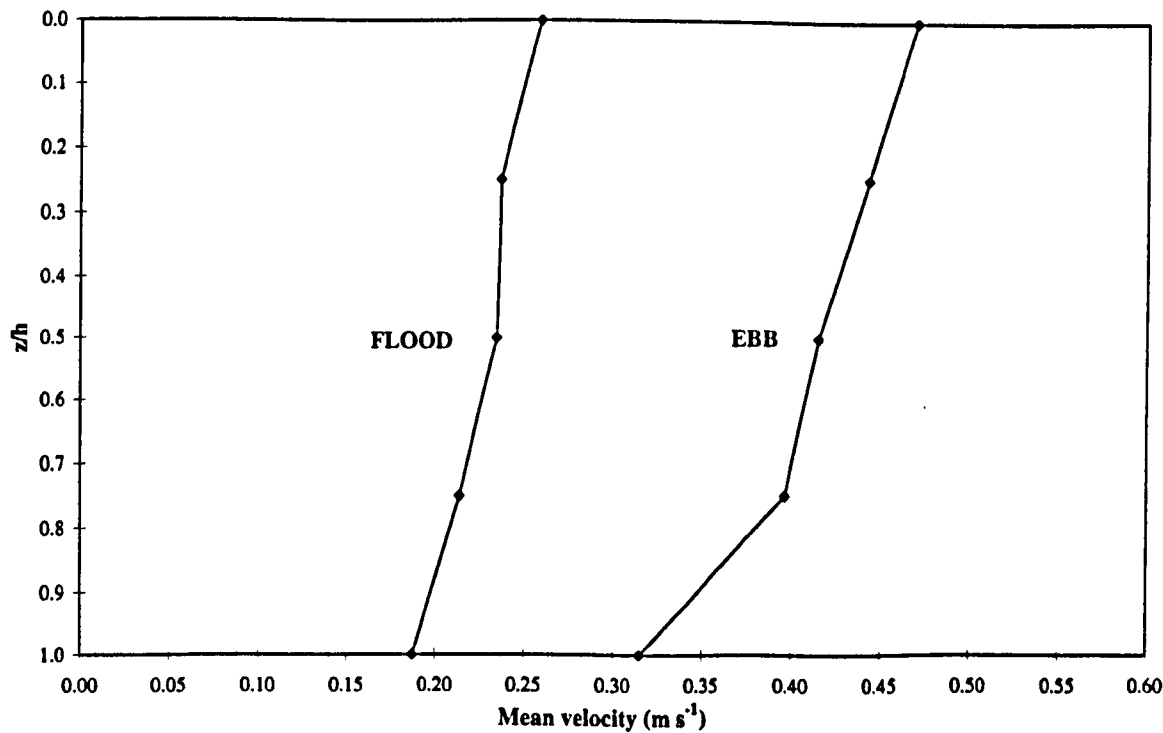
Figure 4-11 – Mean spring flood and ebb current-velocity profiles – Swatch Way (Range = 3.5m).

Data collected in the Swatch Way during a single spring tidal cycle again show ebb velocities consistently greater than the flood. Surface ebb velocities peak at 0.91m s^{-1}

compared with a flood peak of 0.42m s⁻¹. Bottom ebb velocities peak at 0.62m s⁻¹ compared with 0.34m s⁻¹ during the flood. The mean ebb velocity profile is also consistently greater than the flood.
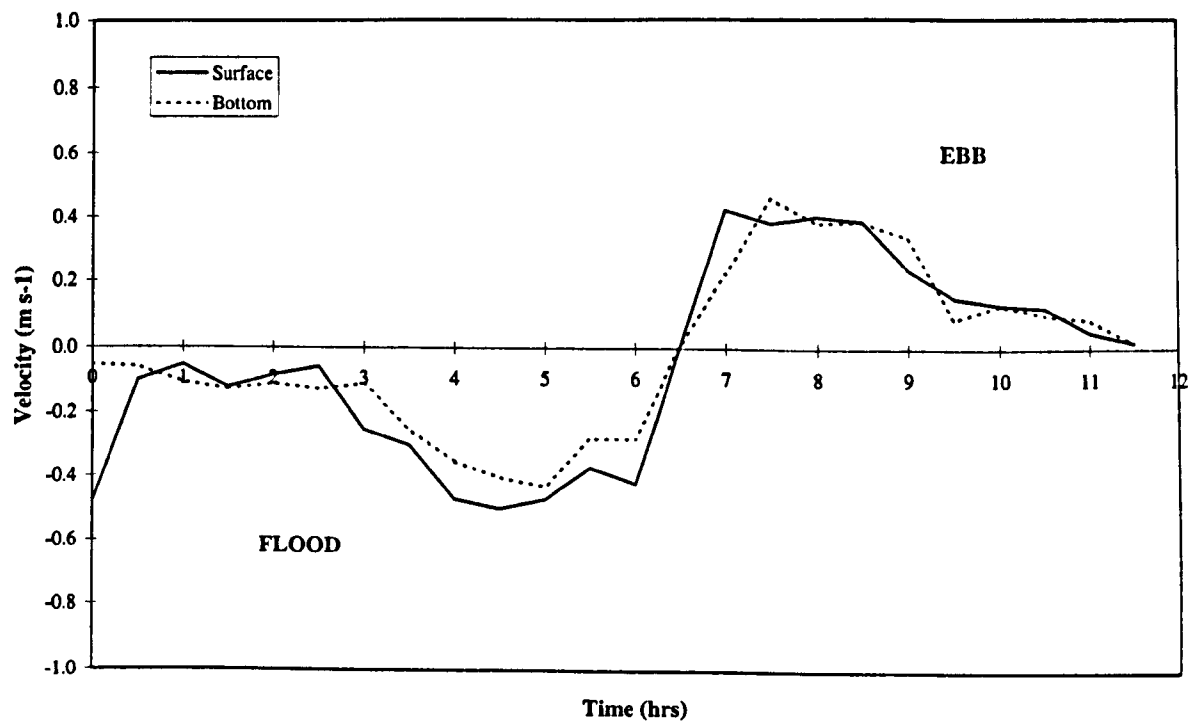
Figure 4-12 – Velocity variations during a spring tide in Walton Channel.
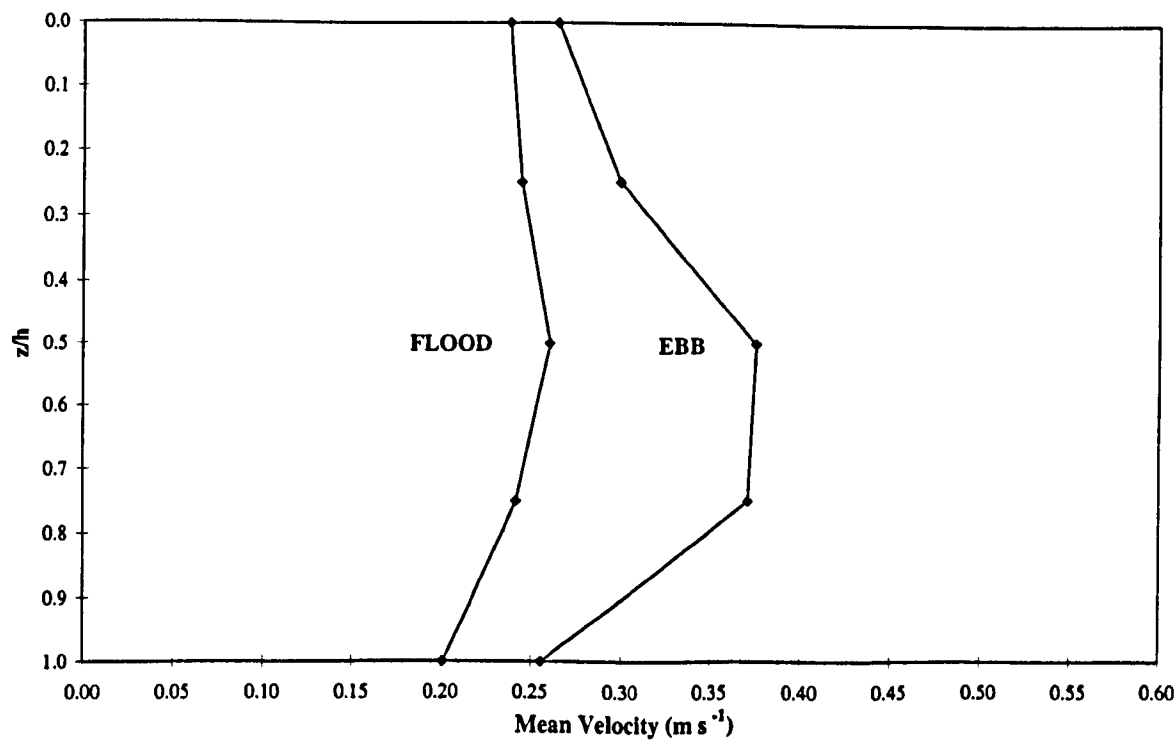
Figure 4-13 – Mean spring flood and ebb current-velocity profiles – Walton Channel (Range = 3.4m).

Data collected in Walton Channel, just off Stone Point, during a single spring tidal cycle are more balanced than Pye Channel and the Swatch Way. Bottom currents flood and ebb simultaneously with those at the surface, and the velocity of each limb of the tide is similar. Surface peak flood velocities are 0.5m s^{-1} compared with the ebb of 0.43m s^{-1}. Surface peak ebb velocity is slightly less in this case at 0.43m s^{-1} compared with bottom peak velocity of 0.46m s^{-1}. However, maximum flood and ebb velocity is reached at mid-depth with velocities of 0.8m s^{-1} being reached on the ebb and 0.52m s^{-1} on the flood.

An illustration of the current velocity variations within Hamford Water would not be complete without including some results from data collected from Velocity Gradient Units (VGU). A full treatment of the VGU and the applicability of the data to boundary layer flow is discussed in a separate section below, Section 4.6. In the present section, data collected at different times but matched according to similar tidal ranges is presented for the inlet throat.

Figure 4-14 and Figure 4-15 illustrate the depth-averaged velocity at the three VGU stations across the inlet throat for a spring and neap tide. Depth-averaged velocity was calculated according to:

$$\bar{\bar{u}} = \frac{1}{z_{max}} \sum_{i=1}^{n} u_i \, \Delta z_i \qquad (4:1$$

Where u_i is the velocity at each current meter, z_{max} is the height above the bottom, and Δz_i is the thickness of the appropriate depth increment for each current meter. Although it is normal convention to plot flood velocities as negative, both flood and ebb are plotted as positive in this case to better illustrate the comparison of velocity peaks. Data from Stations 1 and 3 were collected as part of Deployments 4 and 5 in June 1995. Station 5 data were collected separately in November 1994 (Deployment 3) and were matched with stations 1 and 3 by tidal range and their similar occurrence in a lunar cycle. It is accepted that seasonal meteorological conditions vary greatly, but conditions were similar in wind speed and barometric pressure on both occasions. However, see below in the discussion (Section 4.4.2.2) for problems with matching station 5 to other data.
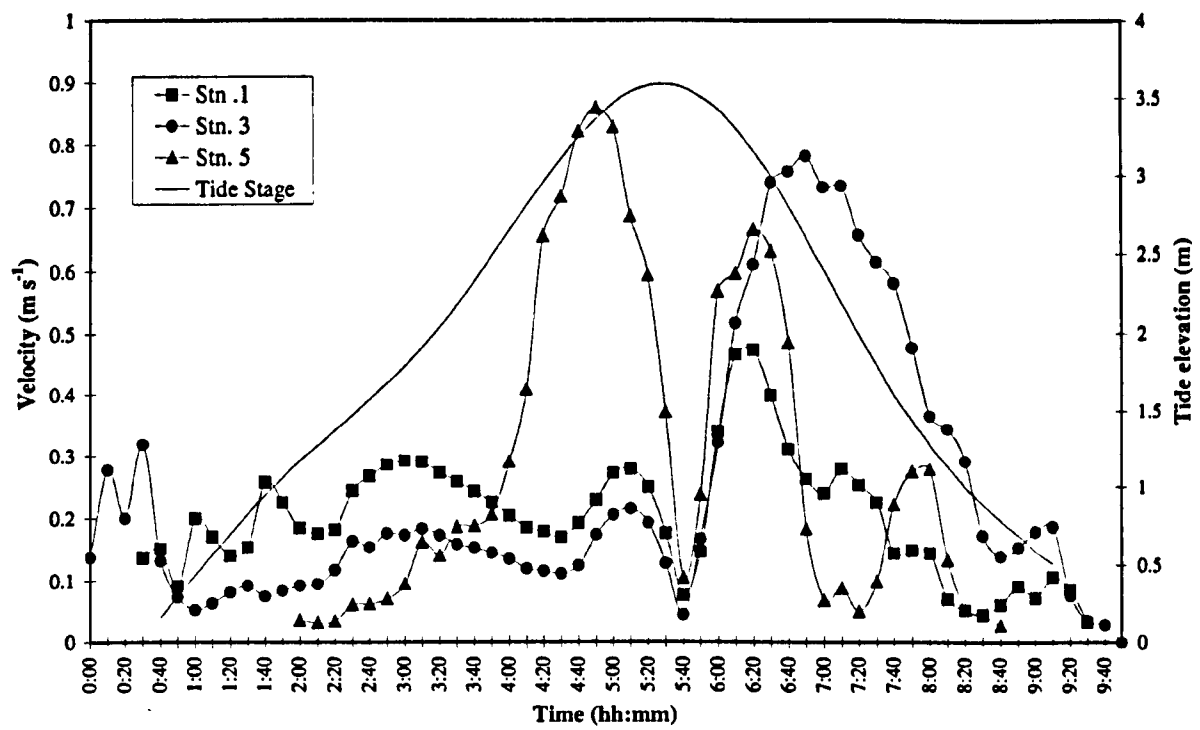
Figure 4-14 – Spring tide depth average velocity for VGU stations 1, 3 and 5

Figure 4-14 is a plot of spring tide depth-averaged velocity (m s⁻¹) at the three VGU stations across the inlet throat (*see* Figure 4-1). The first data point of each curve does not coincide because the base elevation of each VGU mast is different. Station 3 (Pye Sand) is at the lowest elevation, thus the first to record, and shows an initial peak of 0.32m s⁻¹ as the flood tide begins to surge over Pye Sand. This is followed by a reduction in velocity to an average of 0.14m s⁻¹ for the remainder of the flood. Flow at Station 1 (Dugmore Creek) tends to mirror the flow at Station 3 but is approximately double the velocity throughout the flood tide. Station 5 (Inner Swatch) begins recording 2 hours after Station 3 and slowly increases in magnitude until about 1hr 40mins before high water when it peaks rapidly to 0.9m s⁻¹. The peak appears to coincide with significant velocity reductions at the other two stations. On the ebb, Station 5 peaks to 0.7m s⁻¹ at 1 hour after high water then reduces to less than 0.1m s⁻¹ then experiences a minor of peak of 0.3m s⁻¹, before the station dries out 3-hours after high water. The rapid reduction in velocity at Station 5 is matched by a velocity peak of 0.8m s-1 at Station 3. Station 1 again mirrors Station 3 but much reduced in magnitude. On neaps (Figure 4-15) the characteristics described above for springs are similar but much reduced in magnitude. The major difference between springs and neaps, however, is the marked reduction of the flood peak at Station 5. Although it is still evident, it has reduced by more than the corresponding decrease of the other

Stations. Although there remains a flood peak at Station 5 it is not matched by an apparent velocity reduction at the other stations although Station 3 and 5 velocity continues to reduce towards high water. On the ebb, flow at Station 3 dominates.
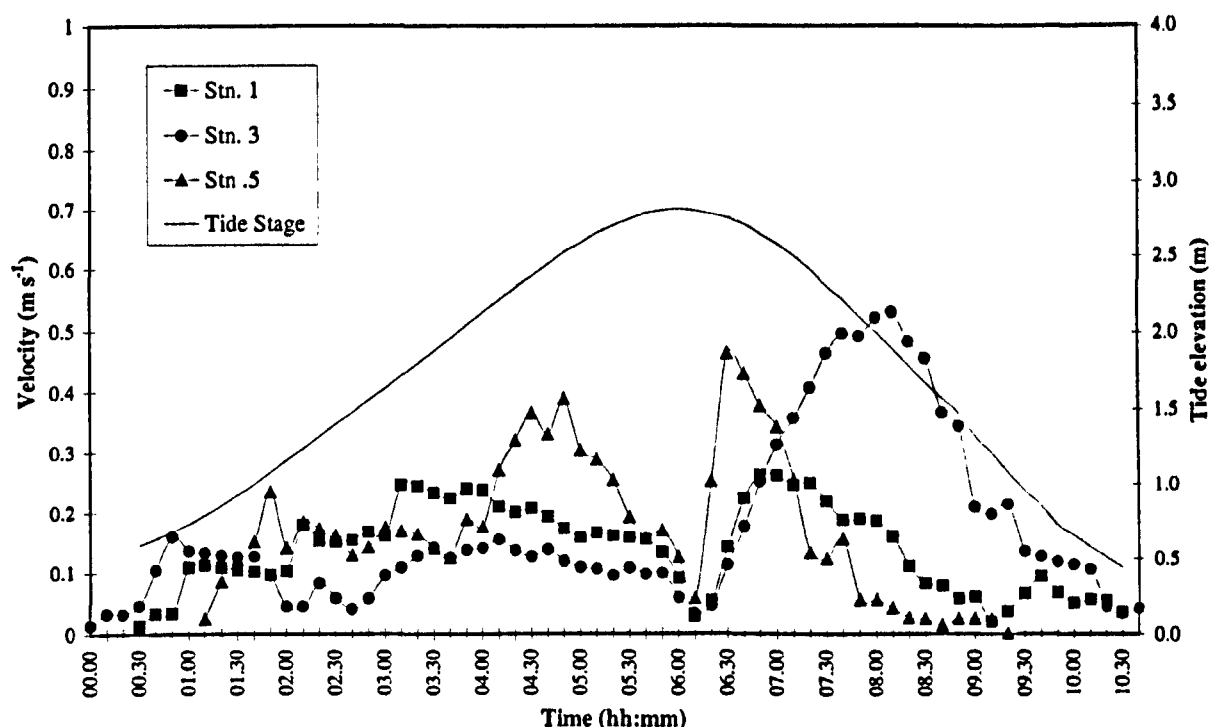
Figure 4-15 – Neap tide depth average velocity for VGU stations 1, 3 and 5 (same scale as Figure 4-14).

In both of the above Figures (Figure 4-14 and Figure 4-15), there is no zero velocity recorded at high water: this is because at slack water normally associated with high water, the current meters continue to record the effects of any waves present. The simple oscillatory motion of an impeller current meter in surface waves is enough to register data.

4.4.2.2 Combined anchor station and VGU results

The above data analysis was presented to illustrate the variation in current velocity at various points in the inlet. In the following discussion, however, the data obtained from the combined VGU/SPM survey in June 1995 (Deployments 4 and 5) is presented exclusively and without inclusion of data from Station 5. Although it is clear that data from Station 5 show a prominent flood peak the fact was not discovered until after Deployment 3, and consequently the survey design did not include Station 5. VGU Station 5 data, collected prior to Deployments 4 and 5, were not fully analysed before the survey and the significance of marginal flood channel velocities not appreciated. In

designing Deployments 4 and 5, no allowance was made to gather velocity and suspended sediment data for the marginal flood channel around Stone Point. The following plots cannot, therefore, accurately represent the conditions being experienced at Station 5. It is, however, accepted that Station 5 velocity data can be combined with Stations 1 to 4 to produce a more comprehensive picture, but the absence of suspended sediment data for Station 5 does not allow a complete picture to be presented when calculations of sediment flux are made (*see later in* Section 6). In the following presentations of cross-sectional velocity and SPM distribution discussion Station 5 is excluded so that both velocity and SPM match.

The following plots of vertical velocity distribution over the cross-sectional profile of the inlet throat, and velocity-time-distribution plots (as well as for all suspended sediment plots (Section 5.5.2)), were generated from data that were first averaged using the method of Kjerfve (1975). A combination of anchor station and VGU velocity data, measured for a spring and a neap tide, were used to calculate non-dimensionlised time-averaged vertical velocity profiles across the inlet throat by the method utilised by Kjerfve (1975). The method is recommended for estuaries with a large ratio of tidal range to mean water depth, ϵ. Most coastal plain and bar-built estuaries have an ϵ-ration of 0.3 and greater. Hamford Water is calculated as 0.4 (*see* Table 2-1). Averaged data were then used in a computer mapping and contouring program (Golden Software's *Surfer* for Windows) and a combination of kriging and spline smoothing were used to generate the plots.

Figure 4-16 and Figure 4-17 illustrate the vertical velocity distribution over the cross-sectional profile of the inlet throat for 5, 3, 1.5 and 0.5 hours before and after high water neaps, respectively. Figure 4-18 illustrates the velocity-depth-time distribution for Stations 1, 2, 3 and 4 for the same tidal cycle.
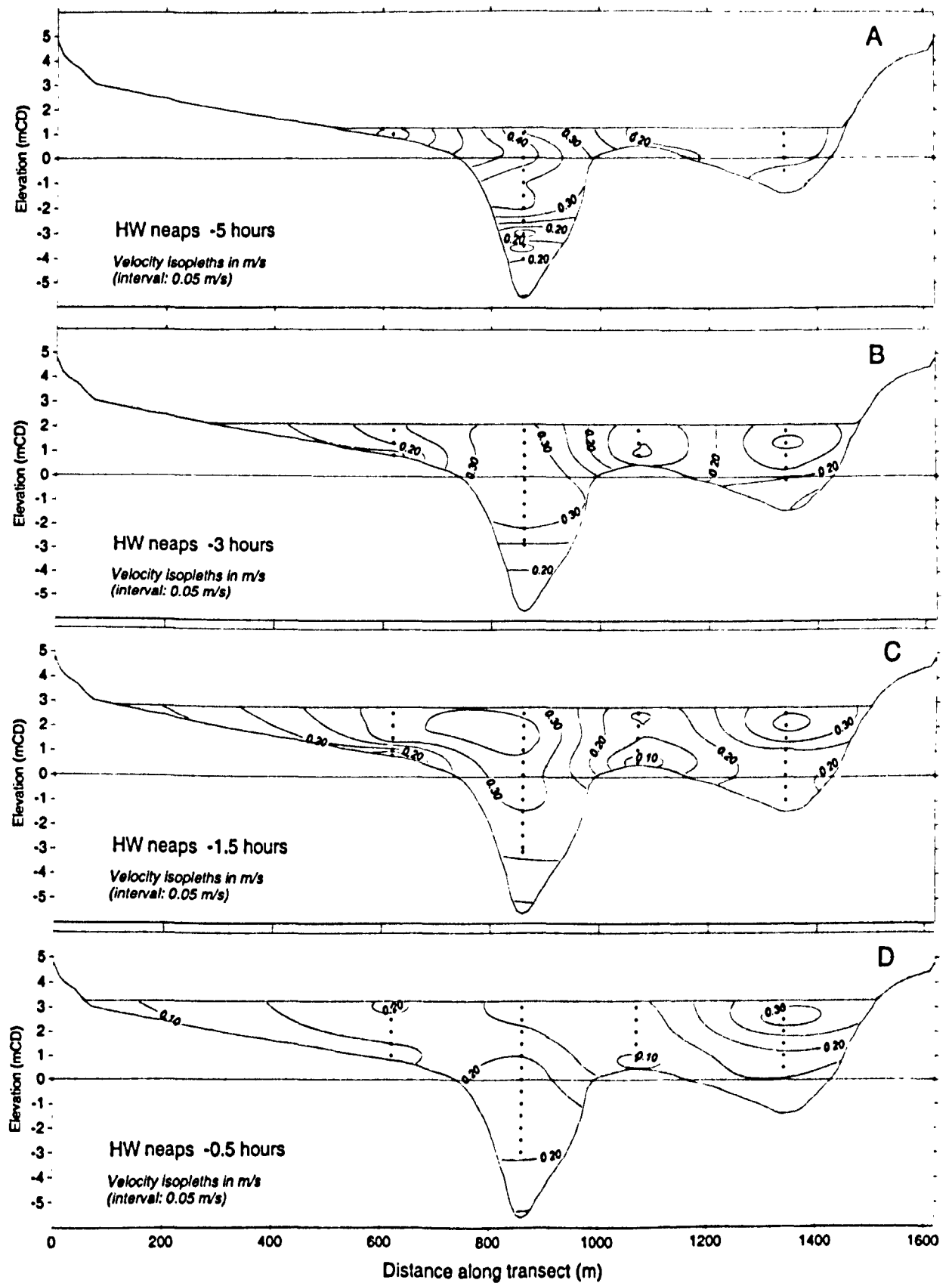
Figure 4-16 – Inlet cross-sectional velocity isopleths – Neap flood tide.
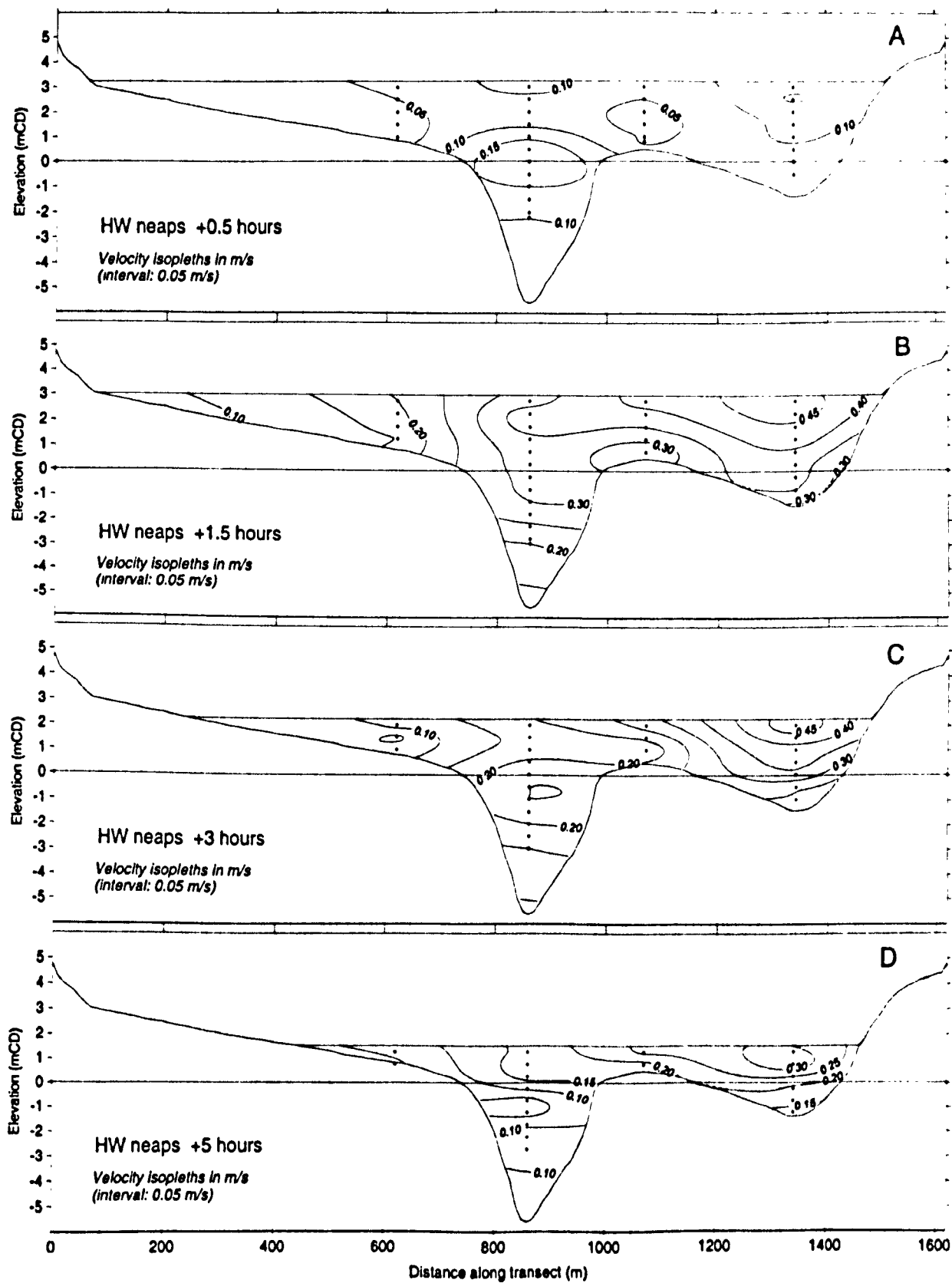
Figure 4-17 – Inlet cross-sectional velocity isopleths – Neap ebb tide.

Figure 4-18 – Neap tide velocity-depth-time distribution – Stations 1 to 4.

On the flood (Figure 4-16), flows of up to 0.4 m s^{-1} are initially confined to the left-hand side of the main channel. It would be expected that flow would be evenly distributed within the main channel rather than to any one side in the case of a relatively linear channel such as Pye Channel. A possible explanation for this anomaly is the effect of small waves (H_s = 10-15cm) on the lower current meters of the VGU at Station 1. The increase in velocity also shows up in Figure 4-18 for Station 1 at about 13:00 (5hrs before HW). As Pye Sand and the Swatch deepen, maximum flow reduces throughout to about 0.3 m s^{-1} at 3 hours before HW, thereafter velocities are relatively steady over the cross-section decreasing towards HW. On the ebb (Figure 4-17), the highest velocities of 0.45 m s^{-1} are experienced mainly in the Swatch from about 1

hour to 4 hours after HW. Flow throughout the remaining cross-section rarely increases above 0.3 m s^{-1}.

In Figure 4-18 it is interesting to note that the time of slack water, or at least of minimum velocity, does not coincide with high water at all stations. The time of minimum velocity is approximately 10 minutes before high water at stations 1 and 2, and about 15 minutes after high water at stations 3 and 4. An immediate plausible explanation is a misalignment of the main survey transect (*see* Figure 4-1) with the opposing banks of the channel i.e., a systematic error in survey design. A more scientific elucidation assumes a satisfactory survey design and attributes the anomaly to the nature of tidal flow through the inlet as recorded. The data would suggest that the tide continues to flood around Stone Point and into Walton Channel up to 15 minutes after high water. Correspondingly, the ebb commences in Pye Channel before high water resulting in a 20-25 minute difference between high water on the north side of the channel with that on the south side.

Turning to spring tides, Figure 4-19 and Figure 4-20 illustrate the vertical velocity distribution over the cross-sectional profile of the inlet throat for 5, 3, 1.5 and 0.5 hours before and after high water springs, respectively. Figure 4-22 illustrates the velocity-depth-time distribution for Stations 1, 2, 3 and 4 for the same tidal cycle.
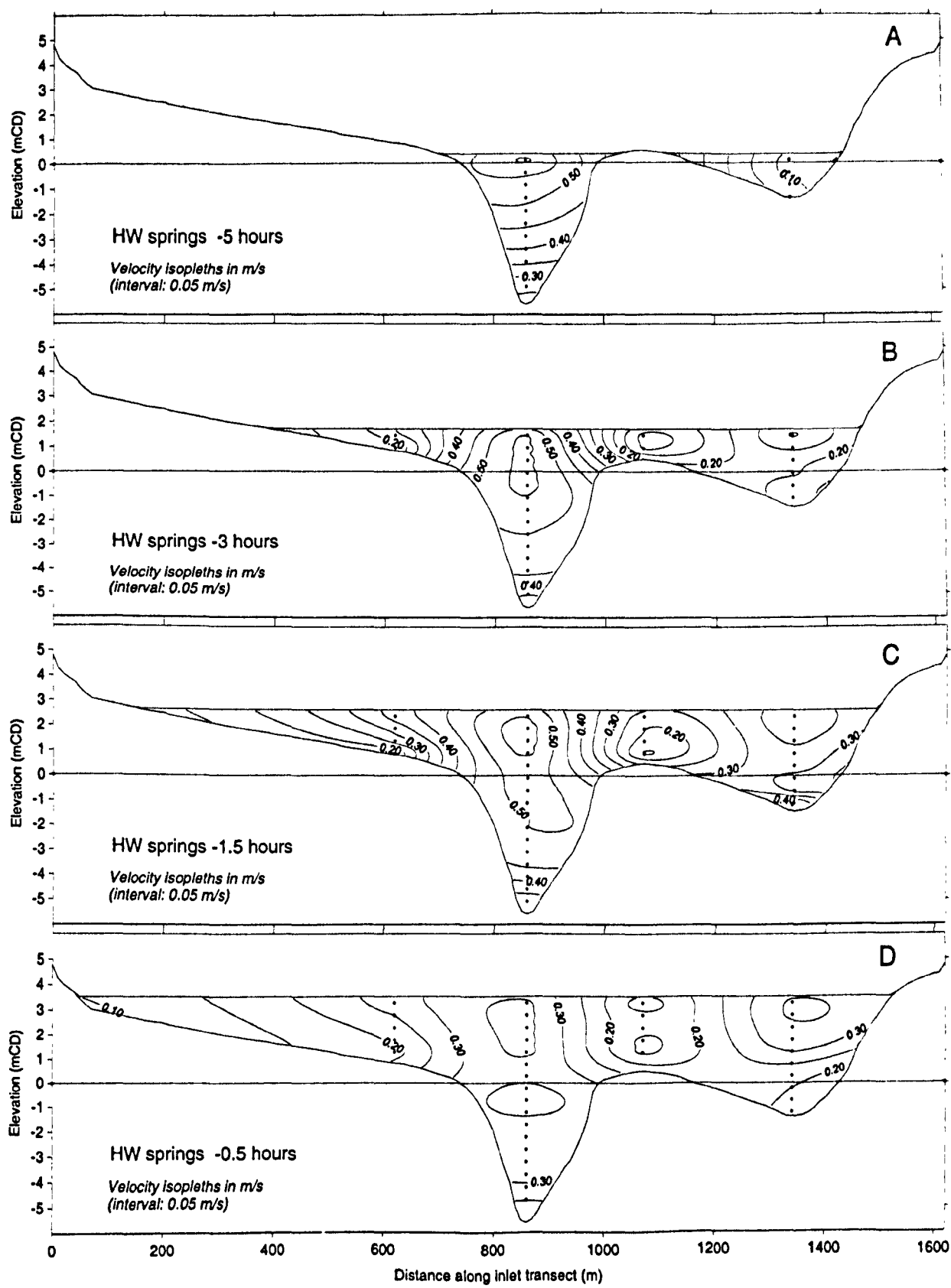
Figure 4-19 – Inlet cross-sectional velocity isopleths – Spring flood tide.
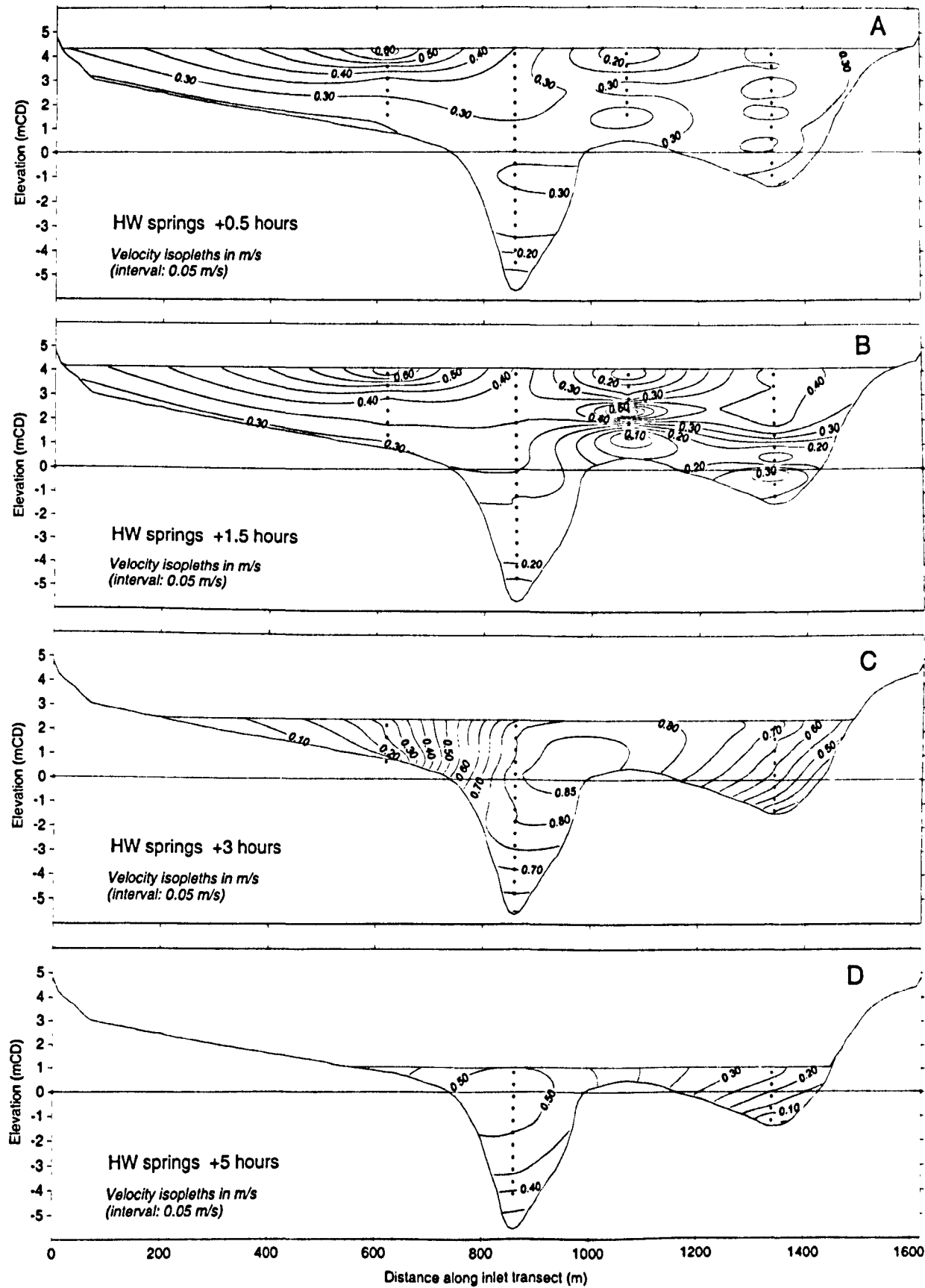
Figure 4-20 – Inlet cross-sectional velocity isopleths – Spring ebb tide.
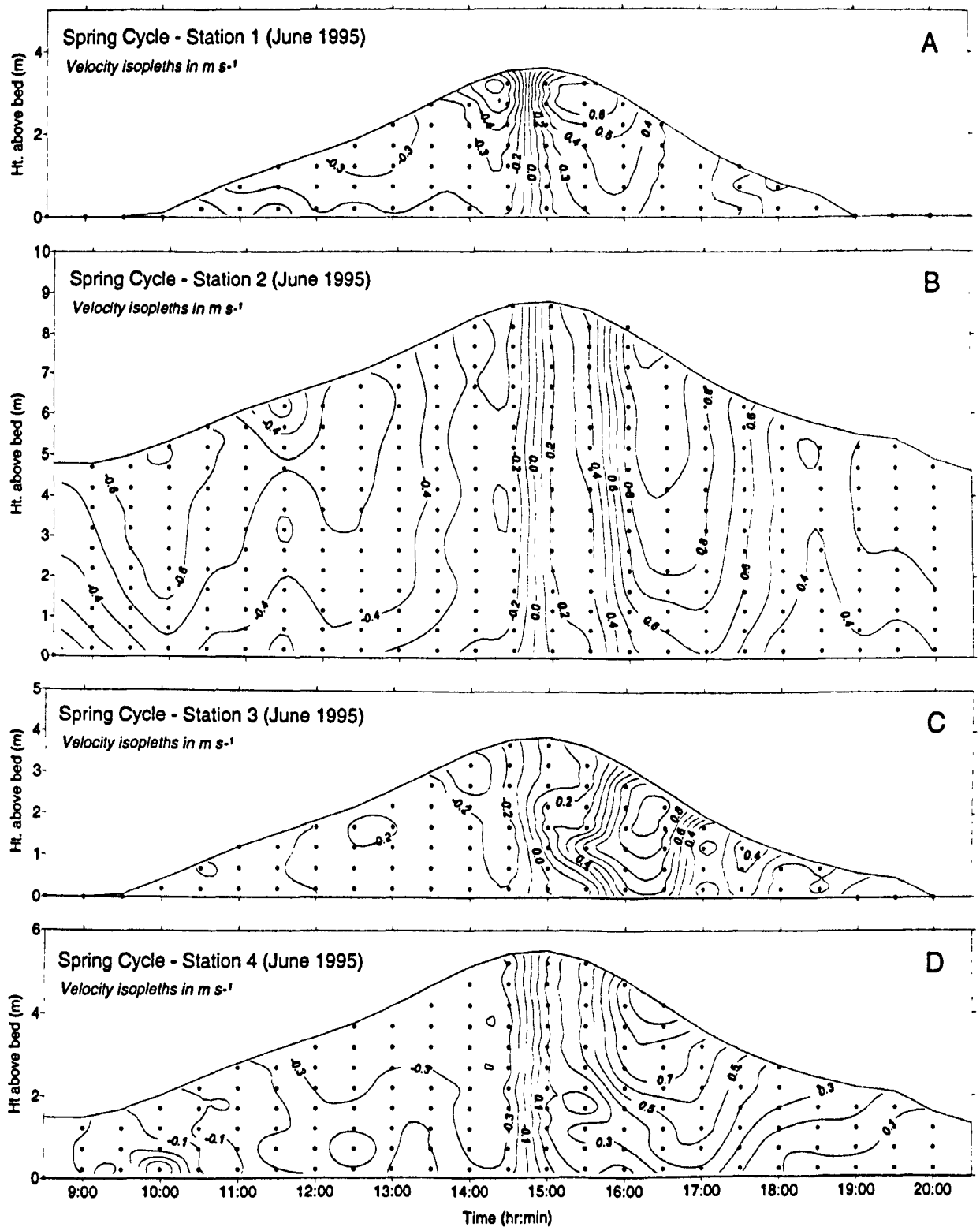
Figure 4-21 – Spring tide velocity-depth-time distribution – Stations 1 to 4.

The immediate difference between springs and neaps is the drying of Pye Sand at low water springs resulting in two apparently separate channels across the inlet. The data suggest that flow is negligible in the Swatch 5 hours before high water, whereas flow has reached 0.5 m s^{-1} in the main channel. When viewed in plan form at Lowest Astronomical Tide (LAT) the Swatch resembles a bay protected by the ebb delta of Pye

Sand (Figure 4-22) which has the effect of preventing any of the flood from entering the Swatch.
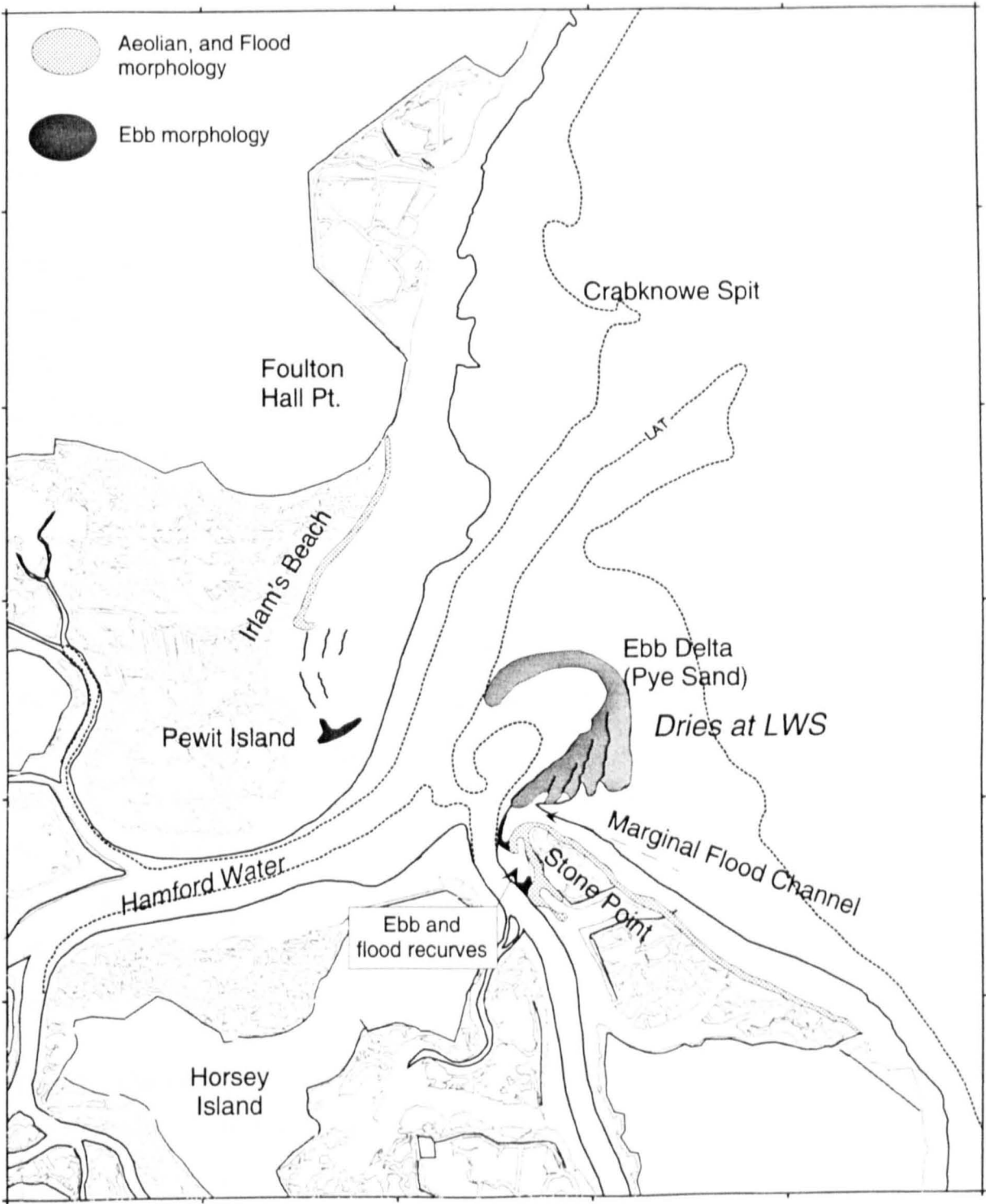
Figure 4-22 – Pye Sand at lowest astronomical tide (LAT).

In fact it was evident from observation that the flow on the last of the ebb reverses in the region of Station 4 as Pye Sand uncovers and the "bay" created by the exposed ebb delta drains into Walton Channel. The duration of reversed flow depends on the length of time Pye Sand remains uncovered. Unlike the neap profiles, there is no apparent increase in flow at Station 1 at the start of the flood suggesting that wave action may be

responsible for the increased velocities during neaps. Maximum flow remains confined to Pye Channel up to 1.5hrs before high water with the point of maximum velocity depressed by about 1 m below the surface. Mehta (1978) stresses that the point of maximum velocity, in open channel flow, is not necessarily at the surface. It is depressed to a level just below the surface due to the presence of secondary flows that move from the banks of a channel to the centre and turn downwards. This characteristic of open channel flow has significant consequences if using instantaneous velocity profiles to directly measure the bed shear-induced boundary layer at the bottom of the channel. On the ebb, 1.5 hours after HW springs, the level of maximum velocity results in a distinctive "jet" at 2 m below the surface. Initially thought to be an error in contouring of the data, the jet is evident on most occasions during springs at about 1m below the surface. The point of maximum velocity also appears to move from over Pye Sand to a position to the left of Pye Channel by the end of the ebb.

4.4.3   DISCUSSION

A distinctive feature of the tidal stage curve of Hamford Water is the short duration ($\approx$10 minutes) of the high water stand as opposed to slack low water, which is approximately 20 to 30 minutes. In general, from slack high water there is a rapid increase in ebb velocity, reaching a maximum about 1 hour after slack water. Thereafter, ebb velocities begin to reduce towards slack low water, which is of a much longer duration than that of slack high water. There is then a gradual flood, peak velocity not being reached until about 5 hours after slack low water (about 1.5 hours before slack high water). Flood velocity then quickly decreases towards high water.

Velocity observations by other workers, for various locations around Hamford Water also illustrate duration asymmetry. Towards the northern end of Hamford Water, at the mouth of Dugmore Creek, Leeks (1975) observed a flood lasting for 6 hours 40 minutes with a corresponding ebb duration of 5 hours 20 minutes. To the north of Horsey Island, HR Wallingford (1990) showed that the flood tide had a longer duration, 4 hours, compared to the ebb, which lasted for less than 2 hours (note these measurements were not taken in a subtidal channel, which means that water completely drained from the sampling site). Both Leeks (1975) and HR Wallingford (1990) graphs of tidal stage are reproduced in the Preliminary Report at Annex A.

A significant feature of the flood tide is the 'spike' of flood current around Stone Point. Whereas tidal inlets in general experience marginal flood currents, the nature of the marginal flood current in Hamford Water is different. The reason for marginal flood currents in the inlets described by Hayes (1980) is that the ebb current is still flowing out of the main ebb channel after the flood current has started. This has the effect of forcing the flood stream up the margins of the inlet and, in doing so, contributes to the formation of marginal flood channels. A distinctive feature of such inlets is the markedly short low water stand (~5-10 minutes). Hamford Water, however, has a long (~30 minutes) low water stand. In addition, the marginal flood channel of Hamford Water is at an elevation of approximately 1.5m above chart datum and therefore the marginal flood current in Hamford Water is much later in the cycle (2-hours). The marginal flood current is, therefore, considered to be related more to the overall flood tidal stream that affects the combined systems of Hamford Water and the Stour and Orwell.

The actual tidal flow, as both recorded and observed in this research, is complex: from low water, the flood tide is initially confined to Pye Channel and flows west up Hamford Water and south into Walton Channel. As Pye Sand covers, approximately 1.5 hours after low water, the flow begins to converge bodily on the north-east point of Horsey Island. Flow around the existing wave break (consisting of sunken Thames lighters) at this convergence point is considerably turbulent. Within Hamford Water the current regime is highly complex being affected by the flow on and off the inter-tidal areas, flow around islands, and the flow in the channels and labyrinth of tidal gullies. The flood tide flows clockwise around Pewit and New Island and into Dugmore Creek. The existence of Horsey Island causes the flood tide to converge in a zone to the south of the island, in the Wade, where the tidal current is effectively zero (Figure 4-23). The same zone then becomes a zone of divergence on the ebb tide. Other tidal convergence/divergence zones were observed between Horsey Island and Hedge End Island, and to the south-west of Skipper's Island. The position of these convergence/divergence zones does not appear to remain stationary within a tidal cycle nor a lunar cycle. Although no current measurements were recorded, it was observed that the Wade zone traversed east to west and west to east on different tides. It is hypothesised that such zones of tidal convergence/divergence may have a significant

effect on sedimentation rates: the zone of slack water may experience increased sedimentation rates, much like a turbidity maximum. They may even cause reduced sedimentation rates due to the lack of current flow and consequently a negligible shear stress. It is noted (Joe Backhouse *pers comm* – owner of Horsey Island) that the road from Horsey Island to the mainland across the Wade, requires routine clearing due to siltation. It is also postulated that the traverse movement of such zones is determined by surface wind conditions: for example, a westerly wind will cause the Wade zone to move to the east and an easterly wind will cause the zone to move to the west. The reasoning behind this is that wind blowing over shallow water can both assist or retard tidal currents depending on whether it is in opposition or supposition. In Hamford Water such movement would then result in differential volumes of water moving either side of the main island, Horsey Island. Consequently, different levels of sedimentation would be experienced in the respective channels of Hamford Water and Walton Channel and the adjacent saltmarsh. Although such differences will have no effect on the total sediment budget of the whole site, different rates of sedimentation within the embayment may be experienced and those variations may be determined by seasonal effects. It has to be stressed that the above hypothesis has not been supported with any real data and is based on extensive personal observation throughout the course of this research.
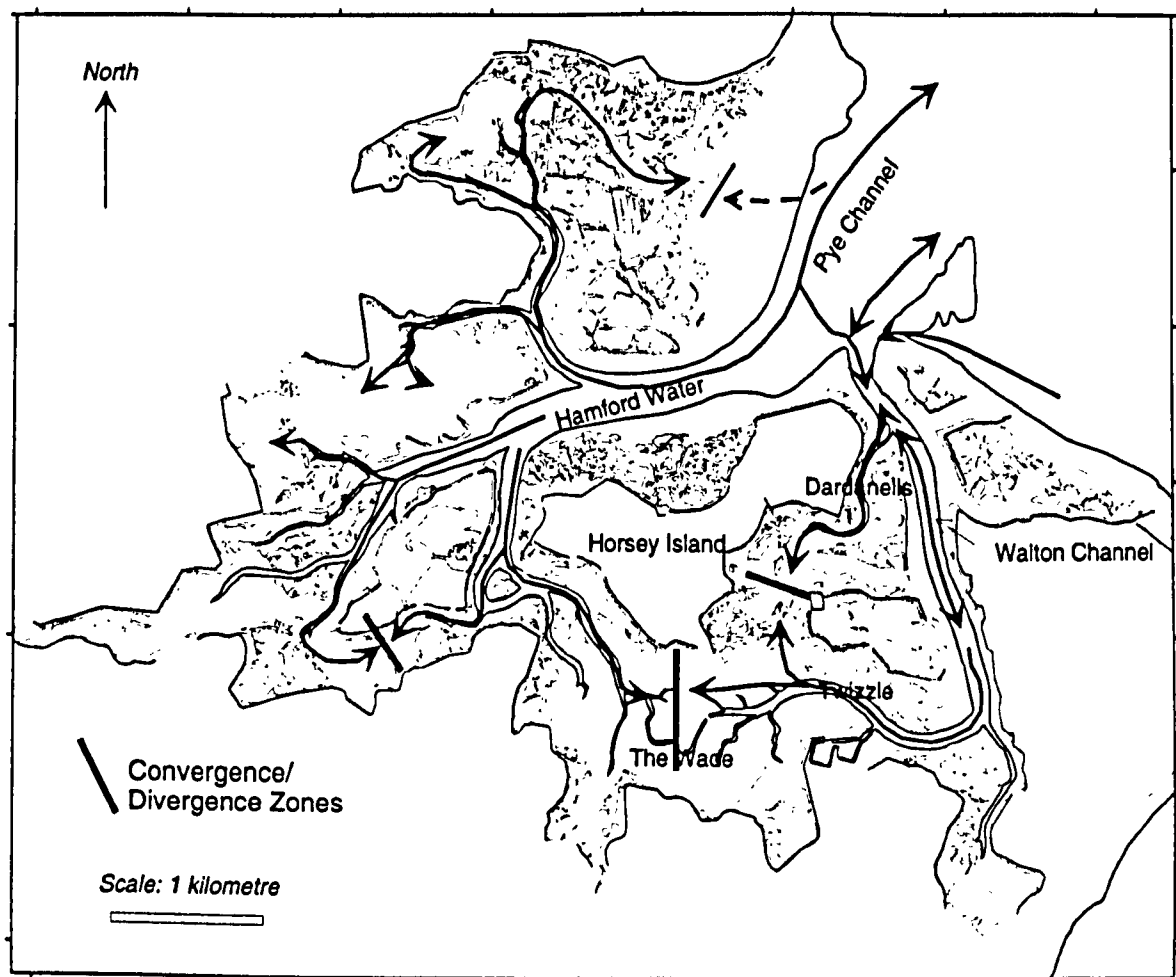
Figure 4-23 – Tidal flow in Hamford Water and the location of Convergence/Divergence Zones.

4.5 Salinity and Temperature

4.5.1 METHODS

Salinity and temperature were recorded simultaneously with current velocity during the initial reconnaissance survey in August 1993 (*see* Section 4.4.1) and the results initially reported in the preliminary report (Annex A). The results are repeated here for re-analysis and discussion.

4.5.2 RESULTS

Figure 4-24 illustrates the variation of salinity (in Practical Salinity Units (PSU)) during a spring tidal cycle, recorded at Stone Point in August 1993. The graph shows a slight dilution of salinity towards high water (≈ 0.7), and a separation of surface and bottom salinity values (≈ 0.1) from well mixed on the flood, to higher bottom salinity on the ebb. The results would suggest that in the summer the salinity of the embayment remains marginally higher than the North Sea due to, presumably, evaporation. It is interesting to note that Hamford Water has a number of "Red Hills" which are sites of

ancient salt pans of pre-Roman and Roman times. However, solar evaporation only accounted for about 20% of the salt-making process, the remainder was achieved by firing (Fawn *et al.* 1990).
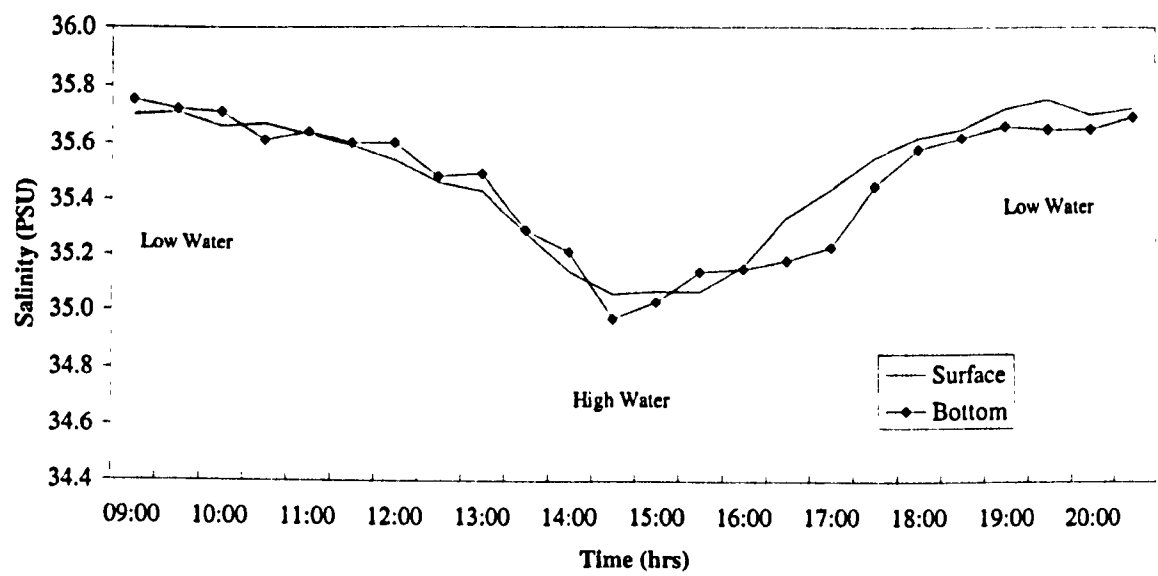
Figure 4-24 – Salinity variation over a spring tidal cycle.

Regarding temperature, in Figure 4-25 there is a consistent rise in temperature ($\approx 1.5°C$) throughout the tidal cycle, seemingly unaffected by either the flooding or ebbing tide. There is also an increasing separation of surface temperature from bottom temperature ($\approx 0.2°C$); the surface temperature being greater.
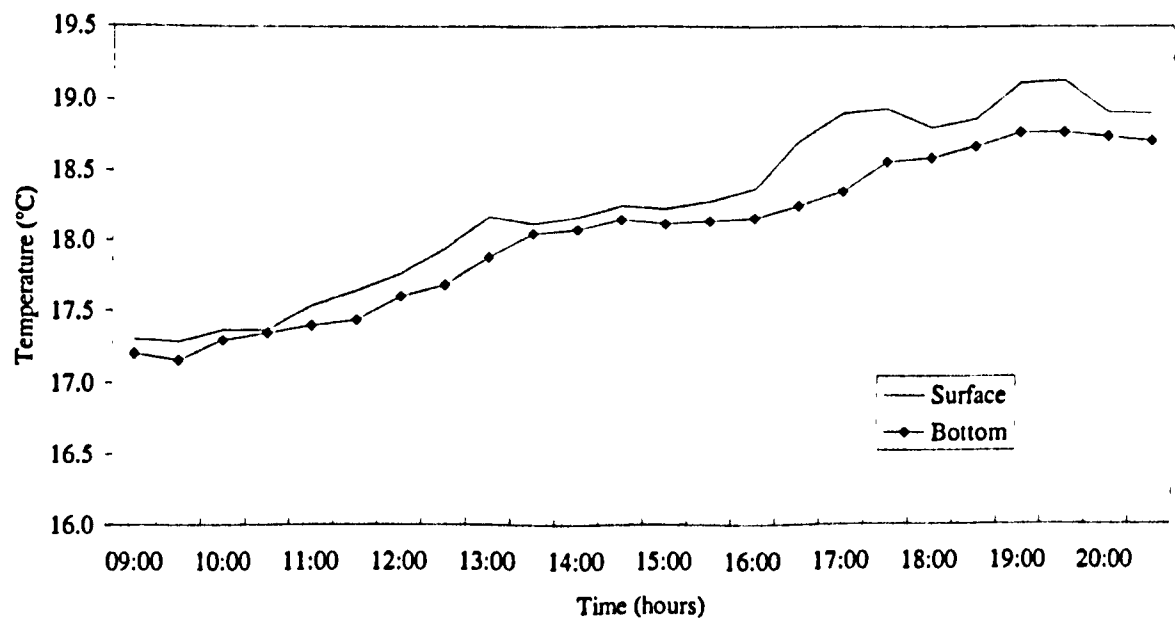
Figure 4-25 – Temperature variation over a spring tidal cycle.

4.5.3   DISCUSSION

Mean temperature and salinity (T&S) recorded for Hamford Water (T=18.15°C and S=35.47) reflect the mean temperature and salinity of the southern North Sea in summer (Lee and Ramster, 1981; Howarth *et al*, 1994). Winter means for the southern North Sea (not recorded in this research) are 6°C and 34.0 respectively (Lee and Ramster, 1981). Given the absence of any freshwater input and therefore no significant mixing, any further data collection of salinity and temperature was considered unnecessary.

The respective effects of temperature and salinity on the inlet circulation are considered negligible. An embayment such as Hamford Water, where there is a negligible freshwater input, is considered to be well mixed in terms of freshwater/saltwater mixing when compared to estuaries with large freshwater input such as the Humber and Thames (Pritchard, 1955). There is negligible stratification and density-induced currents through the inlet entrance and any surface indications of density fronts, such as foam and flotsam, were not apparent. Within the embayment, however, the presence of a slow flood stage and hence a gradual inundation of extensive mud flats, such as The Wade, combined with hot summer days, may alter background temperature and salinity characteristics. Heavy rainfall during tidal flat inundation may dilute salinity and alter the temperature of the flood tide as it moves across warm mudflats. Similarly, evaporation may cause a rise in salinity to such an extent that it may affect the physico-chemical properties of the suspended sediment. An increase in salinity enhances flocculation and hence the settling velocity and thus the rate of deposition. Similarly, increases in temperature affect the viscosity and decrease the double-layer repulsive energy resulting in an increase in aggregation of sediment flocs.

The total salt concentration affects the erosion properties of a mud layer. At higher salt concentrations, the cohesiveness of the soil increases, resulting in a decrease of the erodibility. This follows directly from the diffusive double layer theory. Another influence on the erodibility of a mud layer stems from differences in salt concentration of the pore water and that of the eroding fluid. When the pore water is less saline than the eroding fluid this may cause swelling of a cohesive bed due to osmotic pressure and can thus effect the strength of the bed.

The strength of the bed decreases, and thus the erosion rate increases, with increasing temperature. This is due to a change in the viscosity of the water and the soil, a thickening of the diffuse double layer and an increase in the osmotic potential. Furthermore, the effect of temperature on the biological and chemical processes is likely to occur affecting the erosive properties of the sediment layer (Kandiah, 1974; EC MAST-I, 1993). The subject of salinity and temperature and their effects on the erosion and deposition of sediments is complex and not studied in this research. The reader is referred to Anderson (1983), Amos *et al.* (1988) and Amos (1995) for a more comprehensive review and analysis of the subject. Also, Jago and Mahamod (1999) note that the relationship between threshold velocity and settling velocity is mediated by temperature (by changing the kinematic viscosity of the water).

4.5.4 SUMMARY

Hamford Water may be classified as well mixed after Pritchard (1955): there is a negligible supply of fresh water and a correspondingly negligible degree of mixing. CTD data collected as part of a reconnaissance survey produced T&S values comparable with the North Sea. However, the effect of high summer temperatures was noted as creating a difference between surface and bottom temperature and a diurnal change in salinity levels. The effect of small-scale variations in T&S during the flooding of tidal mudflats is highlighted as an area for future work.

4.6 Boundary Layer Flow

4.6.1 INTRODUCTION

Tidal inlet processes, like estuarine processes, are an interaction of ocean and bay systems. The main forces involved in shaping the morphology of the inlet are a combination of tides and waves. These combine to produce current patterns that determine sediment transport patterns and so define the geometry of the inlet which in turn may influence the flow of currents. There is, therefore, a feedback mechanism between inlet geometry and inlet hydraulics. The most important control on sediment transport is the nature of the flow in the boundary layer.

This section is concerned with the actual boundary layer flow and the nature of shear stress at the bed as recorded at individual stations across the inlet throat. The theoretical

application of boundary layer flow to sediment transport has already been discussed in Section 3.2.3 above, and the method used to measure velocity profiles in the boundary layer has been described in Section 4.4.1.2 and Appendix D. This chapter is divided up and discussed as follows:

- Representative logarithmic velocity profiles are presented, described and analysed.

- Depth average velocity is compared with velocity at 100cm above the bed.

- Shear Velocity, Roughness Length and Drag Coefficient data are presented and discussed.

4.6.2   RESULTS – VELOCITY PROFILES

Presentation and analysis of results from boundary layer measurement centres on those data recorded at Dugmore Creek, Pye Sand and Inner Swatch, Stations 1, 3 and 5, respectively (*see* Figure 4-26). Emphasis is placed on velocity profiles that coincide with the suspended sediment flux surveys of Deployments 4 and 5 (*see* Section 4.1). Notwithstanding data matching problems mentioned previously (*see* Section 4.4.2.2, *p*.67), data from the Station 5 has been matched to coincide with the individual spring and neap flux surveys on the 16 and 20 June 1995. The matching of deployments is summarised in Table 4-4 and Table 4-5, below.
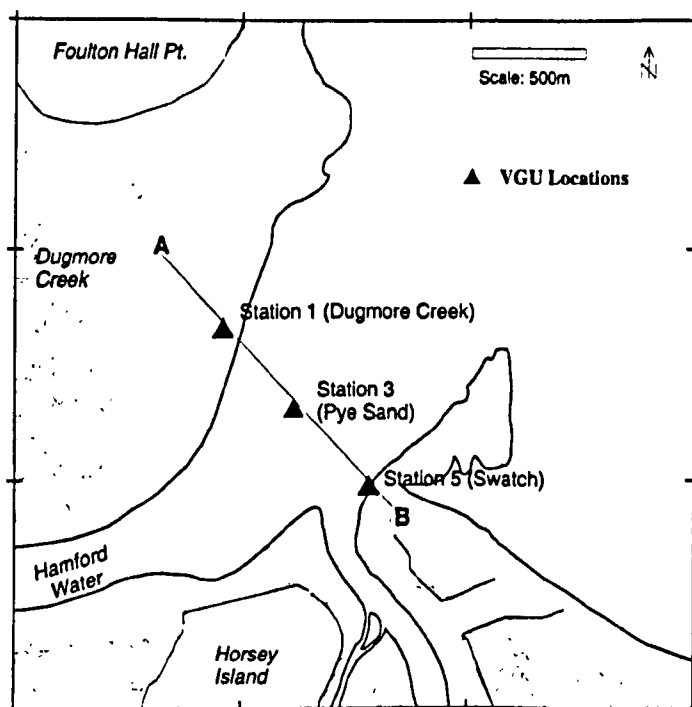
Figure 4-26 – Stations locations for profile analysis.

Table 4-4 – Summary of spring velocity profiles

| Station | Data File | Date/Time (BST) | Profile | | | Tide | |
			Flood	Ebb	Total	Age of Moon*	Mean Range
1 - Dugmore	DUG9502	16/1034 – 1824Jun95	27	21	48	18	3.7m
3 - Pye Sand	PYE9502	16/1004 – 1844Jun95	30	23	53	18	3.7m
5 - Swatch	SWT9422	07/1223 – 1803Dec94	20	15	35	4	3.6m

* Age of moon at springs taken to be 2 and 17 days (2 days after new and full moon respectively).

Table 4-5 – Summary of neap velocity profiles.

| Station | Data File | Date/Time (BST) | Profile | | | Tides | |
			Flood	Ebb	Total	Age of Moon*	Mean Range
1 - Dugmore	DUG9510	20/1314 – 2204 Jun95	31	23	54	22	2.7m
3 - Pye Sand	PYE9510	20/1244 – 2214 Jun95	33	25	58	22	2.7m
5 - Swatch	SWT9401	26/1328 – 2048 Nov94	28	17	45	23	2.5m

*Age of moon at neaps taken to be 9 and 24 days (7 days after springs).

The results are initially divided into three categories depending on a general description of their reliability. Reliability, in this sense, is based on the number of current meters submerged and assumed to be recording:

- **Complete** reliability – all 5 current meters submerged, i.e., greater than 1.5m depth of water.

- **Partial** reliability – submerged up to, and including u_{100} (1m above the bed, 4 current meters).

- **Unreliable** – below u_{100}, 3 or less current meters.

Both *complete* and *partial* reliability implies that the data can be used to calculate sediment transport rates using methods that utilise u_{100}. It should be noted, however, that reliability does not assume the data are reliable *per se*; only subsequent analysis of the r^2 values and further statistical analysis will indicate the suitability of the profiles for sediment transport calculations. Statistical analysis of logarithmic profiles is conducted in Section 4.6.6 below. All logarithmic profiles are presented in the following order for each station (Station-1, 2 and 3):

- Complete *spring flood* relative profiles,

- Complete *spring ebb* relative profiles,

- Selected *spring flood* profiles plotted to scale,

- Selected *spring ebb* profiles plotted to scale.

The above order is then repeated for a neap tide. The respective logarithmic profiles on each graph are produced by simply increasing the velocity value of each profile by 0.1m s^{-1}. The result is a visual separation of the profiles to better assess their changing relative form. (Heathershaw and Langhorne (1988) use a similar technique to present numerous velocity profiles.) Selected profiles for the flood and the ebb are produced to better assess real values of u.

In the following assessment, the shape of individual profiles is described as concave upwards, concave downwards or straight as illustrated in Figure 4-27, below. A full discussion on reasons for observed variations of the profiles is continued after the presentation of results, in Section 4.6.7.
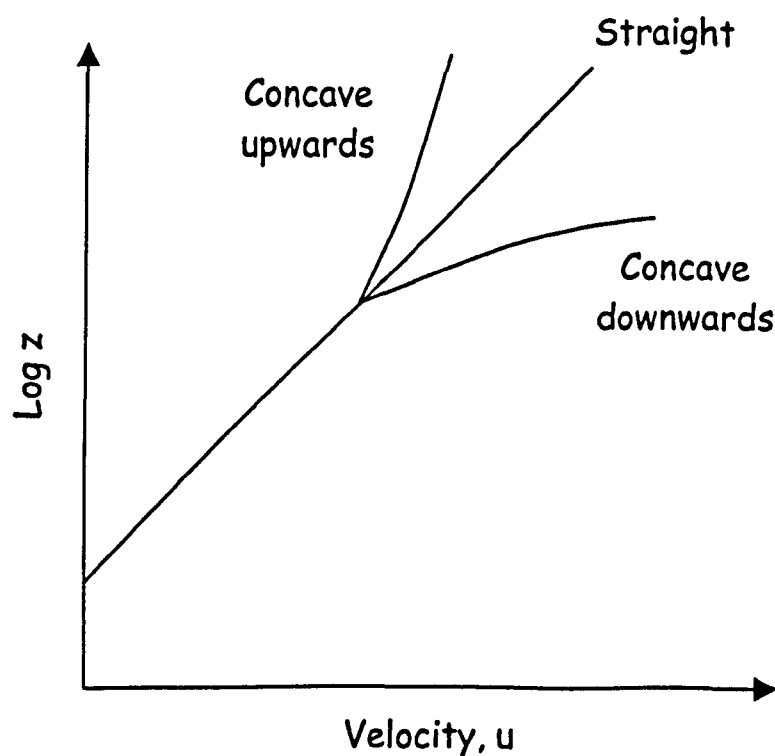
Figure 4-27 – Departures from theoretical logarithmic profile.

4.6.3   VELOCITY PROFILES AT STATION 1 (DUGMORE CREEK)

Appendix E summarises the reliability of velocity profiles recorded at Station 1 (Dugmore Creek) for the full VGU deployment of 13 tidal cycles between 15 and 22 June 1995. At Station 1, of 756 profiles recorded, 405 (54%) are flood profiles and 351 (46%) are ebb. Of all 756 profiles, 69% were determined as being either *complete* or *partially* reliable. When separated into flood and ebb profiles, 73% of the flood and 64% of the ebb profiles were determined as either *complete* or *partially* reliable. An analysis of r^2 values for the 13 tidal cycles between 15 and 22 June (springs to neaps) show that 80% of all profiles record r^2 of ≥ 0.8, however, only 66% of ebb profiles record ≥ 0.8 as opposed to 88% of flood profiles.

Figure 4-28 and Figure 4-29 show logarithmic profiles for a spring flood and ebb tide respectively at Station–1 (Dugmore Creek). The profiles are at 10-minute intervals and represent a 60-second averaging period. Figure 4-30 and Figure 4-31 show selected profiles for the same flood and ebb period at –4, –3, –2, –1 –0.5 hours before high water, and 0.5, 1, 2, 3, and 3.5 after high water (no 4–hour after HW reading was recorded).

There is clearly a marked difference between the general form of the flood and the ebb: flood profiles are more evenly spaced and uniform. The first three profiles of the flood (just after low water) are suspect: it is most likely that the middle current meter was fouled for a time. When plotted to scale, in Figure 4-30 and Figure 4-31, it can be seen that the flood profiles are grouped together for most of the flood duration but there is a marked deceleration of the flow from 2–hours before HW followed by an acceleration of the flow from 1–hour before HW. This contrasts with the ebb where the flow shows a marked acceleration from 30 minutes after high water to 1–hour after, thereafter the flow decelerates and reduces rapidly to 3.5 hours after high water. There is, however, a brief period of acceleration around 2 hours after high water.
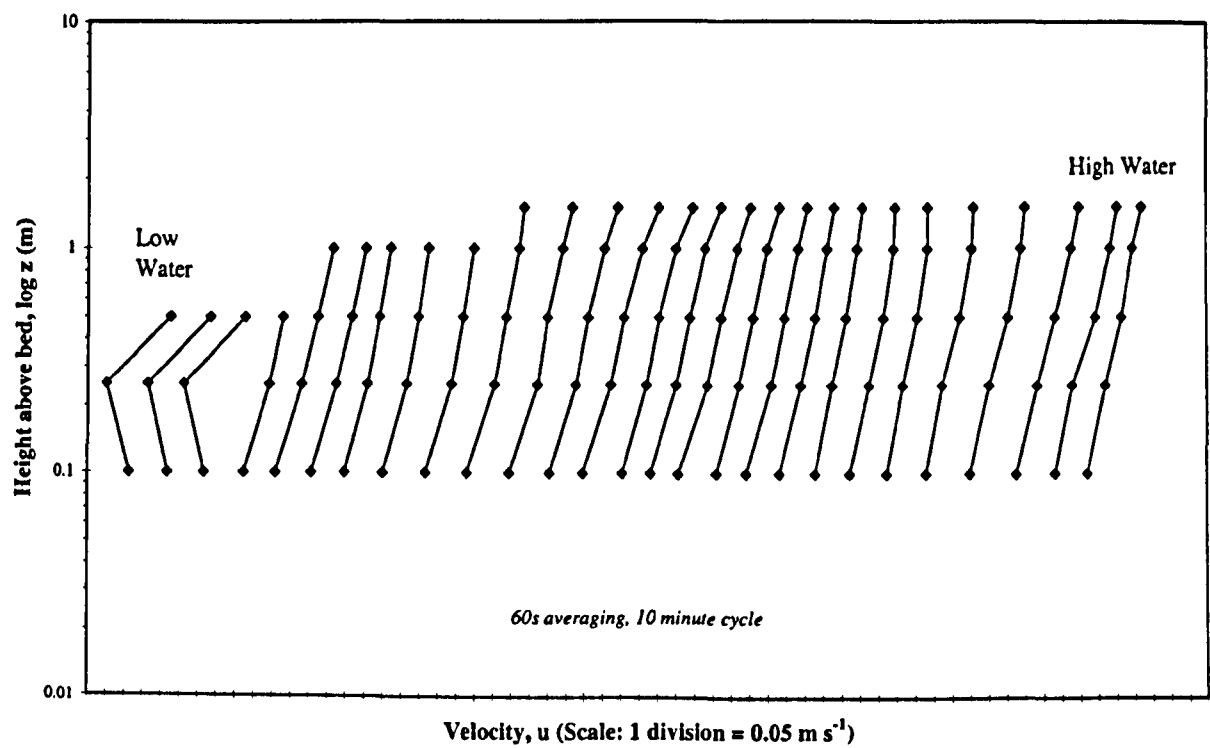
Figure 4-28 – Spring flood log velocity profiles at Station 1 (Dugmore Creek).
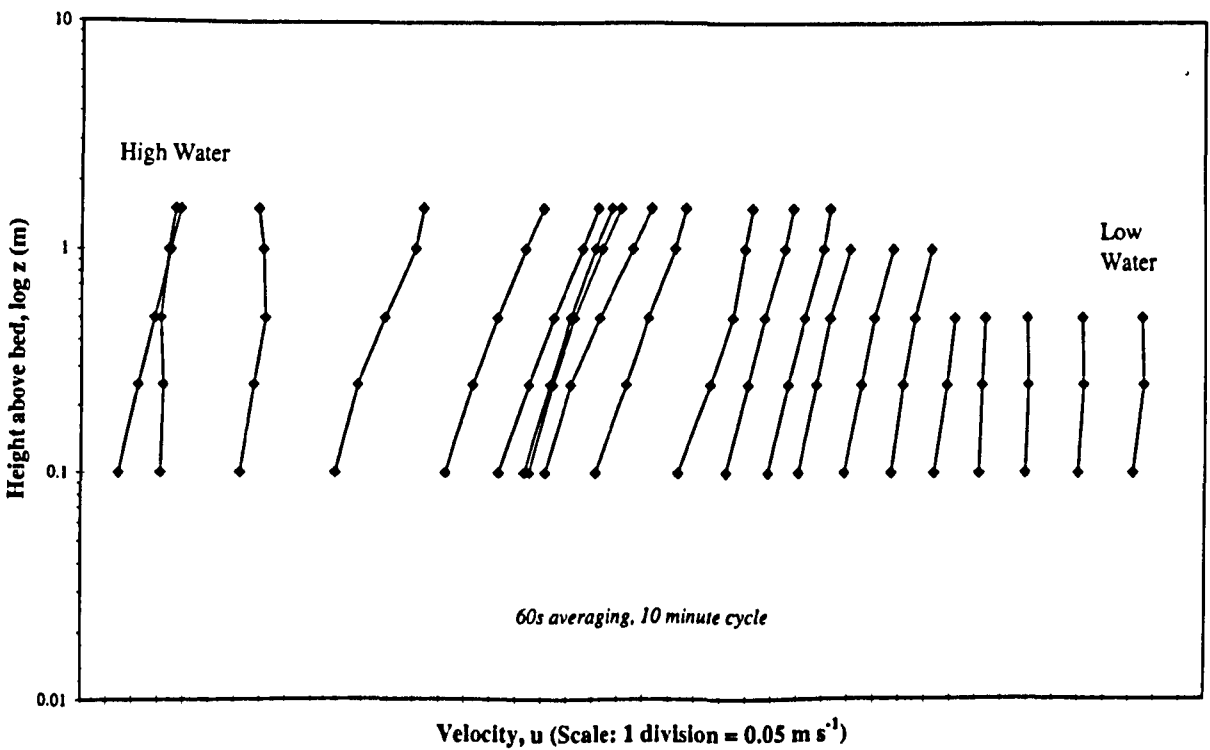
Figure 4-29 – Spring ebb log velocity profiles at Station 1 (Dugmore Creek).
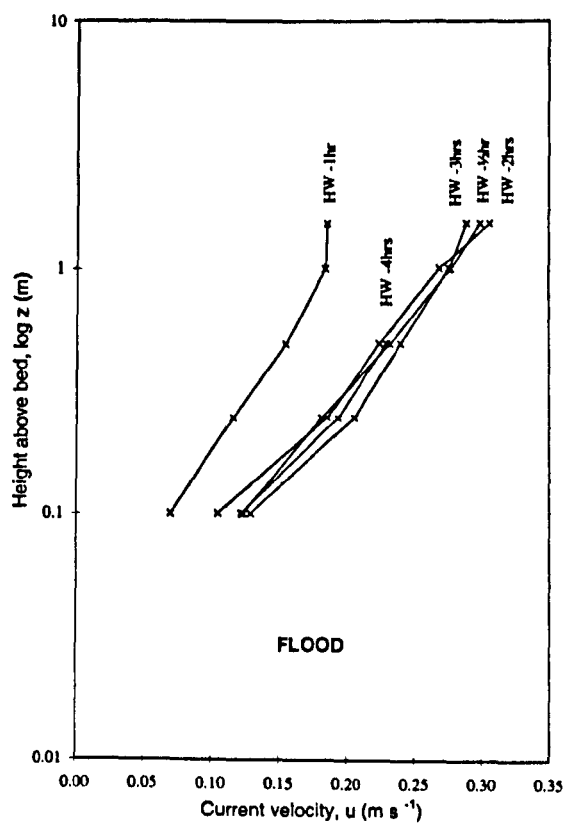
Figure 4-30 – Selected spring flood log velocity profiles at Station 1 (Dugmore Creek).
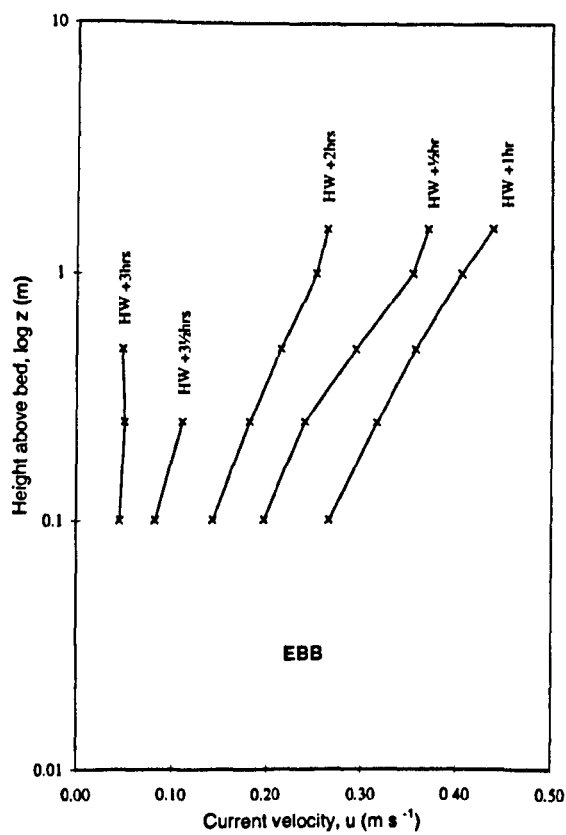
Figure 4-31 – Selected spring ebb log velocity profiles at Station 1 (Dugmore Creek).

Figure 4-32 and Figure 4-33 show logarithmic profiles for a neap flood and ebb tide respectively at Station-1 (Dugmore Creek). The profiles are at 10–minute intervals and represent a 60–second averaging period. Figure 4-34 and Figure 4-35 show selected profiles for the same flood and ebb period at –4, –3, –2, –1 –0.5 hours before high water, and 0.5, 1, 2, 3, and 4 hours after high water.

The contrast between flood and ebb is not as marked as the spring profiles although the flood profiles are still more evenly spaced and uniform. From Table E-, 94% of the flood profiles have an r^2 value of ≥ 0.8 as opposed to 79% of the ebb. For reasons discussed above regarding reliability of profiles, the first 7 flood profiles and last 5 ebb profiles are considered unreliable. For the remainder of the profiles, as with the spring profiles, they constitute a mixture of concave upwards and concave downward forms. On a number of profiles on the flood there are marked departures from a straight line at lower current meters. When plotted to scale, in Figure 4-34 and Figure 4-35, it can be seen that the flood profiles display a sinusoidal form: concave upwards in the lower half of the profile and concave downwards in the upper half. This contrasts with the ebb where the profiles show a change from concave upwards 30 minutes after high water to concave downwards for the remainder of the ebb. The profile for +3 hours is considered unreliable: most probably caused by a fouled rotor.
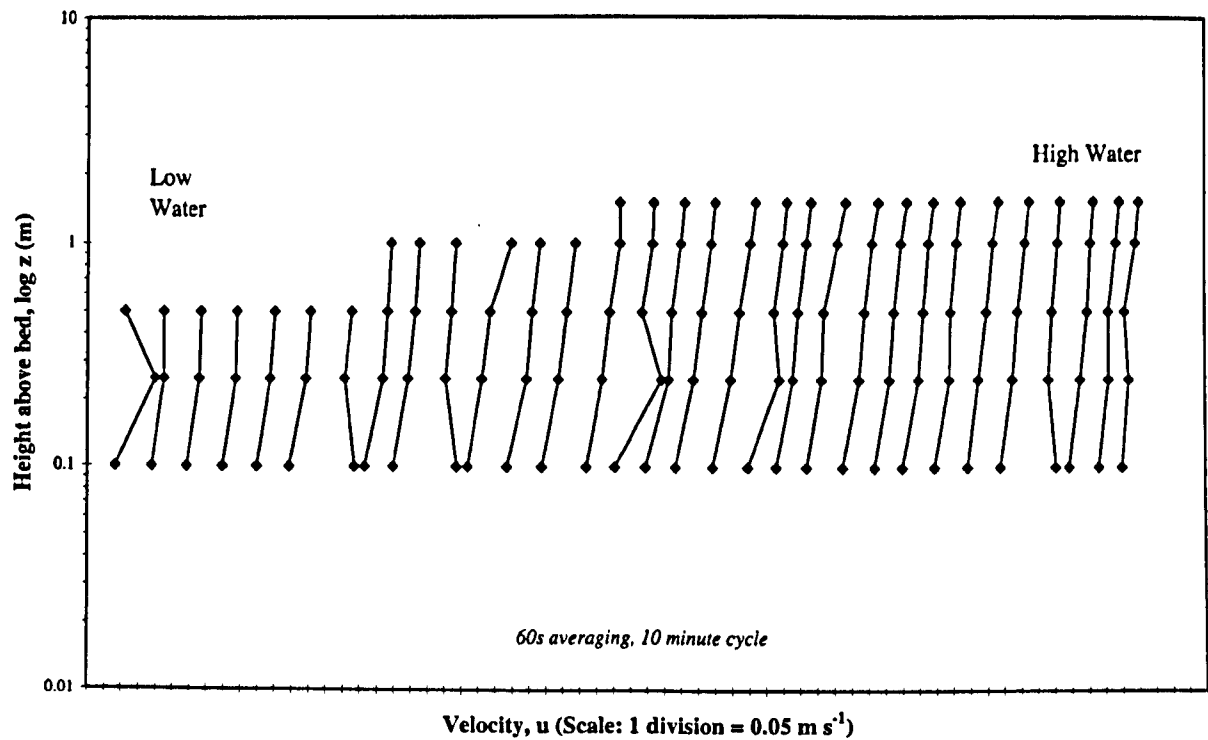
Figure 4-32 – Neap flood log velocity profiles at Station 1 (Dugmore Creek).
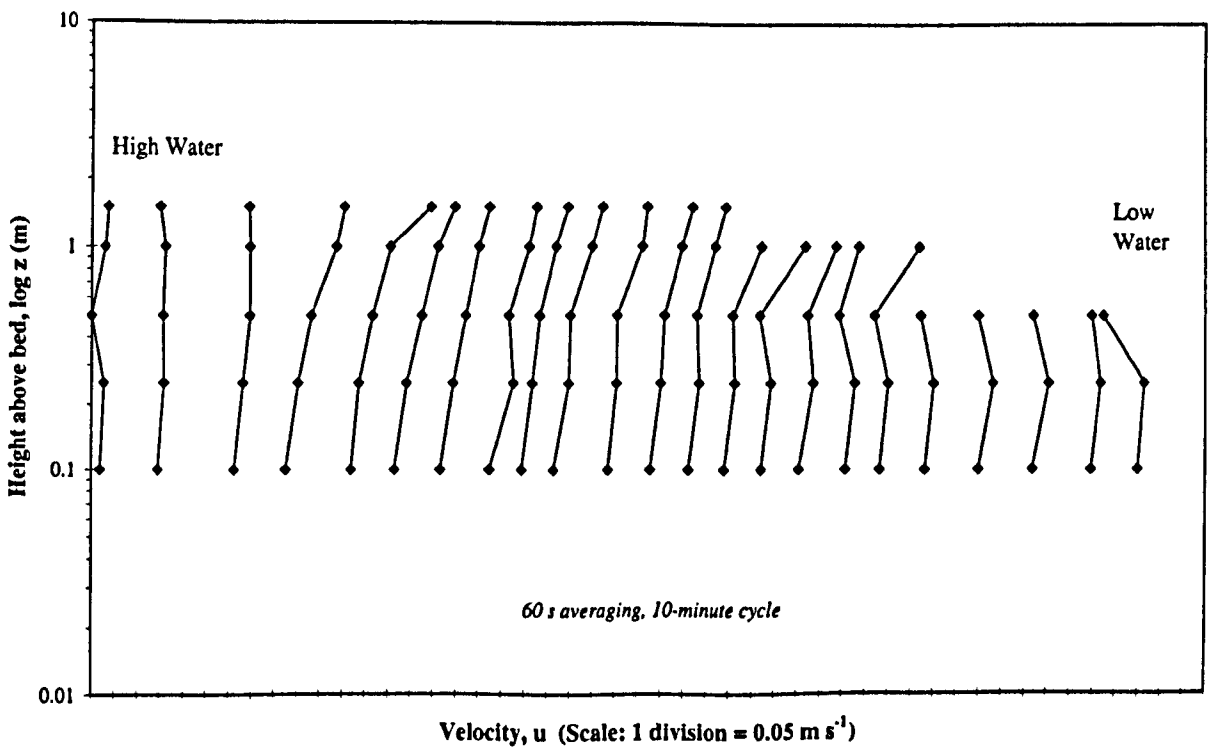
Figure 4-33 – Neap ebb log velocity profiles at Station 1 (Dugmore Creek).
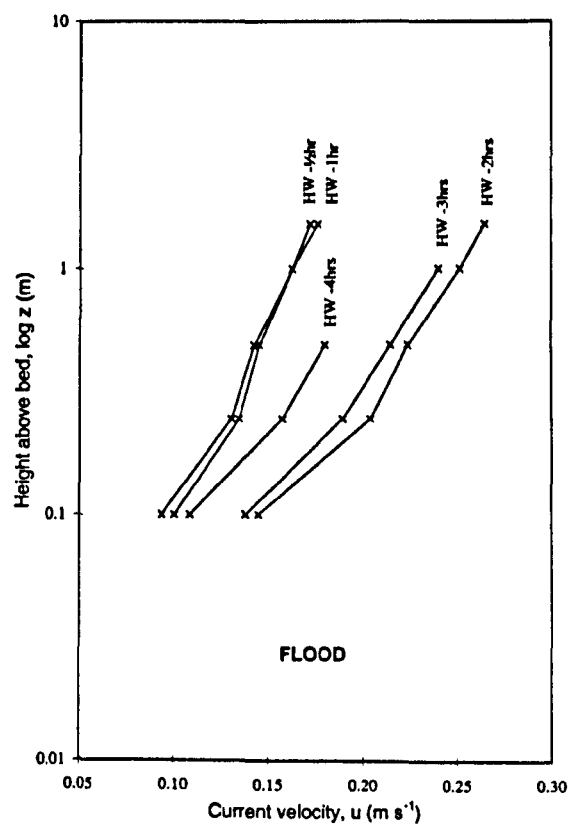
Figure 4-34 – Selected neap flood log velocity profiles at Station 1 (Dugmore Creek).
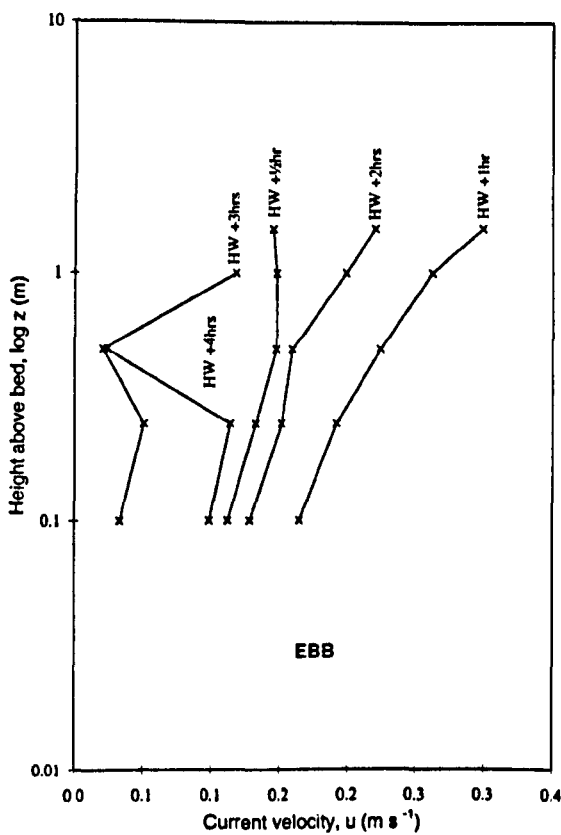
Figure 4-35 – Selected neap ebb log velocity profiles at Station 1 (Dugmore Creek).

4.6.4   VELOCITY PROFILES AT STATION 3 (PYE SAND)

Appendix E summarises the reliability of velocity profiles recorded at Pye Sand station for the full VGU deployment of 13 tidal cycles between 15 and 22 June 1995. At Station 3 (Pye Sand), of 795 profiles recorded, 426 (53%) are flood profiles and 369 (46%) are ebb. Of all 795 profiles, 74.3% were determined as being either *complete* or *partially* reliable. When separated into flood and ebb profiles, 76.5% of the flood and 71.8% of the ebb profiles were determined as either *complete* or *partially* reliable. An analysis of r^2 values for the 13 tidal cycles between 15 and 22 June (springs to neaps) show that 78% of all profiles record r^2 of ≥ 0.8, however, only 76% of ebb profiles record ≥ 0.8 as opposed to 80% of flood profiles.

Figure 4-36 and Figure 4-37 show logarithmic profiles for a spring flood and ebb tide respectively at Station–3 (Pye Sand). The profiles are at 10–minute intervals and represent a 60–second averaging period. Figure 4-38 and Figure 4-39 show selected profiles for the same flood and ebb period at –5, –4, –3, –2, –1 –0.5 hours before high water, and 0.5, 1, 2, 3, 3.5 and 4 hours after high water.

As with Station 1, there is clearly a marked difference between the general form of the flood and the ebb: flood profiles are more evenly spaced and uniform. Although when plotted to the same horizontal scale (Figure 4-38 and Figure 4-39), the flood profiles tend towards concave downwards. The ebb profiles also display a concave downward form but with a marked sinusoidal form.
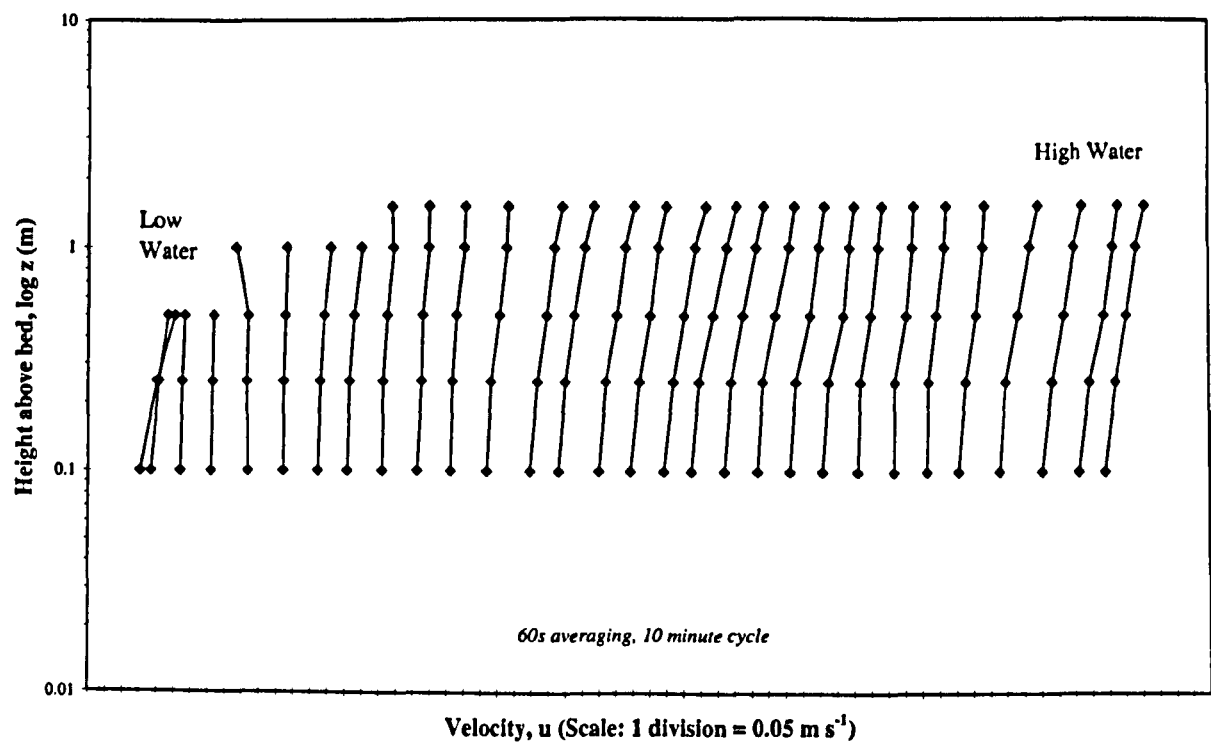
Figure 4-36 – Spring flood log velocity profiles at Station 3 (Pye Sand).
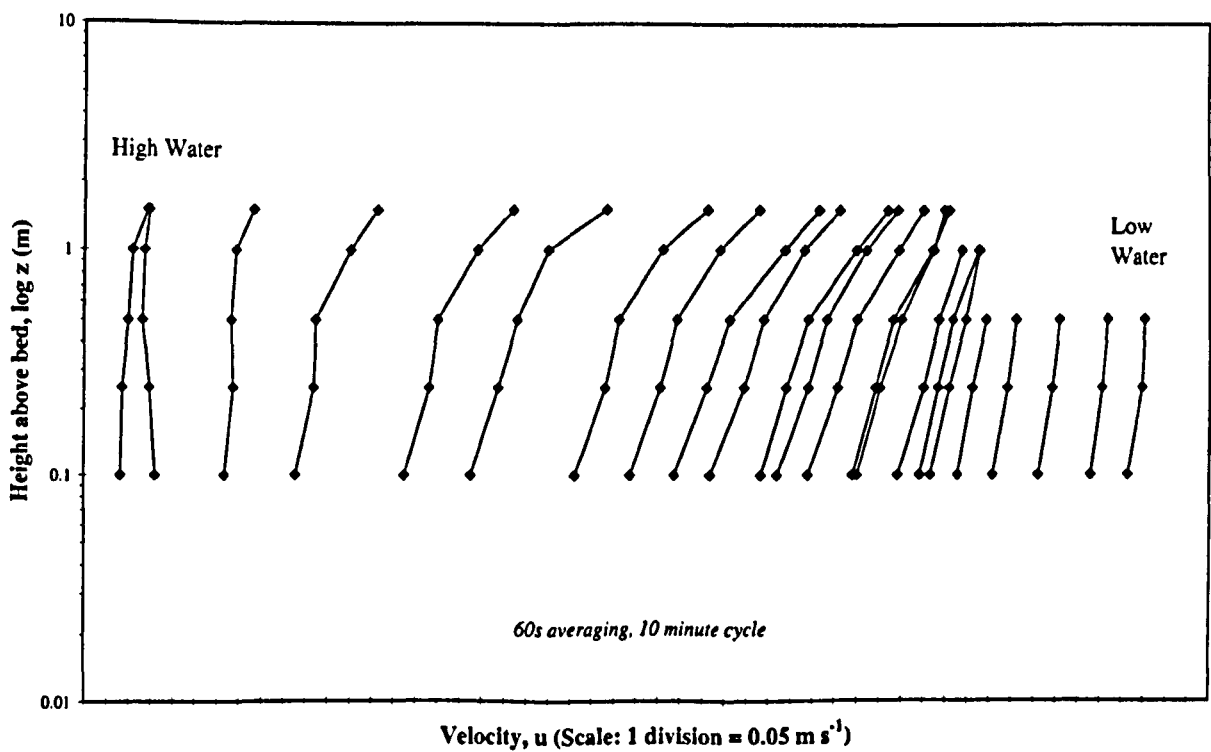
Figure 4-37 – Spring ebb log velocity profiles at Station 3 (Pye Sand).
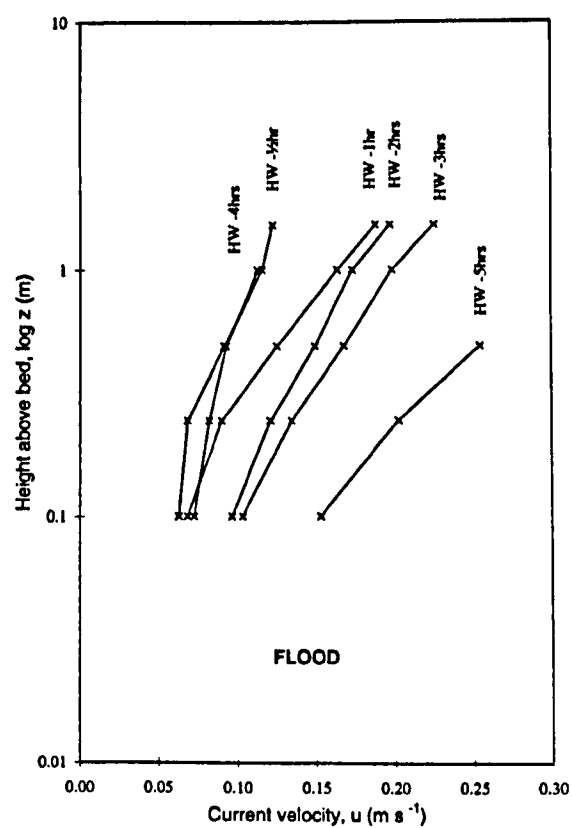
Figure 4-38 – Selected spring flood log velocity profiles at Station 3 (Pye Sand).
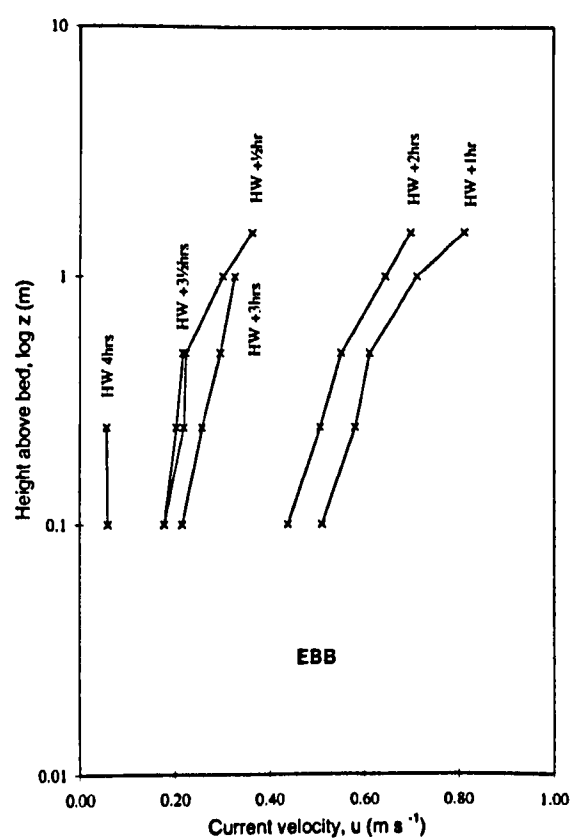
Figure 4-39 – Selected spring ebb log velocity profiles at Station 3 (Pye Sand).

Figure 4-40 and Figure 4-41 show logarithmic profiles for a neap flood and ebb tide respectively at Station-3 (Pye Sand). The profiles are at 10-minute intervals and represent a 60-second averaging period. Figure 4-42 and Figure 4-43 show selected profiles for the same flood and ebb period at -5, -4, -3, -2, -1 -0.5 hours before high water, and 0.5, 1, 2, 3, and 4 after high water.

As with the spring profiles at Station 3, the flood profiles are more uniform and tending towards logarithmic, but when plotted to scale in Figure 4-42, the profiles tend towards concave upwards apart from -5 and -4 hours which are concave downwards. On the ebb the profiles start nearly logarithmic, show brief concave upwards before remaining concave downwards for most of the remainder of the ebb. When plotted to scale in Figure 4-43, the sinusoidal form is again evident.
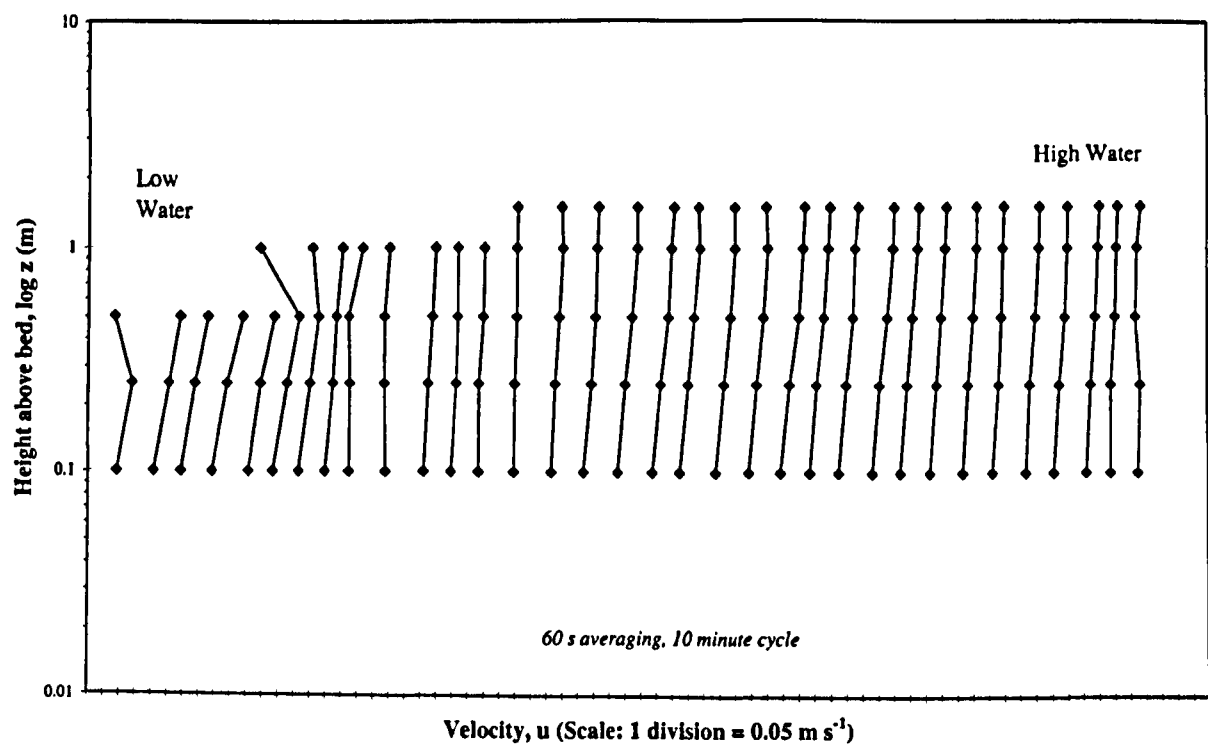
Figure 4-40 – Neap flood log velocity profiles at Station 3 (Pye Sand).
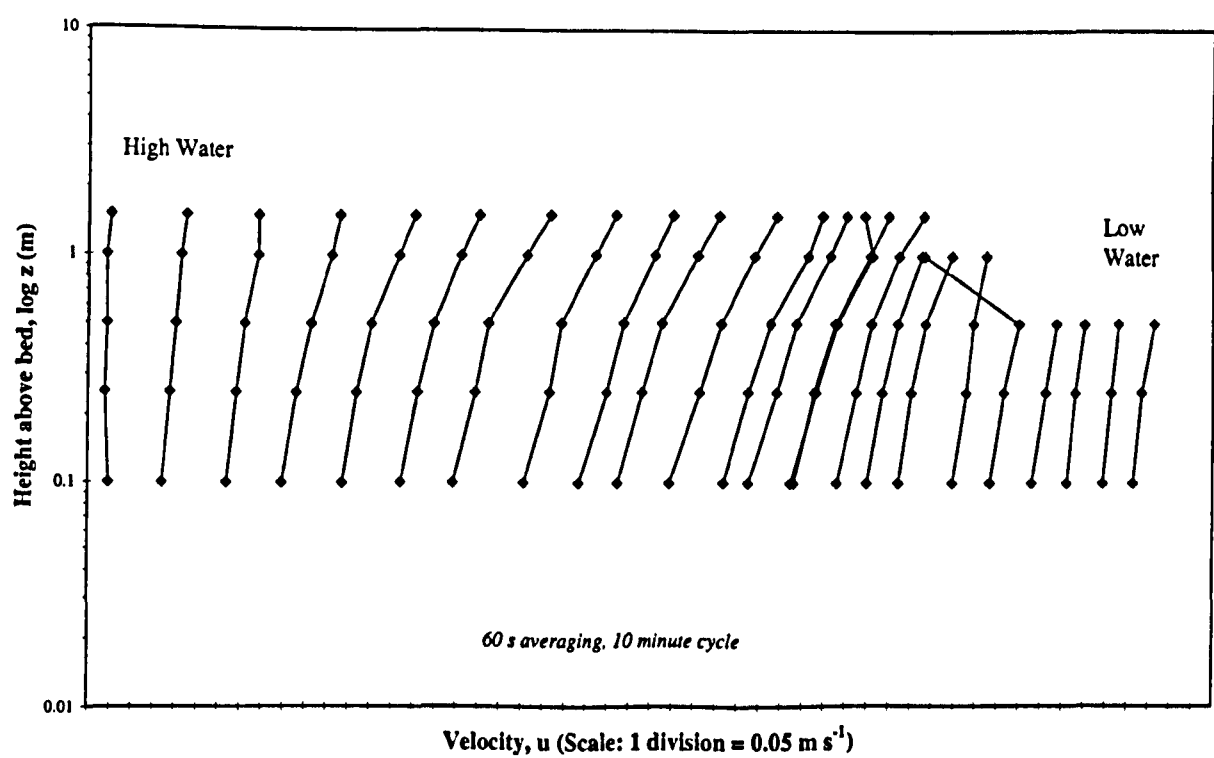
Figure 4-41 – Neap ebb log velocity profiles at Station 3 (Pye Sand).
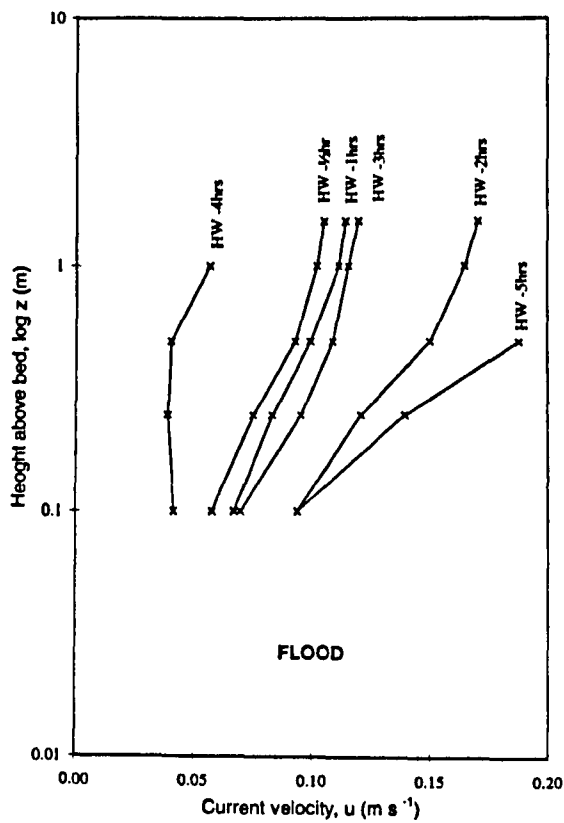
Figure 4-42 – Selected neap flood log velocity profiles at Station 3 (Pye Sand).
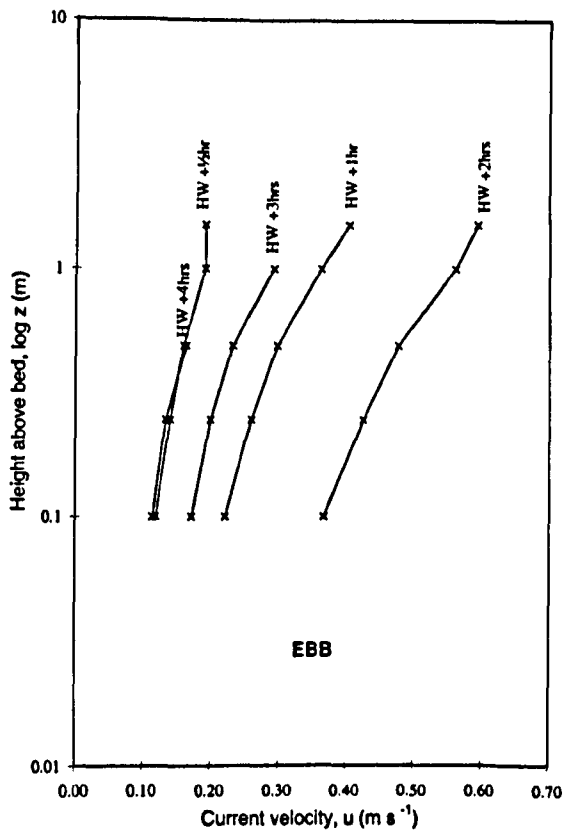
Figure 4-43 – Selected neap ebb log velocity profiles at Station 3 (Pye Sand).

4.6.5   VELOCITY PROFILES AT STATION 5 (INNER SWATCH)

For reasons discussed above (Section 4.4.2.2, *p.*67), velocity profiles for Station 5 (Inner Swatch) were matched to the data for Stations 1 and 3 and therefore, only one spring and one ebb profile are available for analysis as opposed to a whole spring-neap cycle.

At Station 5 (Inner Swatch), of 46 spring profiles recorded, both flood and ebb profiles number 23 (Appendix E). Of all 46 profiles, 60.9% were determined as being either *complete* or *partially* reliable. When separated into flood and ebb profiles, 69.6% of the flood and 52.2% of the ebb profiles were determined as either *complete* or *partially* reliable. An analysis of r^2 values show that 57% of all complete and partially reliable profiles record r^2 of ≥ 0.8, and only 45% of ebb profiles record ≥ 0.8 as opposed to 65% of flood profiles.

Figure 4-44 and Figure 4-45 show logarithmic profiles for a spring flood and ebb tide respectively at Station–5 (Inner Swatch). The profiles are at 10–minute intervals and represent a 60–second averaging period. Figure 4-46 and Figure 4-47 show selected profiles for the same flood and ebb period at –3, –2.5, –2, –1.5, –1 and –0.5 hours before high water, and 0.5, 1, 1.5, 2, and 2.5 hours after high water.

The contrast with Stations 1 and 3, of Station 5 is dramatic: both flood and ebb profiles show significant departures from a logarithmic form. The degree of departure would suggest that the highest rotor in the profile was defective although there was no evidence of this at the time. If the upper rotor is excluded, the form of the remainder of the profiles tends towards concave downwards in most cases. However, if the upper rotor is included, the profiles approximate to a sinusoidal form.
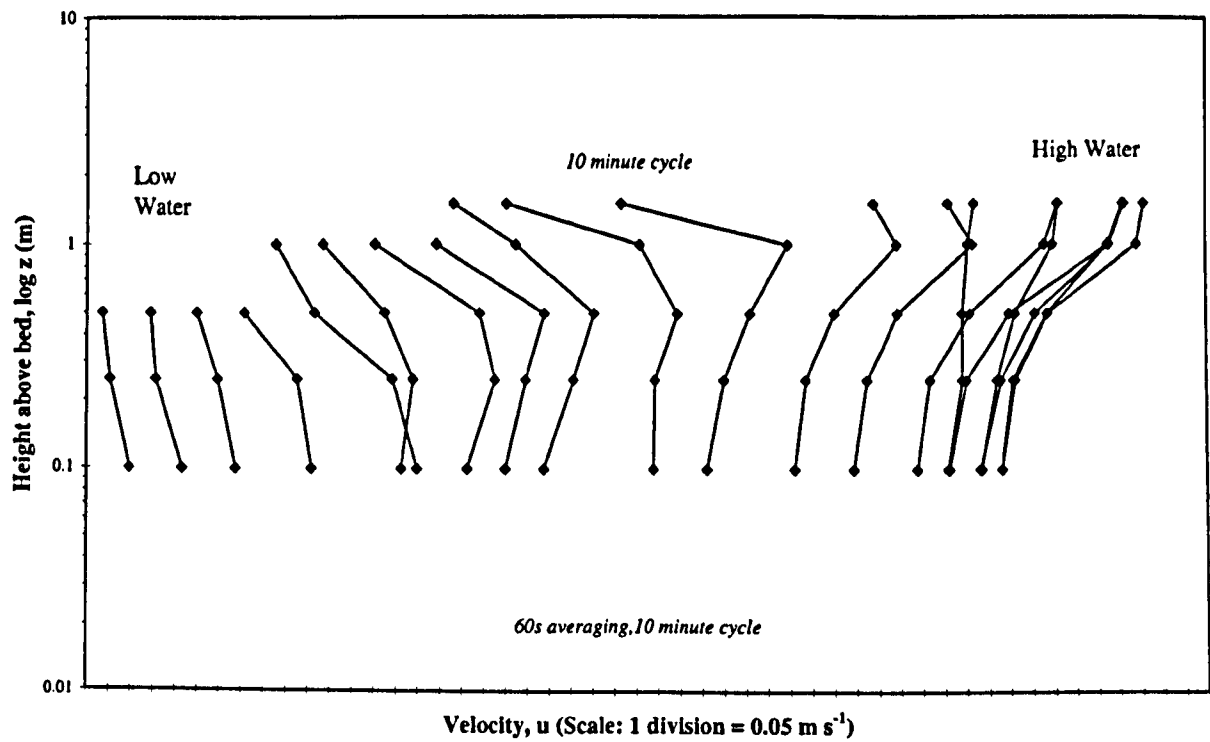
Figure 4-44 – Spring flood log velocity profiles at Station 5 (Inner Swatch).
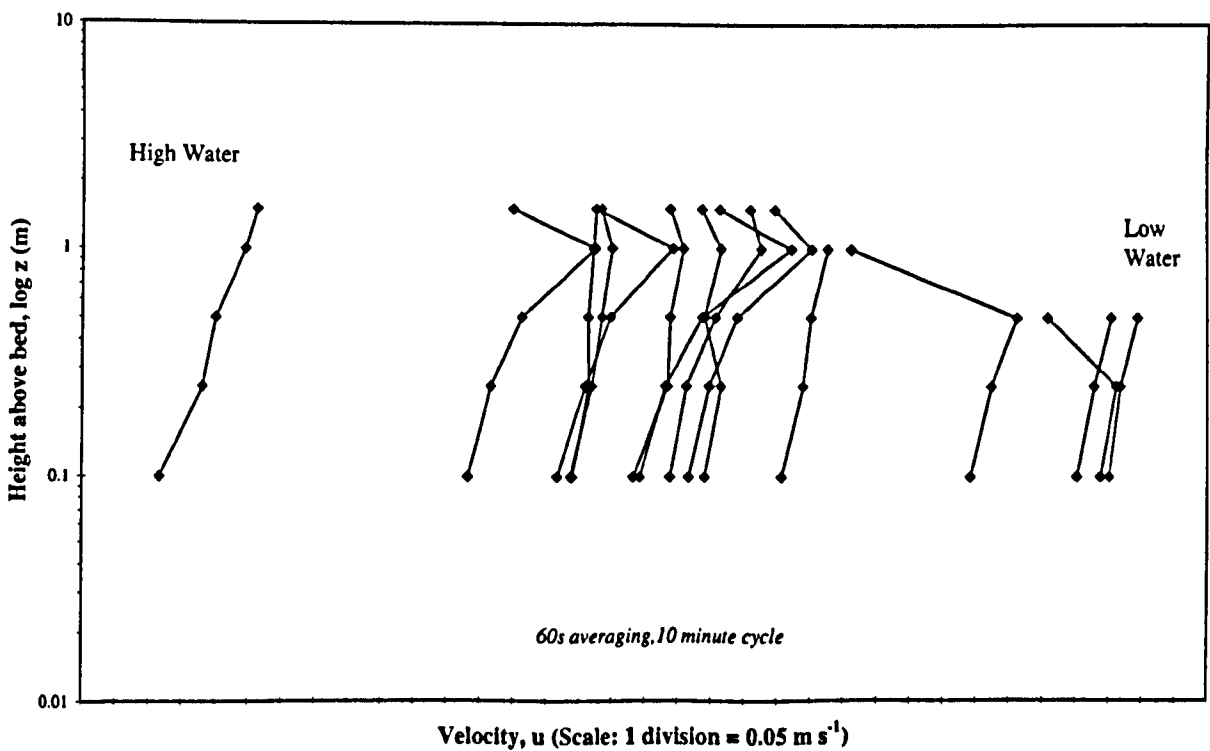
Figure 4-45 – Spring ebb log velocity profiles at Station 5 (Inner Swatch).
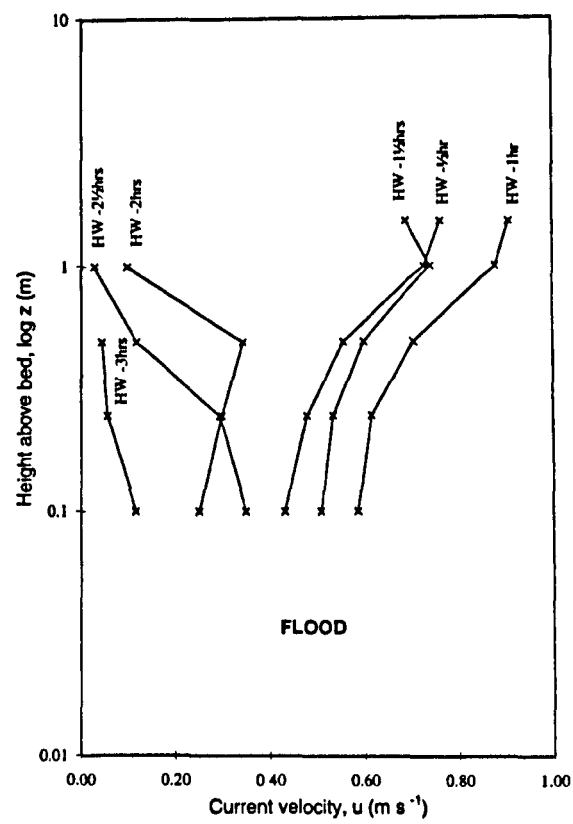
Figure 4-46 – Selected spring flood log velocity profiles at Station 5 (Inner Swatch).
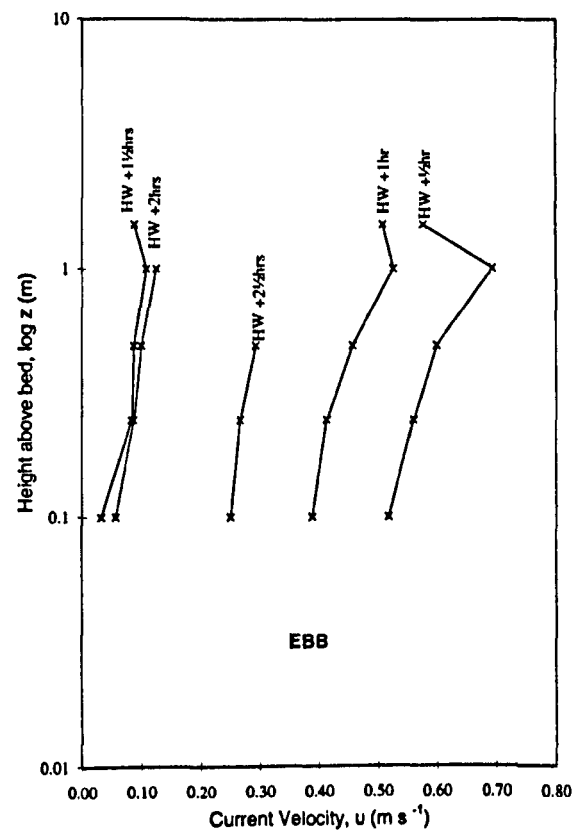
Figure 4-47 – Selected spring ebb log velocity profiles at Station 5 (Inner Swatch).

At Station 5 (Inner Swatch), of 49 neap profiles, 27 flood and 7 ebb profiles were recorded. Of all 49 profiles, 67.3% were determined as being either *complete* or *partially* reliable. When separated into flood and ebb profiles, 59.3% of the flood and 85.7% of the ebb profiles were determined as either *complete* or *partially* reliable. An analysis of r^2 values show that 56% of all complete and partially reliable profiles record r^2 of ≥ 0.8, however, only 45% of ebb profiles record ≥ 0.8 as opposed to 62% of flood profiles.

Figure 4-48 and Figure 4-49 show logarithmic profiles for a neap flood and ebb tide respectively at Station-5 (Inner Swatch). The profiles are at 10-minute intervals and represent a 60-second averaging period. Figure 4-50 and Figure 4-51 show selected profiles for the same flood and ebb period at $-4, -3, -2, -1$ and -0.5 hours before high water, and $0.5, 1, 1.5, 2,$ and 3 hours, after high water. The departures from a true logarithmic form are not as dramatic as the spring profiles but are still more marked than both Stations 1 and 3. As with spring profiles, the shape of the upper part of the profiles appears to be influenced by the top rotor resulting in a sinusoidal form throughout.
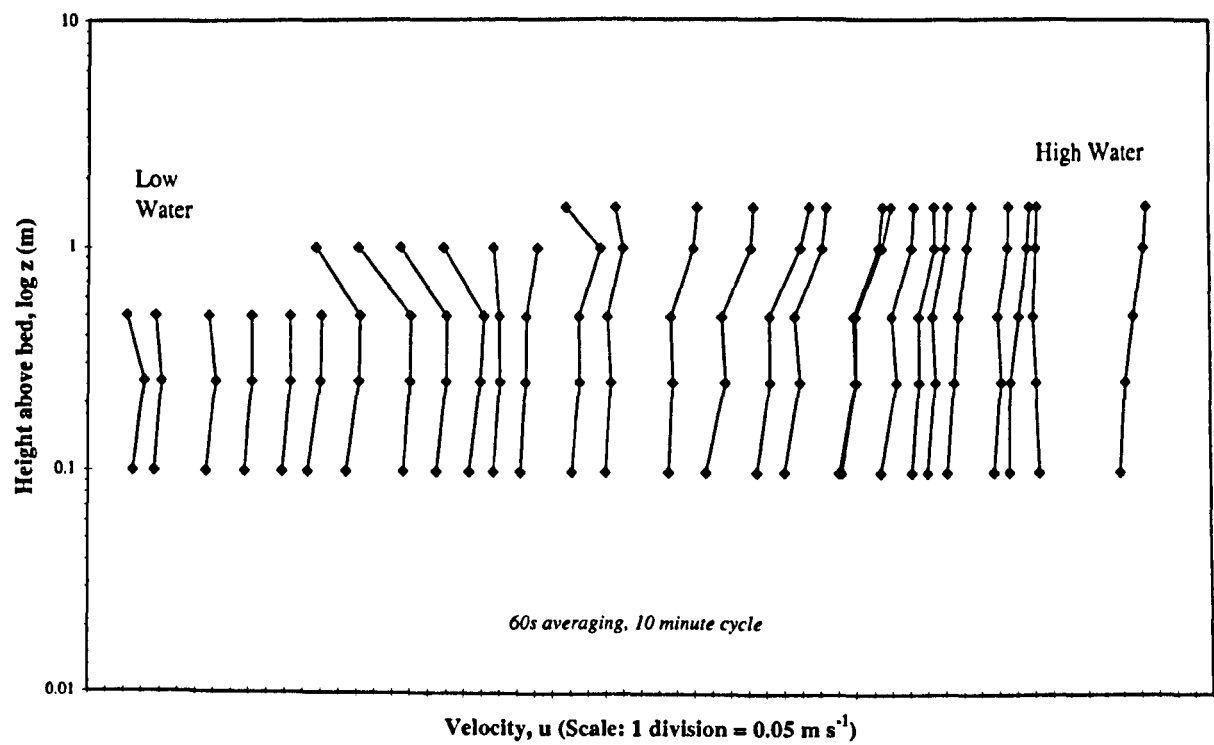
Figure 4-48 – Neap flood log velocity profiles at Station 5 (Inner Swatch).
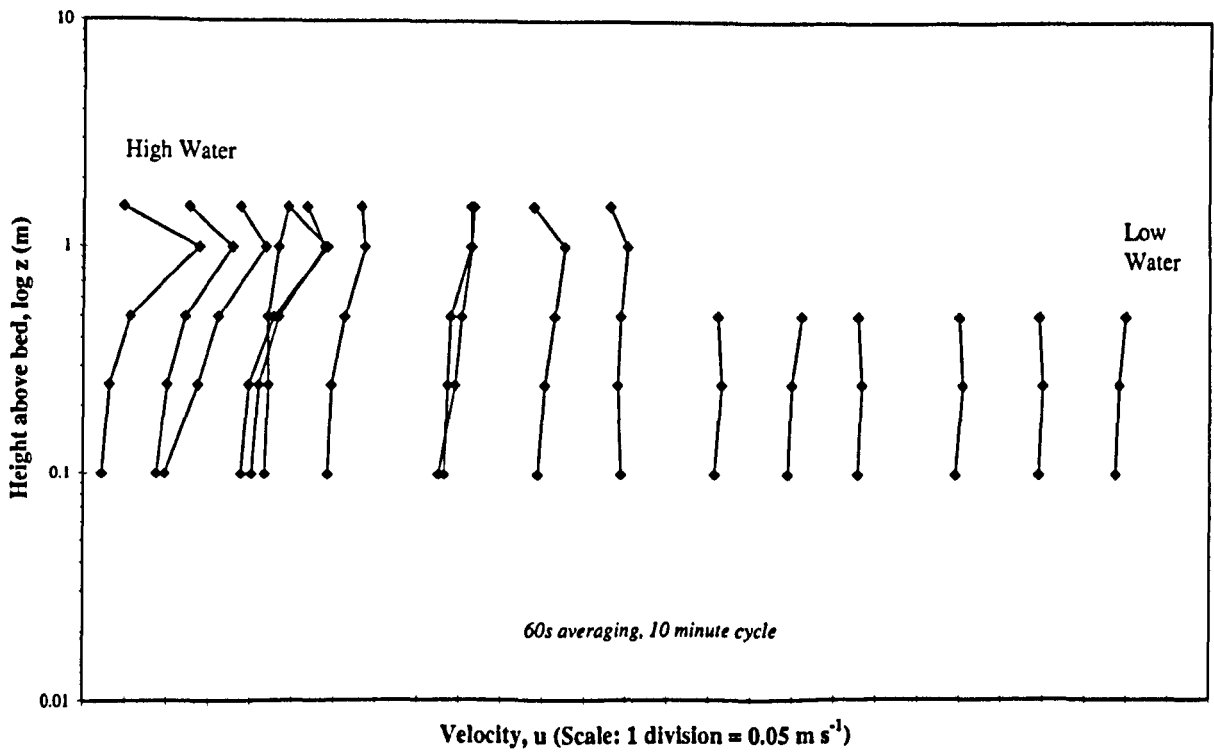
Figure 4-49 – Neap ebb log velocity profiles at Station 5 (Inner Swatch).
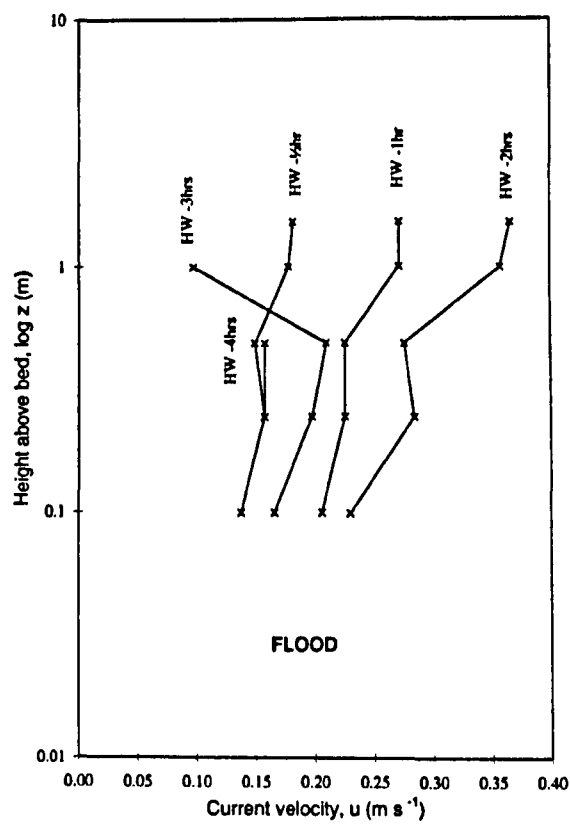
Figure 4-50 – Selected neap flood log velocity profiles at Station 5 (Inner Swatch).
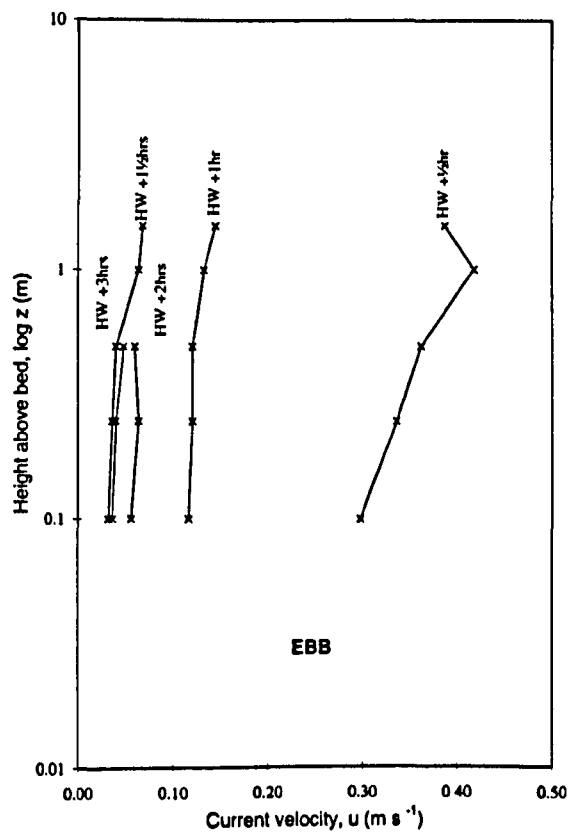
Figure 4-51 – Selected neap ebb log velocity profiles at Station 5 (Inner Swatch).

4.6.6 STATISTICAL VARIABILITY OF VELOCITY PROFILES

Wilkinson (1984) uses a method for evaluating statistical errors associated with logarithmic velocity profiles. He stresses that although the correlation coefficient (r) between u and ln z, calculated as part of the linear regression, gives a good indication of the quality of fit of the straight line to the data, it does not indicate the errors associated with the estimated values of $u*$ and z_0. He found errors in shear stress of $\pm35\%$ and in roughness length of $\pm77\%$, using 95% confidence limits. Using Wilkinson's (1984) method, statistical variability associated with estimates of the bed shear stress and bottom roughness for selected profiles from the data set were calculated and are detailed in Table 4-6 and Table 4-7. It can be seen that much of the temporal variability is contained within the error bars and therefore not significant, implying that a smoothed line could be drawn through the data. It is apparent in all instances that the error bounds for the ebb are considerably greater than the flood indicating that there are processes at work on the ebb that are contributing to increased statistical variability.

Table 4-6 – Error bounds – springs (after method of Wilkinson (1984)).

Spings	Station 1		Station 3		Station 5	
Parameter	δ	+/-	δ	+/-	δ	+/-
$u*(f)$	0.41	17%	0.42	31%	2.55	60%
$u*(e)$	0.42	33%	1.56	53%	1.77	105%
$z_0(f)$	1.10	67%	1.80	126%	0.68	265%
$z_0(e)$	0.46	176%	0.44	243%	0.80	781%
$\ln z_0(f)$	0.45	67%	0.17	126%	-1.53	265%
$\ln z_0(e)$	-1.23	176%	-2.14	243%	-4.56	781%
$\tau_0(f)$	1.99	34%	1.25	63%	24.39	121%
$\tau_0(e)$	1.74	66%	11.31	106%	6.96	210%

Table 4-7 – Error bounds – Neaps (after method of Wilkinson (1984)).

Neaps	Station 1		Station 3		Station 5	
Parameter	δ	+/-	δ	+/-	δ	+/-
$u*(f)$	0.38	29%	0.22	28%	0.99	111%
$u*(e)$	0.66	78%	0.85	30%	1.02	158%
$z_0(f)$	0.46	120%	0.31	125%	0.19	1174%
$z_0(e)$	0.58	761%	0.46	126%	0.51	1658%
$\ln z_0(f)$	-1.07	120%	-1.50	125%	-4.54	1174%
$\ln z_0(e)$	-2.99	761%	-1.22	126%	-7.18	1658%
$\tau_0(f)$	1.09	58%	0.37	56%	2.62	221%
$\tau_0(e)$	1.93	155%	5.10	61%	2.03	315%

Notwithstanding Wilkinson's (1984) method, the significance of the correlation coefficient between $\ln z$ and u was more conventionally estimated using a t–statistic for $r = 0.8$:

H_0: $\beta = 0$

H_0: $\beta \neq 0$

Test statistic:

$$t = r\sqrt{\frac{n-2}{1-r^2}}$$ (4:2

$n = 5$

$t = 2.309$

Degrees of freedom $= n - 2 = 4$

$\alpha = 0.05$

From statistical tables (Swan and Sandilands, 1995), critical $t = 2.352$, therefore for $r = 0.8$ the calculated t is less than the critical t, so the null hypothesis is accepted. However, $r = 0.8$ represents the threshold of significance because for $r = 0.81$ to 0.99, the calculated t exceeds the critical t so the null hypothesis can be rejected. Therefore, for all values of $r > 0.8$ there is deemed to be a significant correlation between $\ln z$ and u.

4.6.7   DISCUSSION – VELOCITY PROFILES

In general, all velocity profiles on springs and neaps and at each station appear to follow similar patterns: all flood velocity profiles are consistently more logarithmic than ebb velocity profiles, with some random variations. The even spacing of the flood profiles implies a uniform, steady flood tidal cycle. The erratic spacing of the ebb profiles highlights the higher recorded velocities and more turbulent nature of the ebb. The curvature of the profiles vary from straight to convex upwards, or convex downwards, to sigmoidal. Sigmoidal profiles were observed by Heathershaw and Langhorne (1988) in an assessment of velocity profiles in the Solent, England. It was

observed that although the seabed near the study area was generally level and devoid of regular bedforms, the observed velocity profiles were consistently concave downwards. They attributed it to the presence of an internal boundary layer that was due to the form drag on irregular topography upstream of the measurement location.

The departures from a true logarithmic form of the velocity profiles in this research seem to be most pronounced just after high water, during the highest velocities. However, in addition to the effects on velocity profiles described by Dyer (1986) and summarised at the beginning of this section, it is felt that the chosen VGU locations in this survey may have contributed to the variations in logarithmic form for the reasons similar to those outlined by Heathershaw and Longhorn (1988). Due to the predominantly soft nature of Hamford Water intertidal sediment, VGU's were only sighted where it was firm enough for the mast to be safely rigged. Apart from Station 1 (Dugmore Creek), all other sites were slightly raised banks with the steepest side of the bank facing the ebb current. The result may be an increase in turbulence and the development of an internal boundary layer resulting in the erratic nature of the profiles at the peak of ebb flows.

4.6.8   ROUGHNESS LENGTH

The applicability and importance of the roughness length z_0, has already been discussed in Section 3.2.4 above; in the following discussion, the variation of z_0 at each Station is considered.

Springs (Figure 4-52, Figure 4-53 and Figure 4-54):

At Station 1, on a spring tide, the maximum value of z_0 is 0.024m on the flood and 0.030m on the ebb with a mean over the whole cycle of 0.027m (Figure 4-52). The value of z_0 varies from 0.01m at the start of the flood, rises to approximately 0.02m at mid-flood, then falls to below 0.005m just after high water. On the ebb, z_0 rises abruptly to a peak of 0.03m about 1.5 hours after high water before dropping back to 0.004m. Throughout the cycle, r^2 values remain consistently above 0.8 with the exception of just after high water.

At Station 3, on a spring tide, the maximum value of z_0 is 0.032m on the flood and 0.013m on the ebb with a mean over the whole cycle of 0.023m (Figure 4-53). The

value of z_0 varies from approximately 0.003m at the start of the flood, rises to a peak of 0.032 at 2-hours before high water, then falls to below 0.005m just after high water. On the ebb, z_0 rises briefly to a peak of 0.01m about 0.5 hours after high water before dropping to approximately 0.002m. Throughout the cycle, r^2 values remain consistently above 0.8 with the exception of just after high water.

At Station 5, on a spring tide, the maximum value of z_0 is 0.007m on the flood and 0.0011m on the ebb with a mean over the whole cycle of 0.009m (Figure 4-54). The value of z_0 averages 0.005m throughout the flood, peaks just after high water at 0.01m, before falling to 0.001 for most of the ebb. Throughout the cycle, r^2 values remain consistently above 0.8 on the flood, but fall below on the ebb.
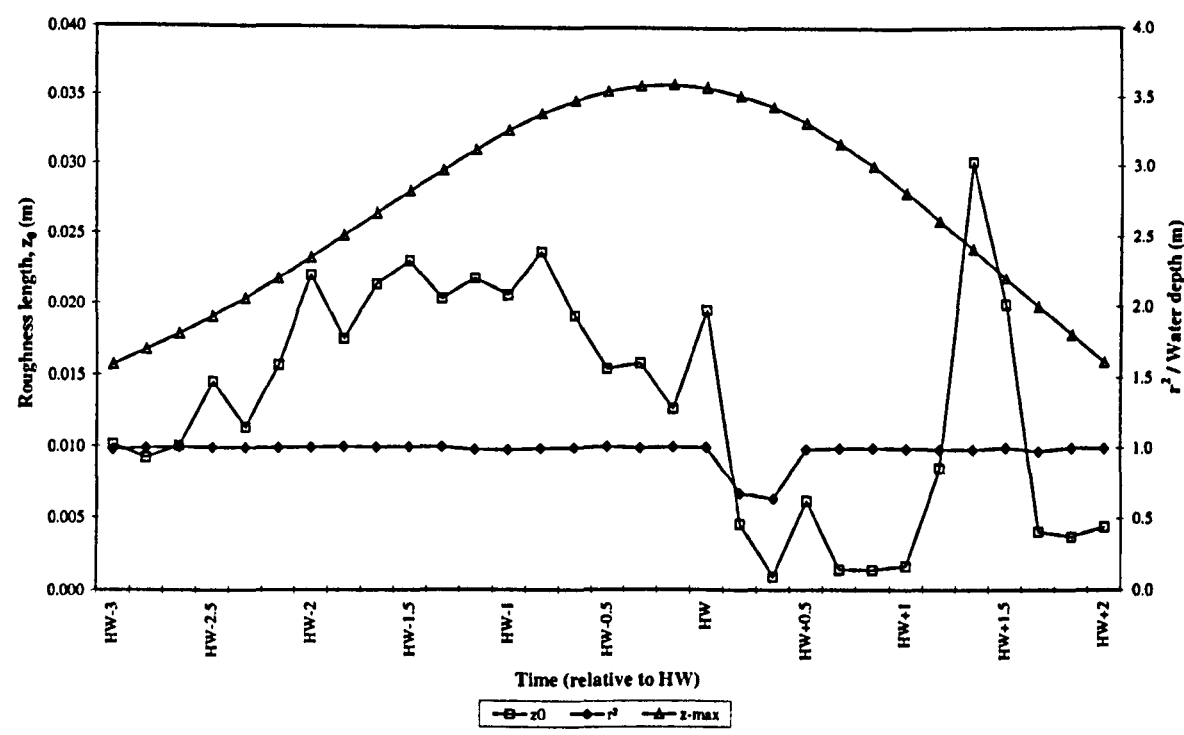
Figure 4-52 – z_0, r^2, z_{max} – Station 1 (Springs)
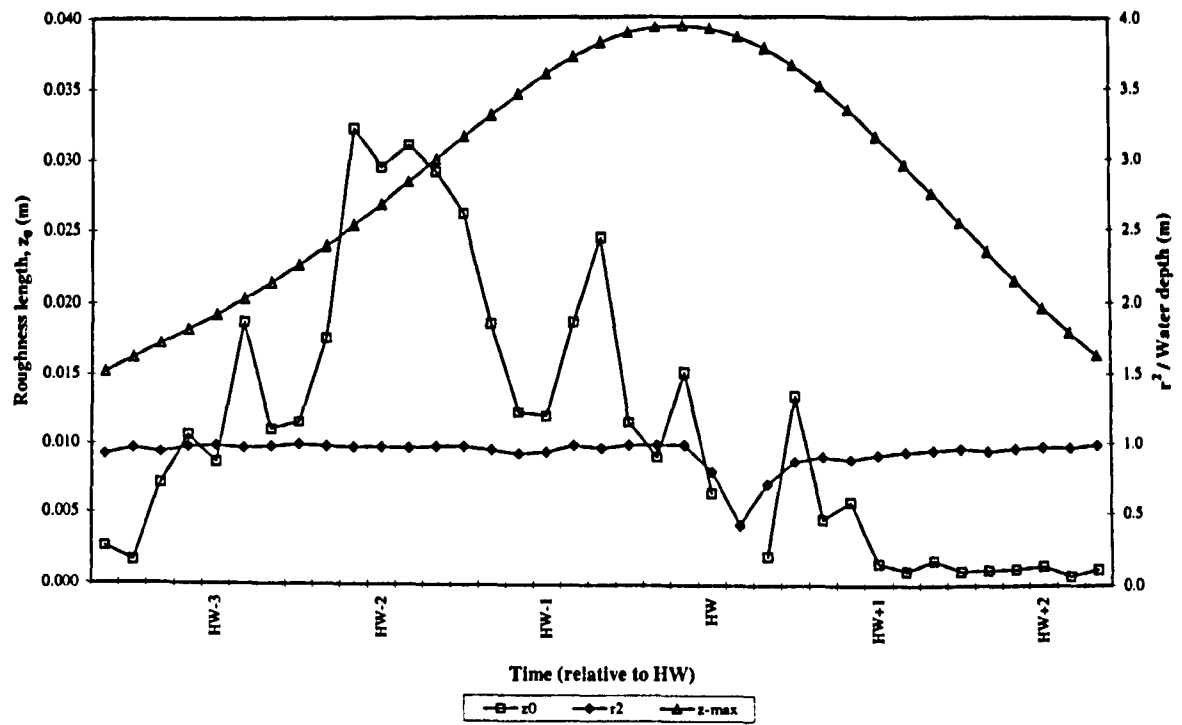
Figure 4-53 – z_0, r^2, z_{max} – Station 3 (Springs)
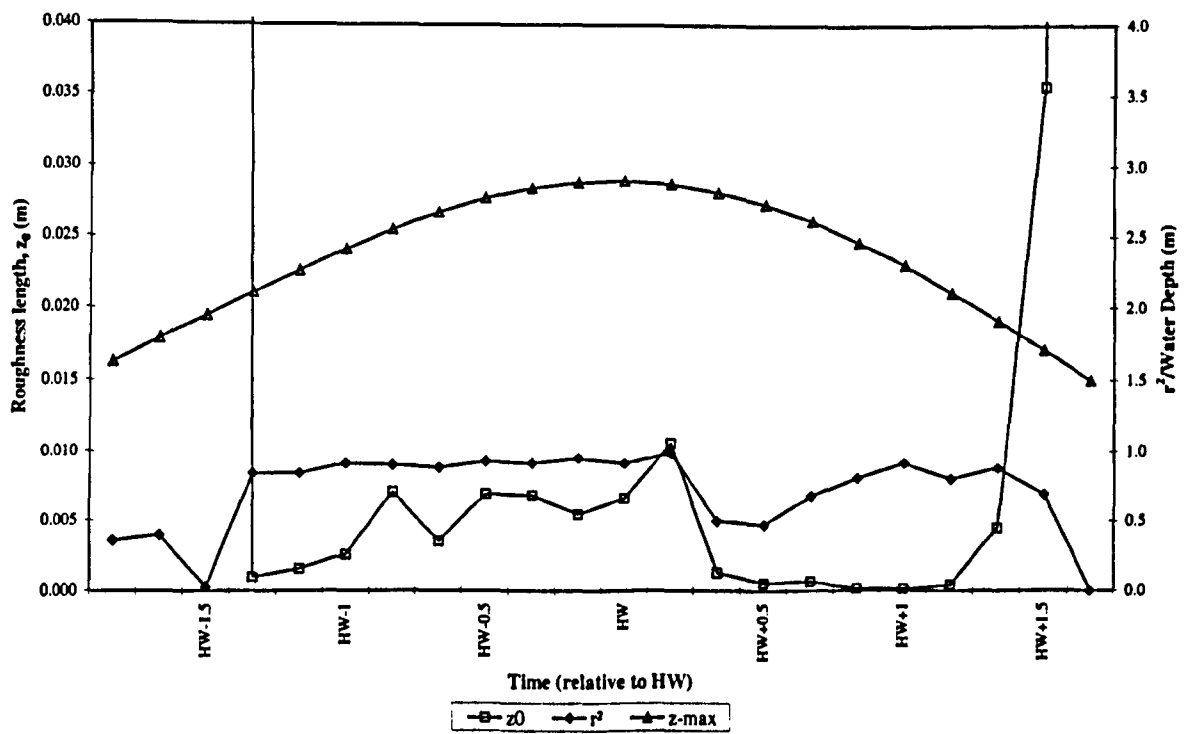
Figure 4-54 – z_0, r^2, z_{max} – Station 5 (Springs)

Neaps (Figure 4-55, Figure 4-56 and Figure 4-57):

At Station 1, on a neap tide, the maximum value of z_0 is 0.007m on the flood and 0.011m on the ebb with a mean over the whole cycle of 0.009m (Figure 4-55). Throughout the flood cycle, r^2 values remain consistently above 0.8 apart from just after high water.

At Station 3, on a neap tide, the maximum value of z_0 is 0.006m on the flood and 0.008m on the ebb with a mean over the whole cycle of 0.007m (Figure 4-56). r^2 values are consistently above 0.8 throughout the flood and ebb apart from high water.

At Station 5, on a neap tide, the maximum value of z_0 is 0.007m on the flood and 0.001m on the ebb with a mean over the whole cycle of 0.004m (Figure 4-57). r^2 values remain above 0.8 up to 15 minutes either side of high water, but are markedly less on the ebb than the flood.
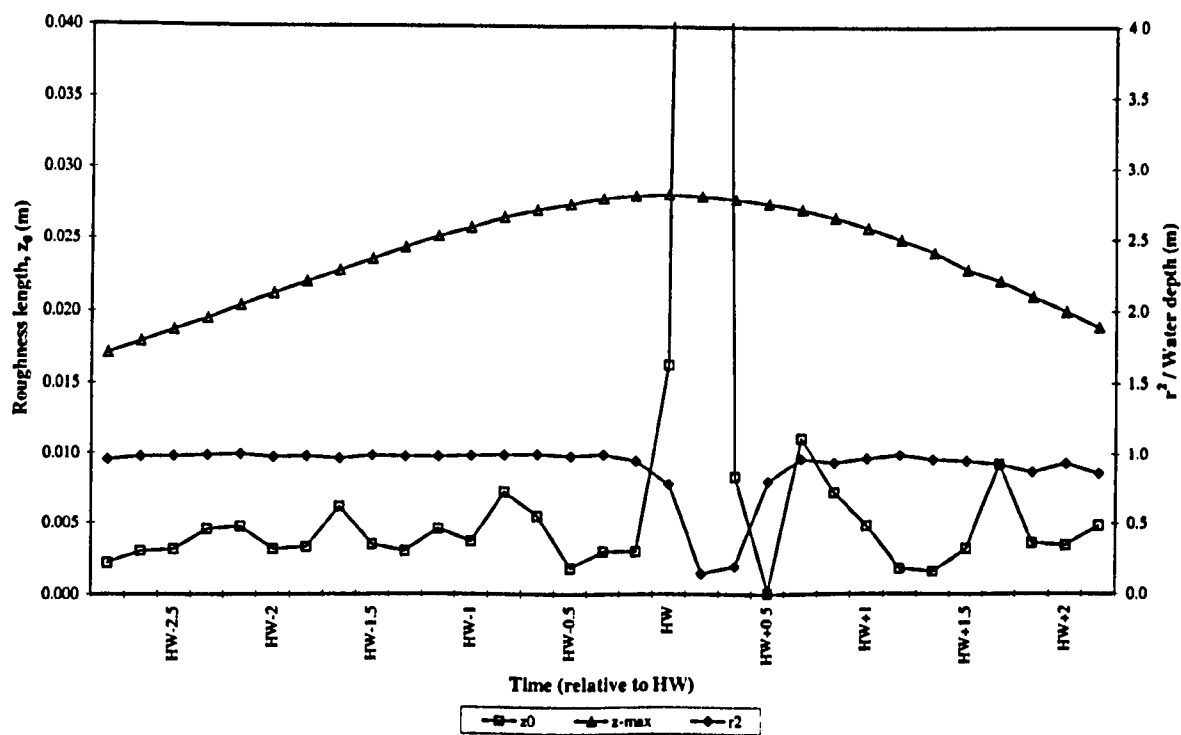
Figure 4-55 – z_0, r^2, z_{max} – Station 1 (Neaps)
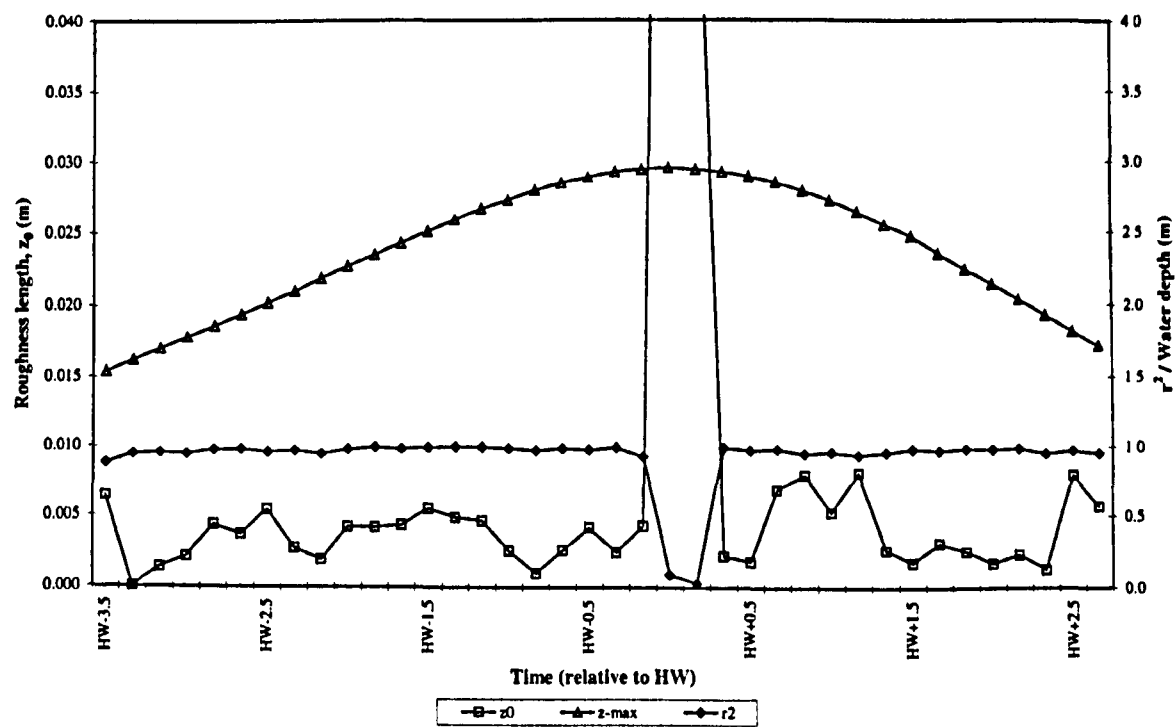
Figure 4-56 – z_0, r^2, z_{max} – Station 3 (Neaps)
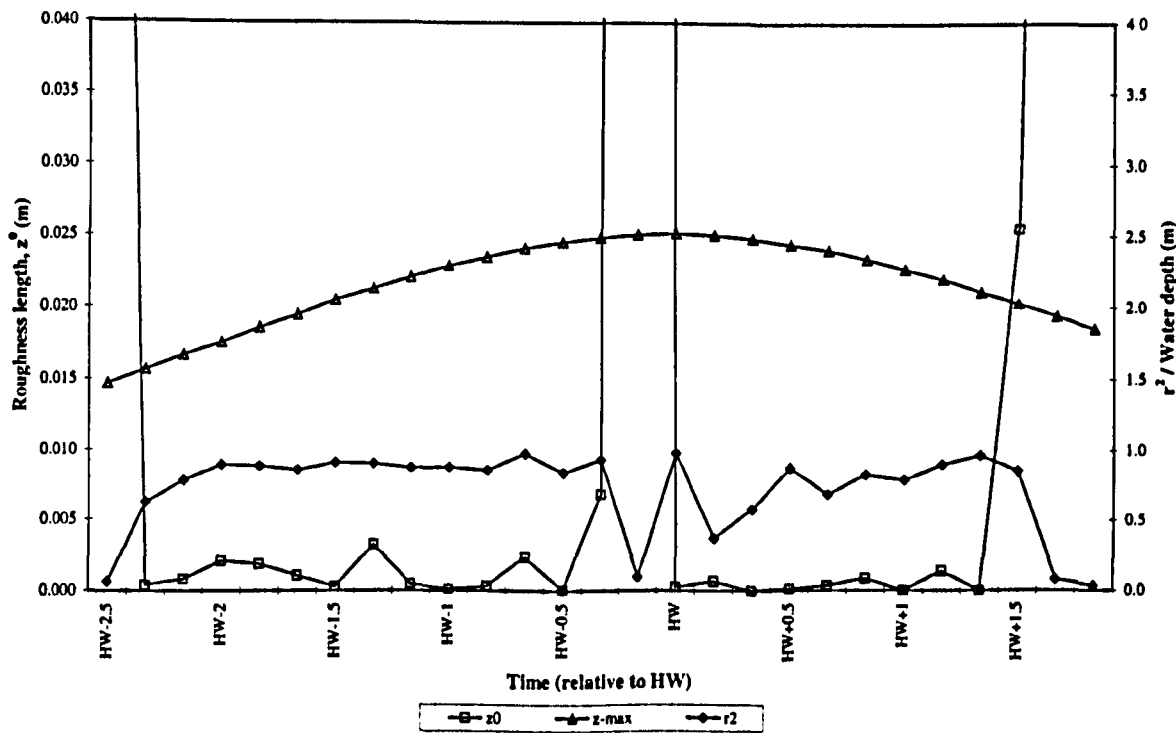
Figure 4-57 – z_0, r^2, z_{max} – Station 5 (Neaps)

4.6.9 SHEAR VELOCITY AND DRAG COEFFICIENT

As with roughness lengths, the applicability and importance of shear velocity and drag coefficient have been discussed in Section 3.2.4 above. Figure 4-58 through to Figure 4-63 are time series plots of shear velocity and drag coefficient over a spring tide and a neap tide at Stations 1, 3, and 5 respectively.

At Station 1, on a spring tide (Figure 4-58), the maximum value of u_* is 0.031m s^{-1} on the flood and 0.031m s^{-1} on the ebb with a mean over the whole cycle of 0.031m s^{-1}. The maximum value of C_{100} is 0.011 on the flood and 0.013 on the ebb with a mean over the whole cycle of 0.012.

At Station 3, on a spring tide (Figure 4-59), the maximum value of u_* is 0.020m s^{-1} on the flood and 0.048m s^{-1} on the ebb with a mean over the whole cycle of 0.034m s^{-1}. Values for high water have been omitted because of unreliable data during slack water. The maximum value of C_{100} is 0.014 on the flood and 0.009 on the ebb with a mean over the whole cycle of 0.011.

At Station 5, on a spring tide (Figure 4-60), the maximum value of u_* is 0.060m s^{-1} on the flood and 0.0221m s^{-1} on the ebb with a mean over the whole cycle of 0.041m s^{-1}. The maximum value of C_{100} is 0.007 on the flood and 0.008 on the ebb with a mean over the whole cycle of 0.007.

At Station 1, on a neap tide (Figure 4-61), the maximum value of u_* is 0.019m s^{-1} on the flood and 0.021m s^{-1} on the ebb with a mean over the whole cycle of 0.020m s^{-1}. The maximum value of C_{100} is 0.007 on the flood and 0.008 on the ebb with a mean over the whole cycle of 0.007. The mean excludes the spike just after high water for the same reasons as for Station 3 (springs).

At Station 3, on a neap tide (Figure 4-62), the maximum value of u_* is 0.011m s^{-1} on the flood and 0.036m s^{-1} on the ebb with a mean over the whole cycle of 0.024m s^{-1}. The maximum value of C_{100} is 0.006 on the flood and 0.007 on the ebb with a mean over the whole cycle of 0.007. Again, the spike at high-water has been excluded from averaging.

At Station 5, on a neap tide (Figure 4-63), the maximum value of u∗ is 0.022m s^{-1} on the flood and 0.013m s^{-1} on the ebb with a mean over the whole cycle of 0.018m s^{-1}. The maximum value of C_{100} is 0.006 on the flood and 0.004 on the ebb with a mean over the whole cycle of 0.005. As with previous Stations, high-water slack spikes have been removed.
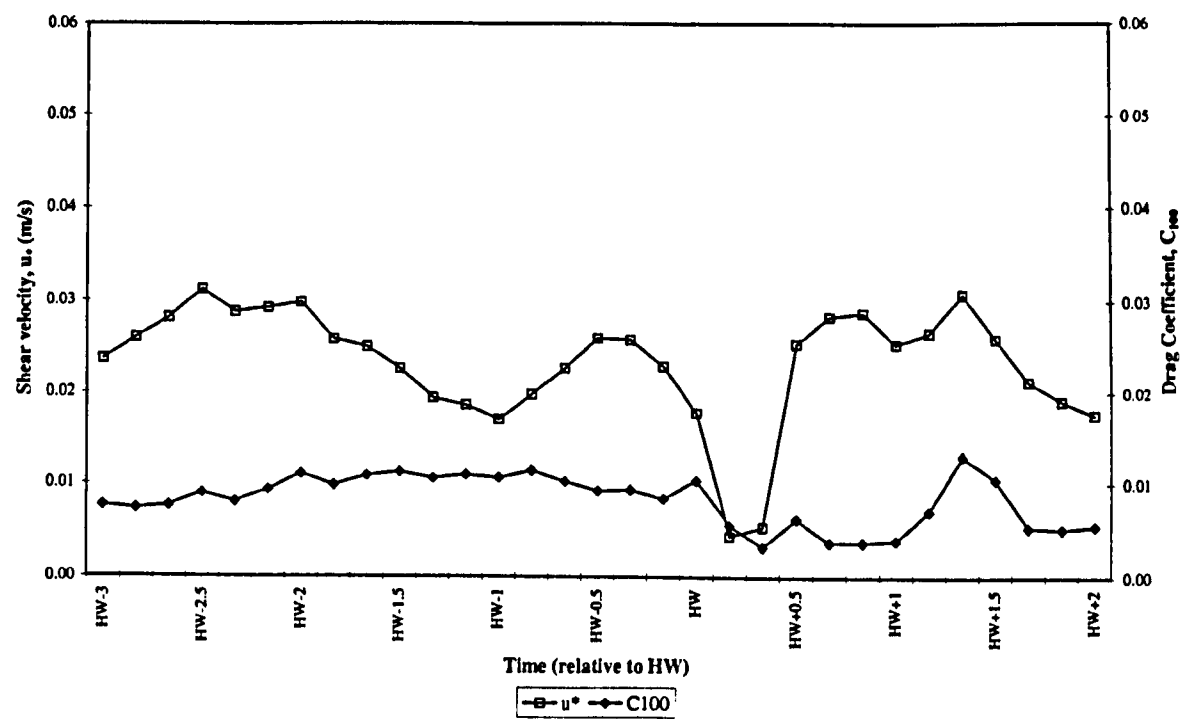
Figure 4-58 – u∗, C_{100} – Station 1 (Springs)
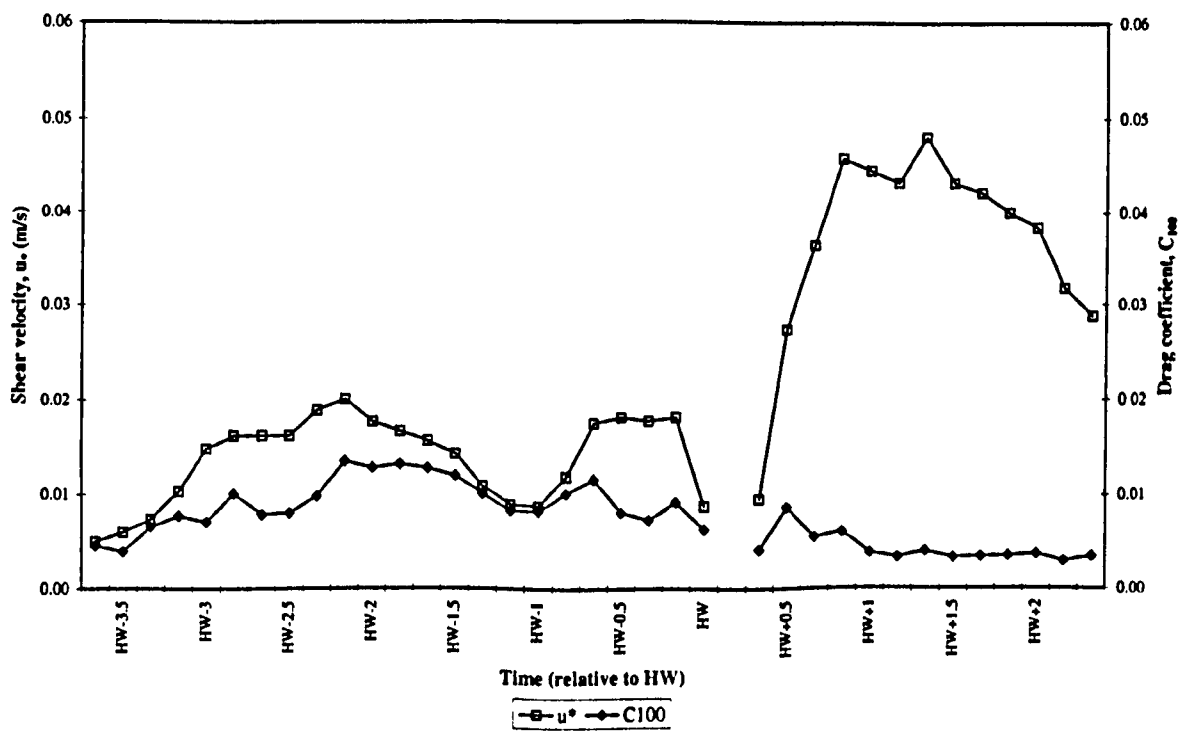
Figure 4-59 – u∗, C_{100} – Station 3 (Springs)
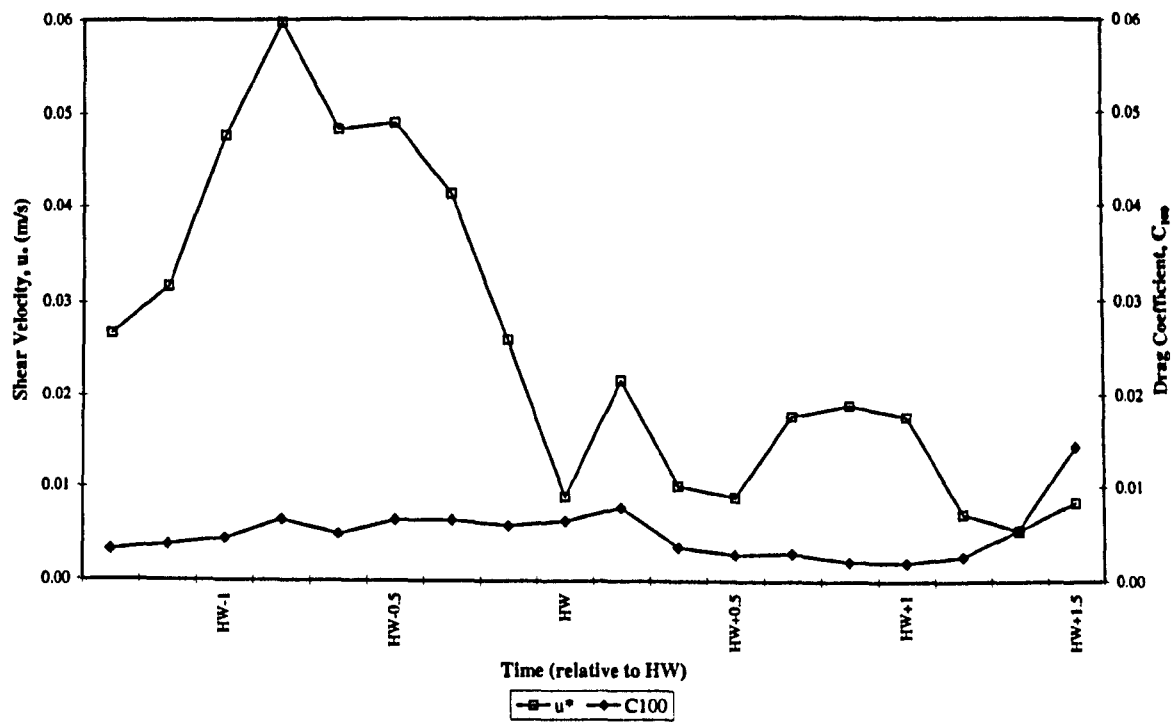
Figure 4-60 – u*, C_{100} – Station 5 (Springs)
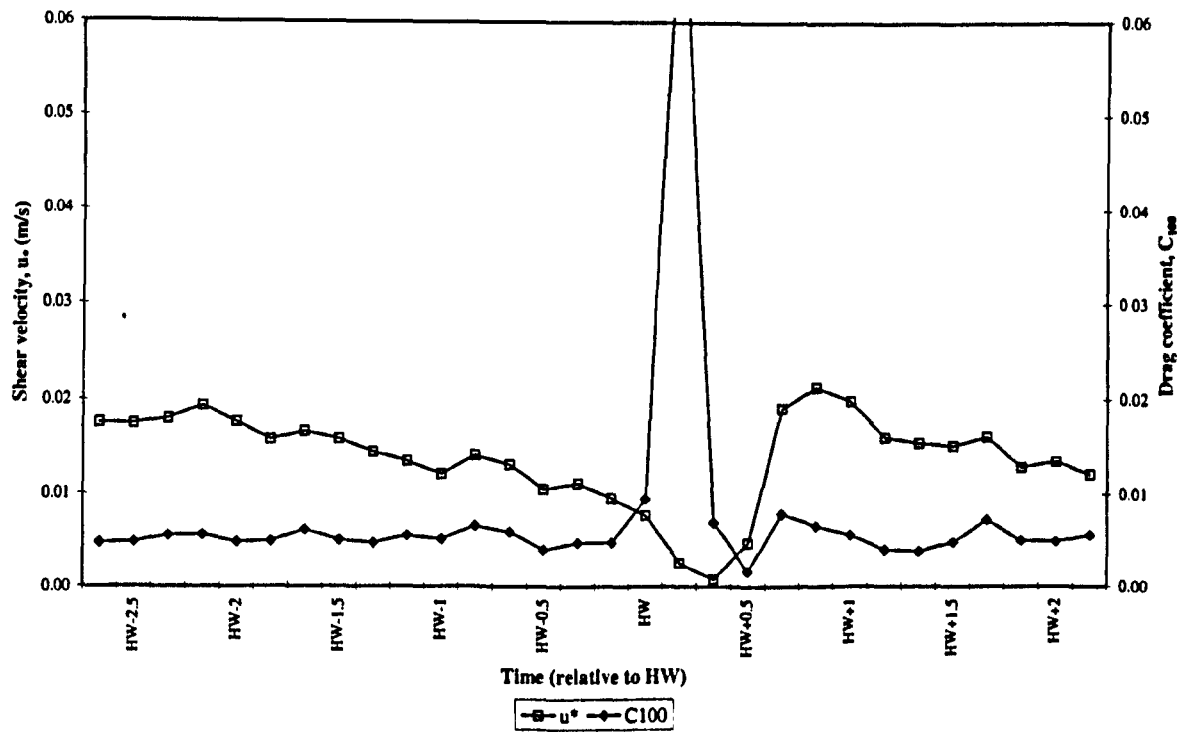
Figure 4-61 – u*, C_{100} – Station 1 (Neaps)
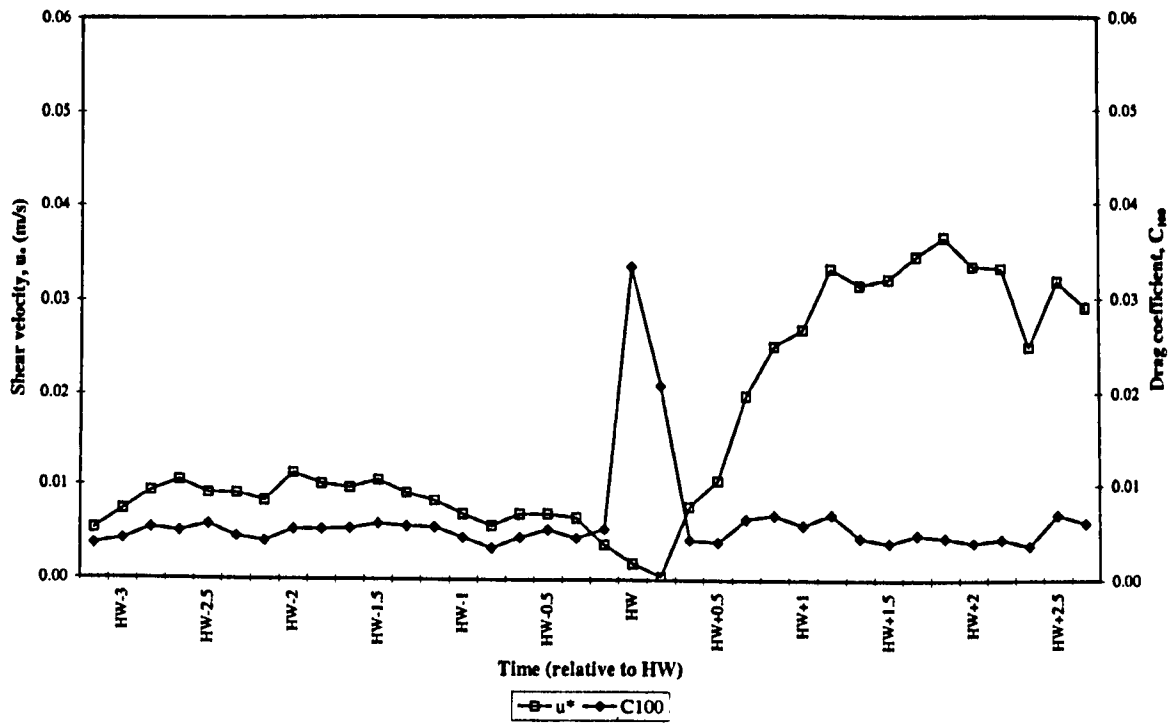
Figure 4-62 – u*, C_{100} – Station 3 (Neaps)
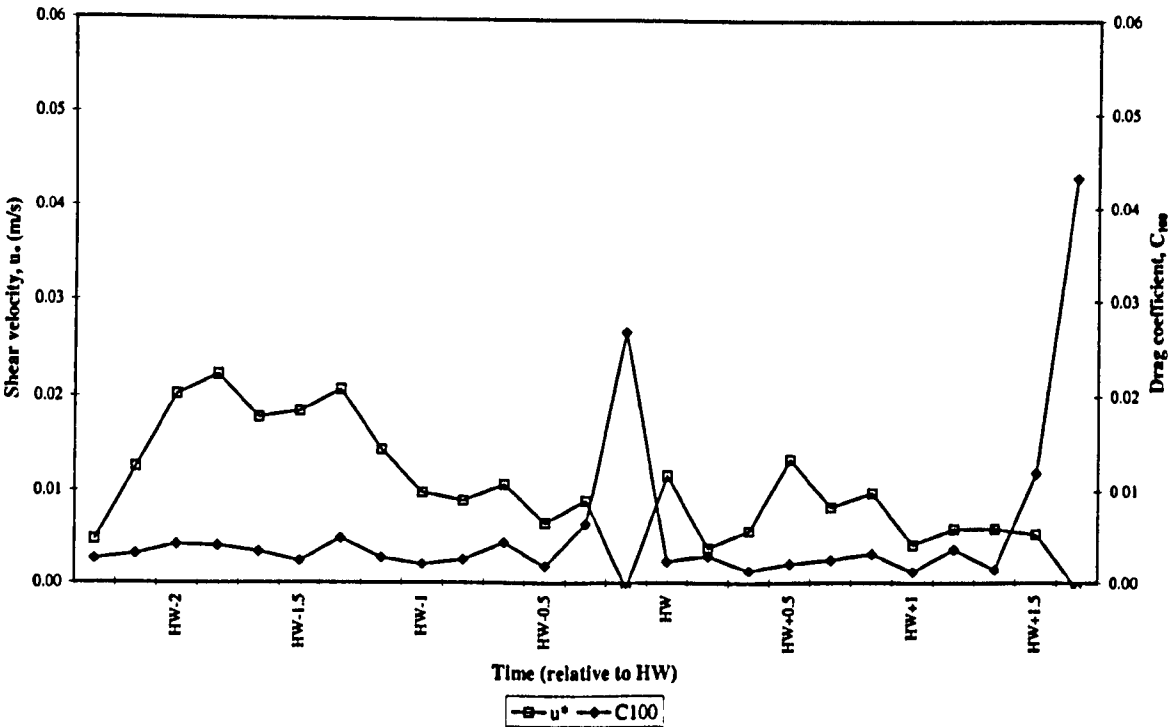
Figure 4-63 – u*, C_{100} – Station 5 (Neaps)

4.6.10   DISCUSSION OF FLUID FLOW PARAMETERS

The nature of flow in the boundary layer is a fundamental control on sediment transport since it is the shear stress generated by the flow that ultimately moves the sediment. The shear stress is in turn determined by the strength of the flow, together with the

sediment grain size and the topography, or roughness of the bed. It follows therefore, that the interaction between current flow strength and the bed roughness will determine the nature of the boundary layer and consequently the magnitude of bed stress.

It has already been discussed that the von Karman–Prandtl logarithmic profile, Equation (3:6), represents a straight line when u is plotted against $\ln z$ and therefore the shear velocity u_*, can be determined by using a least-squares fit of the logarithmic velocity profile. However, it was noted by Whitehouse (1995) that Equation (3:6) may be valid for heights of a few centimetres to several metres above the bed. He compared u_* values calculated using Equation (3:6) of the lowest three data points with that of the lowest six data points. Whereas all data points represent the same boundary layer characteristics, the lowest three heights should be more sensitive to changes in bed level. It was found that there were no systematic differences between u_* calculated from the lowest three data points and u_* calculated from lowest six data points. In Figure 4-64 and Figure 4-65 data from the lowest three data points are compared with data from all data points on springs and neaps at Station 1 (Dugmore Creek). The difference amounts to 64% on neaps and 71% on springs and contrary to Whitehouse's findings is considered significant in this case. The probable reason behind these differences is that Whitehouse did not use a fixed vertical array of current meters, as in this research; velocity profiles were compiled from vertical traverses with a single current meter and interpolated in time to provide quasi-simultaneous profiles.
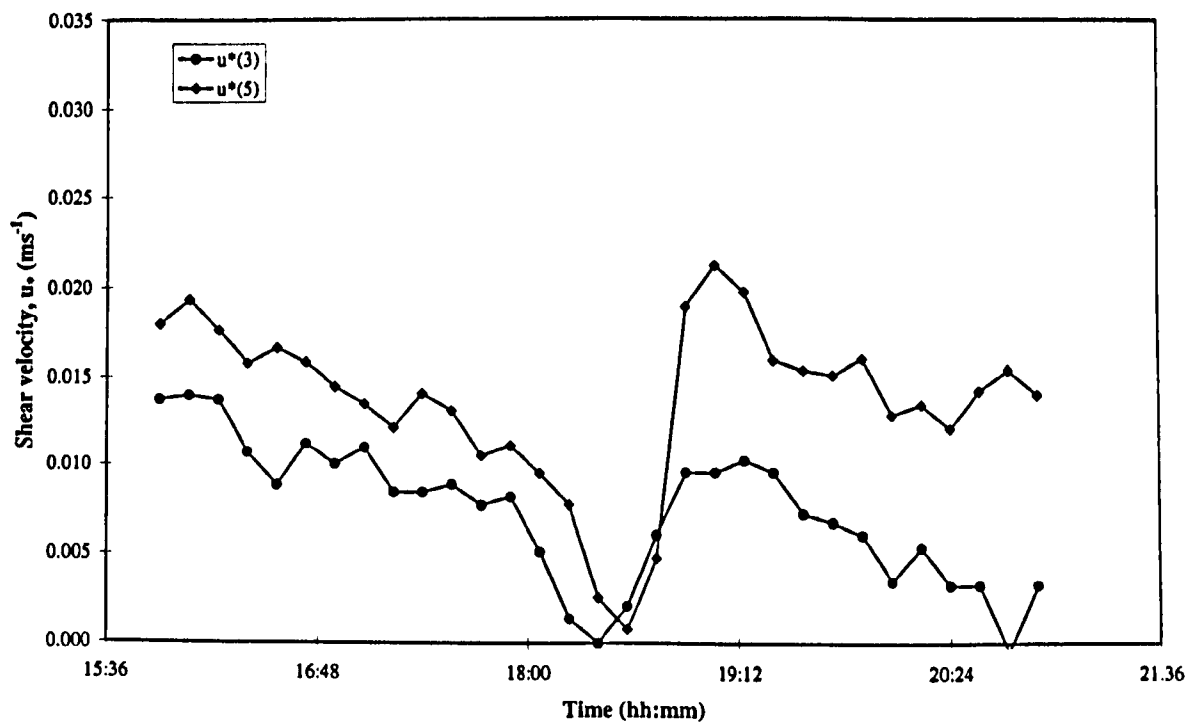
Figure 4-64 – Comparison of u∗(3) and u∗(5) Station 1 (Neaps).
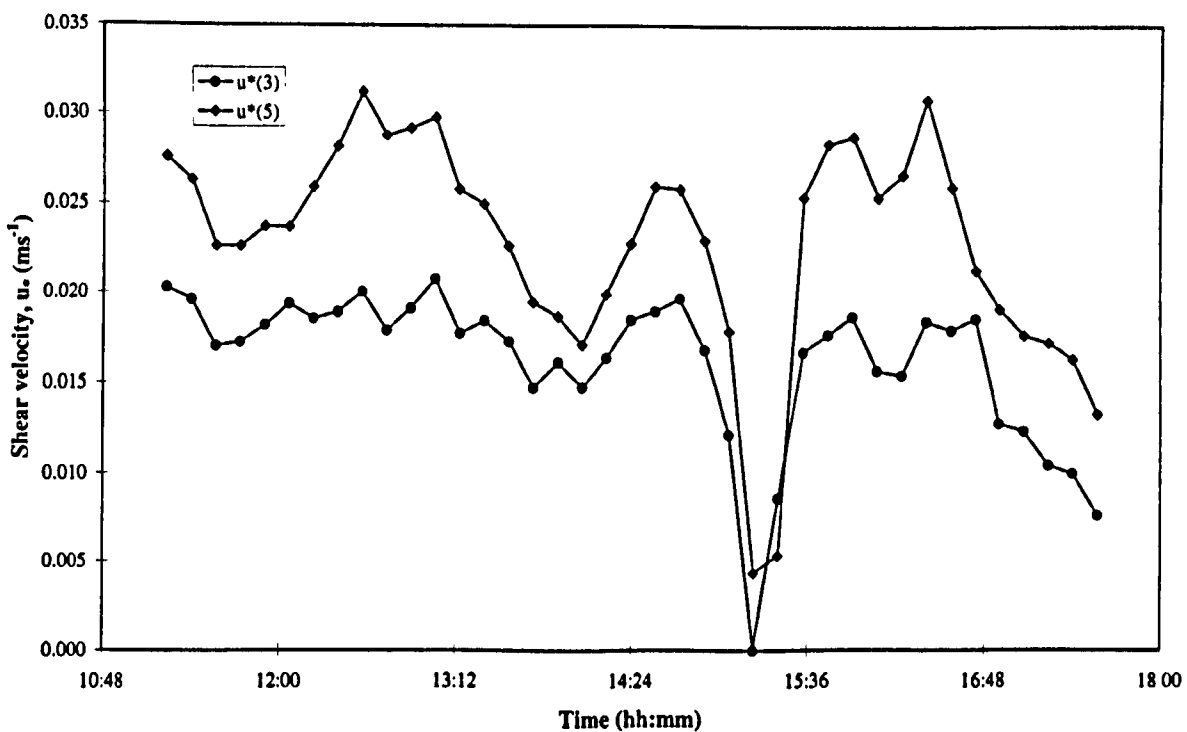
Figure 4-65 – Comparison of u∗ (3) and u∗(5) Station 1 (Springs)

It was discussed in Section 3.2.4 that in practice, real velocity profiles often show departures from a theoretical logarithmic form and the main disturbing effects on the form of the profile were: accelerating or decelerating flow; variations in upstream roughness; the presence of bedforms; stratification in the water column due to salinity or suspended sediment; errors in determining the zero datum of the current meter array;

and waves (Dyer, 1996). It can be seen that vestiges of most of these effects are apparent in the profiles studied in this research.

A critical influence on the form of the velocity profiles is the nature of the bed and the form of the downstream and upstream bottom topography. At each of the stations the morphology of the bed were markedly different. Station 1 is a marginal tidal flat site (D_{50} = 0.056 mm (ϕ4, coarse silt)) with a flat, relatively stable topography; Station 3, a central sand and gravel bank (D_{50} = 7.34 mm (-2.9ϕ, gravel)) with a convex topography both upstream and downstream; and Station 5, a marginal sand bank (D_{50} = 0.25 mm (2ϕ, medium to fine sand)) with a convex topography both upstream and downstream. (A full analysis of sediment grain size parameters is given in the following section, Section 5.) Because of the lateral variation in bed morphology, it follows that at each station the morphology will influence the velocity profiles in a different way.

Variations in shear velocity mirror both the variations in tidal current velocity throughout respective tidal cycles and the location across the mouth of the inlet. Higher shear velocity exerts a stronger influence and can lead to rougher sea bed topography and therefore, equate to higher boundary stresses and increased bed mobility. In general, on springs the roughness lengths appear to be greater on the flood than on the ebb implying that sediment dynamic processes may be weaker on the flood than the ebb. High r-squared values are recorded at all stages apart from around high water slack and just after high water.

Throughout the period of survey no significant mobile bedforms were observed at any station. Station 1 remained coarse silt, Station 3 continued to indicate an erosive surface, and the sand around Station 5 did not appear to change its form and there were no signs of basal scouring. It is concluded that any change in the form of the velocity profiles is due mainly to changes in density of the water column resulting from suspended sediment or due to the upstream bed morphology of the chosen station as discussed above.

5 Sediment

5.1 Introduction

This chapter is concerned with the collection, analysis and environmental interpretation of sediment within Hamford Water. It includes tidal and inter-tidal surficial sediment collected by grab sampler, and suspended particulate matter (SPM) assessed with a transmissometer.

5.2 Surficial Sediment

The principal objective is to determine the general sediment grain size characteristics and distribution of surficial sediments within the site and discuss the environment of deposition. The secondary objective is to present data for use in sediment transport formulae in Chapter 6 below and therefore assess rates of sediment transport and infer sediment transport pathways within the site. A basic principle is accepted in this study of sediment grain size: that any variations in the deposited sediment parameters are due mainly to hydrodynamic conditions operating in the embayment. However, it is also assumed that sediments deposited as part of sediment recharge schemes (as mentioned in Section 1) may influence the overall characteristics of some sediment samples. Generally, it is hypothesised that some major variations in characteristics may exist between the hydrodynamically calm interior of the embayment and the more turbulent hydrodynamics of the inlet throat region. A considerable amount of sedimentary information had already been gained from both published and grey literature (HR Wallingford, 1990; IECS, 1994, CCRU, *pers. comm.*) and this was accounted for when determining the sampling strategy. Unpublished grain size data is reproduced in Appendix B. It has also been assumed in this study that the source of the majority of the contemporary sediment in Hamford Water is marine: there being negligible fluvial input with which to supply terrestrial sediment.

5.2.1 DATA COLLECTION

Surficial sediment samples were collected from in and around Hamford Water in the summer of 1994. The sampling method adopted was a combination of systematic, random and clustered depending on the requirement. Systematic sampling based on the Ordnance Survey (OS) one-kilometre grid was conducted over Pye Sand and

Pennyhole Bay where samples could only be obtained using a boat. The OS grid was used because it enabled a systematic grid to be easily established and was easy to navigate to pre-determined positions using differential Global Positioning System (dGPS). Salt marsh was randomly sampled depending on access to the main areas of marsh. Clustered sampling was conducted at sites of current meter stations to provide suitable statistics for sediment transport calculations.

Samples were collected using either a hand operated grab or sampling ring. Sub-tidal and most intertidal samples were collected by boat using a van Veen-type hand operated grab, which collected about 1kg of wet sediment when fully loaded. The remaining inter-tidal and saltmarsh samples were collected using a 73 x 35mm sampling ring allowing collection of approximately 100g samples. The sampling ring consists of a 3mm-thick plastic ring 73mm in diameter and 35mm in height, bevelled at one end to produce a sharpened edge. It is pushed into the sediment to be sampled until flush with the surface and then the ring, plus sample, is removed with the help of a trowel. The location of all sample positions is illustrated in Figure 5-1.
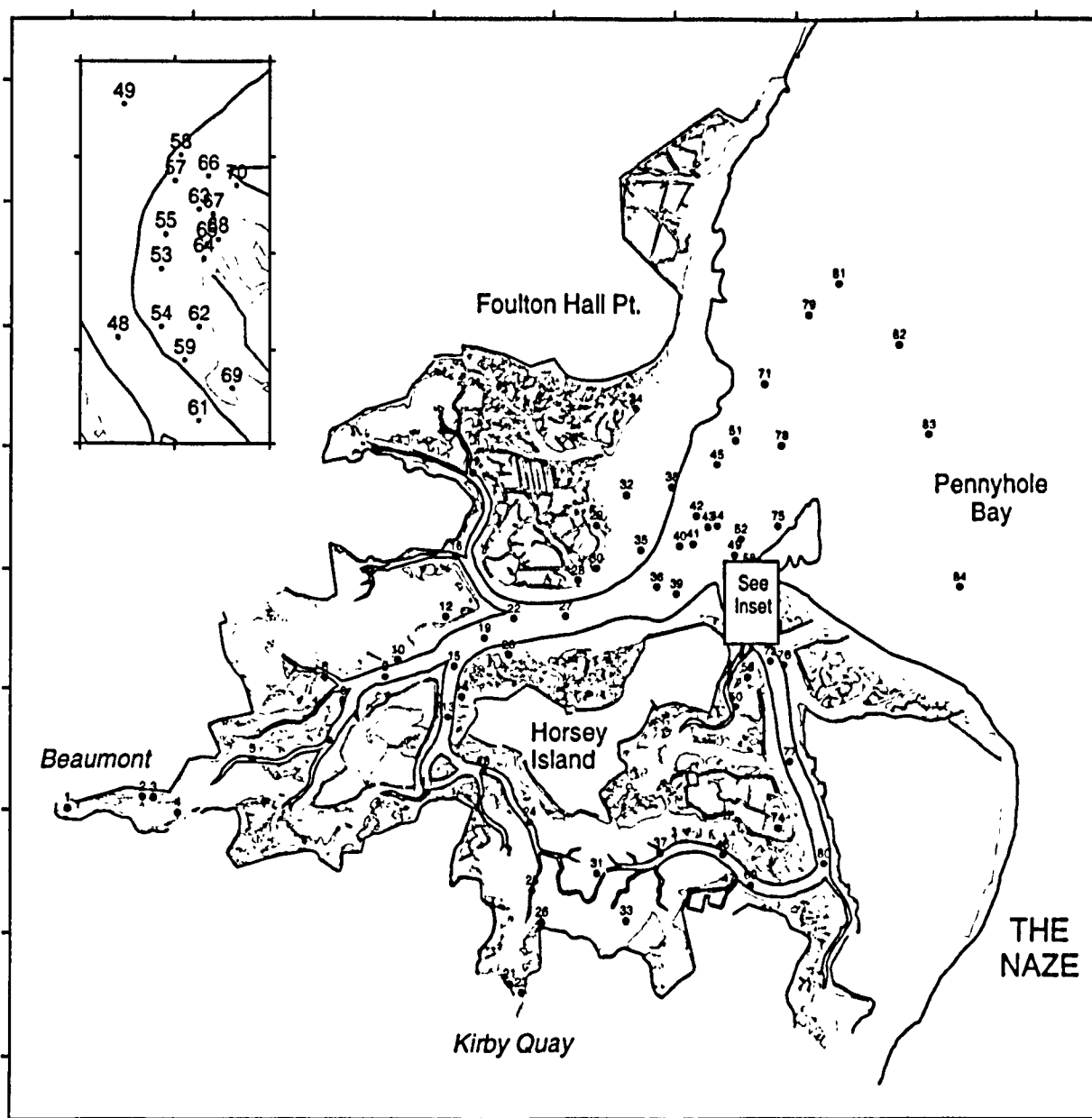
Figure 5-1 – Sediment Sample Locations.

5.2.2 GRAIN SIZE ANALYSIS

In the laboratory, saltmarsh samples were first separated from sub- and inter-tidal samples. Saltmarsh samples proved problematic: the presence of considerable amounts of macro-organic material made pre-treatment difficult. Large root fragments (>10mm length) were first picked from the sample by hand and the remaining material lightly pestled before treating with hydrogen peroxide to remove remaining organics. All samples, including sub- and inter-tidal samples, were then washed through a 63μm sieve with distilled water and the coarser than 63μm fraction placed in a pre-weighed evaporating basin and dried in an oven. The dried sand fraction was weighed, then split

to produce a sub-sample of approximately 100g which was then sieved through a set of sieves at ¼ phi intervals. Each size fraction was weighed cumulatively to 0.01g.

The finer than 63μm fraction was washed by centrifuging to remove salt. The sample was placed in a 1-litre centrifuge bottle, topped up with distilled water, shaken and centrifuged until the sediment separated from the water and collected at the bottom of the bottle. The supernatant was then poured off and the process repeated. The sample was washed from the centrifuge bottle using distilled water, air dried in a pre-weighed evaporating basin, and weighed. For those samples with only a small amount of fine material the washed sample was placed directly in an evaporating basin, dried in an oven at 105°C and weighed. This weight was then added to the pan fraction from the sieve analysis before grain size analysis.

Prior to SediGraph analysis, dried samples were first split to obtain sub-samples of approximately 3.0g, and then treated to remove organic matter. Samples with high organic carbon (>10%) or carbonate (>2%) can hinder proper dispersion of the sample (Coakley and Syvitski, 1991). Organic matter was removed by adding hydrogen peroxide (H_2O_2) and warming for at least 72 hours. Each 3.0g sample was made up with distilled water to obtain a suspension concentration of 0.02-0.1 g ml^{-1} (1% or 2% in aqueous suspensions). The samples were then dispersed using sodium hexametaphosphate and mechanically stirred before analysis by SediGraph.

The procedure adopted for SediGraph analysis is as described by the manufacturers handbook and discussed by Coakley and Syvitski (1991). The SediGraph method assumes that particles are dispersed in a fluid and settle in accordance with Stokes Law. The rate at which the particles fall below a certain depth in a sedimentation column is monitored using a collimated beam of x-rays, from which a measure of the cumulative size distribution of the sediments is obtained.

The combined sieve and SediGraph data were then entered into a spreadsheet to calculate statistical parameters by the method of moments after Lindholm (1987). The method of moments for detailed grain size analysis in muddy environments is, however, not satisfactory. McManus (1988) stresses that moment methods should not be applied unless all grain sizes present, lie within the defined grain size limits. If more

than 1% of the population is undefined, reliability of the moments method decreases and should not be used. Accepting these limitations, it was decided to use moment methods based on the original research requirement to only gather sufficient information to describe the general morphology of the site and provide grain size data for sediment transport computations.

5.3 Results from surficial grain size analysis

The results from moments analysis together with percentages of sand, silt and clay are tabulated and presented in Appendix B. As mentioned above, the primary aim of grain size analysis in this study is to provide an environmental interpretation of the grain size characteristics and give some idea about their provenance. In addition, relating the grain size distribution to the fluid flow relies on a definition of the ways in which sediment grains are transported (Dyer, 1986). The grain size distribution is, therefore, an essential property for assessing the likely behaviour of the grains under fluid forces (McCave and Syvitski, 1991) and as such is a necessary precursor to the following section on Sediment Transport.

The percentages of sand, silt and clay are plotted on a traditional triangular diagram after Shepard (1954) (Figure 5-2) and on a modified form by Pejrup (1988) (Figure 5-4). Classification of estuarine sediments by means of statistical parameters derived from grain size distributions is usually hampered by large percentages of clay (Pejrup, 1988). Estuarine samples are typically multimodal and triangular diagrams based on sand, silt and clay content are often used which forms a means of comparative description and can illustrate trends in suites of samples from particular environments (Dyer, 1986). Shepard's diagram is often used to classify sediments and to distinguish different sedimentary facies from estuarine environments (*see* for example, Evans, 1965). Often, however, samples from single facies are clustered in ellipses in triangular diagrams but the long axes of the ellipses are rarely parallel to any lines in a traditional Shepard–type diagram. The diagram is not best suited for separating the different estuarine depositional facies (Pejrup, 1988).
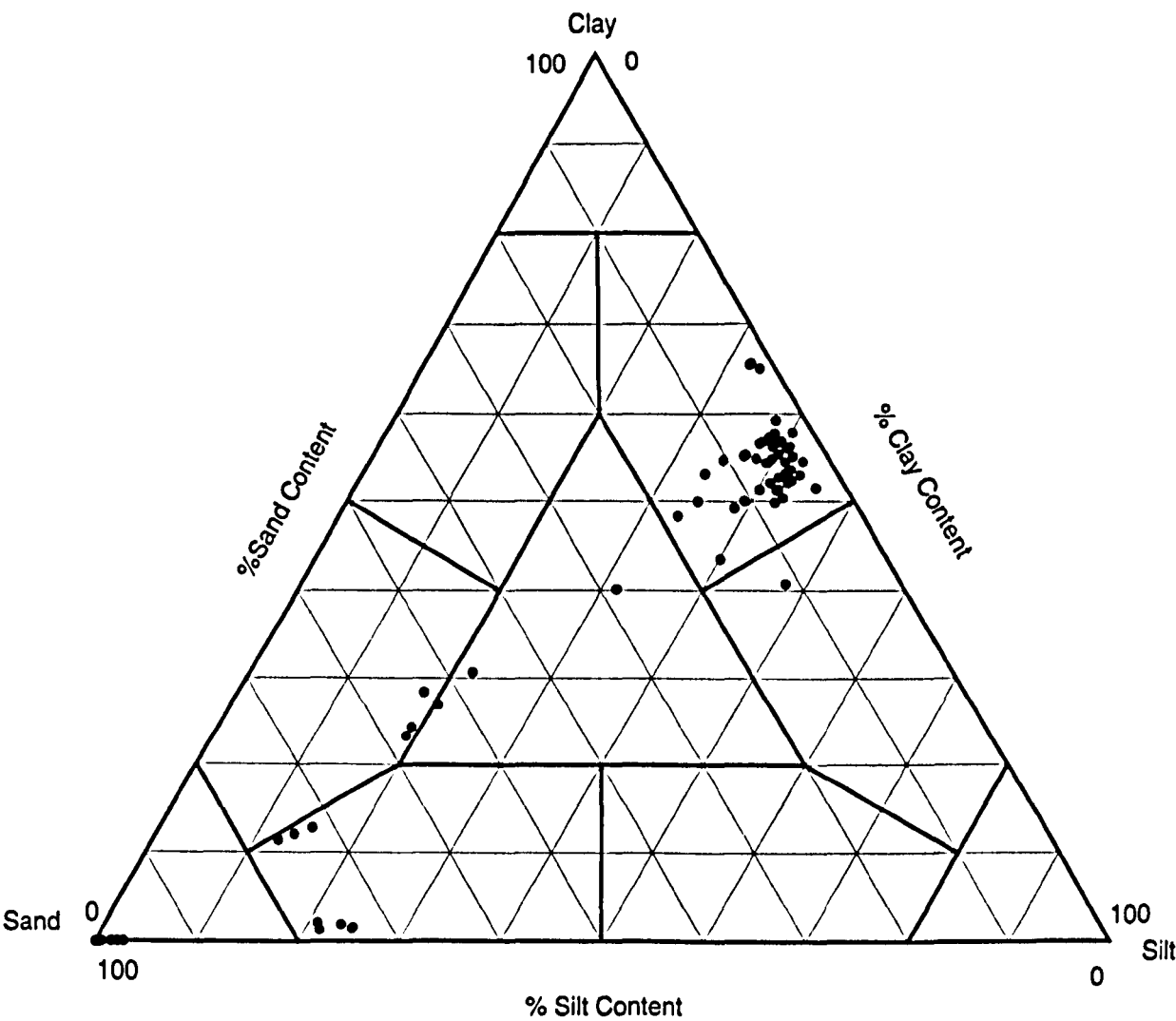
Figure 5-2 – Hamford Water sediment data plotted on a Shepard triangular diagram.
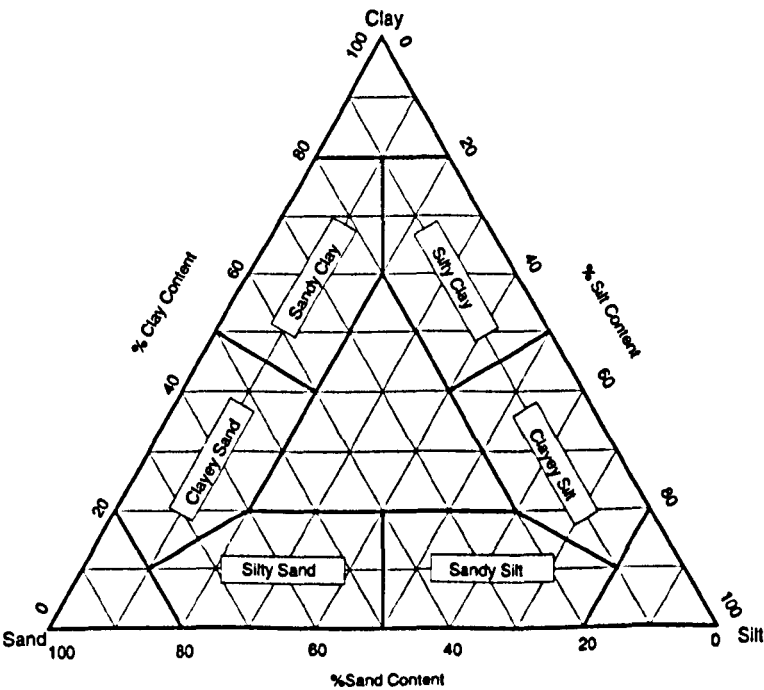
Figure 5-3 – Triangular diagram for classification of sediments (after Shepard (1954)).
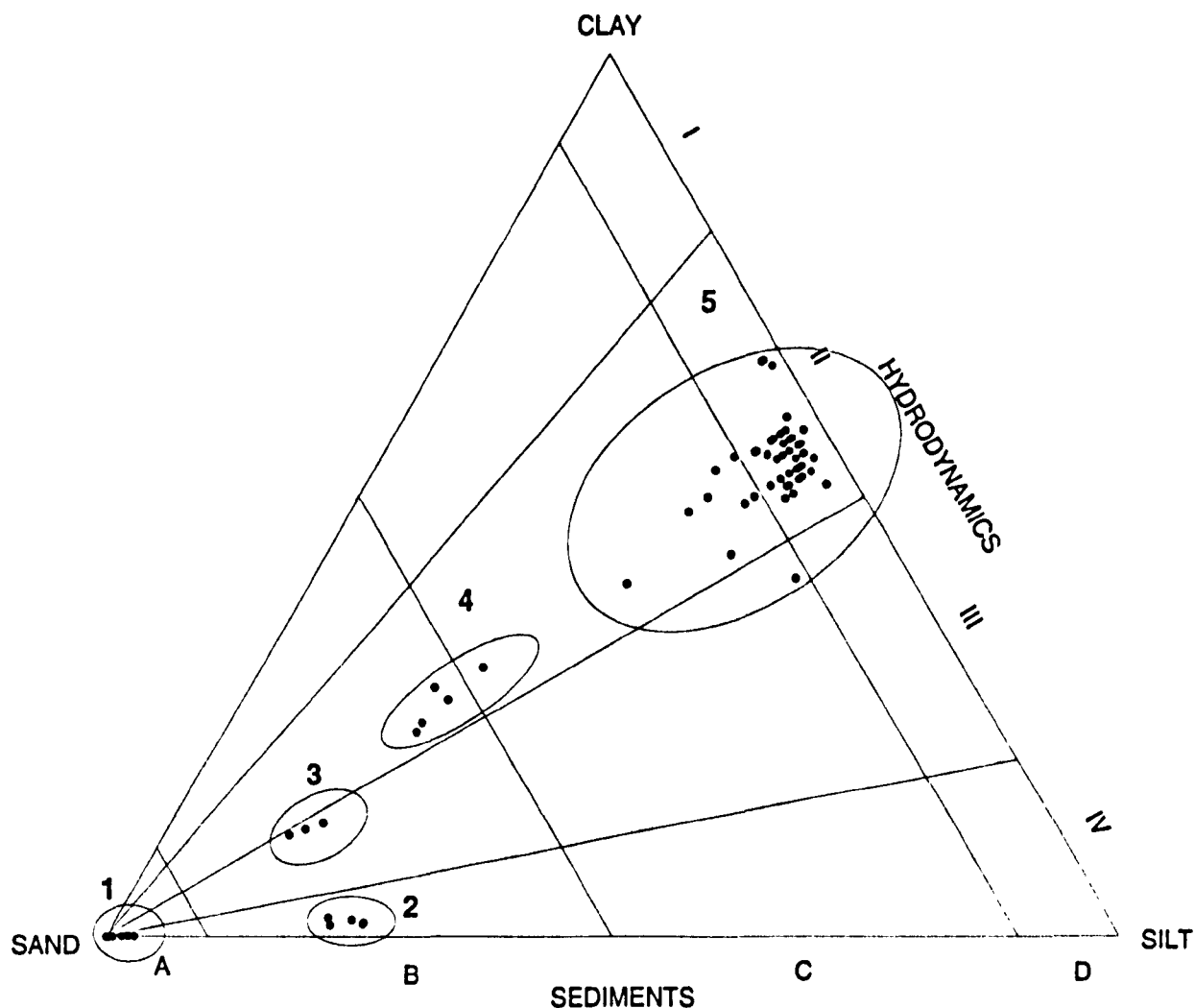
Figure 5-4 – Hamford Water sediment data plotted on a Pejrup triangular diagram.

In Pejrup's diagram (Figure 5-4) the hydrodynamic conditions of the depositional environment are described by the percentage of clay in the mud fraction; sections I to IV reflect increasingly "violent" hydrodynamic conditions. The sediments are classified according to their sand content into four sections, A to D. The triangle is thus divided into 16 groups, each labelled by a letter and a number. For example, group C-III represents sediments containing between 50% and 10% sand deposited under rather violent conditions (Pejrup, 1988). Because of the predominantly bimodal nature of the majority of the Hamford Water samples the method of Pejrup (1988) has been adopted in this research to interpret the distribution of surficial sediment.

On the Shepard diagram most samples plot in the silty clay and on the border between clayey sand and silty sand. On the Pejrup diagram, most samples plot within hydrodynamic section II indicating relatively calm hydrodynamic conditions. However, there are clearly a number of sub-groups within the spread of data (ellipses

1 to 5 in Figure 5-4). Figure 5-5 to Figure 5-9 are plots of cumulative weight percent and weight percent histograms for the 5 ellipses identified from the Pejrup diagram (Figure 5-4).
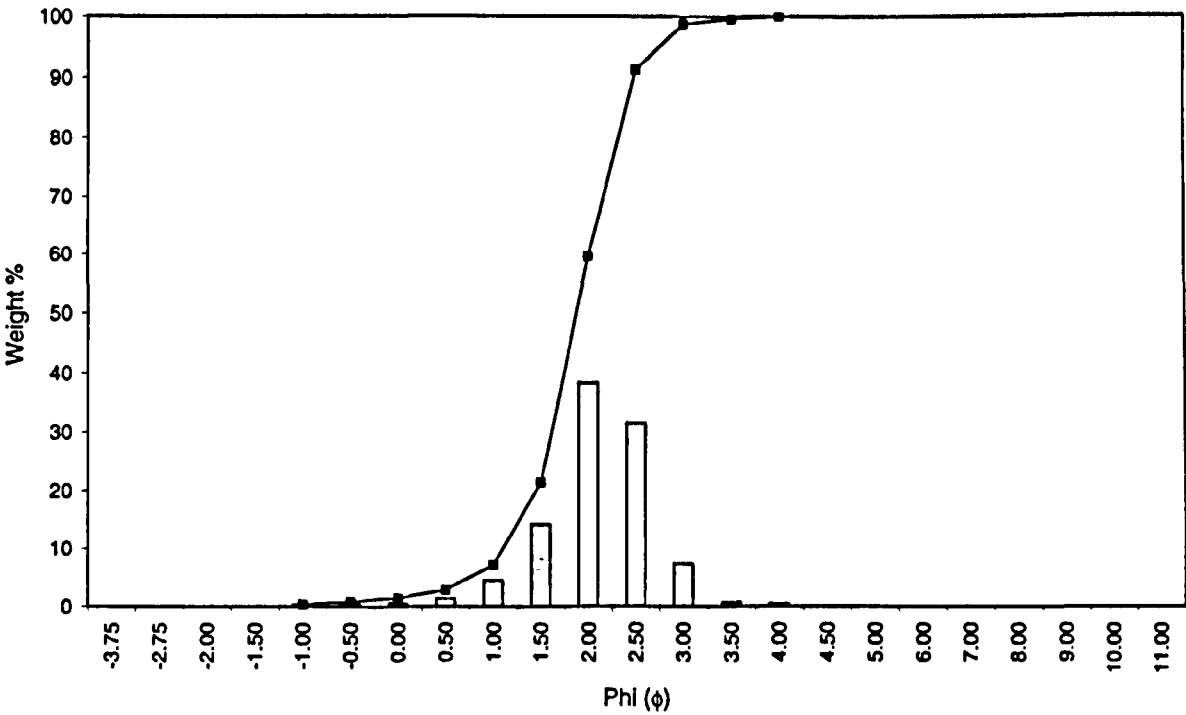
Figure 5-5 – Cumulative weight % curve and weight % histogram for Ellipse 1.
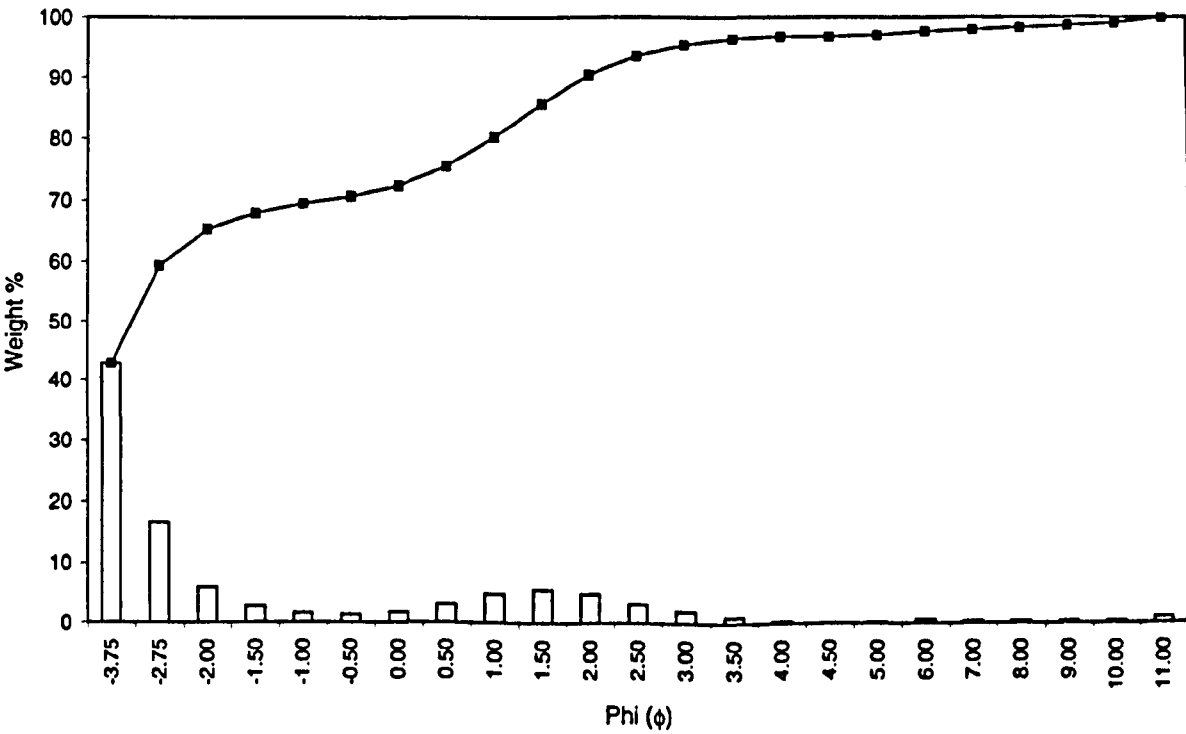
Figure 5-6 – Cumulative weight % curve and weight % histogram for Ellipse 2.
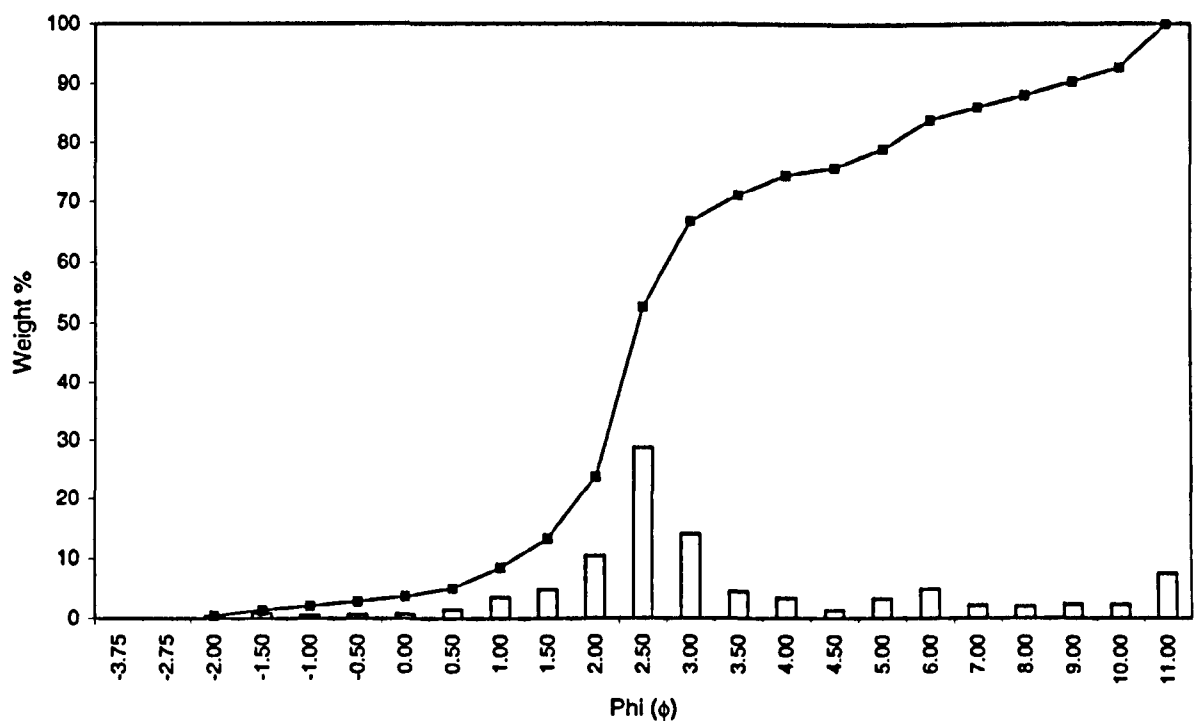
Figure 5-7 – Cumulative weight % curve and weight % histogram for Ellipse 3.
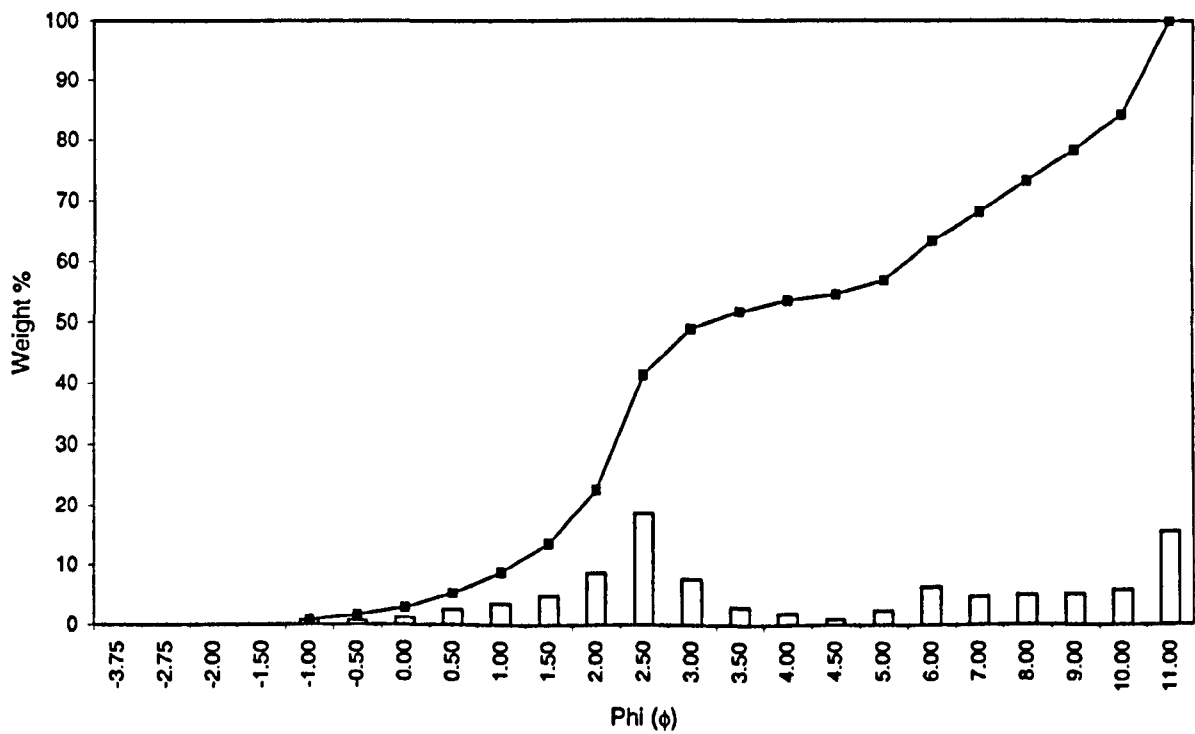
Figure 5-8 – Cumulative weight % curve and weight % histogram for Ellipse 4.
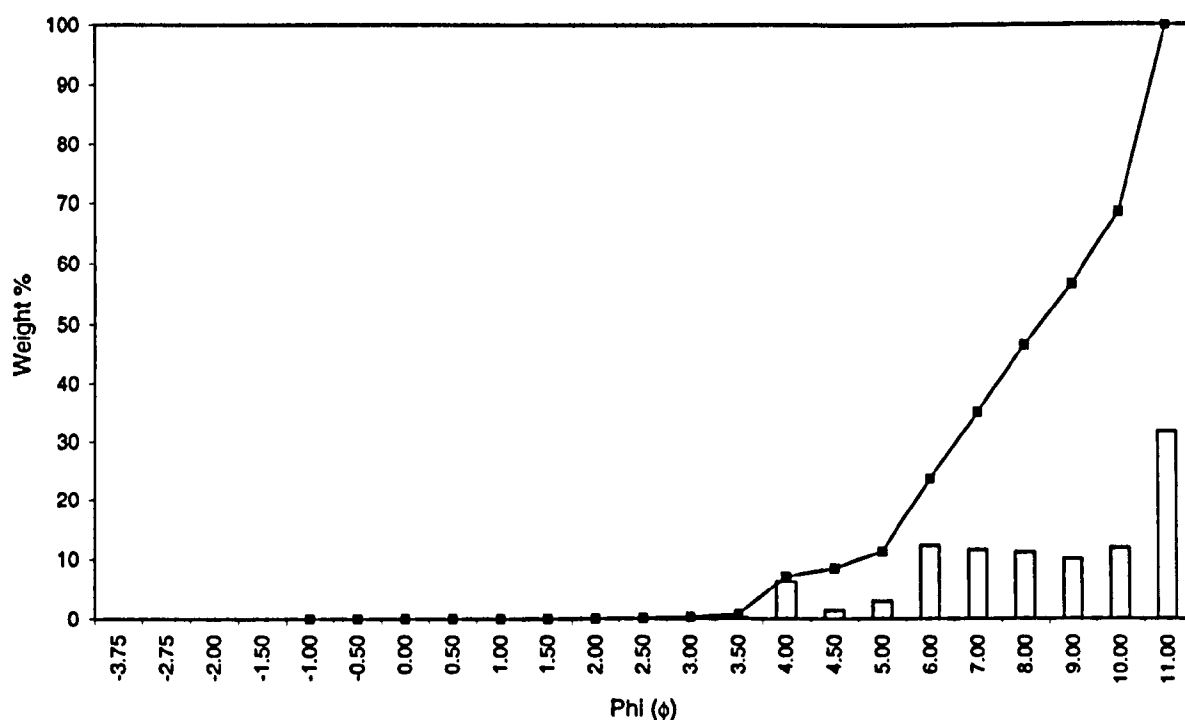
Figure 5-9 -- Cumulative weight % curve and weight % histogram for Ellipse 5.

Ellipse-1 (Figure 5-5) represents the beach, and ebb-delta, well sorted sands. They all fall within the violent hydrodynamic section IV. Ellipse-2 (Figure 5-6) also falls in section IV but are all bimodal, poorly sorted samples representing erosive areas of Pye Sand and Stone Point. Ellipse-3 (Figure 5-7) represents bimodal, poorly sorted silty channel sediments adjacent to the main areas represented by Ellipse-2. Ellipse-4 (Figure 5-8) and Ellipse-5 (Figure 5-9) represent the majority of the Hamford Water sediments: poorly sorted, bimodal silty clays deposited in increasingly calm hydrodynamic conditions. Figure 5-10 summarises the cumulative frequency distribution curves for each ellipse. The classification of Hamford Water sediments using the Pejrup triangular diagram effectively illustrates both the two main hydrodynamic features of Hamford Water: a calm, sheltered interior embayment separated by a very dynamic inlet throat, and the various sub-environments related to the different hydrodynamic conditions of deposition.
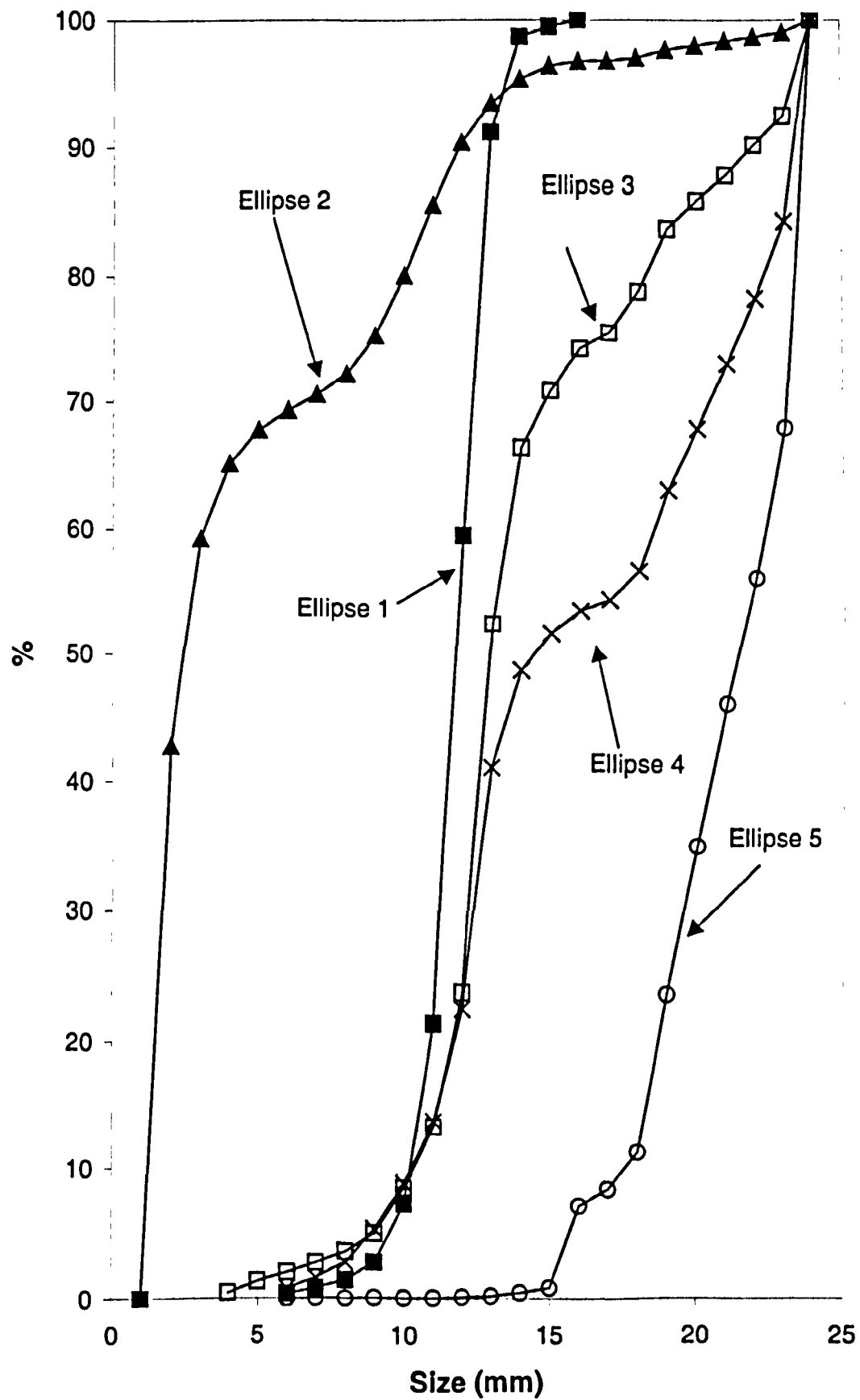
Figure 5-10 – Cumulative frequency distribution curves for each ellipse.
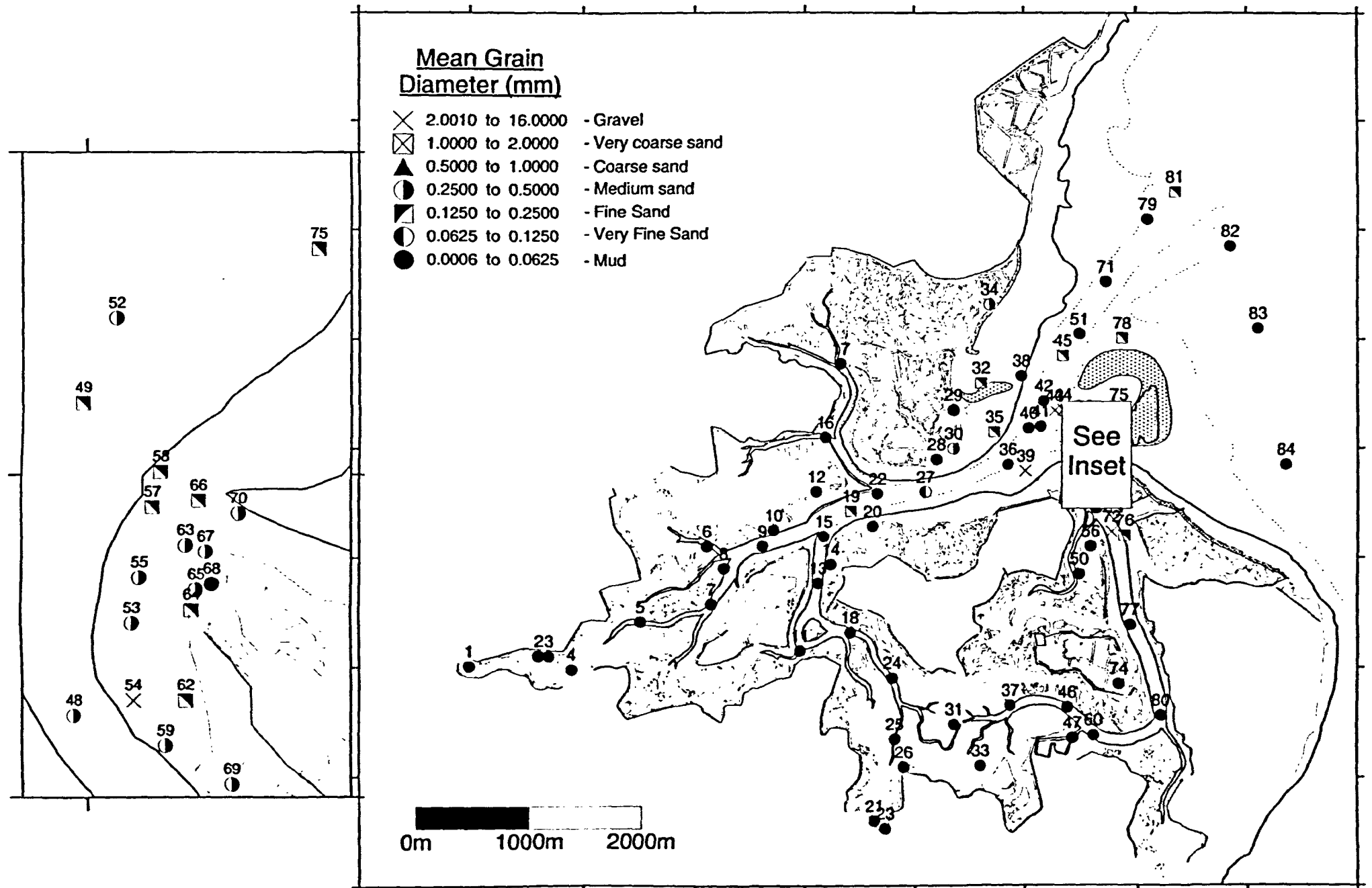
Figure 5-11 – Sediment Distribution map – mean grain size (mm)

5.4 Environmental Interpretation

Figure 5-11 is a map illustrating the mean grain size in millimetres of each sample, the numbers refer to the sample numbers as tabulated in Appendix B. It also shows the main sedimentary features of the site compiled from an analysis of the grain size data and taking into account the ellipses identified from the Pejrup diagram (Figure 5-4), from which various sedimentary regimes can be isolated in Hamford Water. The majority of the saltmarsh, mudflats and subtidal channels in the interior of the embayment consist of mud (<63μm). However, at the inlet entrance and on the ebb delta of Pye Sand the sediment is predominantly sand. However, it was noted during sampling excursions that in places the sand is often only to a depth of approximately 10cm, below which is hard clay characteristic of the London clay (the actual existence of London clay was not confirmed by any analysis). Pye Sand, in particular, can be walked over at low water springs and consists of a layer of fine sand overlying the same clay in depths ranging from 0 to 60 cm and characterised by wave- and current-induced sand ripples. Where the clay is exposed, the surface is covered with a layer of poorly sorted sands and gravels embedded in the clay together with numerous protruding tubes of the tube-worm *Pectinaria belgica*. The sand fraction is evident on the north coast extending south from Harwich to Irlam's Beach, across the entrance of Dugmore Creek, and towards Pewit Island where a bank of sand extends about 150m out into Hamford Water in the form of a recurved spit. To the west of this spit there is no sand. In effect, the width of sand on the north shore beach increases in width from Blackman's Head to Pewit Island. On the south side, the same sand fraction extends from the northern tip of The Naze north-west to Stone Point and around into Walton Channel where the sand fraction stops abruptly. This sand/mud line shows a clear distinction between the different energy regimes of a tide-dominated, estuarine Hamford Water region and a wave-dominated Pye Sand region.

The north shore from Irlam's Beach to Blackman's Point was not sampled in the research but samples taken by HR Wallingford (1990) mainly fall within the very fine silt/clay grade and show a tendency to fine northwards and for sorting to also increase northwards. This was postulated to indicate a northwards moving sediment transport path, although this pattern may be complicated by the relatively low beach levels and the associated exposure of relic gravels. The relevance of a northward fining of

sediment on the north shore with regard to theoretical sediment transport paths at the margins of ebb-dominated tidal inlets is discussed further in Chapter 9.

5.5 Suspended Sediment

5.5.1 DATA COLLECTION

Measurement of suspended sediment was carried out using a *Sea Technologies Inc.* transmissometer interfaced to an *Applied Microsytems Limited* (AML) STD–12 mini-Salinity–Temperature–Depth probe (STD). The STD–12 is a self-logging instrument capable of recording 8-data per second and can be set to record at pre-set depth or time increments. The Sea Tech transmissometer is a compatible unit and was coupled to the STD during the measurement. The accuracy of the transmissometer is ± 0.5% of the transmitted beam. The AML/Transmissometer was deployed for both the combined survey (*see* Section 4.4.2.2 above) and two spatial suspended surveys. For all surveys the method involved lowering and raising the STD–Transmissometer over the side of an inflatable boat at each allotted station at about $0.3m \ s^{-1}$. The instrument was set to log at 10-second intervals for all surveys. Locations of both spring and neap spatial suspended sediment surveys are shown in Figure 5-12. The same cast locations were used for both springs and neaps.

In order to calibrate the transmissometer, occasional water samples were collected in one-litre bottles simultaneously with transmissometer casts for determination of suspended sediment concentration by gravimetric analysis. In the laboratory the samples were filtered through pre-weighed Whatman GF/C glass microfibre filters (measured in grams, to 5 decimal places), washed through with distilled water and dried overnight in an oven at 60°C. The dried filters plus sediment were re-weighed and converted to weight by volume filtered. The final value was recorded in milligrams per litre $(mg \ l^{-1})$. Blank filters were occasionally washed, dried and weighed with the sediment-laden filters to assess any weighing errors. Weighing differences amounted to no more than 0.2%.
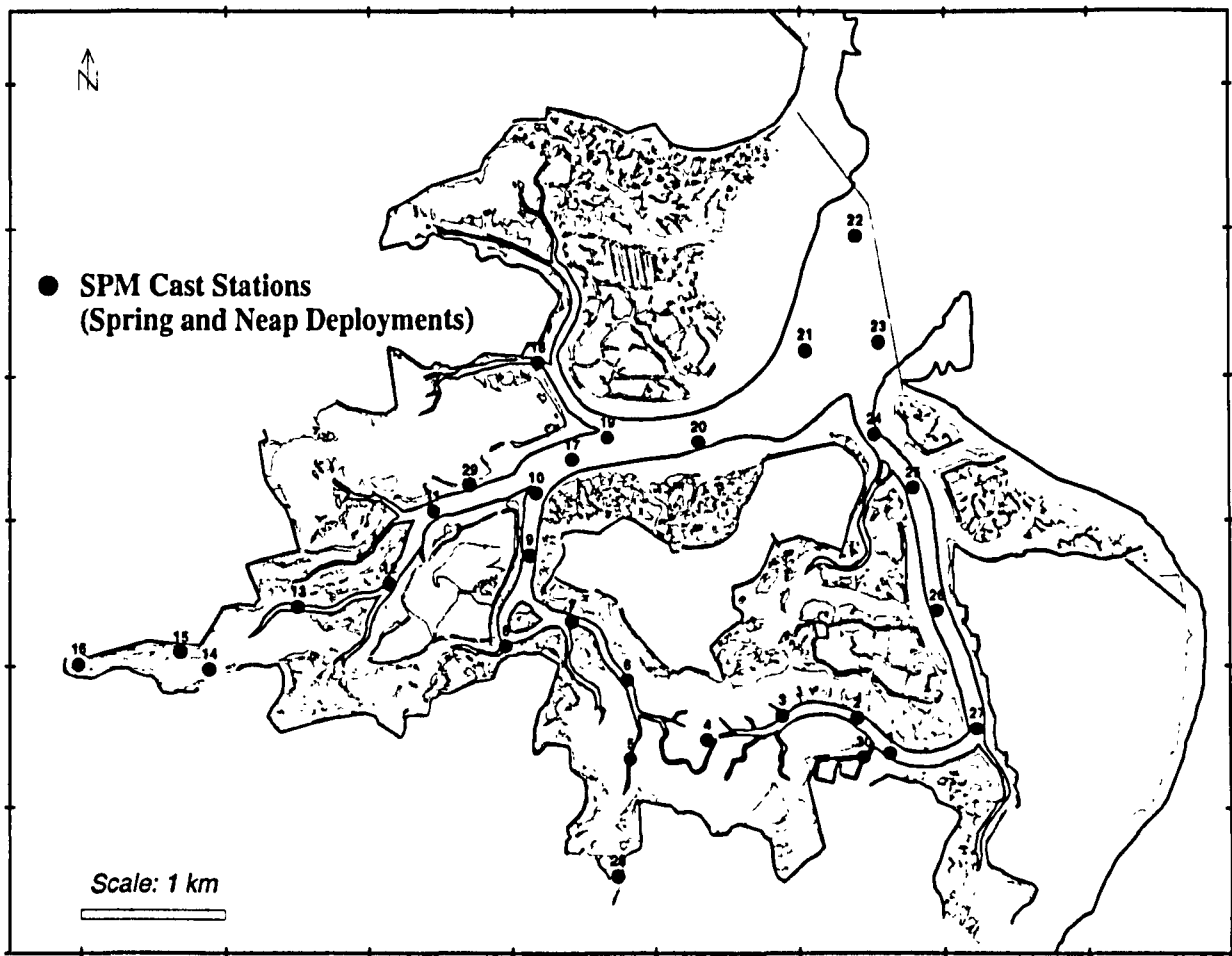
Figure 5-12 – Spatial Suspended Sediment Survey Cast Locations

5.5.2   RESULTS

Raw transmissometer data were de-spiked and split into individual casts by means of a BASIC program, GENSPLIT.BAS (S.E. Jones, *pers. com.*). Output from the program is in the form of averaged values of temperature, salinity and beam transmission (%) for 0.5m depth intervals. The conversion of % transmission T, to beam attenuation coefficient C, is by the following relationship:

$$C = \frac{-1}{L}(\ln T) \qquad (5:1$$

where L is the path length of the transmissometer in metres. Thus for the 10cm path length transmissometer used for this research:

$$C = \frac{-1}{0.1}(\ln T) = -10\ln\left(\frac{T\%}{100}\right) \qquad (5:2$$

Thus, a calibration curve of C against measured values of suspended sediment, as determined from gravimetric analysis can be produced. Calibration was carried out for

each deployment of the transmissometer and separate calibration curves produced from the linear regression analysis of beam attenuation and suspended sediment concentration. Calibration results are tabulated in Table 5-1 and curves for individual deployments and raw data are contained in Appendix F.

Table 5-1 – Transmissometer calibration analysis

Deployment	Regression Equation	r^2	n
Spring Flood	y = 0.455x + 0.0009	0.9571	9
Spring Ebb	y = 0.2419x + 4.8158	0.9807	11
Neap Flood	y = 0.3812x + 1.7131	0.8728	10
Neap Ebb	y = 0.3014x + 3.2185	0.7536	7
Spring Spatial	y = 0.2565x + 11.228	0.935	12
Neap Spatial	y = 0.3741x + 2.3627	0.5627	11

5.5.2.1 Lateral SPM variation

Figure 5-13 and Figure 5-14 are plots of neap tide suspended sediment concentration across the inlet throat in mg l^{-1}, and Figure 5-15 is a plot of neap SPM depth-time distribution. The first two plots appear to contradict expected assumptions about estuarine suspended sediments. If a distinction is made between wash load and bed-material (McCave, 1979), the former being fine material nearly always in suspension and the latter being coarser material transported along the bed given sufficient velocity; it may be expected that the highest concentrations of suspended sediment, both fine and coarse, would occur towards the bed. Apart from B, C and D at Station 1, SPM concentrations reduce towards the bed and at the channel margins. The anomaly can be attributed to this method of data presentation. At Station 2 in particular the data points do not reach the bed and therefore the model has assumed an extrapolation that appears not to represent an increase in SPM that may be expected. Notwithstanding model limitations, maximum SPM values of up to 35 mg l^{-1} on the flood occur around Station 1, 1.5 hours before high water. This does not coincide with points of maximum flow velocity as portrayed in Section 4.4, indicating that wave action may be causing suspension of material over the mudflats around Station 1. On the ebb tide SPM values vary between 20 and 30 mg l^{-1} until after 1.5 hours after high water. Between 3 and 5

hours after high water values increase markedly at the bottom of Pye Channel and around Station 1 with values exceeding 100 mg l^{-1}.

A clearer picture of SPM variation is obtained from Figure 5-15 which shows the SPM depth-time distribution for the whole tidal cycle from which the conclusion can be drawn that the depth-time occurrences of maximum SPM values at each station rarely coincide. At Station 1 maximum SPM occurs just after and just before low water throughout the water column; at Station 2, near the bed at half-ebb; at Station 3, 3 hours before high water and between 1 and 3 hours after; and Station 4, 2.5-3 hours after high water.
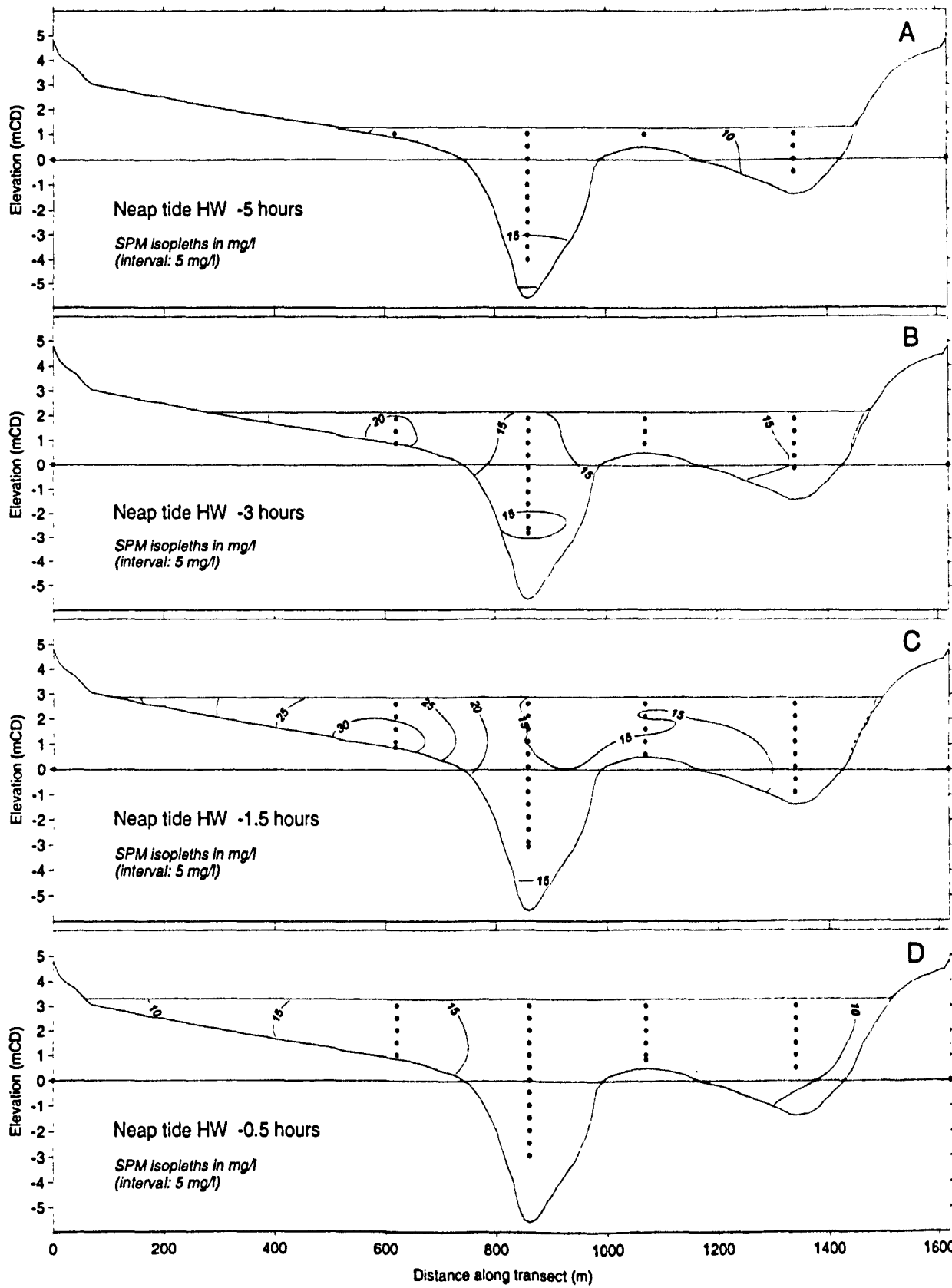
Figure 5-13 – Inlet cross-sectional SPM profiles – Neap flood tide (June 1995)
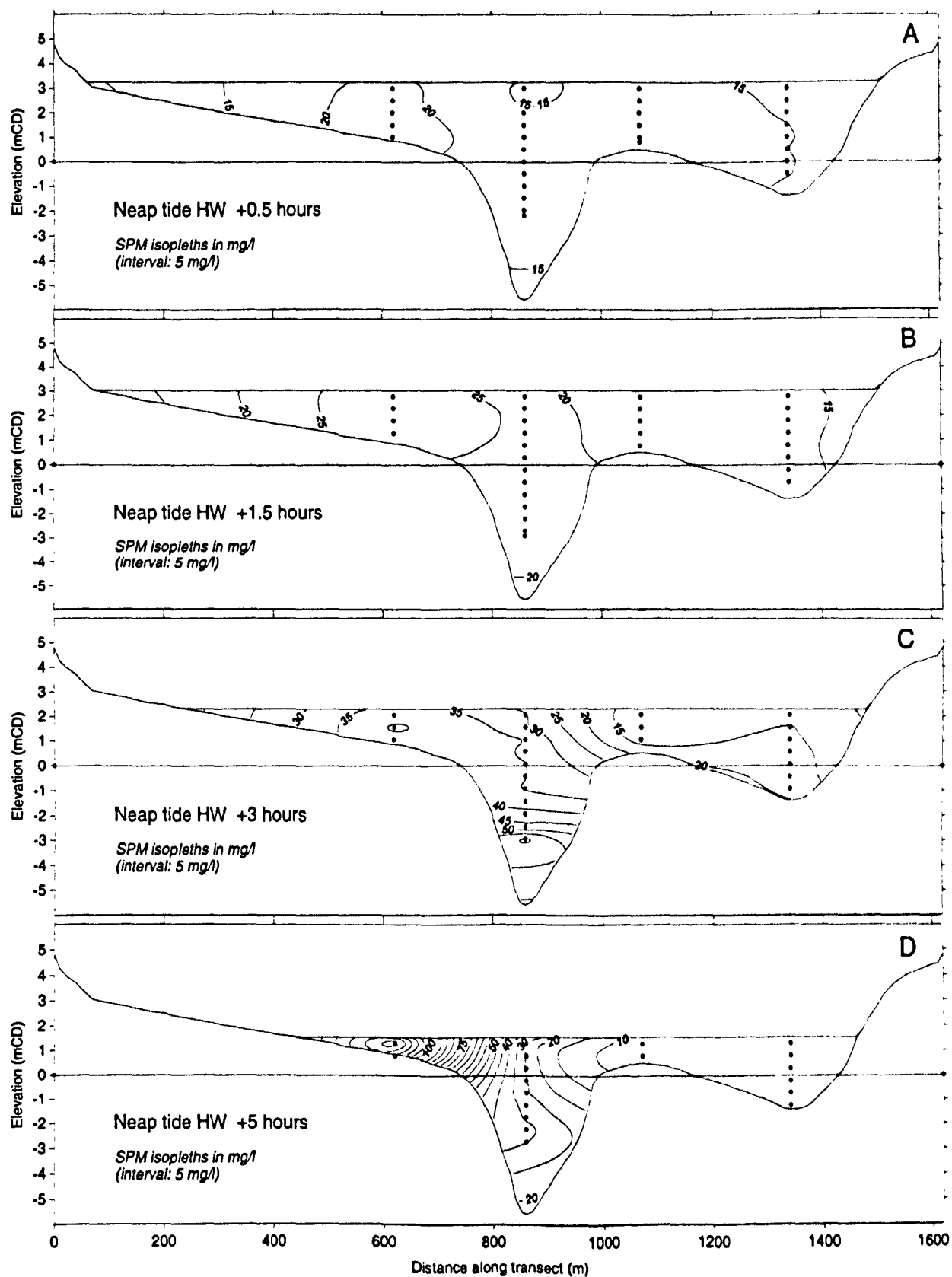
Figure 5-14 – Inlet cross-sectional SPM profiles – Neap ebb tide (June 1995)
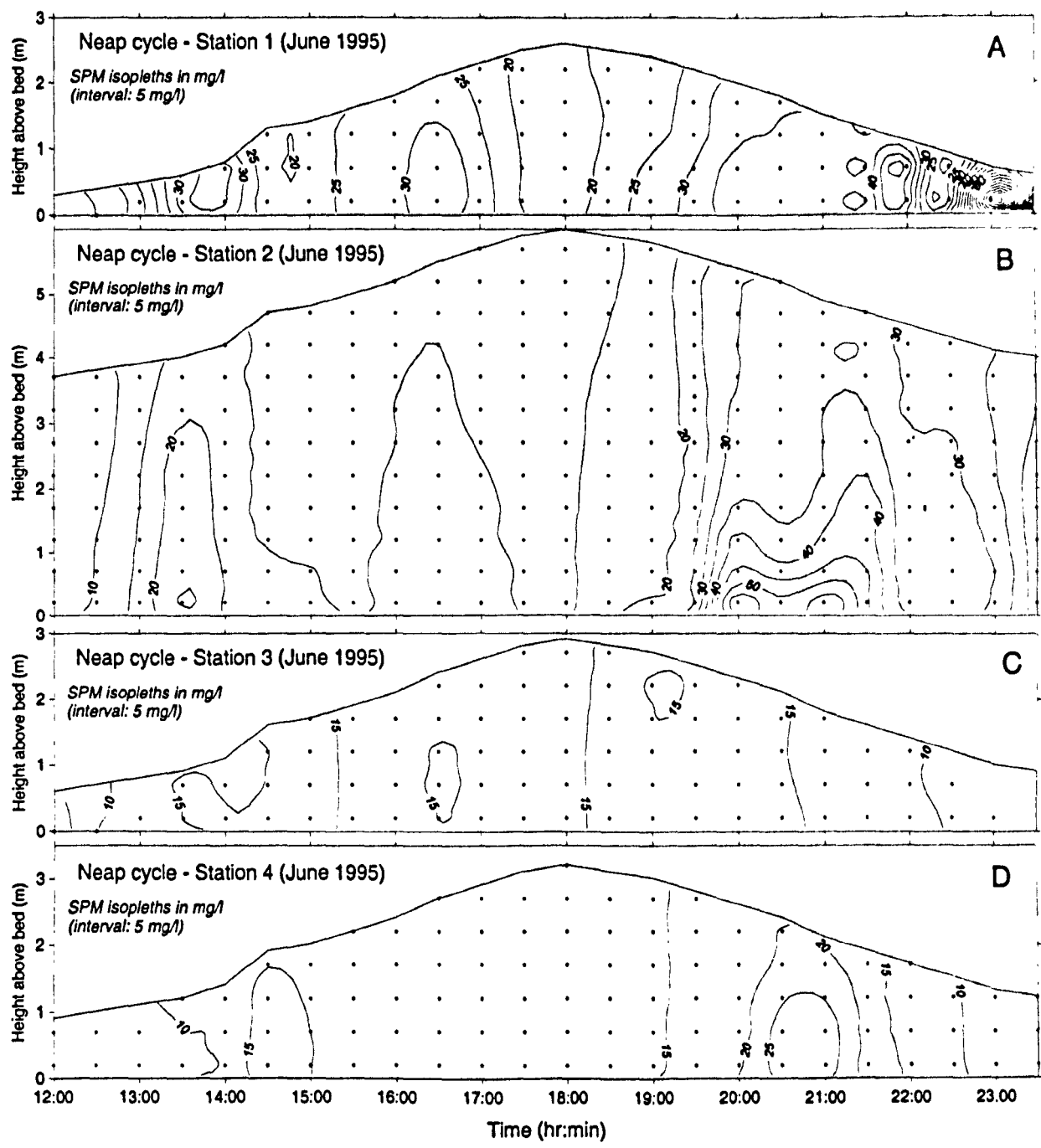
Figure 5-15 – Neap tide SPM-depth-time distribution – Stations 1 to 4.

Figure 5-16 and Figure 5-17 are spring tide plots of suspended sediment concentration across the inlet throat in mg l^{-1}, and Figure 5-18 is a plot of spring SPM depth-time distribution. As with the neap cycle the accurate representation of SPM concentrations near the bed is limited by the method of presentation. Nevertheless, it is evident that SPM values are considerably greater during springs than neaps with the highest values (>60 mg l^{-1}) on the flood occurring around Stations 1 and 3, at 1.5 and 0.5 hours before high water. On the ebb the highest values are concentrated around Stations 1 and 3 until 5 hours after high water.

In Figure 5-18 the maximum SPM values occur about 1 hour after high water at Stations 1, 2 and 4 but not at Station 3 which has maximum values between 3 and 2 hours before high water and a minor peak 2.5 hours after.
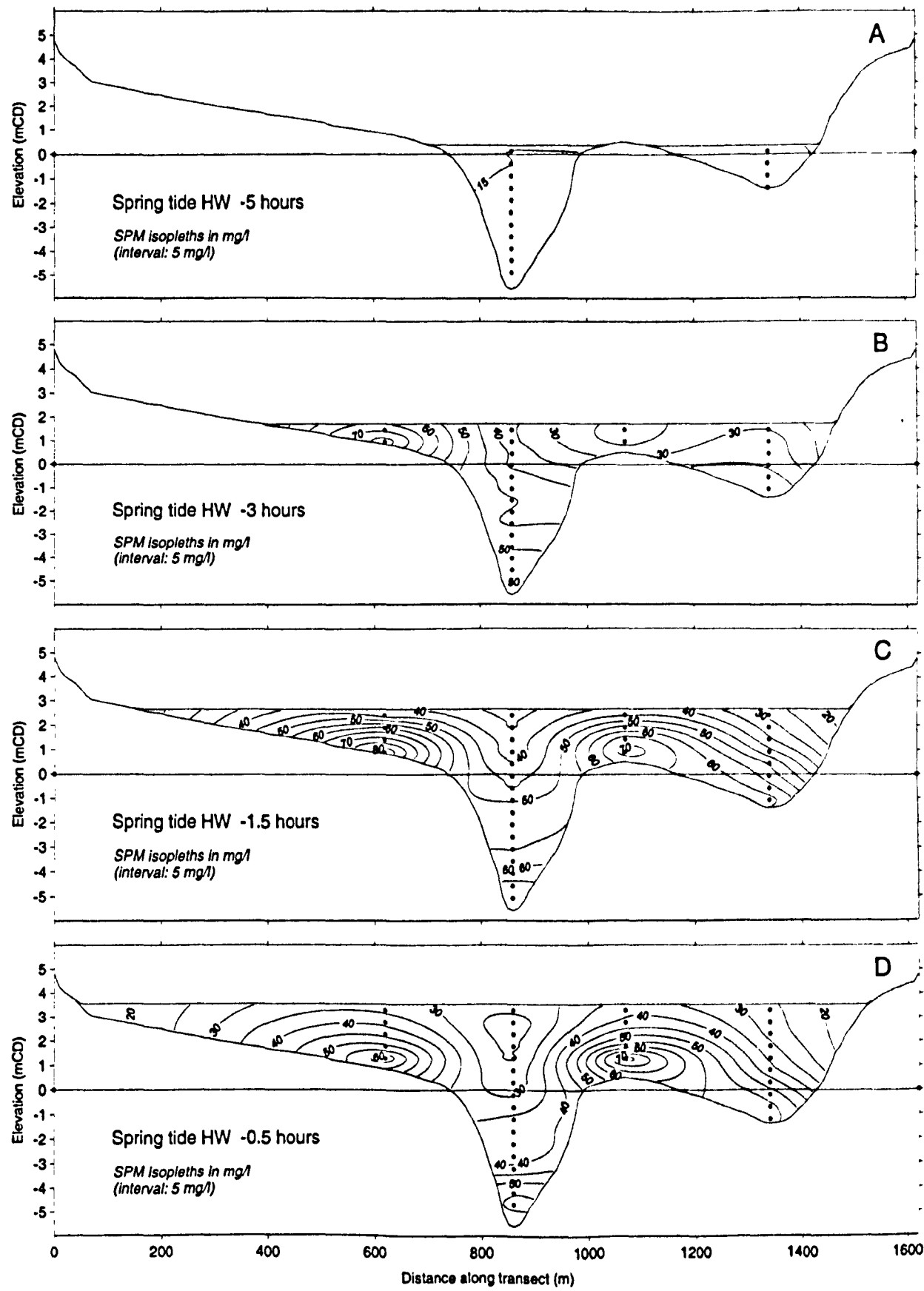
Figure 5-16 – Inlet cross-sectional SPM profiles – Spring flood tide (June 1995)
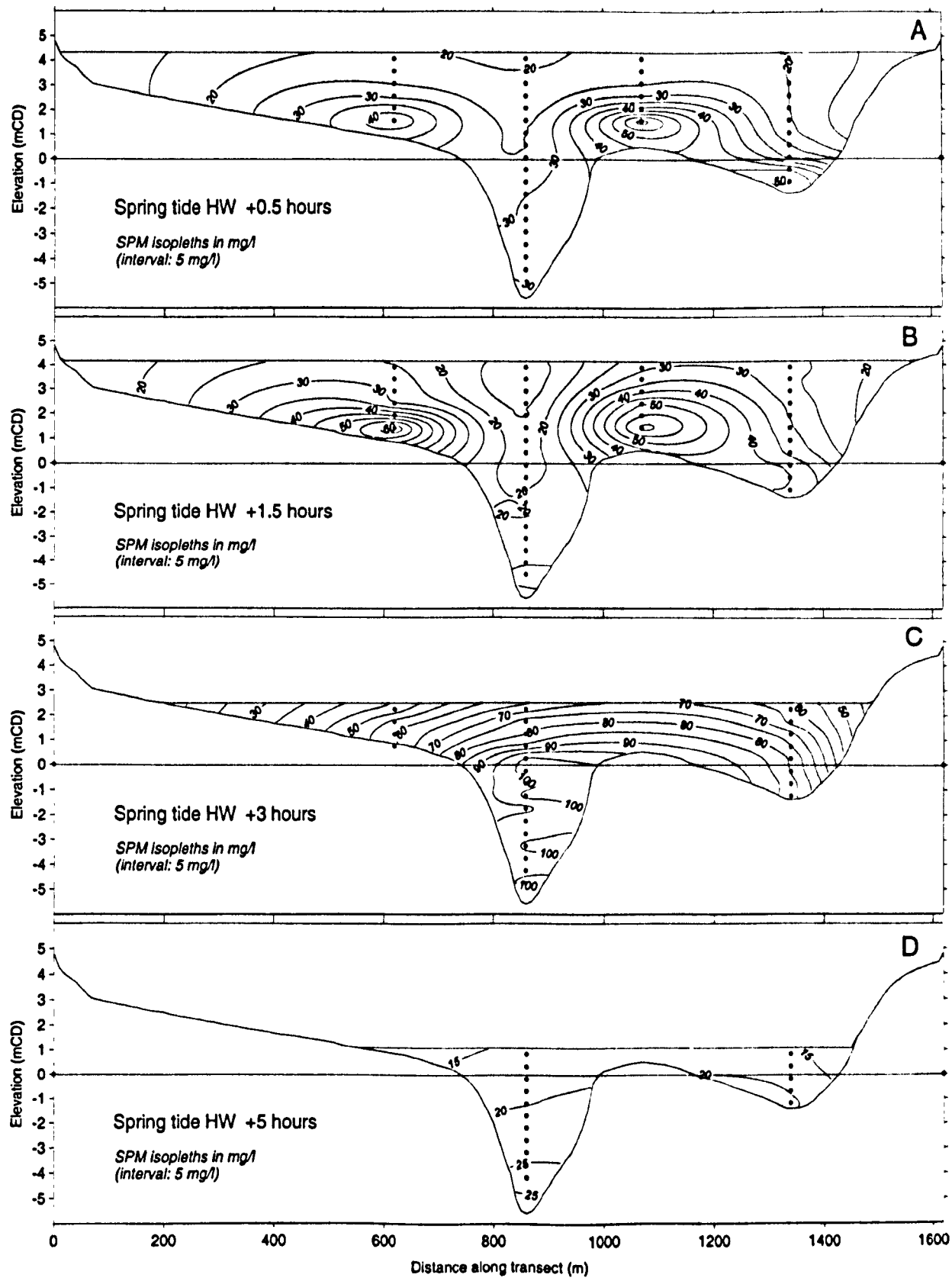
Figure 5-17 – Inlet cross-sectional SPM profiles – Spring ebb tide (June 1995)
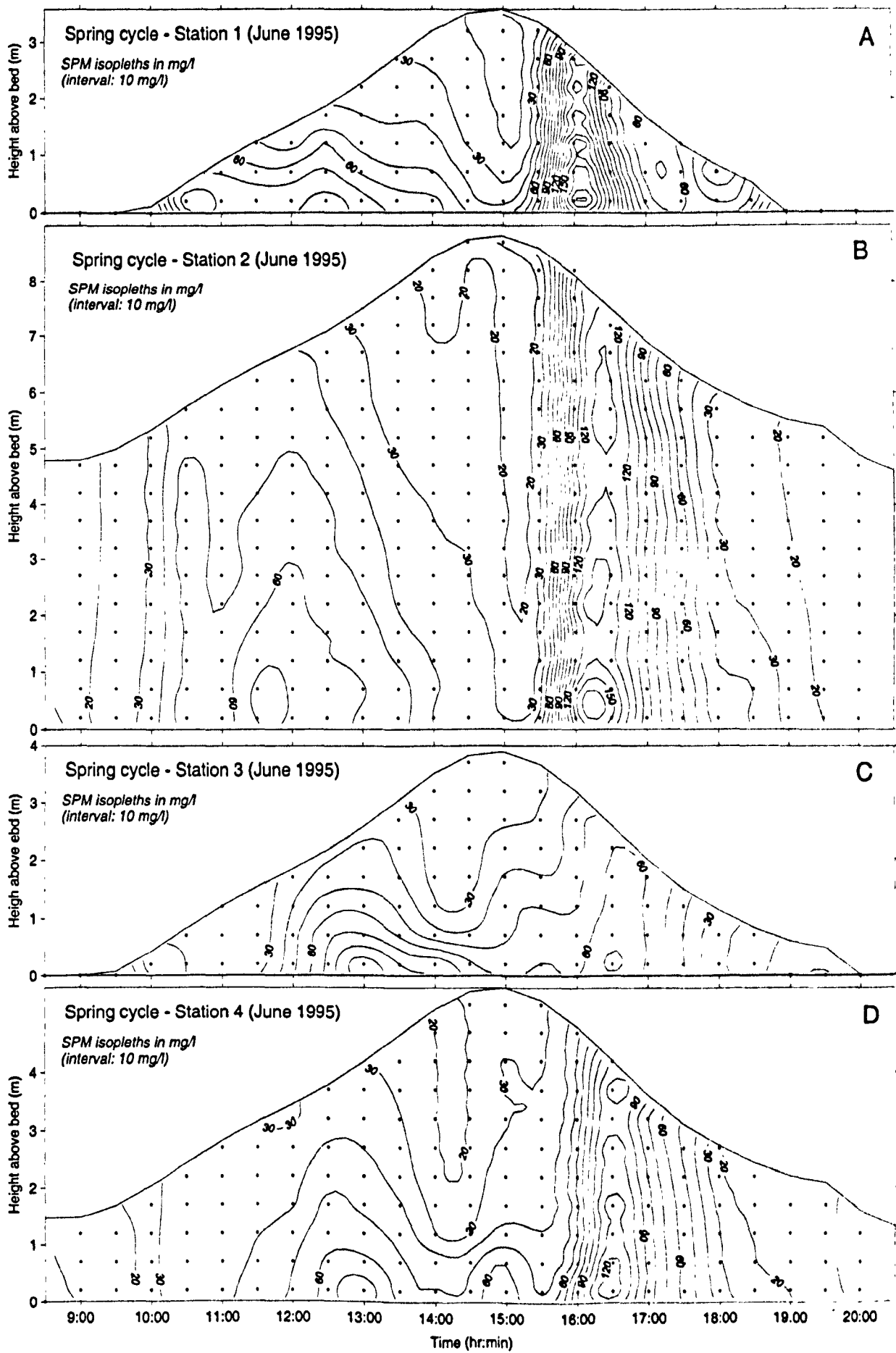
Figure 5-18 – Spring tide SPM-depth-time distribution – Stations 1 to 4

It is evident, from the data presented above, that the varying nature of the bed across the transect (intertidal mudflat at Station 1, subtidal mud at Station 4, intertidal (springs only) sandy-gravel at Station 3, and subtidal sand at Station 4), causes considerable temporal and spatial variation of SPM across the transect on both neaps and springs.

5.5.2.2   Spatial SPM variation

In addition to cross-section SPM profiles, two spatial SPM surveys were conducted, one at a spring high water and one at a neap high water. The objective was to investigate whether there were any significant vertical and lateral variation in suspended sediment concentration at high water springs and neaps throughout the embayment. An inflatable boat with a 20 hp engine was used together with the same transmissometer used for the cross-section survey. The results showed that suspended sediment values were well mixed throughout the water column and averaged 28 mg l^1 on spring and 12 mg l^1 on neaps. Maximum and minimum values were 70 mg l^1 and 13 mg l^1 springs and 23 mg l^1 and 3 mg l^1 on neaps. Figure 5-19 and Figure 5-20 are contour plots of spatial SPM data for a spring high water and a neap high water respectively. The contour level of both figures is plotted to the same scale: minimum of 0 mg l^1 and maximum of 80 mg l^1 with contour intervals at 5 mg l^1. The most significant observation gained from the two surveys is the difference between springs and neaps: spring SPM maximum values are three times maximum neap SPM values. The maximum SPM concentration on springs is in the Walton Channel and at the junction of the three main channels: Walton, Hamford and Pye Channels. It is suggested that this 'plume' of suspended sediment may be directly related to the peak spring flood current velocity experienced in the marginal flood channel around Stone Point (Section 4.4 refers). SPM concentrations throughout the remainder of the embayment are relatively consistent at between 20 and 30 mg l^1 on springs and between 5 and 10 mg l^1 on neaps.
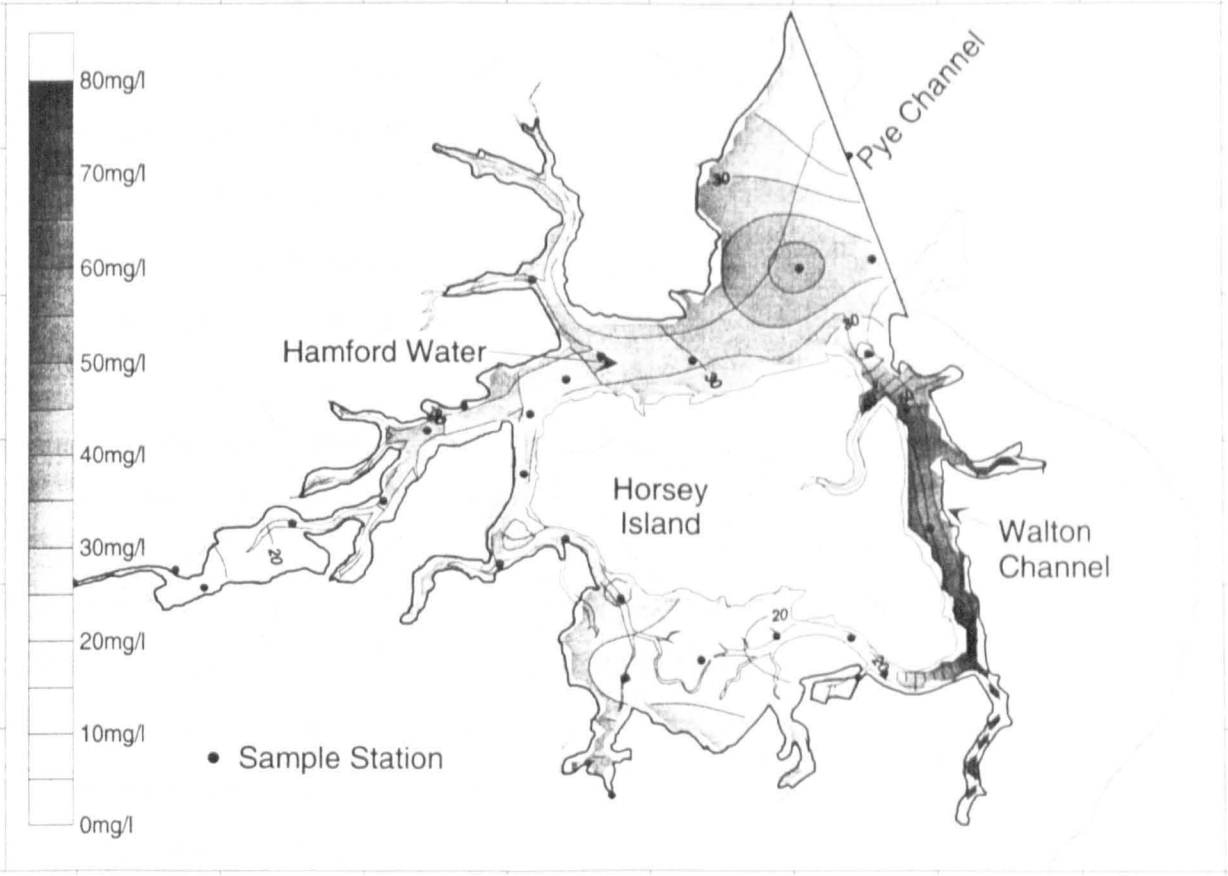
Figure 5-19 – Spring high water spatial SPM distribution.
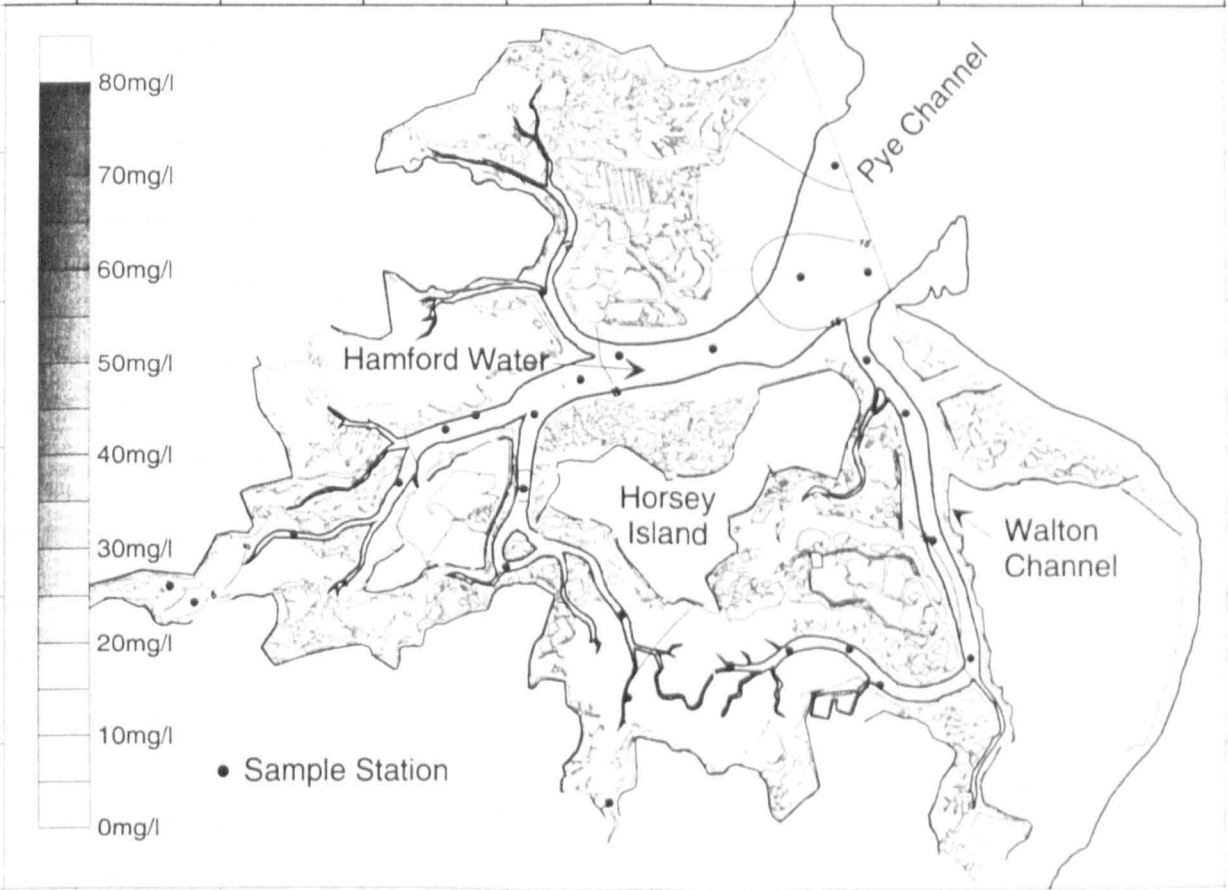
Figure 5-20 – Neap high water spatial SPM distribution.

The results from both surveys are, however, not entirely conclusive. The survey method suffered from a major restriction: it took nearly two hours to sample all points illustrated in Figure 5-19 and Figure 5-20. As discussed in Section 4.3, a feature of the tidal stage curve of Hamford Water is the very short ($\approx$10mins) high water stand. In hindsight, sampling should have been confined to the vicinity of inlet throat, or at least to no more than 10 minutes transit time for the boat used for the survey. No further analysis was made because it was felt that the survey could not effectively cover the site within the short time available at high-water and therefore could not accurately represent the conditions in the embayment.

In hindsight, it would have been interesting to conduct a low water spatial SPM survey on both springs and neaps. With more time available at low water ($\approx$45 minutes) and less area to cover ($\approx$1 km^2 at 0m CD as opposed to more than 8 km^2 at 3.5m CD), such a survey may contribute to an understanding of the amount of residual SPM present in the system prior to the onset of hydrodynamic flow-induced transport. It has already been hypothesised that most fine sediment in suspension has its origin as the Southern North Sea; therefore theoretically, by measuring spatial SPM at low water, a measure of the residual SPM and SPM provenance can be deduced.

5.5.3   SEDIMENT SOURCES

An assumption has been made during the course of this investigation that since Hamford Water has a negligible fluvial input; there will be a correspondingly negligible input of contemporary terrestrial sediment. The source of Holocene sedimentation, as determined from coring and borehole records, is considered to be primarily from the North Sea. Therefore, a detailed analysis of sediment mineralogy, to help determine sediment provenance, was not conducted for this research. However, it is accepted that erosion of exposed sections of London clay within Hamford Water, may contribute to the fine fraction, and the Red Crag and glacial deposits of Naze cliffs may contribute to the sand fraction.

It has been assessed by Eisma and Kalf (1987) that most of the suspended sediment which enters the Harwich to Walton-on-the-Naze area is derived from remote sources and transported either southward along the east coast of Britain from the North Atlantic or northward from the English Channel. A small percentage of the sediment may be

derived from erosion of the littoral zone or from erosion of the sea bed. According to Pethick and Leggett (1993), the concentration of these suspended sediments is low in the open sea, but increases in the Thames outer estuary (between Orford Ness and the North Foreland) where sediments are trapped within a large scale tidal gyre. It is this relatively high concentration of suspended sediments that feeds Hamford Water with fine sediment.

The sand fraction that makes up the majority of the sediments at the mouth of Hamford Water must owe its origin to both the coastal zone and offshore sea bed sediments. The offshore region consists of a mixture of fine and medium sands, but to the north and south they consist of well sorted fine sands with a covering of mud in places. It seems likely that sand and coarser material from the erosional coasts of Norfolk and Suffolk is moved within the nearshore zone southward to the Felixstowe coastal area. This sediment contributes to the Landguard Point spit which has generally extended to the south-west over the past 300 years (Steers, 1964). Material which is not deposited at Landguard Point is then subject to a complex sediment transport system south of Landguard Point, as discussed later in Chapter 9. There is evidence for a significant net movement of sand out of the Stour-Orwell estuary which may also form a source of sediment to the Harwich-Walton Bay and Hamford Water. The original source of this material may be the erosion of the inter-tidal area within the two estuaries which, although it consists of predominantly silt and clay-sized sediment, does contain 5 to 10% sand. A second possible source may be the offshore zone described above, the sand being moved temporarily into the mouth area of the Stour-Orwell where it then appears to be moving out of the estuary when it returns seaward.

To summarise: the source of coarse sediment available for transport through the inlet throat may, therefore, be assumed to be a combination of that supplied by littoral drift, and sediment eroded or retrained from both the embayment and inlet bed. Because of a lack of fresh water input to Hamford Water, sediment of a fluvial origin is considered negligible.

5.6 Summary

Results from an analysis of sediment grain size in Hamford Water can be summarised as follows:

- Hamford Water has two distinct sediment regimes: fine silts and clays in the embayment, and sands in the inlet.

- Most interior fine sediment falls within the relatively calm hydrodynamic stage II on a Pejrup (1988) triangular diagram whereas the inlet sandy sediments fall within the more violent hydrodynamic stage IV.

- The mean grain size of the inlet throat and ebb delta sands is 0.25mm (2ϕ, medium to fine sand) and the majority of the embayment mudflat and saltmarsh 0.011mm (6.5ϕ, medium to fine silt).

- The source of sediment available for transport through the inlet throat is assumed to be a combination of littoral drift sediment; sediment eroded and/or retrained from both the embayment and inlet bed; and, fine sediment in suspension.

- Spatial suspended sediment values were well mixed throughout the water column and averaged 28 $mg\ l^{-1}$ on spring and 12 mg l^{-1} on neaps. Maximum and minimum values were 70 mg l^{-1} and 13 mg l^{-1} springs and 23 mg l^{-1} and 3 mg l^{-1} on neaps.

- Spring spatial SPM distribution appears to be concentrated around Stone Point and the northern end of Walton Channel.

6 Sediment Transport

6.1   Introduction

This chapter is concerned with the movement of sediment through Hamford Water inlet. It includes both the flux of suspended particulate matter (SPM), and the rate of suspended and bedload sediment transport during both a flood and ebb tide, and over a spring-neap cycle. Hamford Water inlet is taken to be the cross-section as previously described in Section 4.1 and illustrated in Figure 4-1.

In considering sediment transport through the inlet, it is hypothesised, from an analysis of grain size in the previous section, that there are two inter-related sediment transport regimes at work: fine, cohesive sediment in suspension (Suspended Particulate Matter – SPM), and coarse, non-cohesive bedload and suspended load sediment, hereinafter referred to as Sand. SPM flux measurements are computed from an evaluation of the tidal prism: the instantaneous discharge being obtained by a vertical and lateral integration of the instantaneous velocity and suspended sediment concentration over a cross-section of the inlet throat. Sand transport rates are calculated based on equations utilising the physical relationships of grain size and current flow. Three sediment transport rate equations are used which utilise either velocity at 100cm above the bed, u_{100} (Hardisty, 1983; Jago and Mahamod, 1999) or depth average velocity, $\bar{u}$ (Engelund and Hansen, 1967).

6.2   Fine, Cohesive Suspended Load Transport (SPM)

In order to determine the volume of SPM passing into and out of Hamford Water on any tidal cycle, it was first necessary to calculate the tidal prism of the embayment. The tidal prism is taken to be the total volume of water the embayment is capable of holding on any single tidal cycle; consequently it will vary from greatest on springs to least on neaps. Tidal prism was calculated by measuring the surface area off Admiralty Chart 2695 (Plans on the East Coast of England, 1989 – Scale 1 : 12,500), for selected datum's relative to chart datum, with an OTT–Type 30.027 Compensating Polar Planimeter. The volume at respective levels above chart datum was then calculated using Simpson's Rule, after Curtin and Lane (1970). The result is a curve of tidal

volume versus tidal elevation from which the predicted volume of the inlet can be determined for any elevation (Figure 6-1).
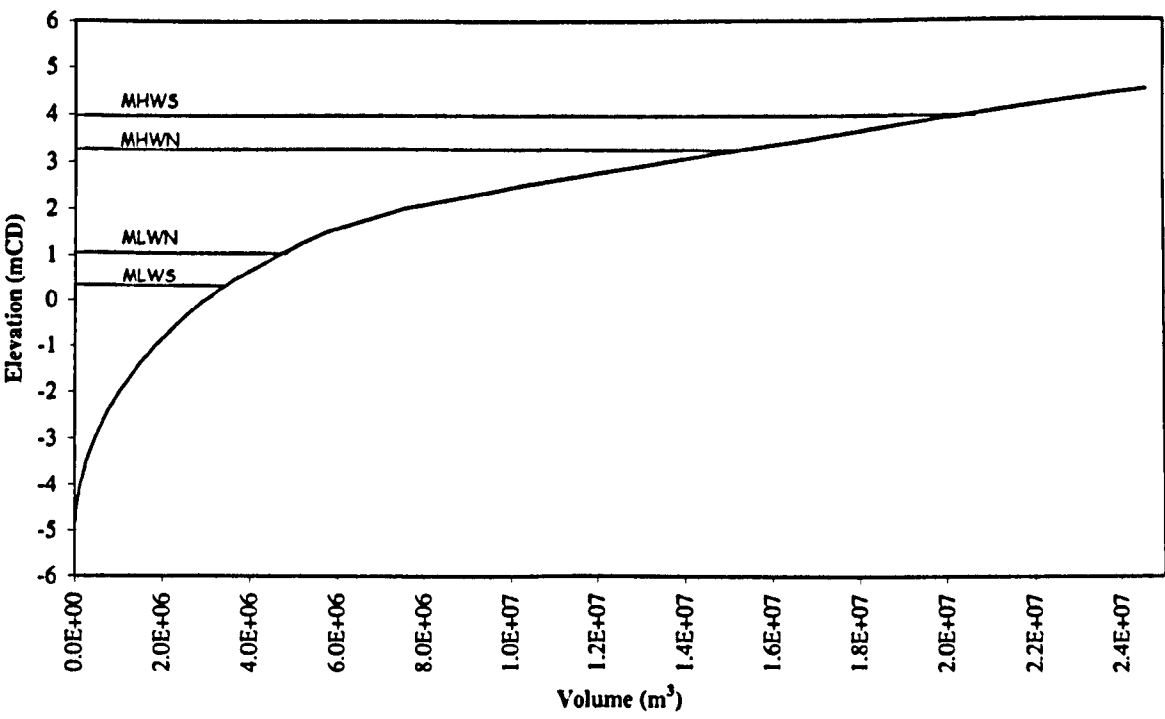
Figure 6-1 – Elevation versus volume

The inlet cross-section was then divided into 5 vertical sectors, each sector representing each VGU and/or anchor station as illustrated in Figure 4-1. The area of each sector was measured by drawing to scale, on metric graph paper, each sector and the area determined using the Planimeter, checked by a numerical count of squares in each sector. This was repeated at 0.1m intervals for a spring and a neap tidal cycle which resulted in two separate data sets of tidal elevation versus cross-sectional area of the inlet. Water and suspended sediment flux measurements were then computed from an evaluation of the tidal prism and the cross-sectional area of the inlet. Instantaneous discharge was obtained by a vertical and lateral integration of the instantaneous velocity and suspended sediment concentration over the cross-section of the inlet throat, according to:

$$q = \sum_{i=1}^{n} C_i \, u_i \, A_i \qquad (6:1$$

where, C is the suspended sediment concentration (g m^3 $^{-1}$), u is the time-averaged current speed (m s^{-1}) and A is the cross sectional area (m) over which C and u are representative. The instantaneous rate is then the flux, q multiplied by the depth

average velocity, $\bar{u}$ calculated according to Equation (4:1). Tabulated data are contained in Appendix H and summarised in Table 6-1 and Table 6-2, and bar charts of sediment fluxes are compared in Figure 6-2 and Figure 6-3. In Table 6-1 and Table 6-2 the *Predicted Tidal Volume* calculation is as already described above. The *Measured Tidal Volume* is the product of the inlet cross-sectional area and depth-averaged velocity. The *Measured Suspended Sediment Flux* is the product of the *Measured Water Flux* and the suspended sediment concentration and expressed in kilograms and tonnes.

Table 6-1 – Spring Sediment Fluxes

Sediment Fluxes and Sediment Transport Rates

Spring Tide - 16 June 1995

Predicted Tidal Volume	Total Flood	-18E+6 m³	
	Total Ebb	18E+6 m³	
	Net (+ebb-flood)	181067 m³	1 % error
Measured Tidal Volume	Total Flood	-19E+6 m³	
	Total Ebb	24E+6 m³	
	Net (+ebb-flood)	4E+6 m³	19 % error
Measured Suspended Sediment Flux	Total Flood	-242361 kg	-242.4 tonnes
	Total Ebb	912236 kg	912.2 tonnes
	Net (+ebb-flood)	669875 kg	669.9 tonnes

Table 6-2 – Neap Sediment Fluxes

Sediment Fluxes and Sediment Transport Rates

Neap Tide - 20-21 June 1995

Predicted Tidal Volume	Total Flood	-15E+6 m³	
	Total Ebb	14E+6 m³	
	Net (+ebb-flood)	-684552 m³	5 % error
Measured Tidal Volume	Total Flood	-14E+6 m³	
	Total Ebb	12E+6 m³	
	Net (+ebb-flood)	-1192804 m³	9 % error
Measured Suspended Sediment Flux	Total Flood	-53466 kg	-53.5 tonnes
	Total Ebb	68544 kg	68.5 tonnes
	Net (+ebb-flood)	15078 kg	15.1 tonnes
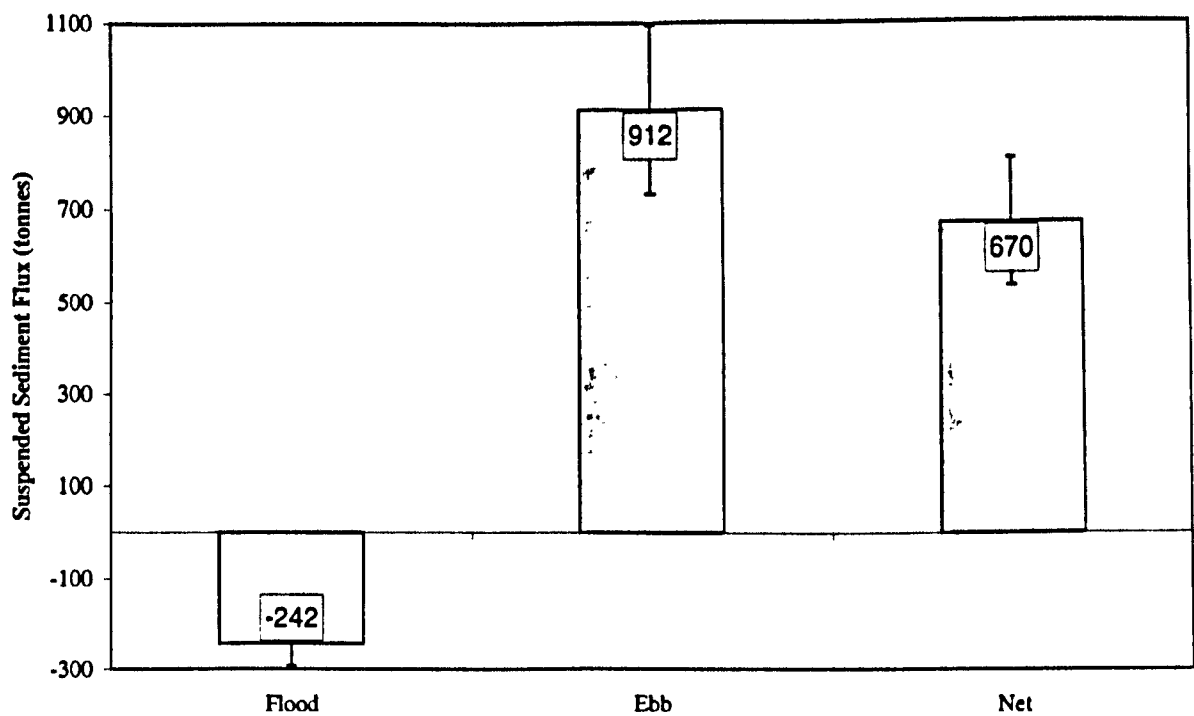
Figure 6-2 – Spring SPM flux.
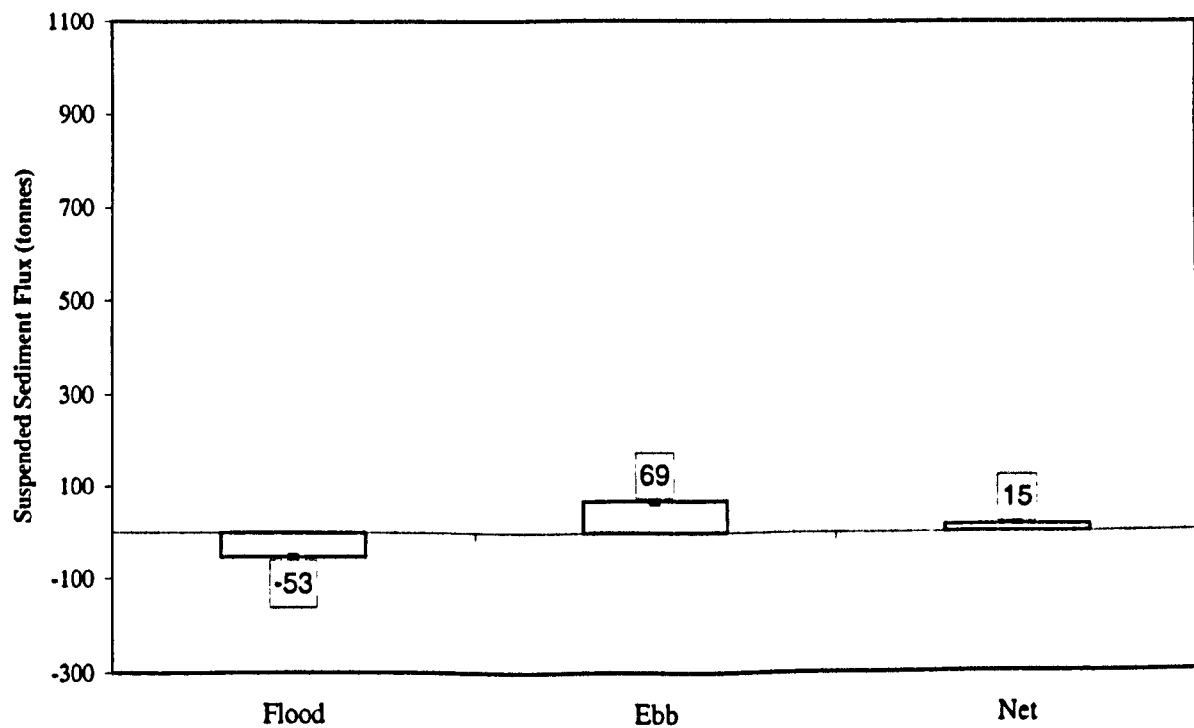
Figure 6-3 – Neap SPM Flux.

The results from measuring a single spring and a single neap tide indicate that there is a net ebb transport of 670 tonnes of SPM on springs and 15 tonnes on neaps. It would be a simple matter to extrapolate these results over an annual cycle and determine an annual budget, however, the results must be considered as more qualitative rather than

quantitative. Hamford Water, as a tidal inlet, presents a particularly difficult system in which to assess sediment flux. An accurate flux calculation depends on being able to balance the tidal prism, and theoretically, the flood and ebb values of both predicted and measured tidal volume should be the same. If the net tidal volume and therefore the net water flux are zero, then any imbalance in suspended sediment flux would represent an accurate indication of net suspended sediment flux through the inlet. In the case of springs (Table 6-1) the predicted tidal volume is 1% in error: 1% of the total volume is imbalanced in favour of the ebb tide. The measured tidal volume is 19% in error: 19% more water flowed out of the embayment on the ebb than entered on the flood. However, on neaps (Table 6-2) the predicted tidal volume is –5% in error: 5% of the total volume is imbalanced in favour of the flood tide. The measured tidal volume is –9% in error: 9% more water flowed into the embayment on the flood than left on the ebb.

The predominant cause of this imbalance is the nature of the tidal basin: Hamford Water does not drain at low water; there is always some residual water volume. Approximately 2.9×10^6 m^3 remain in the system at 0 m CD and the difference in tidal range either side of high water is, therefore, critical to overall flux calculations. In the spring tide survey the tidal range was 0.3m greater on the ebb than on the flood which equates to 0.5×10^6 m^3 additional ebb volume. In the neap tide survey the tidal range was 0.4m less on the ebb than on the flood which equates to 0.6×10^6 m^3 additional flood volume. It is not just a simple matter of removing the volume imbalance due to different tidal ranges; the fact still remains that more or less water may flow in or out of the embayment depending on respective tidal range differences and consequently more, or less SPM is transported depending on the imbalance. In a larger estuarine system such as The Humber or Thames, such difference will be lost within the error bars and account for a very small percentage of the overall flux calculation. An improvement on the current data set would be to continuously monitor SPM flux for a complete spring-neap tidal cycle.

The nature of the inlet cross-section and the nature of the flow through the inlet also make flux calculations difficult. The inlet has two distinct channels, one deep (Pye Channel) and the other shallow (Outer Swatch), and it has gently shoaling margins. It has also been pointed out that the nature of the tidal flow through the inlet is complex

(*see* Section 4.4): the tide is at times stronger at the margins on the flood, and stronger in the center on the ebb. All these factors do not however, detract from the fact that due to the nature of the tidal cycle, the net direction of SPM transport as recorded in this research, is mainly seawards.

6.3 Coarse, Bedload and Suspended Load Transport (Sands)

Sand sediment transport rates are calculated using the methods of Engelund and Hansen (1967), Hardisty (1983), and Jago and Mahamod (1999) for VGU stations 1, 3 and 5. The form and derivation of the formulae has already been covered in 3.2.4 above. This section covers the results, presented firstly as individual spring and neap events for all three survey stations, and then as composite time series for a spring–neap cycle. Full tabulated results are contained in Appendix I.

6.3.1 ENGELUND AND HANSEN (1967)

The form of Engelund and Hansen's (1967) equation has already been described in 3.2.4 above.

$$ q_t = 0.05 \, \rho_s \bar{u}^2 \left[\frac{D}{g(\rho_s - \rho)/\rho} \right]^{0.5} \left[\frac{\tau_0}{(\rho_s - \rho)gd} \right]^{1.5} (g \, cm^{-1}s^{-1}) \qquad (6:2 $$

It is a simple matter to calculate q_t given D and $\bar{u}$: D is the mean grain size and was taken to be 0.025cm, and $\bar{u}$ is the depth-averaged velocity calculated according to:

$$ \bar{u} = \frac{1}{z_{max}} \sum_{i=1}^{n} u_i \Delta z_i \qquad (6:3 $$

Where u_i is the velocity at each current meter, z_i is the height above the bottom, and Δz_i is the thickness of the appropriate depth increment. The time-varying depth of water, z_{max} at each station was determined with reference to tidal predictions at Harwich and computed using TIDECALC (*see* Section 4.3.1 above). Calculated depth averaged velocities, ($\bar{u}$) were used to assess the correlation with velocities at 100cm above the bed (u_{100}) and therefore the validity of using u_{100} in subsequent sediment transport rate formulae. Plots of $\bar{u}$ versus u_{100} are illustrated in Appendix G and values are summarised in Table 6-3. It can be seen that in all cases there is a high correlation of $\bar{u}$

and u_{100}, and therefore the use of u_{100} is justified in sediment transport calculations. It would also indicate that the use of $\bar{u}$ would be applicable in place of u_{100} if necessary.

Table 6-3 – Correlation values for u vs u$_{100}$

Station	r^2
Station 1 (springs)	0.9885
Station 3 (springs)	0.9939
Station 5 (springs	0.9818
Station 1 (neaps)	0.9879
Station 3 (neaps)	0.9972
Station 5 (neaps)	0.9919

6.3.2   HARDISTY'S (1983) BEDLOAD TRANSPORT

As discussed in Section 3.2.4, Hardisty's (1983) bedload equation originates from Bagnold (1963) and Guy *et al.* (1966) but modified to include a threshold term in a parameter describing excess bed stress:

$$q_b = k_1(u_{100}{}^2 - u_{100t}{}^2)u_{100} \ (gcm^{-1}s^{-1})$$

(6:4

where, k_1 is an empirical constant, depending on grain diameter, calculated from a regression analysis of flume transport data of Guy *et al.* (1966) and Williams (1967).

Table 6-4 – Hardisty's (1983) values of calibration coefficient, k_1 (g cm^{-4} s^2)

D (mm)	Correlation Coefficient	Calibration Coefficient
0.18	0.97	0.68×10^{-5}
0.27	0.96	0.47×10^{-5}
0.45	0.81	0.21×10^{-5}
1.45	0.96	0.16×10^{-5}

The computed values of k_1 were regressed onto the grain sizes to provide a calibration coefficient in terms of sediment grain size:

$$k_1 = \frac{1}{6.6 \, d^{1.23}} \, x \, 10^{-5} g \ cm^{-4}s^2$$

(6:5

The figure shows a plot with y-axis "Calibration coefficient, k_1 ($g\,cm^{-4}\,s^2$)" ranging from 0.0E+00 to 1.2E-05, and x-axis "Grain diameter (mm)" ranging from 0 to 1.6. The fitted curve equation is $y = 2E\text{-}06x^{-1.23}$. Legend shows "◆ Sand Sizes". A vertical line marks "0.25 mm".
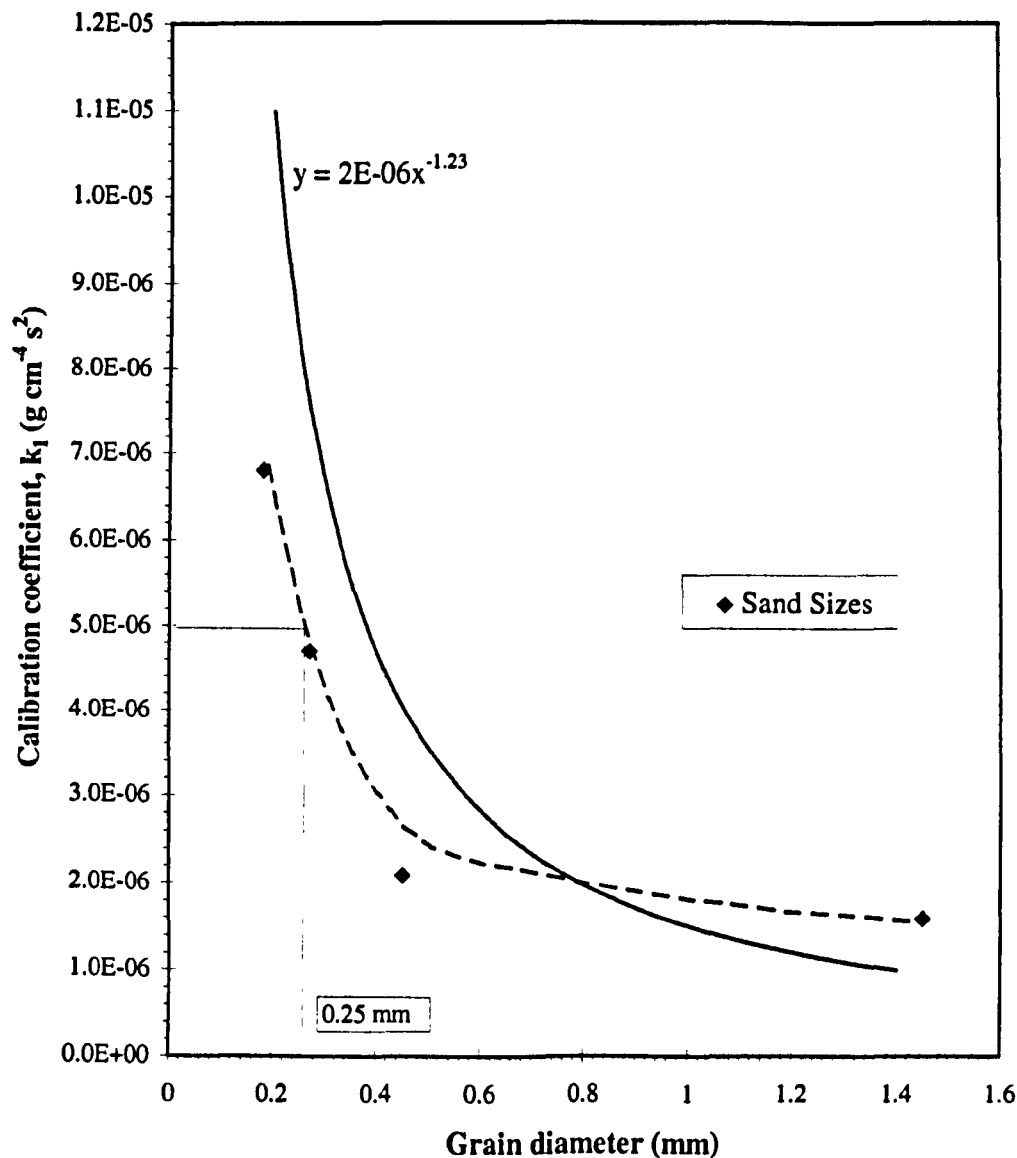
Figure 6-4 – Calibration diagram for k_1 in Equation (6:5).

It can be seen that for a mean grain size of 0.25mm, taken to be the mean for sand that circulates through the inlet throat as discussed in 5.3 above, the value of k_1 is taken to be 0.49×10^{-5} if estimated from the fitted curve (Figure 6-4), and 0.83×10^{-5} if calculated from Equation (6:5). The value calculated from Equation (6:5) is considerably greater than that picked from Figure 6-4, and for the following calculations of q_b the value estimated from Figure 6-4 is used in Equation (6:4).

6.3.3   JAGO AND MAHAMOD (1999)

As discussed in Section 3.2.4, Jago and Mahamod's (1999) total load algorithm is suggested as being suitable for total load sand flux in high-energy environments where

currents are fast enough to cause significant sand transport. The algorithm is a power relationship given by:

$$q = k \left[(u_1 - u_{1t}) / u_{1t} \right]^n \qquad (6:6$$

where q is total sand flux, u_1 and u_{1t} are mean current velocity and threshold current velocity at 1 m above the bed, respectively, k is an entrainment parameter, and n an exponent, both of which are dependent on grain diameter D.

The derived dependence of n on D is given by:

$$n = 5.028 - 5564D + (3225 \times 10^3) D^2 \qquad (6:7$$

The entrainment parameter, k is given by:

$$\log_{10} k = -2.465 - 1163D + (2973 \times 10^3) D^2 \qquad (6:8$$

From which, for sands of 0.25 mm, k is determined as **2.7 x 10⁻³** and n as **3.84**. These values are used in Equation (6:6).

6.3.4   SPRING SAND SEDIMENT TRANSPORT RATE RESULTS

Spring sediment transport rates for VGU stations 1, 3 and 5 are summarised in Table 6-5 and the variation of sediment transport rate over a spring cycle at the respective stations is illustrated in Figure 6-5 to Figure 6-7 with tidal stage and depth-averaged velocity for the same period illustrated in Figure 6-8. Although flood values are represented as negative in Table 6-5, Figure 6-5 to Figure 6-7 are plotted positive so that the scale can be plotted logarithmically in order to compare each method.

Table 6-5 – Spring sediment transport rates compared.

Springs 16 June 1995		E&H (1967)	Hardisty (1983)	J&M (1999)
Station 1	Flood	-1001.7	0.0	-2.0
	Ebb	884.3	22.9	22.6
	Net	-117.4	22.9	20.6
Station 3	Flood	-89.6	0.0	0.0
	Ebb	13913.6	1024.9	774.6
	Net	13824.0	1024.9	774.6
Station 5	Flood	-19303.0	-1429.1	-1301.0
	Ebb	379.7	496.2	371.2
	Net	-18923.3	-932.9	-929.8
	Flood	-20394.3	-1429.1	-1303.0
	Ebb	15177.6	1544.0	1168.4
Net Total (kg m^{-1})		-5216.7	114.9	-134.6

From Table 6-5 the following significant points are noted:

- Values produced by Engelund and Hansen's (1967) (E&H) equation are orders of magnitude greater than Hardisty (1983) and Jago and Mahamod (1999) (J&M).

- Hardisty and J&M accord in magnitude but not in net direction.

- At Station 1, Hardisty and J&M show net ebb transport but E&H show net flood.

- At Station 3 all equations show a net ebb transport direction.

- At Station 5 all methods show a net flood transport direction.
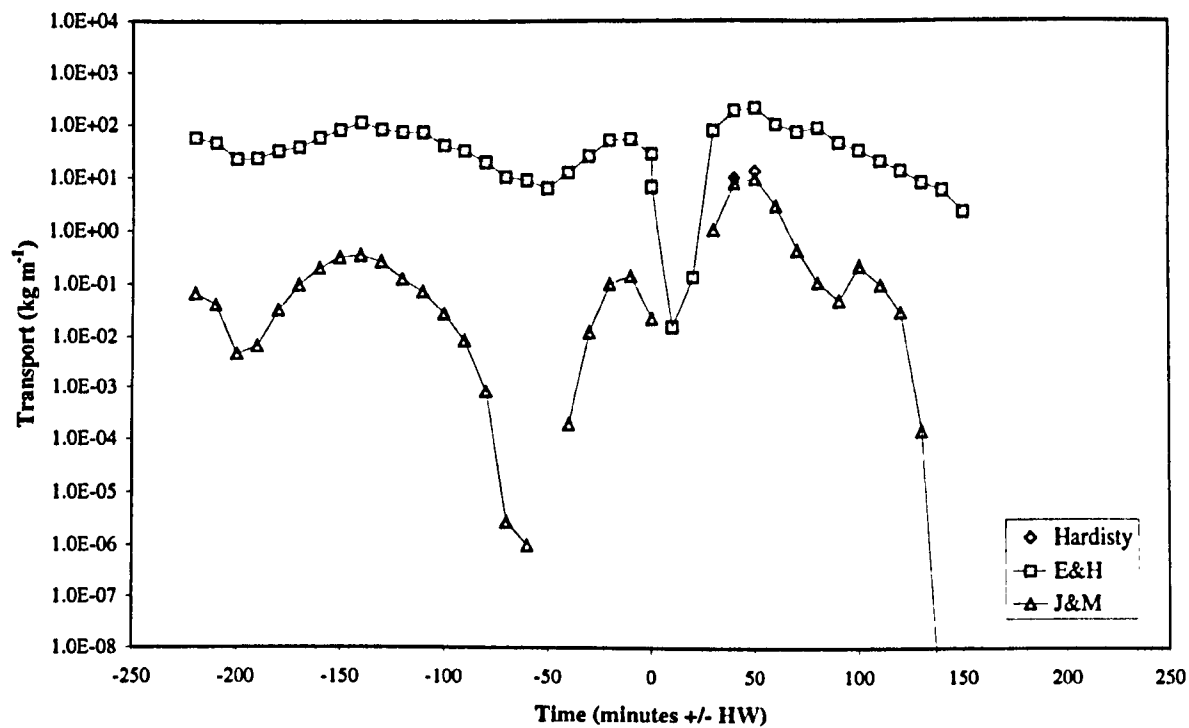
Figure 6-5 – Spring sediment transport rates – Station 1.
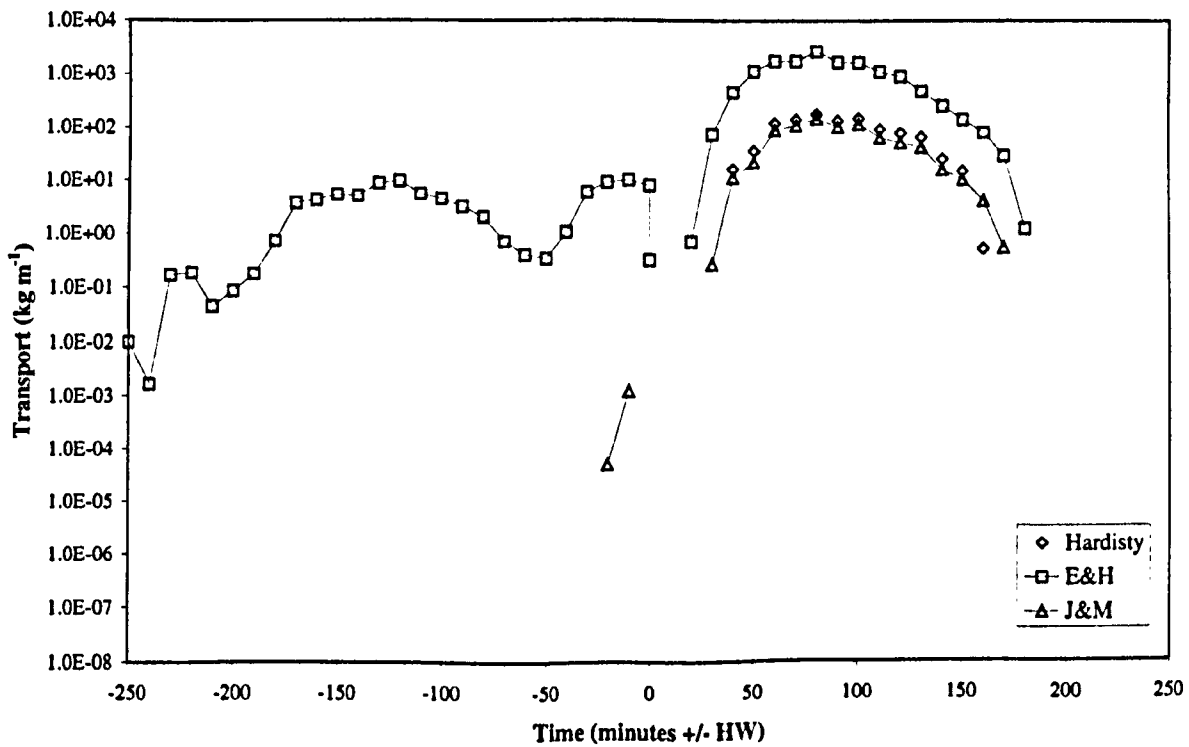
Figure 6-6 – Spring sediment transport rates – Station 3.
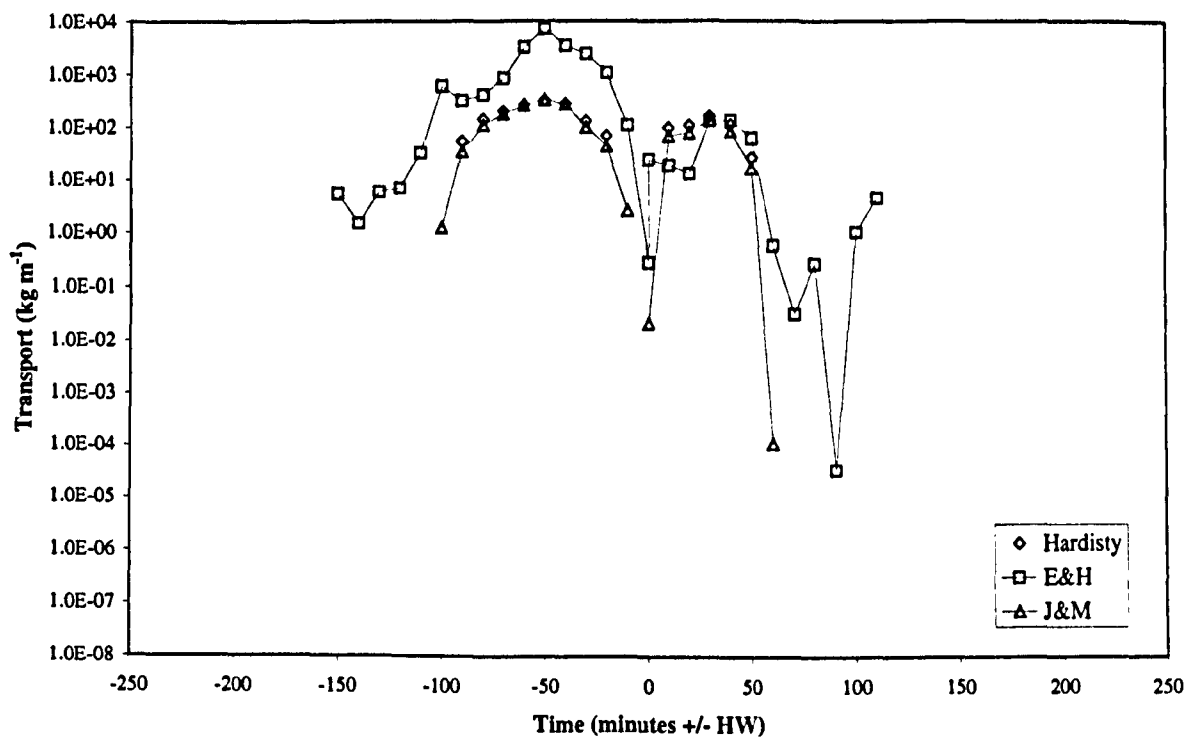
Figure 6-7 – Spring sediment transport rates – Station 5.
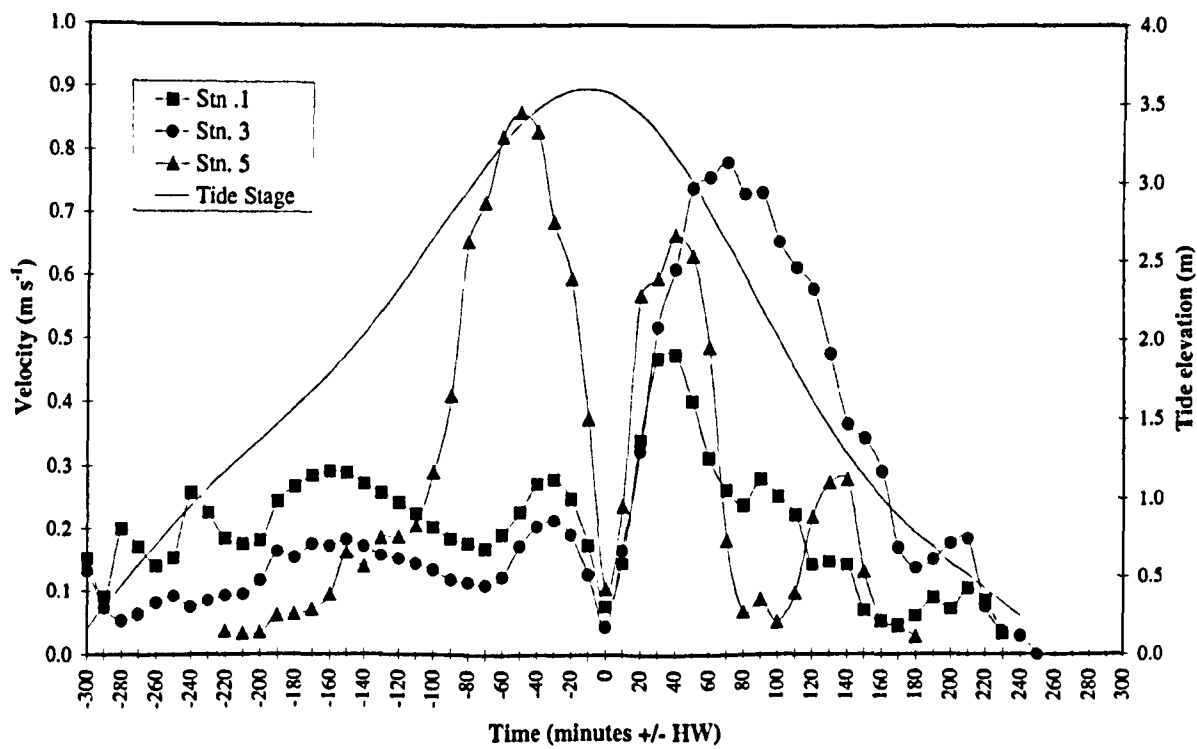
Figure 6-8 – Spring tidal stage and depth-averaged velocity curves.

6.3.5   NEAP SEDIMENT TRANSPORT RATES

Neap sediment transport rates for VGU stations 1, 3 and 5 are summarised in Table 6-6 and the variation of sediment transport rate over a neap cycle at the respective stations is illustrated in Figure 6-9 to Figure 6-11, with tidal stage and depth-averaged velocity for the same period illustrated in Figure 6-12.

Table 6-6 – Neap sediment transport rates compared.

Neaps 20-21 June 1995		E&H (1967)	Hardisty (1983)	J&M (1999)
Station 1	Flood	-167.6	0.0	-0.3
	Ebb	111.6	0.0	0.2
	Net	-56.0	0.0	-0.1
Station 3	Flood	-9.8	0.0	0.0
	Ebb	3355.8	164.5	116.2
	Net	3346.0	164.5	116.2
Station 5	Flood	-242.5	0.0	-9.7
	Ebb	24.9	42.6	34.3
	Net	-217.5	42.6	24.6
Totals	Flood	-419.8	0.0	-10.0
	Ebb	3492.3	207.2	150.7
Net Total (kg m^{-1})		3072.5	207.2	140.7

From Table 6-6 the following significant points are noted:

- E&H shows the same pattern of net sediment transport direction as during springs: flood transport at Station 1, ebb at Station 3, and flood at Station 5.

- Hardisty and J&M show negligible or ebb transport across all stations.

- All methods show a net ebb sediment transport.
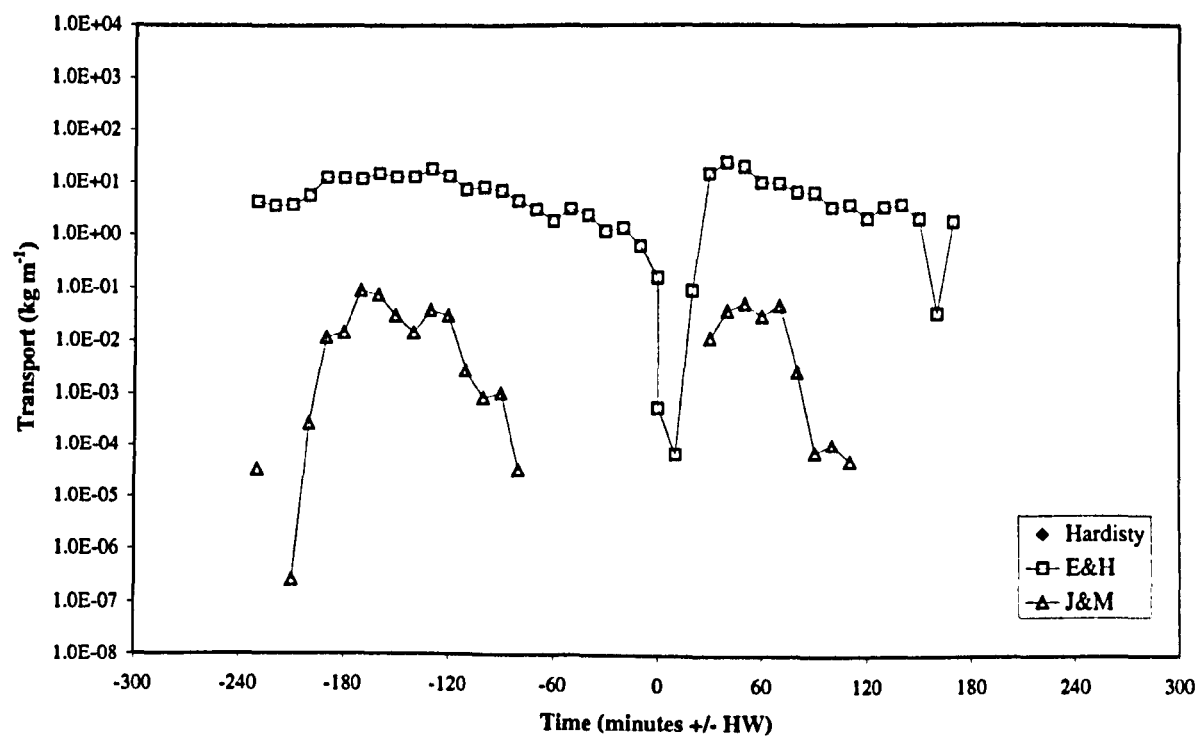
Figure 6-9 – Neap sediment transport rates – Station 1.
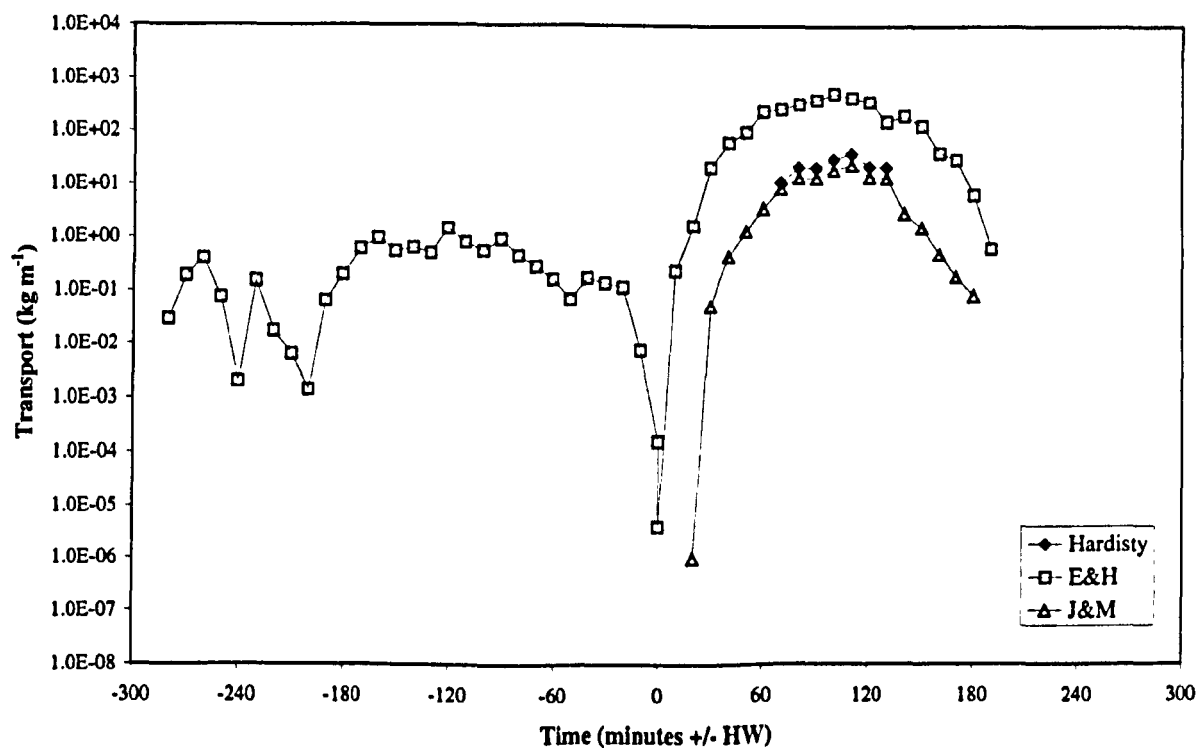
Figure 6-10 – Neap sediment transport rates – Station 3.
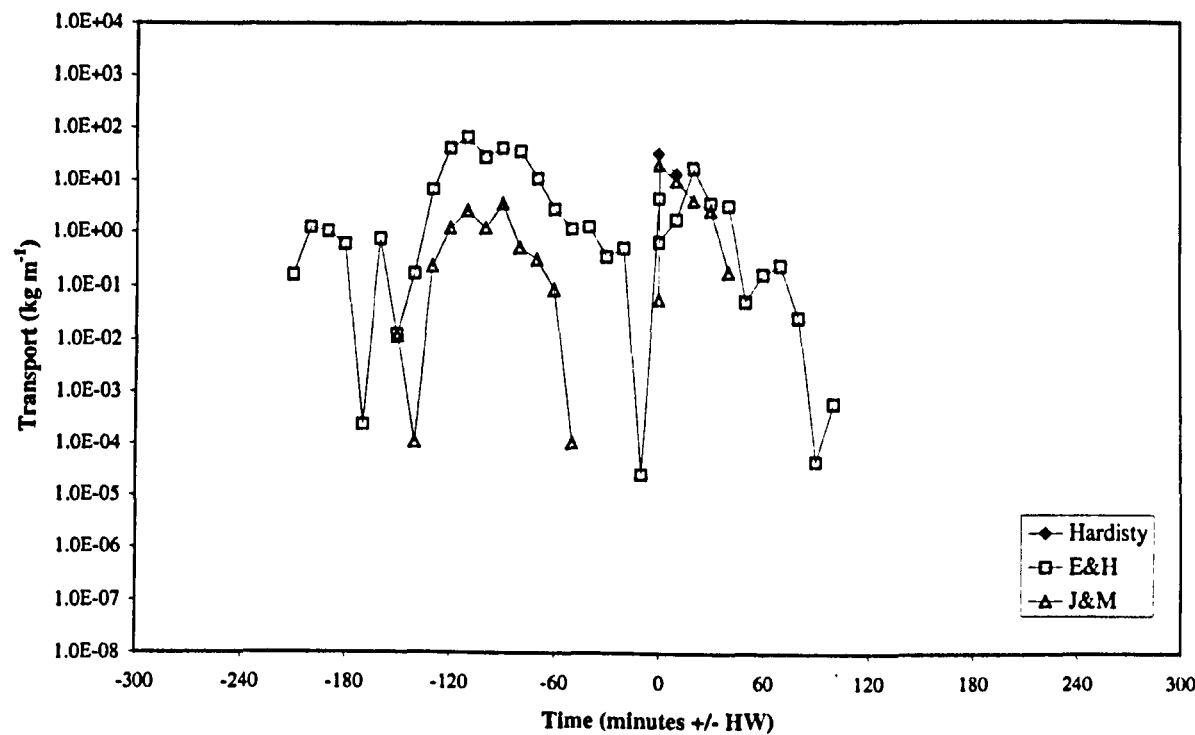
Figure 6-11 – Neap sediment transport rates – Station 5.
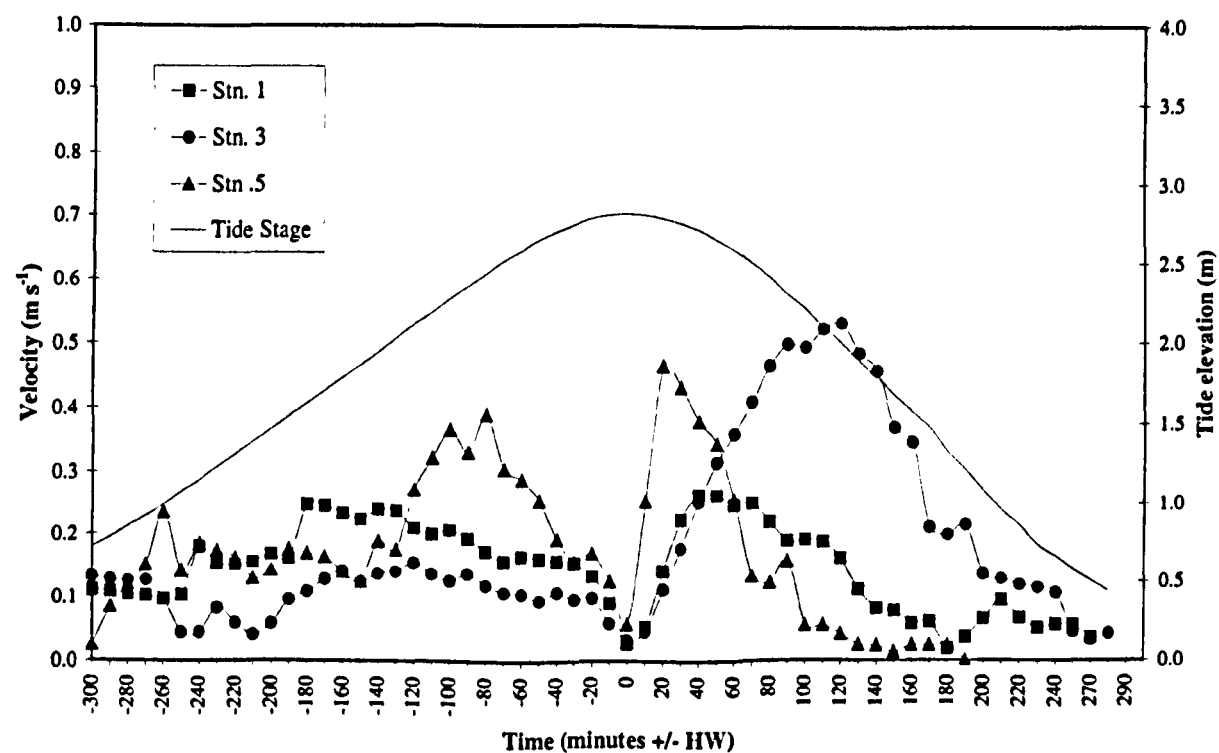
Figure 6-12 – Neap tidal stage and depth-averaged velocity curves.

6.4 Discussion

A time series of sediment transport rates for the inlet throat for all flood tides using all three methods is illustrated in Figure 6-13, and for all ebb tides in Figure 6-14. The data for each Figure are contained at Appendix I.
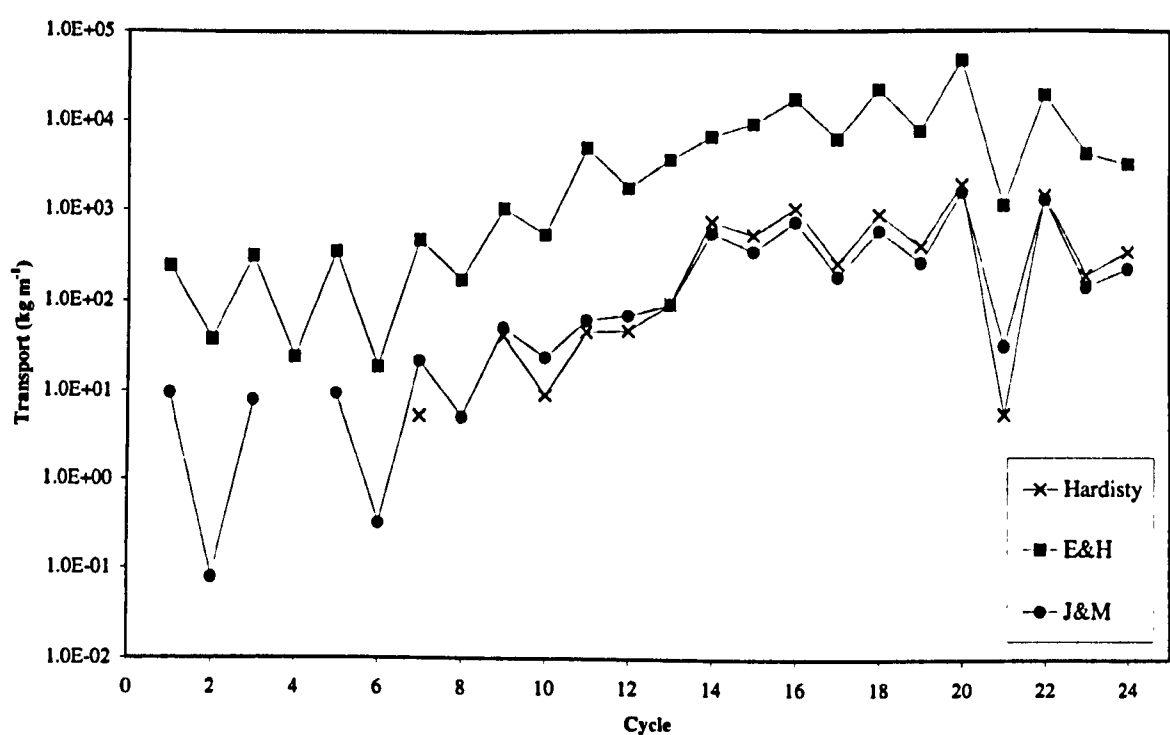
Figure 6-13 – Time series of sand sediment transport rates – Flood tides.
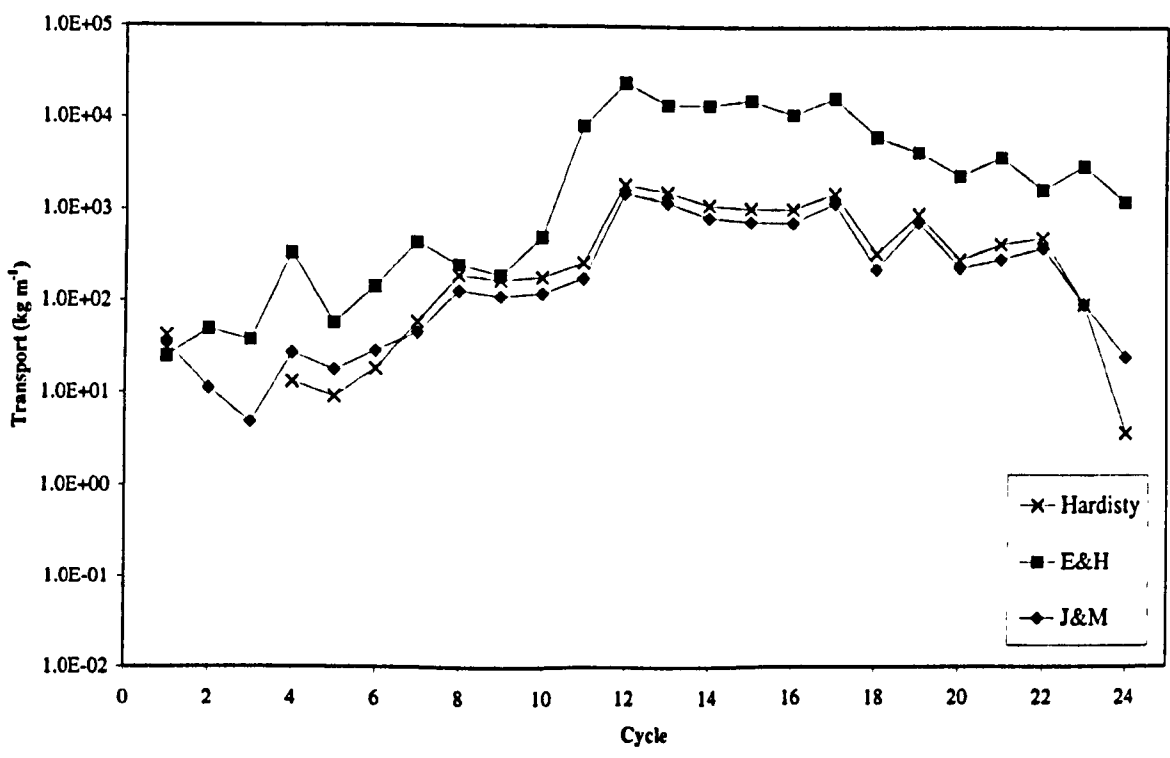
Figure 6-14 – Time series of sand sediment transport rates – Ebb tides.

In Figure 6-13 and Figure 6-14 the x–axis represents tidal cycle in days, Day 13 being springs, and Days 0 and 24 being neaps. The y–axis is sediment transport rate plotted linearly to accommodate negative values (–ve corresponding to flood and +ve, to ebb

after the convention adopted by Dyer, (1979)). Table 6-7 is a qualitative summary of the net direction of sediment transport on springs and neaps.

At first sight, and on balance, there is a net ebb transport of both fine and coarse sediment. At neaps all results indicate ebb transport, whereas at springs both Engelund and Hansen (1967) and Jago and Mahamod (1999) indicate flood transport. It is interesting to note that in all cases, if Station 5 is excluded, results would show net ebb sediment transport throughout. As discussed in Section 4.4.2.2, Station 5 was not part of the comprehensive inlet survey and has only been included by matching similar tidal range data from a previous individual survey at Station 5. The inclusion of Station 5 data significantly alters the net sediment transport direction and thus highlights the importance of careful planning and the ability to be able to survey as much of an inlet cross-section as possible. The significance of marginal channels in tidal inlets cannot be ignored.

Table 6-7 – Summary of net transport directions

Method	Net Direction of Transport	
	Springs	Neaps
SPM Flux	EBB	EBB
Engelund & Hansen (1967)	FLOOD	EBB
Hardisty (1983)	EBB	EBB
Jago & Mahamod (1999)	FLOOD	EBB

If Engelund and Hansen's (1967) formula is considered to be the more applicable formula to use, as discussed in Section 3.2.4, it can be seen that Hamford Water may be experiencing a net flood flux on springs and a net ebb on neaps. Such a situation for SPM flux is demonstrated by Dobereiner and McManus (1983) for the Tay estuary. If a similar situation exists in Hamford Water, then as a rough calculation, in 1995 there were 706 high tides of which 354 were spring high waters (exceeding 3.8m above OD), and the remaining 352 were neaps. Of the 354 spring tides only 100 were over 4.0m, which is the mean height that all saltmarsh is deemed to be submerged. Therefore, if it assumed that on spring tides there is a flood transport of suspended sediment, as predicted by E&H, and on neaps an ebb transport, 14% of the tides transport sediment to the saltmarsh, 36% of the tides are flood dominant but most of the sediment does not reach the saltmarsh, and 50% of the tides are ebb dominant. This would suggest that

the system is experiencing some measure of dynamic balance throughout an annual cycle of SPM flux.
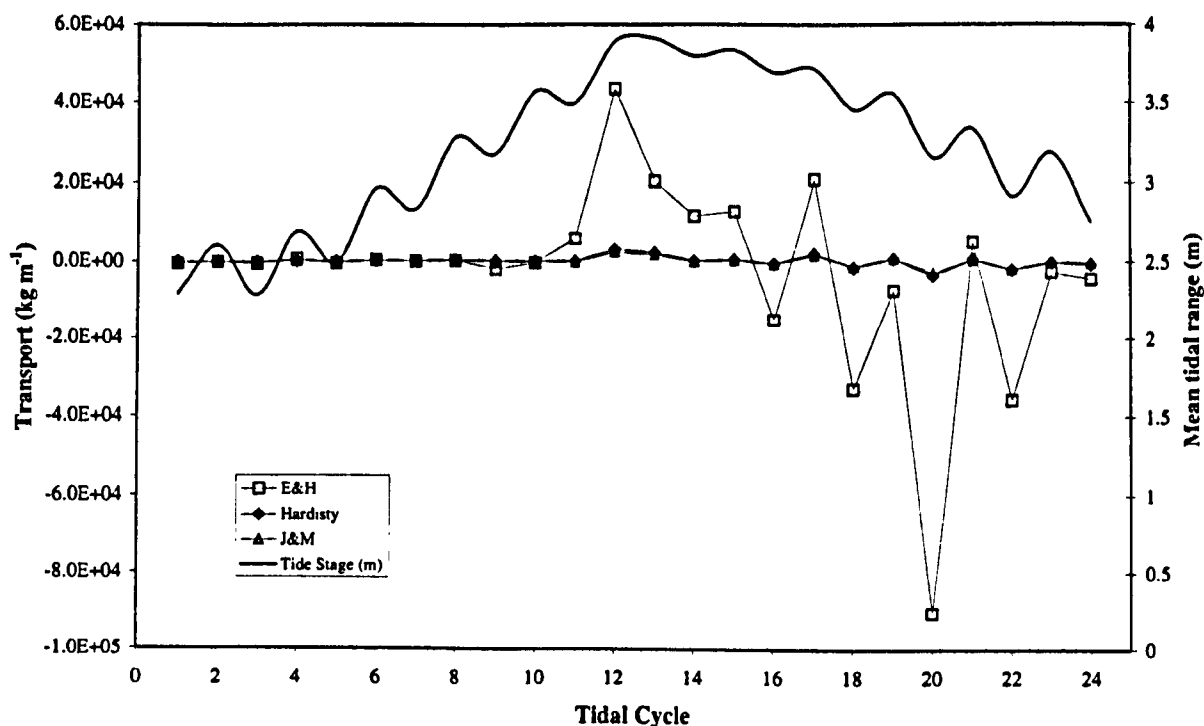
Figure 6-15 – Time series of sand sediment transport rate tidal range.

If a time series over a full spring-neap cycle is considered (Figure 6-15), net transport appears to remain minimal in the lead up to springs and then dramatically increases just prior to peak springs followed by a general decline towards neaps. This could suggest factors other than a direct relationship with current velocity and bed shear stress. One such effect may be attributed to the weather. The weather can affect the movement of sediment in a shallow embayment in a number of ways: firstly, precipitation on exposed mudflats at low tide can increase erodibility which results in increased SPM levels on the next high tide. Secondly, wind strength increases wave height which erodes mudflats and saltmarsh depending on the state of tide. Thirdly, wind direction can enhance or retard the ebb or flood current depending on whether the wind is in opposition or supposition. Such forcing is obviously difficult to predict although seasonal predictions can be attempted based on short-term climatic records. For the duration of the period of the above data set there were no significant meteorological events that may have contributed to increased wave action and therefore increased sediment transport.

The sediment transport rate can be considered to be directly dependent on the tidal range since the tidal range determines the current velocity. It is hypothesised, from an analysis of the results of this research, that in Hamford Water a threshold range is reached, normally before springs, when shear stresses are such that a plume of fine sediment is forced into suspension. The result is a phase advance between tidal range and average sediment transport rate (*cf.* Figure 6-15 and Figure 6-16).
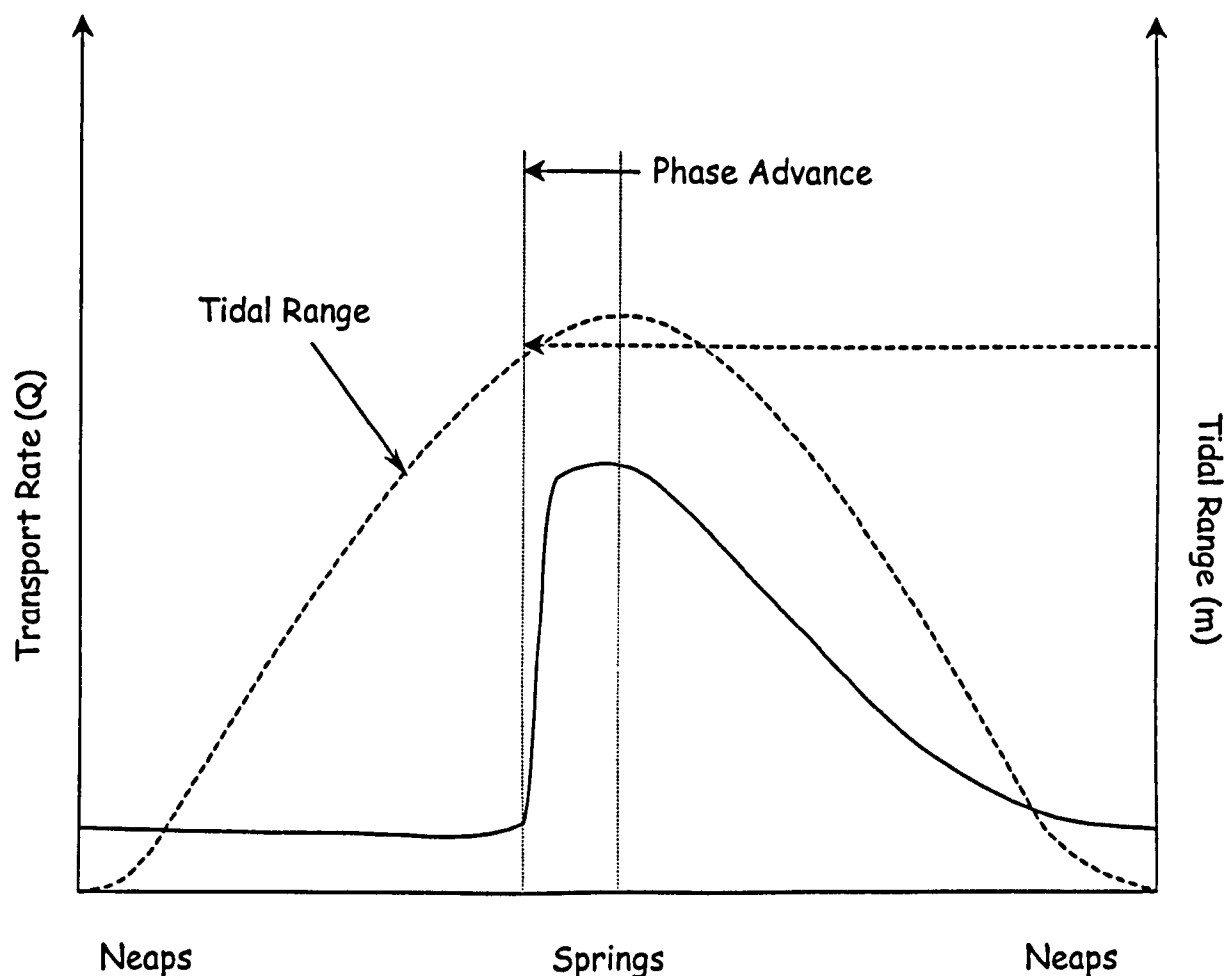
Figure 6-16 – Sediment transport rate phase advance.

Tidally averaged suspended solids was highlighted by Parker (1994) as being an area of research that required more data. As longer data sets are becoming available it is evident that physical processes are modulated on longer periods by non-physical forces. Parker (1994) describes a long term summer decline in tidally averaged suspended sediment and a repeated phase advance of SPM. The proposal in this thesis is that the overall sediment transport of Hamford Water mirrors the processes by which cohesive sediment beds erode: the critical shear stress for erosion is reached in steps; in this case a single step is reached at some point prior to peak springs. It is also hypothesised that the form of the tidal basin contributes to the observed stepped, rapid increase in SPM as

opposed to a gradual build up as velocities increase towards springs. Figure 6-17 illustrates a stylized form of a longitudinal section of Hamford Water. The actual profile of the thalweg from Beaumont Quay to Pye End buoy is illustrated in Figure 6-18.
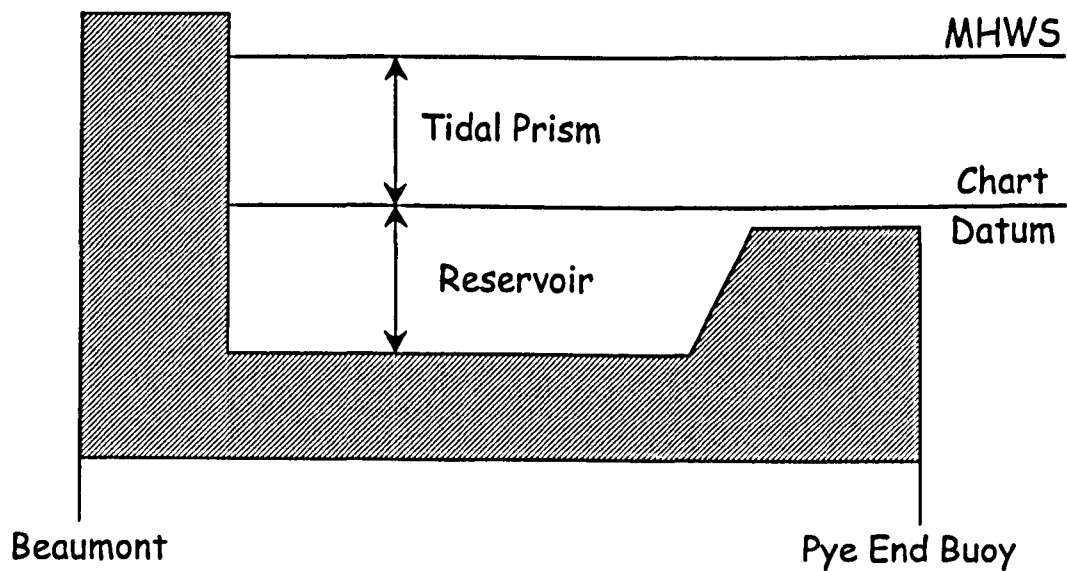
Figure 6-17 – Stylized longitudinal cross-section of Hamford Water
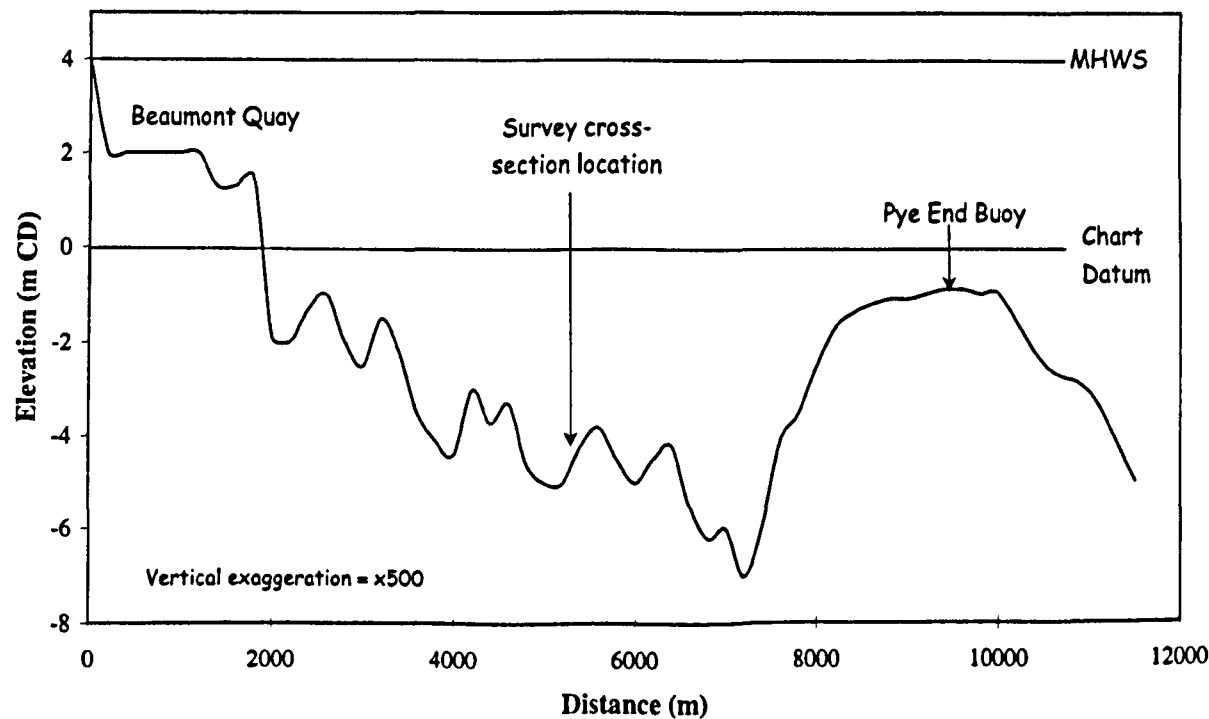
Figure 6-18 – Hamford Water thalweg from Beaumont Quay to Pye End Buoy

As discussed in Section 6.2 above regarding SPM, Hamford Water never drains completely, there is always a reservoir of water remaining at low tide. It is suggested that this reservoir is filled, to some extent, with a high concentration of fine sediment, similar to a fluid mud layer, with a correspondingly high density. Under low flow

velocities during neaps, the flood and ebb current flow over the reservoir with minimal mixing due to the density difference. At some stage during the build up to springs a velocity is reached whereby the density boundary is broken down and the fluid mud layer is incorporated in the main flood and ebb flow. Unfortunately, the existence of such a layer was not detected conclusively during profiling with the transmissometer (*see Section 5.5*). It was assumed that if it did exist then it should be evident at Station 2 (Pye Channel). If the original SPM data is reassessed and each individual cast of the transmissometer is plotted for both the spring and the neap survey, the result is as illustrated in Figure 6-19 and Figure 6-20. On Figure 6-19 and Figure 6-20 the separation between surface and bottom SPM levels are bounded by an envelope, and Figure 6-21 is depth averaged velocity for the same period. If it is assumed that there is very little coarse sediment in Pye Channel, as indicated from grain size analysis in Chapter 5, the predominant sediment movement should consist of SPM. On neaps (Figure 6-19) there is very little variation between surface and bottom SPM levels apart from a short period just after low water and for approximately two hours after high water. Throughout the tidal cycle, surface SPM varies only gradually, increasing only on the ebb tide. On springs (Figure 6-20), the separation between surface and bottom SPM is much more marked. On the flood the surface SPM levels mirror the bottom SPM levels but with a marked separation between the two. On the ebb, however, there is a rapid increase in SPM levels, but a reduction in the size of the separation between surface and bottom. The two graphs illustrate that at a certain critical velocity, plumes of fine sediment are lifted into the water column and that at an even greater critical velocity the whole of the bed is turbulent and well mixed. There is also an indication of a stepped approach to erosion of cohesive beds: on the spring flood and the neap ebb when current velocity increases are steady, SPM levels peak and then subside before peaking again. In general, Figure 6-19 and Figure 6-20 illustrate rather simply the possible existence of a bed of high concentration SPM, the actual existence of which is highlighted for further investigation.
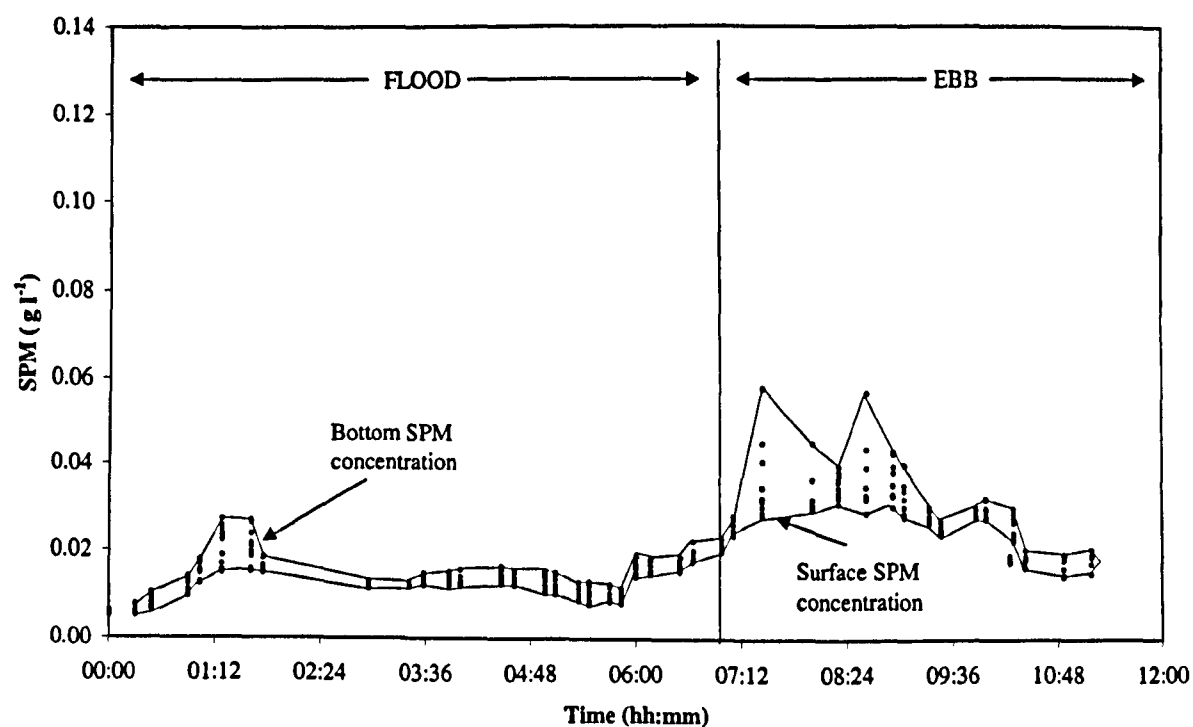
Figure 6-19 – Transmissometer casts at Station 2 for a neap cycle.
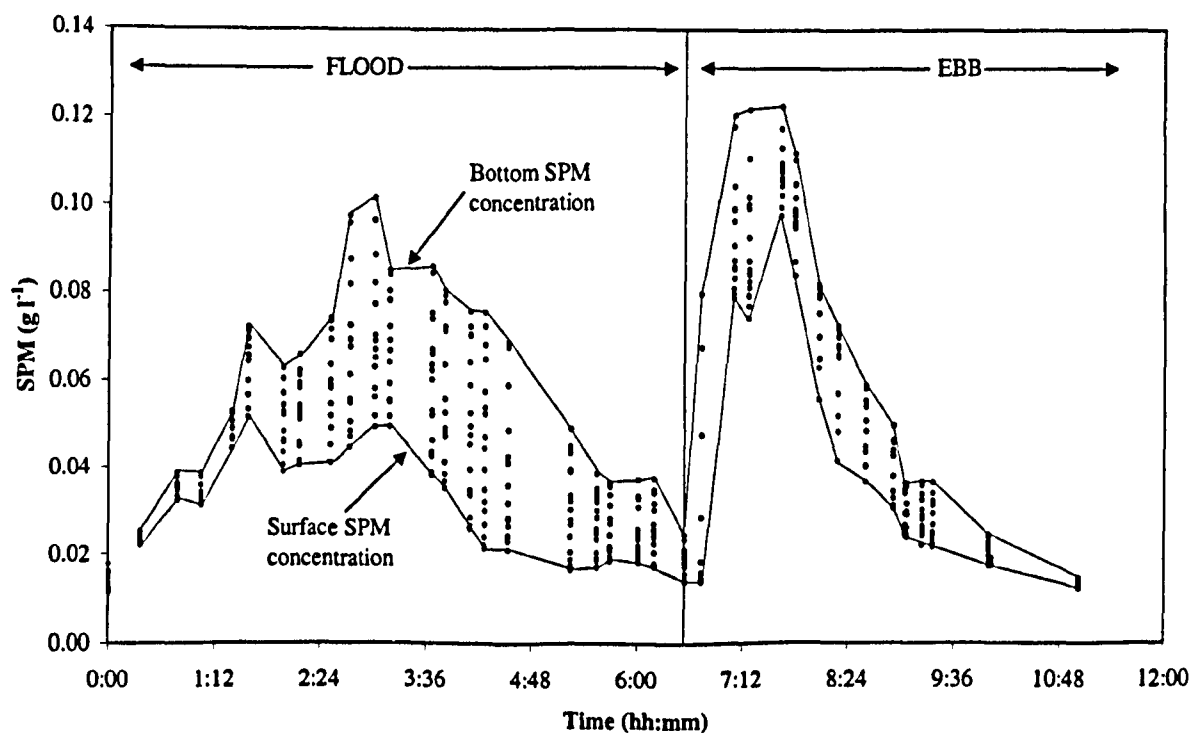
Figure 6-20 – Transmissometer casts at Station 2 for a spring cycle.
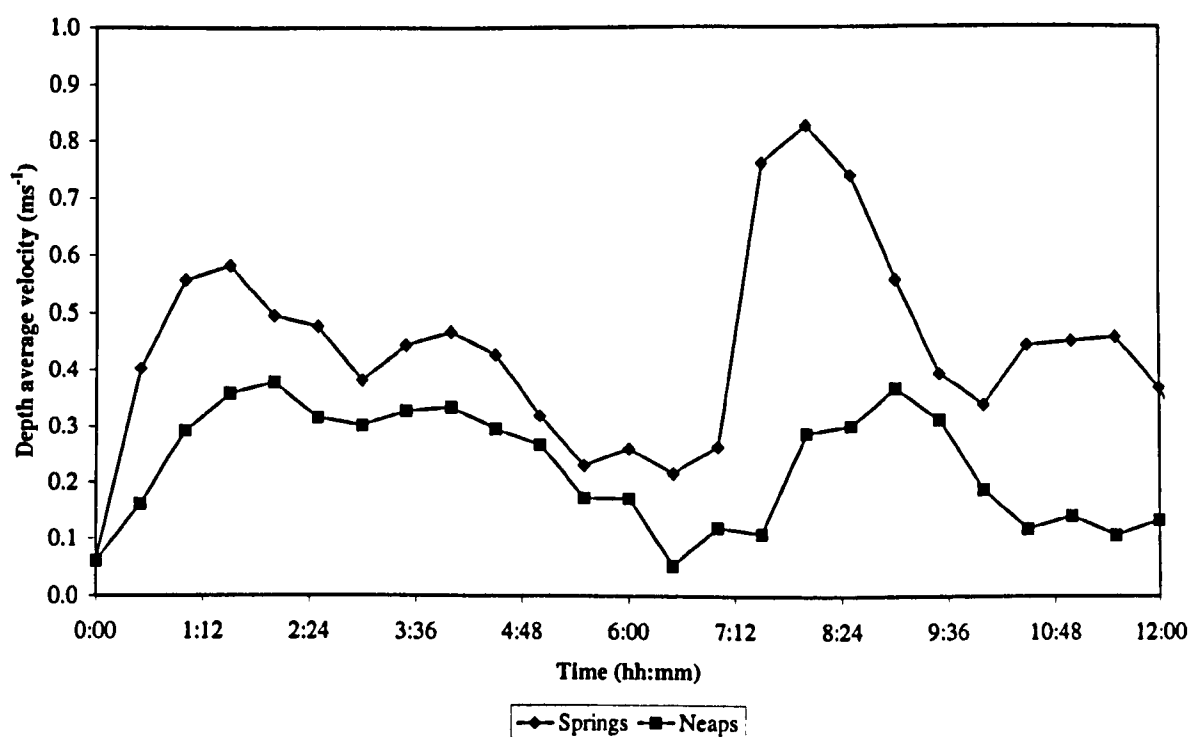
Figure 6-21 – Station 2 depth average velocity.

The above analysis of sediment transport serves to present a qualitative understanding of the movement of sediment through the inlet throat of Hamford Water. There is, however, a great deal of uncertainty; the most significant cause of which is the various predictive methods used. The first point to note is the difference between the three methods: Engelund and Hansen's method produces results considerably greater than Hardisty's, and Jago and Mahamod's. The simple explanation for this is the difference in the methods as previously mentioned in Section 3.2.4: Hardisty's method is for bedload transport and includes a threshold term; Engelund and Hansen's method has no threshold term and is for total load transport; Jago and Mahamod's method is for total load and involves a threshold condition. Although the attraction of the Hardisty's equation is the need only to measure u_{100}, u_{100t} and k_1, the limitations are that it is based on only four data points, and the calibration is based on low flow velocities (<0.55 ms^{-1}) using flume data and therefore is not suitable for fast currents and suspended load. Hardisty's method tends to overestimate q at low velocities and underestimates q at high velocities (Jago and Mahamod, 1999). Jago and Mahamod (1999) criticise their formula (Equation 6:6) pointing out that since q is sensitive to changes in n, and n is very sensitive to changes in D, under field conditions Equation (6:6) may give

uncertain values of q. They demonstrate that, for fine sand, and high velocities and transport rates, the velocity/transport rate relationship is not linear.

It has to be accepted that no single method or even a combination of methods can accurately determine the sediment transport rate or the sediment flux through the inlet. Each method has its limitations and therefore an accurate quantitative value of the direction of net sediment transport through the inlet is not possible. What can be achieved, however, is an qualitative assessment of the net sediment transport direction, from which inferred pathways of sediment transport can be attempted.

6.5   Summary

This chapter has assessed the flux of SPM and the rate of suspended and bedload sediment transport during both a flood and ebb tide, and over a spring-neap cycle. The results from measuring the SPM flux for a single spring and neap tidal cycle indicate that there is a net ebb transport of 670 tonnes on springs and 15 tonnes on neaps. However, the errors involved in the calculation of SPM flux mean that the results can only be viewed as qualitative rather than quantitative.

Three individual methods used for calculating Sand sediment transport rate produced a complex mixture of both ebb and flood net transport direction. If the total load formula of Engelund and Hansen (1967) is seen as offering the most applicable net transport direction, it is suggested that Hamford Water experiences a net flood transport on spring tides and a net ebb transport on neap tides. It is hypothesised that the change from ebb to flood transport is not linear; instead, a phase advance in peak transport is determined by tidal range and, by implication, peak velocities. It is also hypothesised that the morphology of Hamford Water enables a fluid mud reservoir to form that is incorporated into the overall sediment budget only after a critical shear stress is reached.

7 Contemporary rates of accretion and erosion

7.1 Introduction

This chapter is a study of the contemporary, spatial and temporal patterns of erosion and accretion in the embayment. Temporal variations are assessed by measuring the vertical rate of change using discrete markers on saltmarsh, in tidal creeks, and on mudflats. Spatial variations are assessed by reference to any published literature, maps and charts of the site.

7.2 Methods

7.2.1 TEMPORAL VARIATIONS

A total of 78 markers on 9 separate transects were set up in the Kirby Creek and the Wade area of Hamford Water (Figure 7-1). The setting-up procedure involved establishing a temporary bench mark (TBM) on, or at the foot of the sea wall, and levelling back to a known Ordnance Datum bench mark where possible. A second TBM was established at the seaward limit of the saltmarsh and, using the level for sighting, a series of markers were positioned between the two TBMs. The markers consist of 10 x 10cm steel plates buried in the saltmarsh at a depth of approximately 10cm, and 5mm diameter stakes driven into the bottoms of creeks where they occur along the transect. After allowing a settling period of a month, all markers were monitored at approximately 3-monthly intervals for a total of 26 months.

The problems of monitoring and maintaining such transects are considerable. Ideally some comparison between spring and neap measurements should have been made; unfortunately the timing of the tidal cycle rendered this impractical. The time of high water during springs in Hamford Water occurs around midday and midnight.
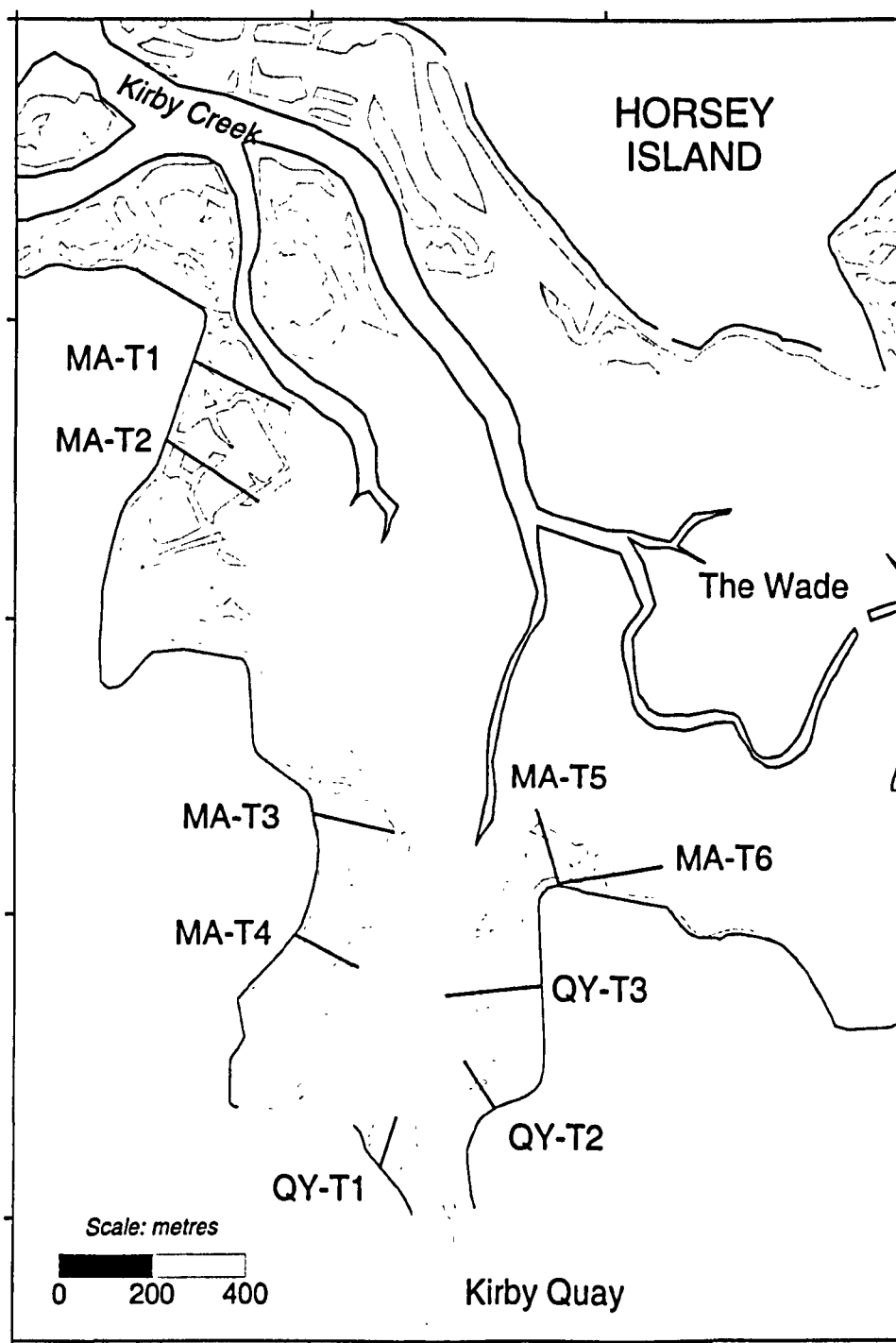
Figure 7-1 – Transect location map.

From a safety point of view this did not leave enough daylight hours to monitor all markers. During neaps, however, low water occurs around midday leaving almost the entire period of daylight to take measurements. The actual window of opportunity was about 5 to 7 days depending on time of year and available daylight hours. In the results discussed below, the data are averaged to whole months, so the error bounds in the horizontal are effectively ±15 days. Only the saltmarsh and the edge of the mudflats were monitored simply because the mudflats of Hamford Water are generally too soft to walk on and, even if markers were positioned, monitoring would destroy the surface

being measured. The successful use of vertical markers for measuring accretion is commonly considered limited because of the effects of scouring around the base of the marker. It was found during this research, however, that scouring rarely occurred and a bigger problem was the seasonal build-up of an algae cone at the base of the marker. This was most evident on creek and mud flat markers and in the spring resulted in cones up to 3.0cm in height with a diameter at the base of 5.0cm. It was decided in all instances to carefully dislodge the cone before measuring the marker. In hindsight plates should have been placed in the creeks and mud flat sites as with the saltmarsh sites and the vertical markers used for re-location and identification only.

Errors in measuring the plates and stakes are difficult to ascertain. When measuring plates the mean of at least four separate readings were taken around the centre of the plate using a spike, or dibble, and the depth of penetration measured to ±1mm with a standard millimetre rule. Measuring stakes in creeks proved more problematic since the very act of approaching the stake can disturb the level of mud around the base. The decision to remove algal cones prior to measuring also imposed an unknown random error on the bed elevation. However, as with the plates, the height of the stake above the bed was measured to ±1mm using a standard millimetre tape-measure. It is assessed, purely from experience, that the vertical error bounds are ±2mm for saltmarsh and ±4mm for creeks.

7.2.2   SPATIAL VARIATIONS

Actual physical measurement of spatial variations of the extent of saltmarsh was not conducted in this research. Burd's (1992) extensive assessment of erosion and vegetation change between 1973 and 1988 is the only reliable study to-date and this is used in conjunction with old maps and charts that cover the area. In addition, Kodz (1994) assessed changes in the spatial extent of saltmarsh for a section of Kirby Creek from aerial photography. Physical methods of determining the lateral rate of saltmarsh cliff erosion were not attempted. Saltmarsh cliff retreat is not a uniform process and can only be assessed with any reliability from detailed cartography. The use of discrete markers on the cliff edge can only provide data for a very small section which cannot be extrapolated more than a few metres: saltmarsh cliff erosion tends to be a result of slumping and rotational slip confined to a very small area (Frey and Basan, 1985).

7.3 Results and Discussion

7.3.1 TEMPORAL VARIATIONS

The results from saltmarsh and tidal creek monitoring are summarised as mean values in Table 7-1. Averaged data and details of statistical analysis are contained in Appendix J. For the period of observation, the annual rate of change of salt marsh and creek bed elevation was calculated from the slope of the linear regression of data for 26 months.

Table 7-1 – Summary of mean annual vertical rates of change

Location	n	Rate (mm yr-1) (dz)
All	78	4.2
All Creek	37	5.9
All Marsh	41	2.7
All West-facing	36	3.6
West facing Creeks	20	5.3
West facing marsh	16	1.4
All East-facing	42	4.8
East-facing creeks	17	6.6
East-facing marsh	25	3.5

At the outset of this research, published reports tended to support the principal hypothesis of this thesis: that Hamford Water was experiencing net *erosion* of saltmarsh. However, the obvious conclusion from Table 7-1 is contrary: Hamford Water is subject to a significant net *accretion* on both saltmarsh and mudflat: the annual rate of change for all markers being 4.2 mm yr^{-1}. This supports Leeks (1975) who investigated vertical accretion rates over a 9–month period (April to December 1974) for 20 sample points of saltmarsh on the north side of Hamford Water and found the sample mean rate of accretion to be 1.4mm yr^{-1}. Although his method and the exact location of sample points is unknown, it is clear that a net erosion rate is not apparent on either the north or south saltmarsh. It would be tempting to extrapolate the above results (Table 7-1) to the whole site but it is suggested that localised variations cannot be ignored. In Annex B, it was proposed from a cursory look at available data, that saltmarsh and tidal creek elevations might be affected by meteorological conditions. It was postulated that there may be lower activity and corresponding lower accretion on

the marsh than in the creeks. West-facing marsh accretion (i.e., towards the prevailing wind) was suggested as being minimal, whereas east-facing marsh was showing approximately 5mm y^{-1}. Superimposed on this is the additional hypothesis: although Hamford Water is experiencing a net loss of saltmarsh, the loss is being translated into a net gain on the mudflats and in tidal creeks. In other words, creek sedimentation should be greater than saltmarsh sedimentation. It is also proposed that given the sheltered nature of Hamford Water, there is a local effect of waves (as discussed in Section 4.2), determined by aspect to the prevailing wind; east-facing (sheltered from the prevailing wind) areas should experience more accretion than west-facing. The forcing mechanism behind the above variations in sedimentation is suggested as resulting from a direct relationship between seasonal, and therefore, meteorologically driven levels of SPM. The following variations are proposed:

- Higher winter SPM than summer SPM due to more winter mixing.

- Higher spring tide SPM than neap tide SPM due to more mixing on spring tides.

- Increased erosion from wind-generated waves in winter; low erosion in summer.

- Increased resistance to erosion in summer from algal binding.

- Possible decreased bed erodibility in winter due to trampling and compaction by over-wintering birds.

Given the restrictions on monitoring due to the nature of the tide in Hamford Water (*see* Section 7.3.1 above), it was not possible to assess whether there were any systematic differences between springs and neaps. It is postulated, however, that spring-neap variations of saltmarsh accretion could be significant: the tide only covers the marsh surface at springs, therefore no marine sediment can be deposited at neaps and most sedimentation occurs at springs. Figure 7-2 illustrates a model of the sedimentation processes during neaps: as the tide rises over the mudflats, depending on wave action, there may be some re-suspension of sediment from the mudflat. Generally, SPM levels, both from re-suspension and ambient levels, are low due to low current velocities during neaps and consequently there are low levels of sedimentation. As the tides reaches high water the saltmarsh cliff may be subject to wave action and

possible undercutting and slumping. Processes on the saltmarsh are unaffected by the tide as long as the marsh remains uncovered: there is unlikely to be any marine sedimentation and compaction and consolidation processes will be at work. On neaps there is more likely to be erosion from the saltmarsh surface if considerable precipitation is experienced.
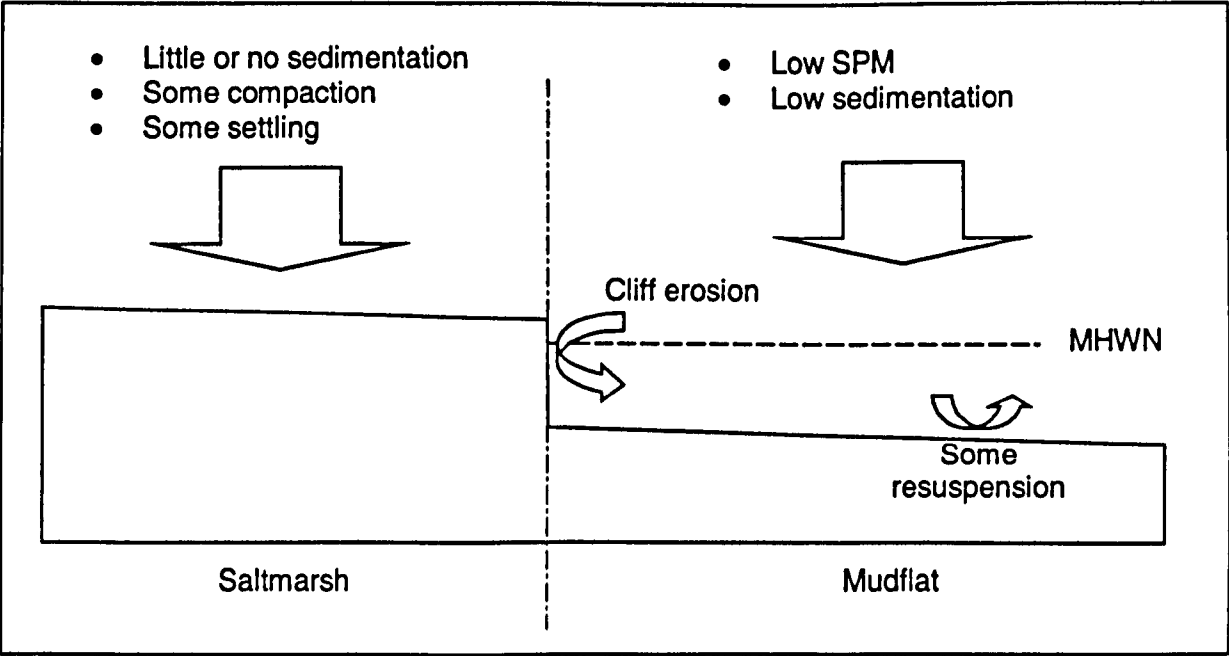
Figure 7-2 – Saltmarsh-mudflat sedimentation – Neaps

During spring tides (Figure 7-3) the rising tide results in re-suspension of sediment from the mudflat fronting the saltmarsh depending on wind/wave action. Some saltmarsh cliff erosion occurs as the tide rises and reaches bankfull stage and covers the saltmarsh. Generally, during springs over the mudflat, SPM levels are high and there is a correspondingly high sedimentation rate. Over the saltmarsh, there is high sedimentation, some erosion, a little compaction and some settling of the marsh.

178
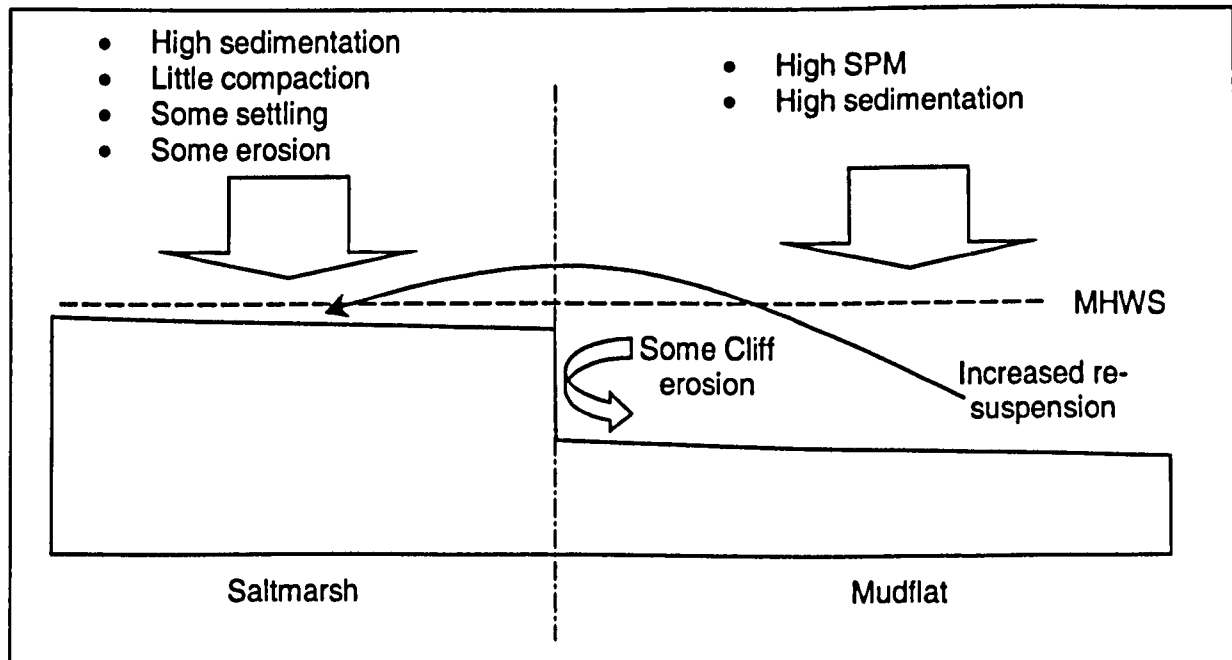
Figure 7-3 – Saltmarsh-mudflat sedimentation – Springs

With the above model in mind and given the evidence for seasonal variability in saltmarsh and mudflat accretion and erosion rates, it was decided to test whether there are seasonal and localised variation in saltmarsh and tidal creek sedimentation in Hamford Water. It can be seen from Table 7-1 that the average rate of change in elevation of all points (Δz) was found to be +4.2 mm yr^{-1}. A t-test of whether the rate of change of elevation of creek markers (δz_{ck}) is significantly greater than Δz at the 95% confidence level gives 0.62 which according to statistical tables (Spiegel, 1992) for 36 degrees of freedom, the null hypothesis, $H_0 : \delta z_{ck} = \Delta z$ should be rejected if $t <$ 1.69. Similarly, a t-test of whether the rate of change of elevation of saltmarsh markers (δz_{sm}) is significantly lower than Δz at the 95% level gives –2.66, which for 40 degrees of freedom, $H_0 : \delta z_{sm} = \Delta z$ should be rejected if $t >$ 1.68. In both cases, therefore, H_0 is rejected implying that there is a significant difference between creek and saltmarsh sedimentation: creek sedimentation is greater than saltmarsh. Comparing the two main morphological features, it is hypothesised that δz_{ck} is greater than δz_{sm}, and a two-sample t-test assuming unequal variances gives $t = 0.19$. From statistics tables, the value required for t-statistic with 36 degrees of freedom at the 95% confidence level is 1.69 or higher. Figure 7-4 to Figure 7-6 illustrate the mean rates of vertical change (in mm) for all marsh, all creek, and all samples respectively. In all cases both a linear and a 3rd order polynomial have been fitted to the data. The linear trend simply accords with the mean annual rate of change as calculated and tabulated in Table 7-1. The 3rd

order polynomial is fitted in an attempt to assess trends within the data. It is evident that a there may be some waxing and waning of sediment accretion rate but it is not clear whether it is a seasonal variation with an annual period.
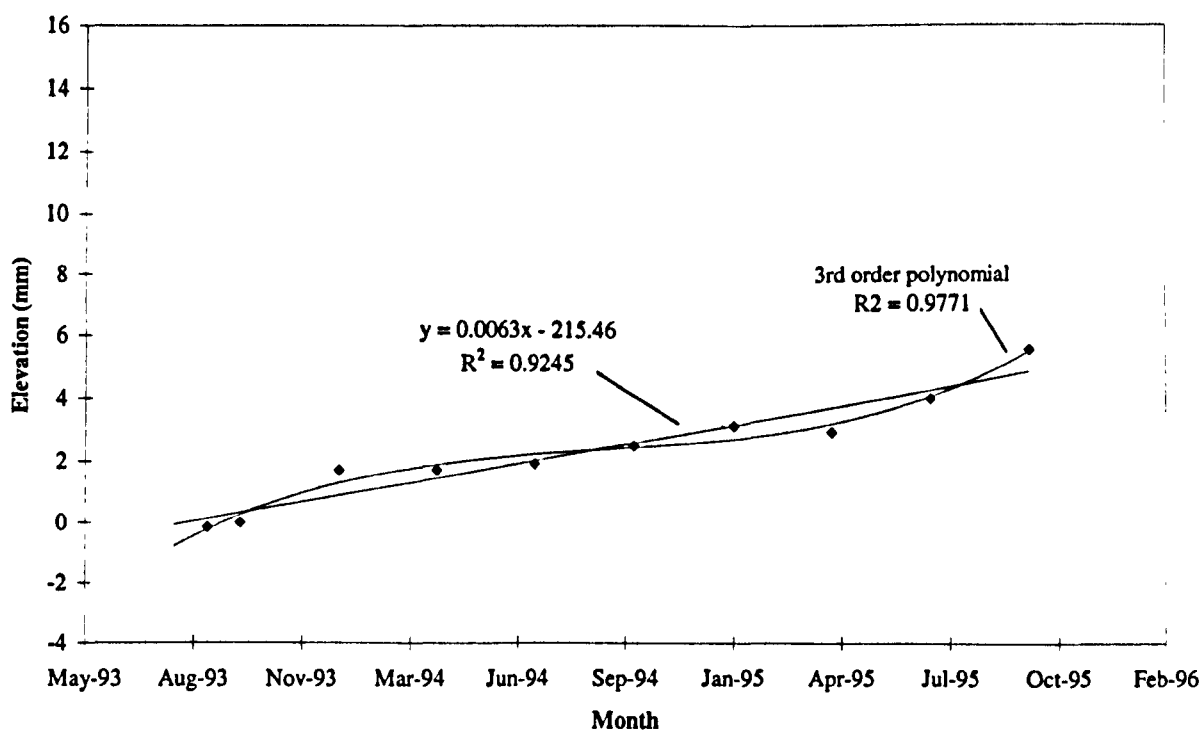
Figure 7-4 – Mean accretion for all marsh samples over 26 months.
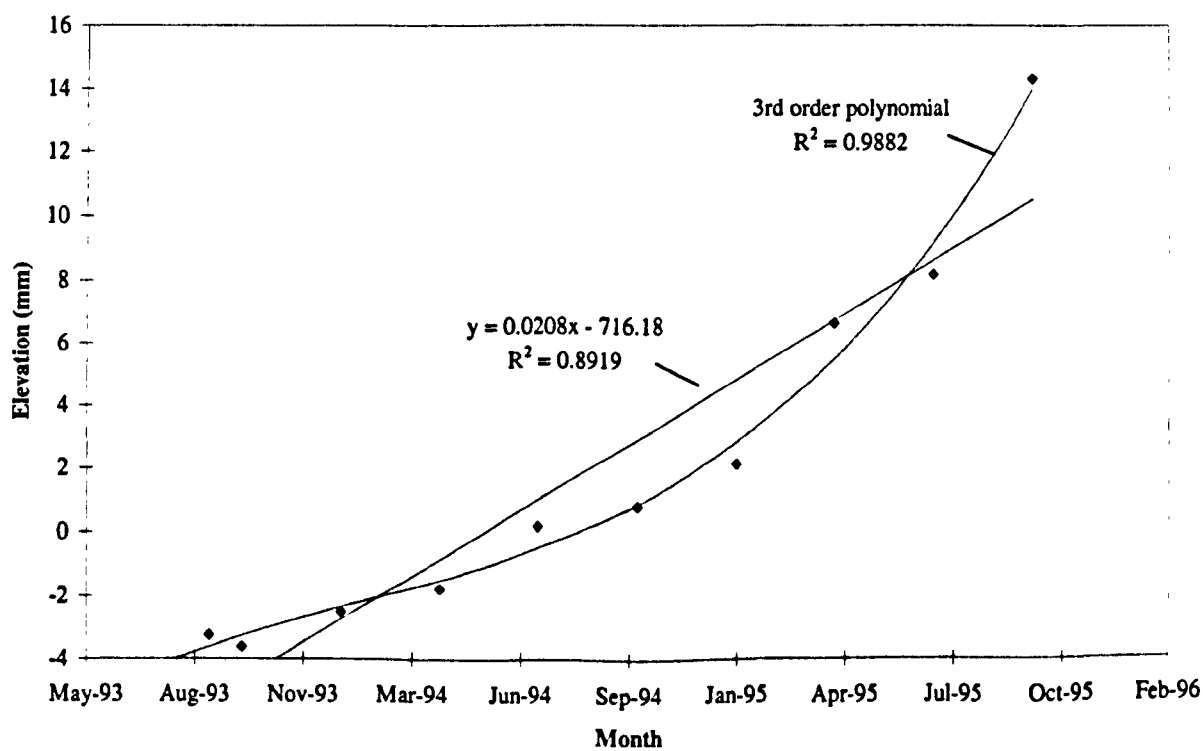
Figure 7-5 – Mean accretion for all creek samples over 26 months.
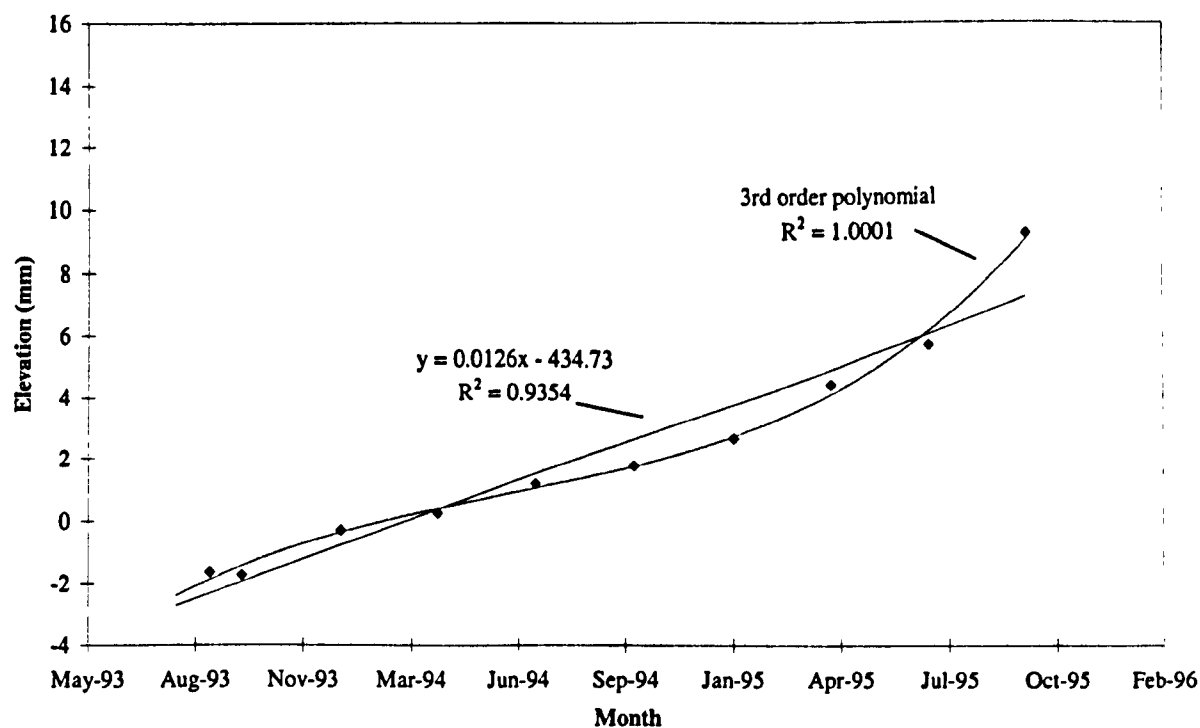
Figure 7-6 – Mean accretion for all samples for 26 months.

In order to further investigate the possibility of trends and possible seasonal variability within these data, time series analysis using an additive forecasting method (Wilkes, 1989; Chatfield, 1996) was conducted on marsh and creek data separately, and on all data. Using the additive method, each observation (Y) is considered to contain a trend (T), a seasonal variation (S), a cyclical variation (C) and a residual variation (r). Wilkes (1989) considers that the cyclical variation is only worth identifying in very long (decadel) time series; and since this analysis is mainly concerned with seasonal variations, the cyclical variation (C) in the following analysis is excluded. The resulting model used is:

$$Y = T + S + R \qquad (7:1$$

Figure 7-7, Figure 7-8 and Figure 7-9 are plots of observed change in elevation with time versus the predicted change as determined by the Additive forecasting model.
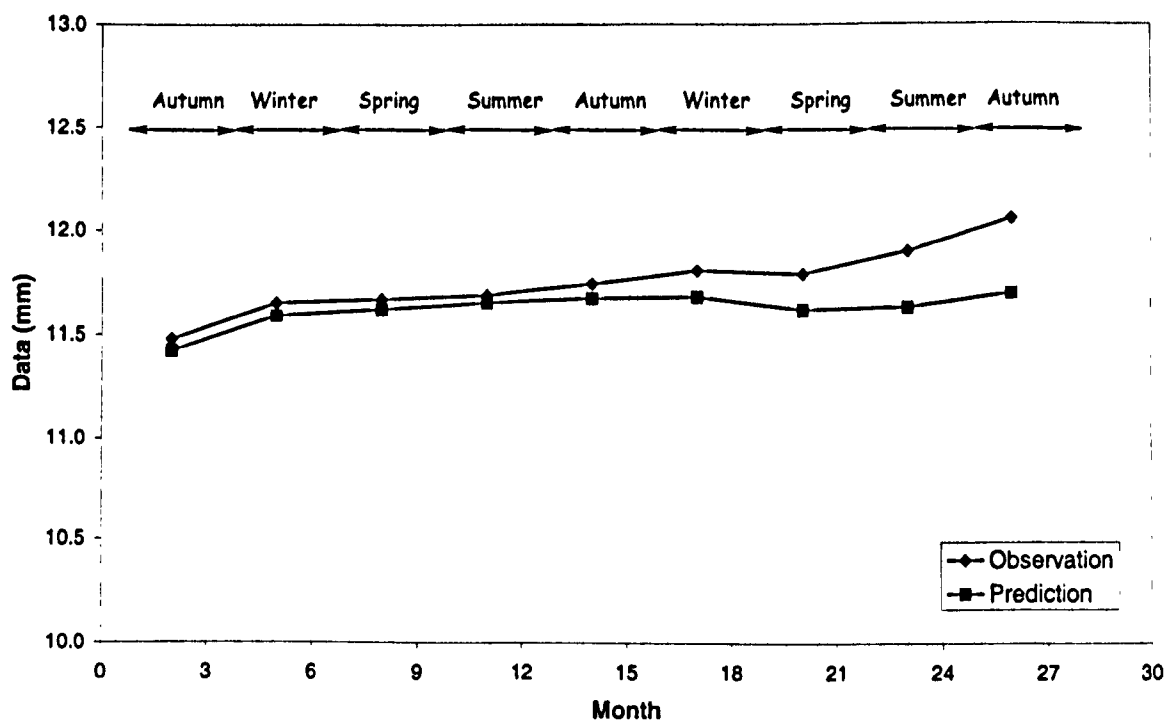
Figure 7-7 – All Marsh Data – Observed versus Predicted.
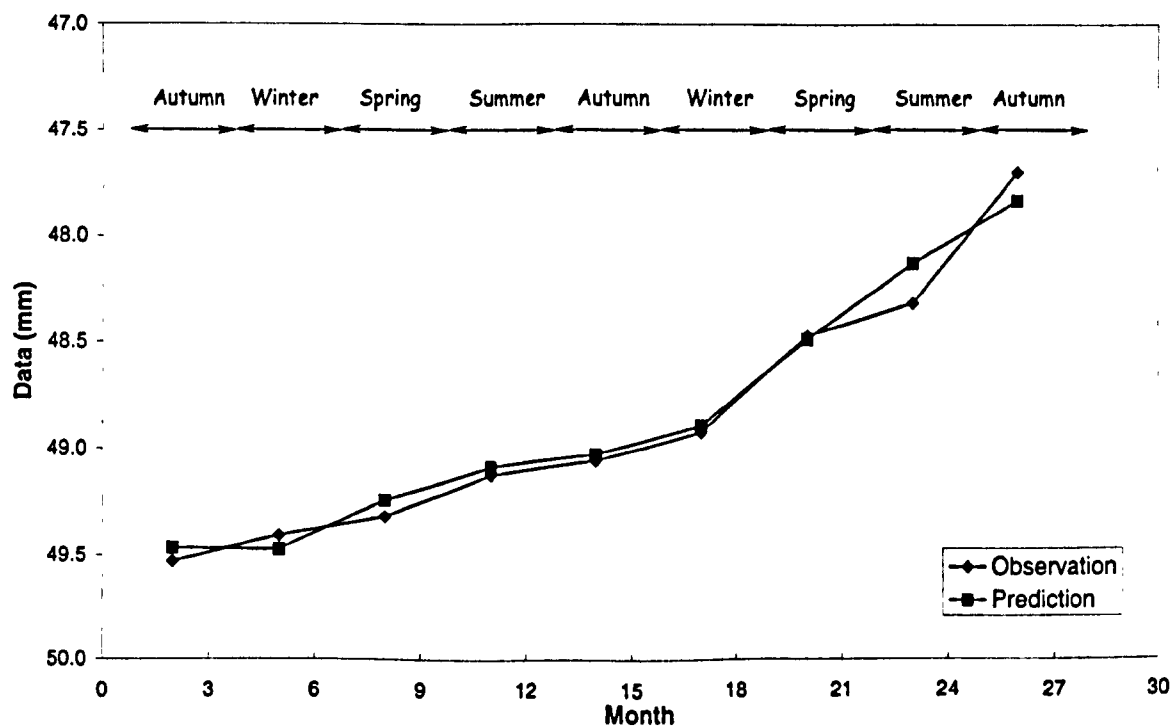
Figure 7-8 – All Creek Data – Observed versus Predicted.
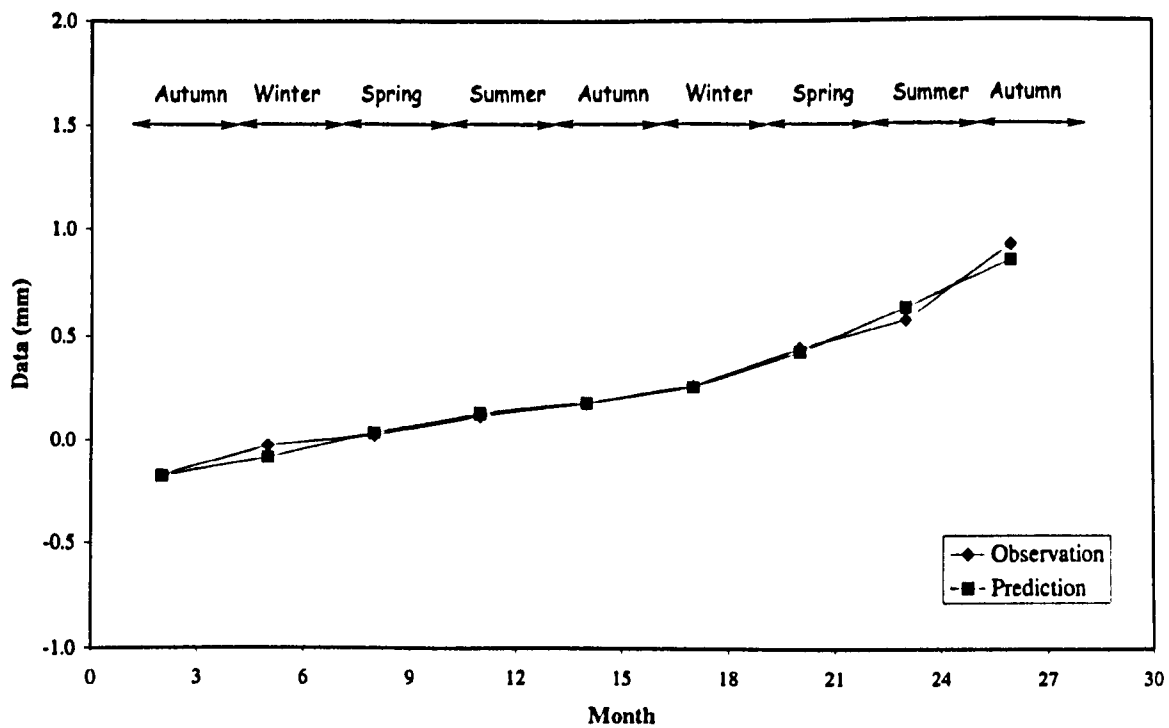
Figure 7-9 – All Data – Observed versus Predicted

The results of attempting to fit a model to the data, as illustrated above, show that the observation and the prediction accord closely when all creek data and all data are considered (Figure 7-8 and Figure 7-9), but the model diverges when all marsh data are considered (Figure 7-7).

It is concluded from a statistical investigation of the data that seasonal variations cannot be determined with any confidence, and for the purposes of this research the results are best considered as having a simple linear trend. The hypothesised model illustrated in Figure 7-2 and Figure 7-3 cannot, therefore, be tested effectively. However, by eliminating seasonality and assuming linear trends in the data, a direct comparison can be made between the marsh data and the creek data. The results summarised in Table 7-1 clearly show the difference in sediment accretion rates between saltmarsh and tidal creeks: 2.7 mm yr^{-1} on saltmarsh and 5.9 mm yr^{-1} in tidal creeks. The data also imply that the effect of the prevailing wind, south-westerly in this case, is to cause more accretion on east-facing saltmarsh and in tidal creeks (4.8 mm yr^{-1}) than west-facing (3.6 mm yr^{-1}). The inference is that the prevailing wind causes more erosion of those surfaces facing the wind than those that are not and it is considered that local wave action is the main cause.

7.3.2   SPATIAL VARIATIONS

Historical coastline changes and spatial variations were discussed in the preliminary report (Annex A); this section expands on that discussion. It was noted, from a comparison of Admiralty Charts dated 1847 and 1993 (respectively, the earliest and most recent Admiralty Hydrographic surveys and considered to the most reliable indication of channel positioning and depths), that there was very little change in the central position of the main channels: Pye Channel, Hamford Water; and Walton Channel. The reason for the stability of these channels is because they are most probably cut into the Eocene London Clay basement and are therefore relatively resistant to meandering. (The actual channel bed rock type was not determined in this survey.)

The most noticeable changes are to channel depths. Comparison between the 1847 and 1993 Admiralty charts indicate that depths have decreased by between 1 and 2m in the Hamford Water channel and approximately 5m across the width of Pye Channel (Figure 7-10). It is noted, however, from discussion with the UK Hydrographic Department (UK Hydrographic Department Curator, *pers. comm.*) that the accuracy of the 1847 survey should be treated with caution; the method and benchmarks used for the survey are uncertain and unlikely to have been the same as in 1983.
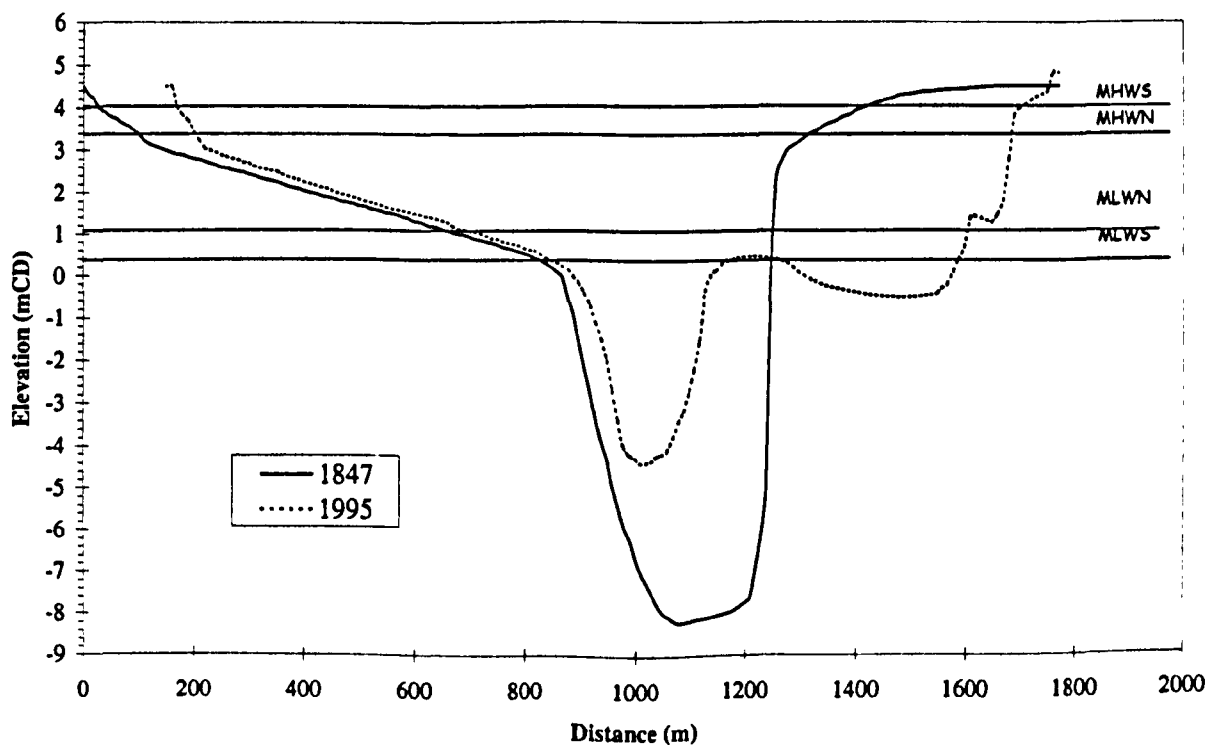
Figure 7-10 – Comparison of inlet cross-sectional profile between 1847 and 1995.

Spatial changes to the smaller creeks and channels is difficult to determine. Minor changes at the head of the main channels and to some of the smaller tributary creeks can be identified; the largest changes being to Dugmore Creek and Salt Fleet. Dugmore Creek is shown on the 1847 Admiralty Chart to be subtidal almost to its head where it drained the saltmarsh to the north of Pewit Island. It has [1999] almost completely silted up, possibly as a result of the beach ridge of Irlam's Beach imposing onto the creek. The creek is now intertidal and although a route to the sea along the line of the old Dugmore Creek still exists, the channel also connects with Bull's Ooze and the main tidal flow is now through Oakley and Bramble Creeks.

Salt Fleet has experienced a similar fate, the subtidal creek having completely silted up so that only an intertidal creek exists. The 1847 Admiralty Chart shows this creek draining the intertidal area between Horsey Island and Hedge End Island and it is possible that the siltation of this creek is a consequence of the attempts to reclaim this area as discussed in Section 2.4. Changes to the intertidal areas of Hamford Water between 1847 and 1984 indicated that there has been a significant increase in intertidal area. Especially around the area of Garnham's Island where erosion of saltmarsh and the reversion of reclaimed areas back to saltmarsh and mudflat has occurred. The study of Burd (1992), who compared aerial photographs from 1973 and 1988, also identified areas where erosion of the saltmarsh has resulted in the increase of mudflats. The main increase in mudflat area as a result of loss of saltmarsh has occurred around the edges of the Wade, Cunnyfur Ooze and Bull's Ooze. The erosion of these saltmarsh areas can be attributed to wave action, as discussed in Section 4.2, waves being able to develop during higher tidal ranges. This process involves positive feedback: the loss of saltmarsh increases the area of mudflat, and hence the fetch length, this in turn increases the size of waves that erode the saltmarsh edge. The result is an increase in the area of mudflat and fetch length.

It is calculated, from Gramolt (1960), that approximately 1067 ha of land were reclaimed by 1880; it is also known that 705 ha of saltmarsh were measured by Burd (1992) as remaining in 1988. The difficulty in marrying the two values so that a reasonable estimate of saltmarsh loss since 1880 can be made, is the lack of a spatial limit to any calculations. It has to be assumed that the present day seawall provided the

limit to Burd's calculations and that the approximate line of the 5m contour line would provided a boundary for unopposed marsh development.

Figure 7-11 is a plot of saltmarsh area in hectares against time since 1600. It is plotted from a point of view of saltmarsh loss as opposed to land gain. This is essentially a reconstruction from Gramolt (1960) and shows phases of reclamation and times of sea defence failure due to abnormally high tides. It assumes no loss or gain of salt marsh between phases. It also shows occurrences of notable floods on the East Anglian coast (data from Grieve (1959), Harland and Harland (1980)). The hatched line is an assumed rate of loss of salt marsh since 1900, no major reclamation has taken place since. Figure 7-12 is the same plot with a fitted linear rate of saltmarsh loss since 1600 – an inferred rate of loss 2.76 ha^2 yr^{-1}.
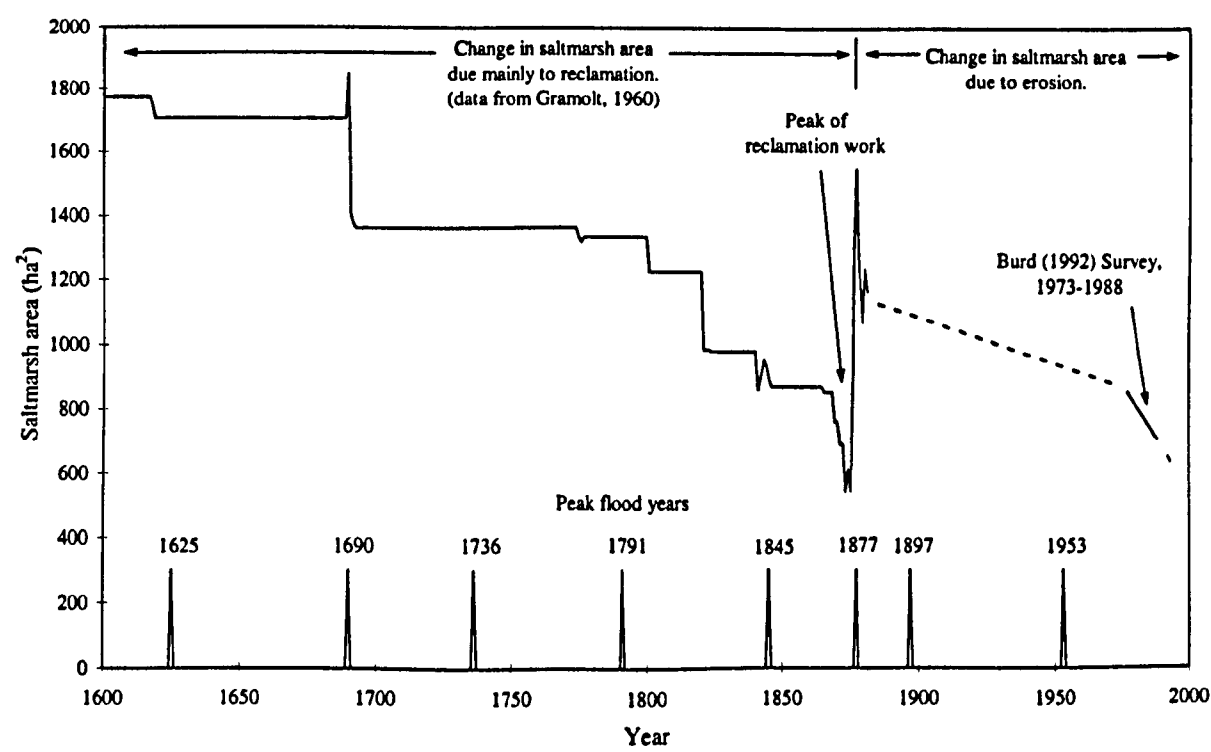
Figure 7-11 – Change in area of saltmarsh since 1600.
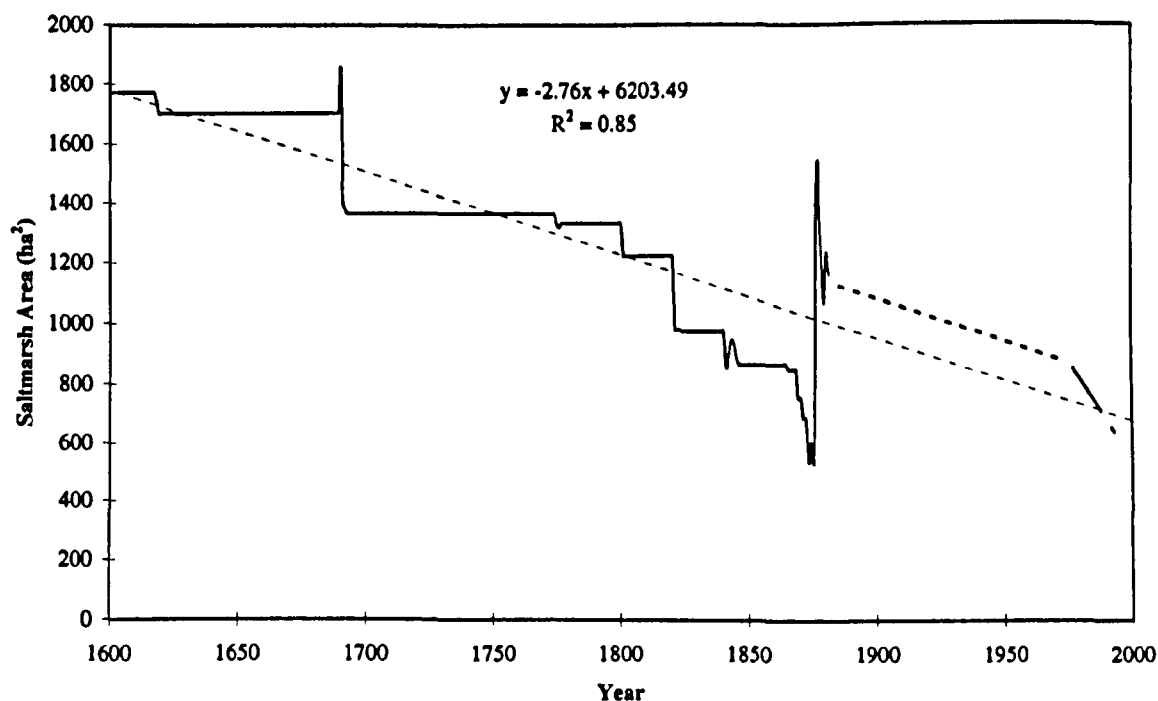
Figure 7-12 – Rate of loss of saltmarsh since 1600.

The greatest loss of saltmarsh is that of Stone Point and Figure 7-13 is the result of an analysis of various maps and charts dating back to 1794. (Appendix K list the maps and charts used to compile Figure 7-13.) The inference is that there has been an average rate of retreat of Stone Point of 2.3m yr^{-1} since 1794. Although by fitting a curve to the data, the rate has considerably increased since the 1930's.
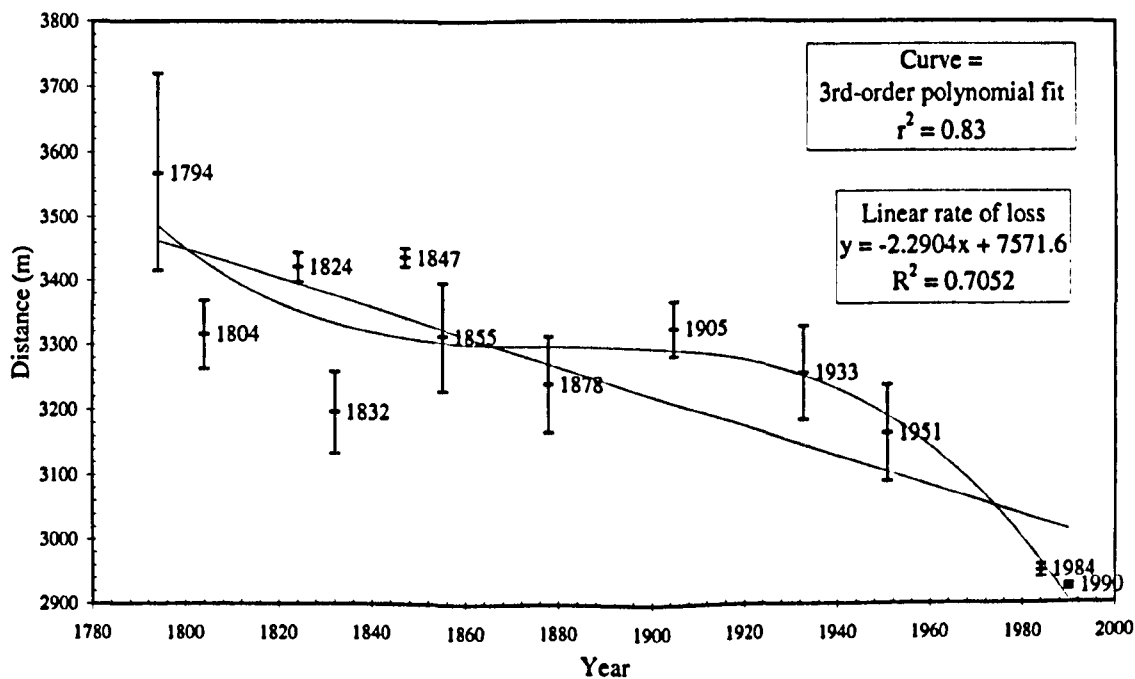
Figure 7-13 – Changing position of Stone Point measured relative to the Naze Tower (1794 to 1990).

The loss of saltmarsh areas to reclamation was detailed in Section 2.4. The subsequent breach of many of the enclosures has resulted in large areas reverting to mudflat and saltmarsh. It is worth noting that during the intervening periods, when some areas are reclaimed whilst others remain open to tidal sedimentary processes, the enclosed areas are often lower than the surrounding unenclosed areas. Results of a field study by Kodz (1994) in which transects were levelled across sea walls in selected locations around Hamford Water, showed height differences of over 2.0m in places: the reclaimed land being lower than the fronting saltmarsh. Therefore, areas which were previously saltmarsh before reclamation, may have reverted, in the first instance at least, to mudflats since the levels of these areas were too low to allow saltmarsh to develop. Between 1940 and 1981 the 0m contour defining Pye Sands experienced a recession amounting to over 500m, although between 1981 and 1989 this contour built seawards by approximately 200m (IECS, 1995). The changes to the extent of this intertidal area, however, did not parallel the changes in the morphology of the marshes at Stone Point discussed below.

It is perhaps significant to note that the shoreline at Blackman's Head used to extend considerably further out from its present position in historical times. Carlyon-Hughes (1939) reproduces a portion of an Admiralty survey dated 1844 with the retreat of Blackman's Head superimposed. Quarrying for septaria has reduced the extent of the headland by approximately 300 metres since 1752. At the same time the southern extent of Languard Point increased by about the same amount, although a cause-and-effect connection between the advance of Languard Point and the retreat of Blackman's Head is not suggested.

To the west of Pye Sands and to the south of Crabknowe Spit the low water mark has remained relatively stable since 1838, despite the fact the intertidal area to the north, which fronts Foulton Marsh and Dovercourt, has receded significantly. The area showing the greatest amount of retreat is that fronting Foulton Marsh, which has retreated by about 800m since 1838, giving an erosion rate of 50m yr^{-1}. There is a marked discontinuity in the width of the intertidal areas to the north and south of Crabknowe Spit, which suggests that this feature is preventing the retreat of the intertidal area to its south. However, if the spit is a free form, then it would be expected that this would retreat with the rest of the shoreline, although this does not

appear to be happening. Therefore, it would seem that the spit is fixed in some way so as to prevent its erosion. Given the fact that the London Clay basement remains close to the surface in this area, in fact outcropping above high water in places, it is feasible that Crabknowe Spit is fixed by the London Clay basement.

Comparison of Admiralty Charts from 1847 and 1983 indicates that Stone Point has retreated approximately 500m. These figures give a retreat rate of between 3.7m yr^1 and 3.12m yr^1. The Admiralty (1983) consider that the retreat of Stone Point may eventually result in the formation of a second channel mouth, draining through Cormorant Creek and taking the discharge from the Walton Channel.

The analysis of Burd (1992) compared aerial photos taken in 1973 and 1988, and found that during this period 19% of the total area of marsh in 1973 (170.6 ha) had been eroded. The largest loss of area was to the pioneer zone, which lost 40% of its original area, while the low zone lost 21% and the low-mid and mid zones lost 15% each (Burd, 1992). The most significant areas of erosion identified were those open to the dominant waves from the north-east, including the open shore sites and the northern edge of Horsey Island. Other significant areas of marsh loss were around the edges of the large intertidal areas of the Wade, Cunnyfur and Bull's Oozes and the area to the west of Skipper's Island. In addition to this many of the creeks have experienced head-ward erosion (Burd, 1992).

7.3.3   DISCUSSION

The erosion of saltmarsh in Hamford Water is variable in spatial intensity; different areas experience different rates of erosion and for different reasons. The saltmarsh loss along the shores of the Harwich-Walton Bay can be attributed to the roll-over of the sand and shingle ridge which fronts the marshes; the landward movement of which is caused by wave action. It is proposed by IECS (1995) that a rise in sea-level has caused wave refraction changes to take place which have forced Stone Point spit to change orientation in an anti-clockwise direction so as to lie in a more protected position in the shelter of the Naze. This does not, however, account for the retreat of the Stone Point Marshes in an eastwards direction. This rapid retreat may be explained by the fact that these marshes were previously enclosed, and thus preventing accretion on the areas inside the wall, while outside the walls accretion continued. Therefore,

when the enclosing walls were finally breached in 1874 (Gramolt, 1960), the land surface which was enclosed would have been lower than the surrounding areas relative to tidal levels. Such a difference in levels would have meant that the marshes would not be able to survive and so the marsh edge retreated.

As Stone Point has retreated, so the mouth of Hamford Water has widened to such an extent that the mouth is now more than double its width in 1839. Such a widening would, at higher stages of the tide, allow more waves to enter the inlet, hence increasing wave erosion of the exposed shores. Such shores would include the western edge of the Stone Point Marshes, as well as those on the northern shore of Horsey Island. Attempts have been made to reduce the amount of wave erosion along the north-eastern tip of Horsey Island by the placing of a series of sunken Thames Lighters approximately 20m offshore from the marsh edge to act as a wave break. The widening of the mouth of the estuary would also have important affects on tidal processes in the inlet. A wider mouth allows a greater discharge to pass through it and, for a constant tidal prism, will mean that depths will have to decrease in order to maintain the tidal equilibrium.

The erosion of the marsh edges at locations such as the Wade, Cunnyfur and Bull's Oozes and the area to the west of Skipper's Island can be attributed to wave action which is able to develop at high water. These processes would be accentuated by any rise in sea-level. A rise in sea-level would force the upper limit of saltmarsh inshore as wave energy is able to propagate further onshore due to the deeper water conditions. Over the mudflats, the locally generated waves would be less affected by friction from the bed resulting in an increase in wave energy and therefore more erosion. Pethick (1992) outlines an additional process causing saltmarsh creeks to enlarge at their head-ward extent: the result of an increase in tidal prism and consequently tidal energy. The creek system of a tidal marsh is finely adjusted to the dissipation of tidal energy so that any change in any incident energy will be accompanied by morphological change in the creek system. Increases in the tidal prism may be brought about by sea-level rise and/or the effects of reclamation. In the latter case reclamation of the inner section of saltmarsh often results in the loss of large areas of tidal creek causing an increase in tidal prism in the channels immediately seaward of the reclaimed area and subsequent erosion of the creek banks. However, large proportions of the enclosed areas of

Hamford Water have reverted to saltmarsh, and although the drainage system of the enclosed marshes has often been modified, the tidal prism would have been decreased once more. The degree of internal contraction of saltmarsh within Hamford Water is less than in estuaries where large amounts of reclamation have taken place and the erosion of the saltmarsh creeks is therefore probably a result of sea-level rise alone.

7.4   Summary

Clearly Hamford Water is experiencing a number of interrelated processes contributing to some dramatic, but also some gradual changes to the general morphology. This research has attempted to record the vertical rate of change of both saltmarsh and intertidal mudflat. The results indicate an overall net sediment accretion of 4.2 mm yr^{-1} (Table 7-1) but with a lesser accretion rate on saltmarsh than mudflat, 2.7 mm yr^{-1} and 5.9 mm yr^{-1} respectively. The hypothesis is that, although there is a net sediment accretion, saltmarsh is being eroded and the eroded sediment is contributing to a greater mudflat accretion rate. In the previous section on sediment transport (*Section* 6.4) it was estimated that there are approximately 100 occasions that all saltmarsh is submerged in any one year and on those occasions a flood sediment transport is predicted. It was also suggested that on the remaining 607 high tides, any sediment in suspension is not being supplied to the saltmarsh and is either directed in a flood direction towards the tidal flats and creeks or is subject to ebb net transport. It was suggested that the system is experiencing a dynamic balance throughout an annual cycle. The fact that flood transport is being experienced only on springs and therefore only when all marsh is covered, would also go some way towards explaining why saltmarsh is showing a net accretion but the whole site is experiencing saltmarsh cliff erosion and a general reduction in the area of saltmarsh. So although the saltmarsh is eroding it does not necessarily imply that the site is losing sediment.

8 Holocene Sedimentation

8.1 Introduction

The aim of this phase of the study was to determine the palaeoenvironmental significance of the Holocene deposits in Hamford Water, and to relate any findings to the pattern of changing sea-level and coastal geomorphology of the East Anglian coast. The main method of environmental reconstruction used was the study of lithological evidence by analysis of the stratigraphy of the sediments using well-established coring techniques.

8.2 Methods

The principal objectives of fieldwork were to: (1) determine the sequence, thickness and lateral extent of Holocene deposits and, if appropriate, the level of any bedrock; (2) to obtain representative samples for radiocarbon dating (^{14}C); and, (3) to obtain Holocene sedimentation rates for comparison with contemporary sedimentation rates.

8.2.1 CORING

The study involved two stages of downcore investigation: exploratory reconnaissance with an auger, and full core retrieval using a vibrocorer. In addition, the literature was searched for previous records of coring within the area. Figure 8-1 illustrates the location of all core sites and Appendix L lists a summary of each borehole record. Nine exploratory cores were taken using either a 0.5m or a 1.0m long, 30mm diameter gouge auger. Samples from two of these cores (A2 and A7) were subsequently used by Cobbold (1995) for foraminiferal analysis. Based on the findings from exploratory coring, two further cores were sunk for more detailed analysis using a 76mm diameter vibrocorer. Ideally, the sites for the vibrocores needed to be free from any anthropogenic disturbance and site A5 appeared to be the most likely site. Unfortunately, due to its remoteness for surveying and logistical purposes, it could not be used.

A hand-operated, Dutch-type gouge auger was used for exploratory coring. It was light and easy to use and ideal for determining the general nature and thickness of soft

cohesive sediments. However, it suffered from problems of contamination since the chamber must repeatedly pass down through the same hole. Exploratory auger samples were described in the field (*see* Cobbold, 1995), but not retained for analysis.
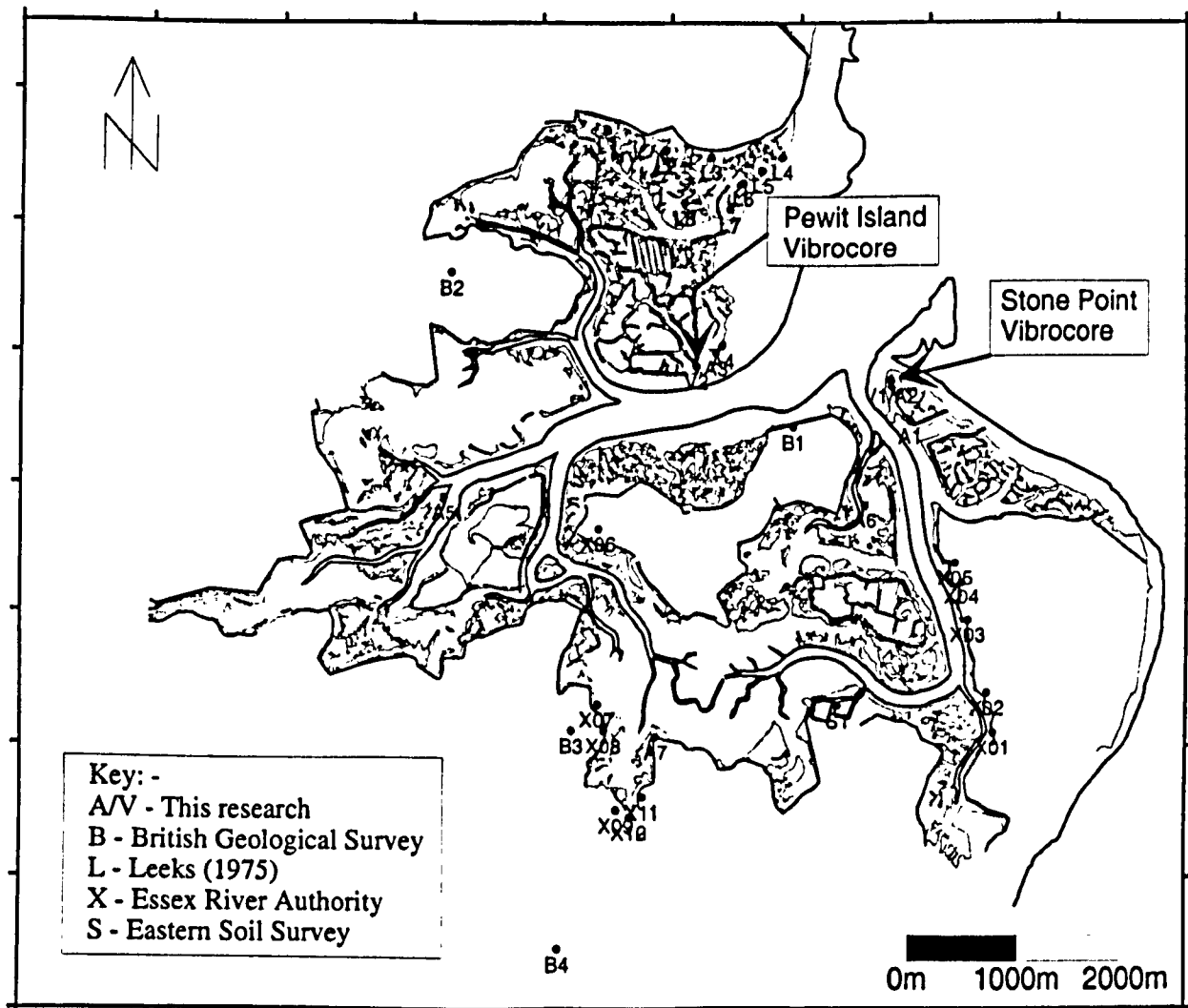
Figure 8-1 – Borehole Location Map

To enable sufficient downcore material for interpretation and ^{14}C dating a larger diameter core was required; a vibrocorer was borrowed from the University of East Anglia (UEA). The UEA vibrocorer utilises a standard industrial vibrator of the kind used to condense cement, fitted with a clamp on the end to facilitate attachment to the core. The core consisted of five–metre lengths of 72-mm diameter aluminium tube, the length being predetermined from the results of exploratory augering. The lower end of the tube was fitted with a brass core catcher to prevent loss of material when withdrawing the tube. The completed assembly was positioned over the spot chosen for coring and pushed by hand into the ground enough to allow the tube to be easily

stabilised and vertically aligned with either a plumb line or spirit level. The vibrator was then attached together with two rope strops tied around the tube to allow a field assistant to apply a downward force to assist the core. The vibrator was then coupled to the motor and the motor started. Depending on the nature of the substrate, the penetration rate of the tube into the ground was at first rapid ($\approx$15cm s-^{1}) then settled into about 2cm s-^{1}. The operation was continued until the core was inserted so that approximately 50cm were exposed or until bedrock was reached. The vibrator was then removed and the end of the core filled with seawater (to reduce decomposition of organics), capped with a tight-fitting plastic cap, and secured with water-resistant tape. To retrieve the core, a tripod was rigged over the exposed end of core and a $Tirfor^{TM}$ winch attached. When the whole core had been retrieved, it was cut with a hacksaw into approximately one–metre lengths to enable easy transportation to the laboratory.

In the laboratory, the cores were opened using a slitting saw on a Bridgeport Universal Milling machine. Two longitudinal groves were cut into the wall of the tube on opposite sides of the core to 0.2mm mean thickness of the tube. The remaining cut was made with a sharp knife to help prevent contamination of the core with aluminium swarf. The core was then sliced in half with a spatula, opened, photographed, described, sub-sampled and re-sealed. The Troels-Smith (1955) system of sediment description, as summarised by Birks and Birks (1980), and Aaby and Berglund (1986), was then used to describe the cores.

8.2.2   RADIOCARBON DATING

Sub-samples for ^{14}C dating were cut from one hemisphere of each core in 10mm-wide slices. The curved edge of each slice was then trimmed by approximately 5mm to prevent any longitudinal contamination due to shearing between core and tube wall. Preparation of peat samples for ^{14}C dating simply involved weighing, bagging, and clearly labelling. Shell samples first had to have all traces of sediment removed, followed by identification of shell type. For the best temporal resolution, at least 6 grams of carbon, in the form of benzene, are required for dating which translates into a requirement for at least 55 grams of shell material. The shell samples were therefore grouped to obtain sufficient weight as illustrated in Figure 8-2 and Figure 8-3, below, before despatch to the Godwin Laboratory, Cambridge for dating.

8.2.3 LEVELLING

Levelling of the core locations was by means of a standard dumpy level and metric levelling staff. The Stone Point core was levelled to the nearest Ordnance Survey benchmark, 1.1km away on the sea wall at the entrance to Cormorant Creek. Conditions for levelling were not ideal due to the nature of the ground. Most of the survey was conducted on soft, marshy ground where body weight can suppress the ground around either the level or the staff by as much as 2cm. Due to a rising tide the survey could not be closed and, as a consequence, it is assessed that an accuracy of no less than ±2.0cm can be stated. The core on Pewit Island could not be levelled due to its remote location. A marker was left at the core position for possible later levelling with more accurate equipment. In hindsight Pewit island should not have been chosen for a core site without accurate levelling facilities immediately available; it is too far out on the marshes to be accurately levelled with a dumpy level. Although a marker was left, it is anticipated that it will now have moved too much to provide an accurate datum.

8.3 Results

8.3.1 STRATIGRAPHY

The stratigraphy of each core is illustrated in Figure 8-2 and Figure 8-3, descriptions of the cores based on the Troels-Smith (1955) method are tabulated in Table 8-1 and Table 8-2, and photographs of Stone Point Core are shown in Appendix N. The cores are remarkably similar: both cores are overlain with a shallow soil horizon, approximately 5 cm thick, marking the present-day saltmarsh surface. Beneath this layer is an homogeneous layer of mottled grey-brown clay; at Stone Point this extends to 60cm below the surface, and at Pewit Island, to 110cm. Immediately beneath this layer, in both cores, there exists a grey/black herbaceous peat layer approximately 5cm thick, from which samples were extracted for ^{14}C dating (Samples WBSPT1 and WBPWT1). Beneath the layer of peat, both cores grade from mottled dark grey clay with plant fragments to blue-grey clay with occasional layers of shell fragments. At Stone Point, shell fragments occur at 240cm, 320cm and a composite band between 370cm and 440cm. The latter shell band was used for the second Stone Point ^{14}C date

(Sample WBSPT2). In the Pewit Island core, a composite shell fragment band occurs between 280cm and 350cm from which the second Pewit Island ^{14}C date was taken (Sample WBPWT2). Further shell fragments from the Pewit Island core occur at 390cm and 430cm. The base of the Stone Point core consists of stiff, dark-grey silty clay fulfilling the description of London clay (*see* Section 2.5.1 above). This was considered to be the bedrock of the sequence since the stiffness of the material meant that the vibrocorer could penetrate no further. Only 5cm of this clay were recovered and the base of the core was taken to be 460cm. No such material was encountered in the Pewit Island core and coring was stopped at 460cm to leave enough tube exposed to withdraw the core. In hindsight, since bedrock was not found during previous exploratory coring at Pewit Island (Cobbold, 1995), a longer section should have been used. However, difficulties with transporting aluminium tubing, with a length greater than 5m, over marsh and across tidal creeks precluded it.

Stone Point

Core Depth (m) / Depth (m OD)

Depth markers	Descriptions
0.0 / +1.62	Brown soil horizon
	Mottled grey-brown clay
0.6 / +1.00	Grey/black herbaceous peat RC sample WPSPT1 Age 590 years.
	Mottled dark grey clay with plant fragments
1.6 / OD(N)	
2.6 / -1.00	Blue grey clay with occasional layers of shell fragments.
3.6 / -2.0	
	Composite shell bands used for radiocarbon dating.
4.2	RC sample WBSPT2 Age 4280 ±126
4.6	London Clay?

Figure 8-2 – Stone Point core description.

Pewit Island

Core Depth (m)	Depth (m OD)		

0.0 — +2.0 — Brown soil horizon

0.2

0.4

Mottled grey-brown clay

0.6

0.8

1.0 — +1.0 — Grey/black herbaceous peat
RC sample WBPWT1
Age 635 years.

1.2

1.4

1.6 — Mottled dark grey clay
with plant fragments

1.8

2.0 — OD(N)

2.2

2.4

2.6

2.8

3.0 — -1.0 — Composite shell bands
used for radiocarbon
dating.

3.2 — Blue grey clay
with occasional
layers of shell
fragments.

RC sample WBPWT2
Age 2850 ±108

3.4

3.6

3.8

4.0 — -2.0

4.2

4.4

?

4.6

Figure 8-3 – Pewit Island core description.

Table 8-1 – Core description – Stone Point

Stone Point Core	
Depth (*below surface (m)*)	**Troels-Smith Description**
0.00 – 0.09	Hue: 7.5YR 4/2; Nig: 2; Strf:. 0; Elas: 2; Sicc: 2; Humo: 1; Upper boundary: Surface of core; Lower boundary: V. Gradual. As 2 Ag 1 Dh 1 – Brown soil horizon.
0.09 – 0.65	Hue: 10YR 4/1 darkening to 4/2; Nig: 2; Strf: 0; Elas: ½; Sicc: 2; Humo: 0. Upper boundary: V. Gradual; Lower boundary: Sharp. As 3, Ag 1 Dh+ – Dark grey clayey silt with plant fragments.
0.65 – 0.75	Hue: 7.5YR 3/0 – 2/0; Nig: 4; Strf: 0; Elas: 3; Sicc: 2; Humo: 4. Upper boundary: Sharp; Lower boundary: Gradual. Th 3 Dh 1 Ag+ – Grey/black herbaceous peat.
0.75 – 1.30	Hue: 7.5 YR 3/0; Nig: 3; Strf: 0; Elas: 1; Sicc: 2/3; Humo: 2. Upper boundary: Gradual; Lower boundary: Gradual. As 3 Ag 1 Dh+ Mottled dark grey clay with plant fragments.
1.30 – 1.60	Hue: 10 YR 5/4; Nig: 2; Strf: 0; Elas: 1: Sicc: ½; Humo: 0. Upper boundary: Gradual; Lower boundary: V.Gradual. As 4 Ag+ Yellowish brown silty clay
1.60 – 4.43	Hue: 10YR 4/1; Nig: 3; Strf: 0/1; Elas: 2; Sicc: 3; Humo: 0. Upper boundary: V.Gradual Lower boundary: Sharp. As 3 Ag 1 Dh+ Ld+ Blue-grey silty clay with occasional layers of shell fragments.
4.43 – 4.60	Weathered London Clay

Table 8-2 – Core description – Pewit Island

Pewit Island Core	
Depth (below surface (m))	**Troels-Smith Description**
0.00 – 0.33	Hue: 7.5YR 3/4 3/0 + 2/0; Nig: 2–3; Strf:. 0; Elas: 1; Sicc: 3; Humo: 3; Upper boundary: Surface of core; Lower boundary: Gradual. Ag2 As 1 Dh 1 – Brown soil horizon.
0.33 – 1.06	Hue: 10YR 4/1 darkening to 3/1; Nig: 2–3; Strf: 0; Elas: 1; Sicc: 3; Humo: 3. Upper boundary: Gradual; Lower boundary: Sharp. Ag 1, As 2 – Mottled and bioturbated grey-brown clay.
1.06 – 1.08	Hue: 7.5YR 3/0 – 2/0; Nig: 4; Strf: 0; Elas: 3; Sicc: 3; Humo: 4. Upper boundary: Sharp; Lower boundary: Gradual. Th 3 Dh 1 Ag+ – Grey/black herbaceous peat.
1.08 – 2.36	Hue: 7.5 YR 4/2; Nig: 3; Strf: 0; Elas: 2; Sicc: 3; Humo: 4. Upper boundary: Gradual; Lower boundary: Gradual. As 3 Ag 1 Dh+ Mottled dark grey clay with plant fragments.
2.36 – 2.71	Hue: 10 YR 4/2; Nig: 3; Strf: 1; Elas: 1: Sicc: 3; Humo: 0. Upper boundary: Gradual; Lower boundary: V.Gradual. As 3 Ag 4 Dh+ Dark grey silty clay
2.71 – 4.07	Hue: 7.5YR 4/0; Nig: 3; Strf: 1; Elas: 1; Sicc: 3; Humo: 0. Upper boundary: V.Gradual Lower boundary: Base of core. As 3 Ag 1 Dh+ Ld+ Blue-grey silty clay with occasional layers of shell fragments.

8.3.2   SHELL SPECIES

Appendix M lists the species found in both cores and their location within the cores. The following is a brief description of the shell species, their habitat and whether they are considered to be auto- or allochthonous to the site.

Cerastoderma edule (Common edible cockle) – inhabits clean sand, muddy sand, mud or muddy gravel, burrowing to a depth of no more than 5.1 cm, from mid-tide level to just below low water-mark. It is common in sandy bays around the British Isles and in estuaries and rivers extending upstream to a salinity minimum of about, or just below 20PSU (Trebble, 1976). Considered to be either autochthonous and/or allochthonous.

Littorina littorea – abundant throughout the British Isles, on rocky shores and others sufficiently firm enough to give some attachment. Their upper limit on a shore depends on the degree of shelter and shade, both raising it. They eat diatoms, young and older algae, and are particularly attracted to *Ulva* and *Enteromorpha,* avoiding tougher fucoids (Graham, 1988). This may suggest that this sample is allochthonous since the site is mainly muddy.

Littorina saxatilis (rudis) – similar to *Littorina littorea* and most probably allochthonous.

Mytilus edulus – very common around the coasts of the British Isles, from high in the intertidal zone down to depths of a few metres, attached by byssus threads to rocks and piers, within sheltered harbours and estuaries and on rocky shores of the open coast, sometimes living in dense masses wherever there are suitable surfaces for attachment (Trebble, 1976). Considered allochthonous because of the lack of suitable attachment surfaces in Hamford Water.

Scrobicularia plana – intertidal species inhabiting soft mud or clay bottoms with abundant organic detritus, in estuaries, etc., where fresh water- seawater mixing causes varying salinity (Trebble, 1976). Considered to be autochthonous and/or allochthonous.

8.3.3 RADIOCARBON DATES

Samples extracted from each core were dated at the Godwin Laboratory, Cambridge. The radiocarbon ages (Table 8-3) are conventional ^{14}C ages based on the zero datum year of AD 1950 and the Libby half-life for the ^{14}C isotope of 5568 ± 30 radiocarbon years, and have been corrected for isotopic fractionation (δ^{13}C).

Table 8-3 – Radiocarbon (^{14}C) Results

Sample ID	Radiocarbon Age	Uncertainty Years	δ^{13}C $^0/_{oo}$	Corrected Age
WBPWT1	635	45	–14.4	
WBPWT2	3255	100	1.32	2850 ± 108
WBSPT1	590	40	–15.25	
WBSPT2	4685	120	1.52	4280 ± 126

There are a number of problems associated with samples from estuarine regions (Switsur, *pers. comm.*). Salt marsh plants such as *Spartina sp.* use the C_4 photosynthetic pathway and so isotopic fractionation is only about half of the fractionation of normal temperate C_3 plants; thus it is essential to ensure that the fractionation is measured for such samples for it can affect the age by around 200 years. However, it is considered to be of minor importance in Hamford Water since most *Spartina sp.* resulted from the accidental introduction of *Spartina alterniflora* to Southampton Water from America in 1870 and its subsequent spread throughout the United Kingdom (Adam, 1990)(*see* also Section 2.3). It is considered that *Spartina sp.* was not established when these deposits were formed.

Marine shells also constitute a problem since the origin of their carbon is not part of the atmospheric carbon cycle, for which radiocarbon dating method was originally devised. The ages are affected by the so-called *reservoir effect* because of the depletion of the ^{14}C concentration in the sea water. Thus living material has an apparent ^{14}C age which can be between 200 and 2000 years, depending on location and is due to the mixing of ancient abyssal waters with those above the thermocline. Around the British Isles the conventional value for this reservoir effect is 405 ± 40 year (Harkness, 1983).

8.4   Discussion

The specific aim of the investigation of Holocene sedimentation was to estimate rates of sedimentation from downcore evidence by radiocarbon (^{14}C) dating of organic layers, and identify the major controls on these patterns (tectonic subsidence, sea-level change, sediment supply). An important influence in the investigation has been several references in the literature to occurrences of peat in either exposed or downcore deposits (*see Section 2.5.4*). There also existed the possibility of constructing a sea-level curve to compare with adjacent estuaries depending on the reliability of the data. The following discussion deals firstly, with the Holocene stratigraphy, followed by sedimentation rates and thirdly, the applicability of the ^{14}C dates as sea-level indicators.

8.4.1   STRATIGRAPHY

The Holocene stratigraphy of the site is generally uncomplicated. As discussed in Section 2.5 the site consists mainly of Holocene marine, estuarine alluvium overlying a basement of Eocene London clay and flanked to the west, north-west and south-east by Plio-Pliestocene Red Crag deposits and Pliestocene glacial sand and gravel. From an analysis of all borehole and core records, a general picture of the sub-surface stratigraphy can be attempted. Figure 8-4 is the same geological sketch-map as previously illustrated in Section 2.5 (Figure 2-4) with cross-sections A-B and C-D superimposed. Figure 8-5 and Figure 8-6 are generalised cross-sections of A-B and C-D, respectively.
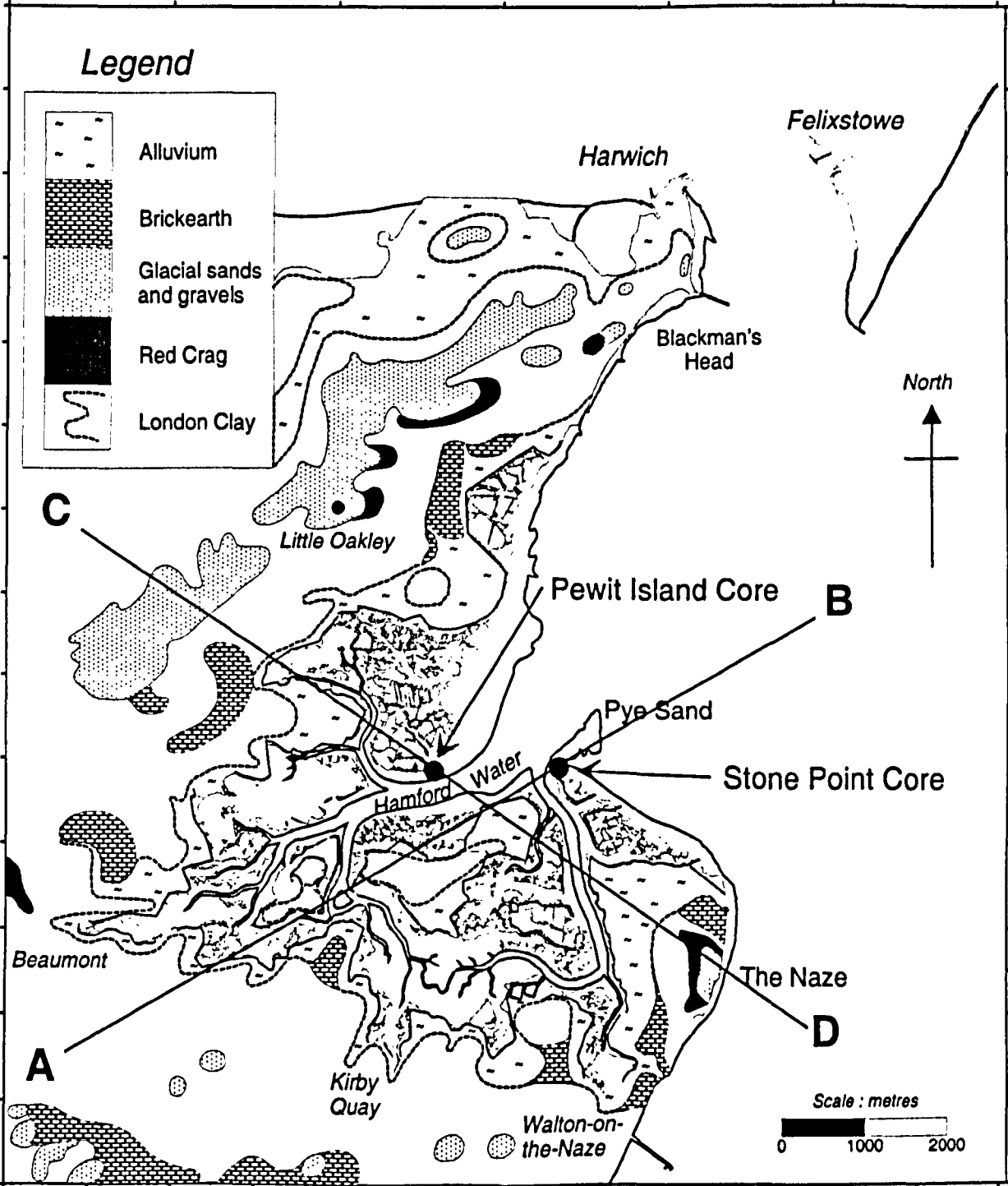
Figure 8-4 – Hamford Water, location of cross-sections.
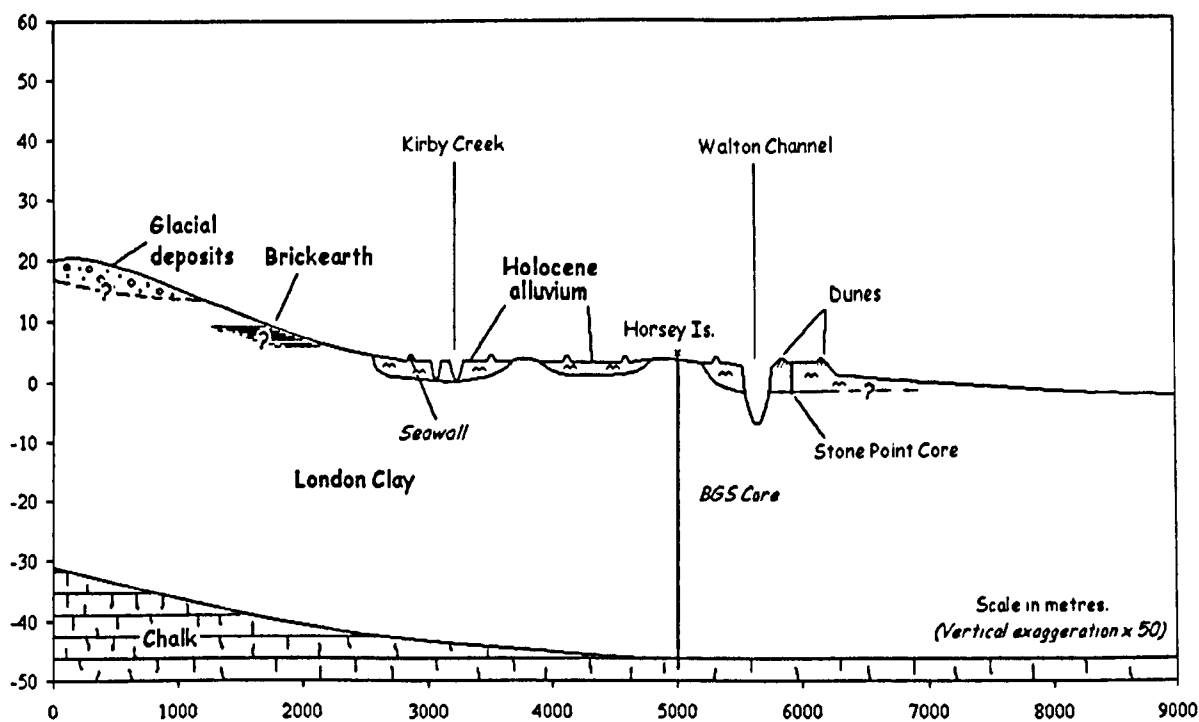
Figure 8-5 – South-west–North-east cross-section of Hamford Water (Line A – B).
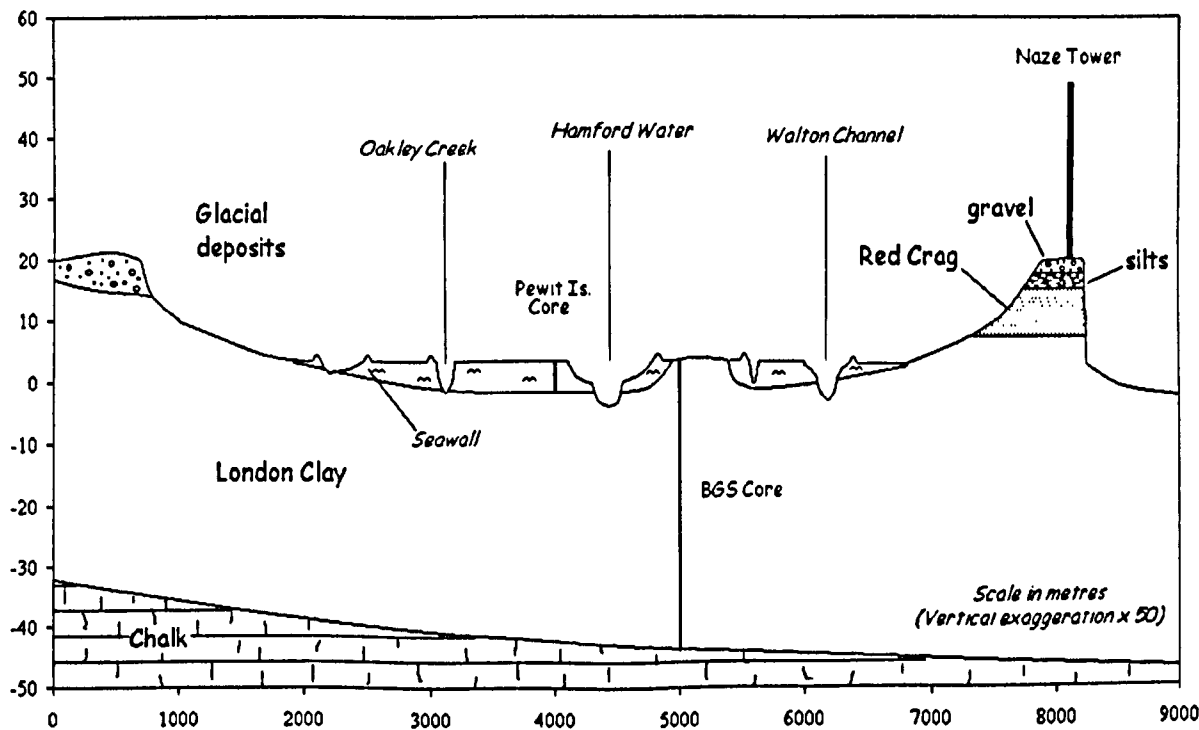
Figure 8-6 – North-west–South-east cross-section of Hamford Water (Line C – D).

The cross-sections illustrate the basin-like occurrence of the Holocene deposits in Hamford Water flanked by older deposits of glacial sands and gravels and Red Crag. The London Clay is depicted as protruding up through the Holocene deposits and outcropping at the surface on Horsey Island (*see Section 2.5.1*). It is also illustrated, although based on considerable conjecture, that the main channels of Hamford Water,

and Walton Channel cut into the under-lying London Clay. The result is an undulating London clay surface crossed by incised channels and filled with Holocene alluvium, the whole area forming part of a much larger channel that probably formed when the proto-Thames and Medway flowed over this region as discussed in Section 2.5.3 and illustrated in Figure 2-5.

8.4.2 SEDIMENTATION RATES

In the previous chapter (Chapter 7) the contemporary rates of accretion and/or erosion were assessed by repeated measurement of both marsh and mudflat surface, revealing a complicated short-term picture. The results from the ^{14}C dates in this section complement those results to some degree but can only really suggest a simple linear relationship between accretion and elevation. Both cores are similar in that they record a lengthy, and presumably uninterrupted, period of estuarine sedimentation from the base of the core to the peat layer. The peat layer records a period of little or no sedimentation and of unknown duration, followed by a continuous, and again presumably uninterrupted period of sedimentation to the present day.

Beneath the peat layer at Stone Point, between 4280 years BP at a mean depth 4.06m, and 590 years BP at a mean depth of 0.69m, 3.37m of sediment was deposited giving a mean rate of accretion of 3370mm in 3690 years, or 0.91mm yr^{-1}. Similarly, at Pewit Island, between 2850 years BP at a mean depth 3.37m, and 635 years BP at a mean depth of 1.08m, 2.29m of sediment was deposited giving a mean rate of accretion of 2290mm in 2215 years, or 1.03mm yr^{-1}. Above the peat layer, Stone Point experienced 0.69m of sedimentation in 590 years or 1.17mm yr^{-1}; and at Pewit Island, 1.08m in 635 years or 1.7mm yr^{-1}.

The difference in depth of the peat layer in both cores is the key to its origin. If it is assumed that sedimentation beneath the peat layer at Stone Point was contemporaneous with Pewit Island, it is reasonable to suggest a mean sedimentation rate of 0.97mm yr^{-1} for the two sites up to the formation of the peat layer. Unfortunately the depth of the peat in both cores does not accord (Pewit Island being up to 0.5m deeper than Stone Point), and since the Pewit Island core could not be levelled to OD there is no way of linking the formation of peat at both sites from elevation alone. In fact, the ^{14}C evidence would suggest that the peat layers are not contemporaneous. The difference

in depth and ^{14}C age lend support to an hypothesis that they represent ancient agricultural surfaces formed during separate, unrecorded periods of marsh reclamation. Subsequent flooding of the land resulting from a breach reverted the land to estuarine saltmarsh and marine sedimentation. Alternatively, if it is assumed that the present level of the top of each core is the same, the Pewit Island site may have experienced greater subsidence than Stone Point and when Pewit Island breached the flooded land would be subjected to a more rapid sedimentation rate by being lower in the tidal frame.

If the differences between the two cores are ignored, the evidence suggested from the combined ^{14}C dates is that Hamford Water has experienced a mean sedimentation rate for the last 4500years BP of approximately 1mm yr^{-1}. If it is assumed that saltmarsh sedimentation rates keep pace with sea-level rise, this equates to an equal change in sea-level over the same period (Figure 8-7). However, there is a problem with combining all ^{14}C dates to form a single sedimentation curve: the level of formation of peat and shell should be different. (Whereas the peat forms in a very narrow band, shell deposits can form over a very broad band.) It is assumed that marsh, and therefore the peat, forms at the top of the sequence and within the morphological boundaries of a typical saltmarsh, i.e., low marsh to high marsh. Shell bands, however, are more likely to form at various elevations relative to the prevailing tidal range. The types of shells recovered from the cores were described in 8.3.2 above. Given the amount of shell material required for a ^{14}C date, shell samples submitted for dating consisted of a combination of the species recovered. Therefore, in addition to an elevation error due to banding of the samples, there is also an elevation error due to the exact unknown original elevation that the shell was deposited.
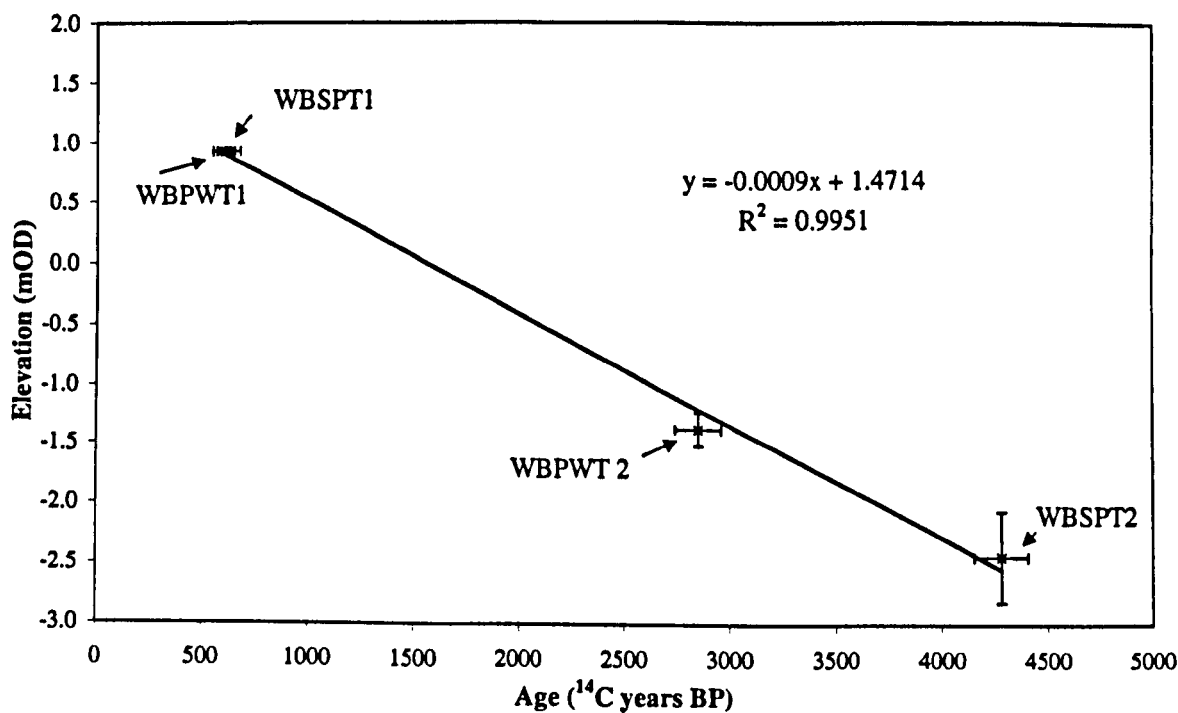
Figure 8-7 – Holocene Sedimentation Rates – Hamford Water

Current estimates of rates of sea-level rise for the Essex coast range vary: 3 mm yr^{-1} (Long and Mason, 1983); 1.4 to 1.7 mm yr^{-1} (Carter, 1988), and 1.75 to 2.75 mm yr^{-1} (Davidson *et al.* 1991). The close proximity of Hamford Water to Harwich and Felixstowe means that sea-level data from these locations is likely to be comparable to the study area. The results from this study imply a much reduced rate of sea-level rise.

8.4.3   SEA -LEVEL INDEX POINTS

Reliable sea-level indicators within an estuarine stratigraphic sequence can usually be attributed to transgressive or regressive overlaps. For example, a succession in which estuarine clay gives way to terrestrial peats suggests that a sea-level regression has occurred. Conversely if a peat layer is overlain by estuarine clay, then a marine transgressive sequence may be inferred (Lowe and Walker, 1984).

In the case of the peat layers of both Stone Point and Pewit Island; their origin can either be attributed to a brief sea-level regression, or to an old land surface formed on reclaimed marsh (as discussed in Section 2.4 above). However, both explanations are difficult to reconcile given the available evidence. If the peat were to be considered as a sea-level index point, the layers should correspond to a sea-level regression between

590 and 635 years BP. Such a layer contrasts with the neighbouring estuaries of the Deben, Stour and Orwell where no such layers are encountered (Brew, 1990 and Brew *et al.*, 1992), and indeed there are no recorded instances of a sea-level regression at this time. Brew's (1990) investigation showed a continuous sequence of estuarine silts without intercalated peat. It is of course possible, although unlikely, that Hamford Water experienced a localised tectonic uplift in contrast with the general downward trend of the North Sea basin although it would be expected that the affected region would extend to neighbouring estuaries. More likely, changes in eustatic sea-level have been complicated by local variations in rates of Holocene sediment subsidence within the area.

Correlating the peat layers with previously reclaimed land surfaces is equally problematic. Although both Stone Point and Pewit Island were subject to saltmarsh reclamation: Stone Point between 1800 and 1840 (calendar years) and Pewit Island sometime before 1774 (Gramolt, 1960), there are no known records of reclamation in the 14th century coinciding with the peat dates: 635–590 years BP (1315–1360 calendar years). There is, however, good evidence for human occupation in this area and that Europe experienced Alpine glacial advance, increased surface wetness and lower-than-average winter temperatures (Roberts, 1998). It is, therefore, possible that a combination of early undocumented attempts to reclaim the land combined with a particularly wet period resulted in the thin layer of peat as recorded. Consequently, it is not appropriate to use the peat dates as sea-level index points.

Only the basal shell date from Stone Point could be termed a sea-level index point, that is, if it is assumed that the Stone Point basal sequence is indeed London Clay. It can be implied that the surface of the London Clay represents a weathered surface before the onset of a transgressive sea-level. A date for material on top of the London Clay would represent the date the sea reached that level. In support of the Stone Point ^{14}C shell date is the work of Zeuner (1958) (previously discussed in Section 2.5.4) in which a discontinuous *"peaty marsh-clay"* layer of only a few inches thick is overlying an occupation layer and underlying an estuarine sequence somewhere near Stone Point. The occupation level is considered by Zeuner to be of Neolithic and Beaker age and it is now known that the Mesolithic/Neolithic transition in Britain is diachronous between 8 and 5.5ka BP and the Neolithic/Bronze Age transition between 4.2 and 4.5ka BP

(Scourse, *pers comm*). The Beaker period represents a ceramic tradition spanning the Late Neolithic/Early Bronze Age between 4.5 and 3.7ka BP. The Stone Point basal shell date of 4.3ka BP accords well, therefore, with the archaeological evidence in that it must immediately post-date the occupation level. However, although there is a good correlation between the Stone Point ^{14}C date and Zeuner's sequence, the evidence merely supports Zeuner's work and does not expand on the record of sea-level change or of sedimentation rates in Hamford Water mainly because the exact location of Zeuner's sequence is unknown.

Regarding the Pewit Island shell date: it could only be regarded as an index point if it were possible to relate the mulluscan assemblage with the inter-tidal, or a specific sublittoral depth range. Species recovered from the Pewit Island core (Sample WBPWT2, *see* Appendix M) are a mixture of *Littorina Sp*, *Cerastoderma edule*, *Mytilus littorea* and various shell fragments including *Rossoidae* and possibly *Scrobicularia plana*. Although *Cerastoderma edule*, *Mytilus littorea* and *Scrobicularia plana* could all inhabit the muddy sediments that make up the Pewit Island core, *Littorina Sp* inhabits the rocky shore, and since the latter species predominates, it is suggested that the majority of shells recovered from both cores are allochthonous and cannot be used as reliable sea-level index points.

There also remains one further problem with using any of the ^{14}C dates as sea-level index points; the accuracy of relating the borehole levels with Ordnance Datum. Before any of the ^{14}C dates can be considered as sea-level indicators, the accuracy of borehole levelling needs to be assessed. In a site investigation involving sea-level studies it is of paramount importance to know accurately to what level, in relation to a national datum, the site is situated. Heyworth and Kidson (1982), in a comprehensive assessment of errors involved with sea-level studies, suggest that levelling of a sample point should introduce an error of no more than ±1.0cm. The use of a dumpy level, in this research, combined with long survey distances over soft terrain resulted in an estimated accuracy of ±2cm. In addition, it was not possible to "close" the survey, thereby introducing a further unknown systematic error. It is quite possible that the final survey error was greater than ±4cm. Consequently, the levelling data is considered too unreliable for accurate sea-level studies. It is therefore concluded that none of the ^{14}C dates can be considered as accurate sea-level index points.

8.5   Summary

This section has focussed on the Holocene history of sedimentation as determined from two cores recovered using a vibrocorer. From a description of the cores and radiocarbon dating of organic material within the cores, the following can be summarised:

- The stratigraphic sequence recorded from the two vibrocores are similar: both cores are overlain with a shallow soil horizon marking the present-day saltmarsh surface, beneath which is an homogeneous layer of mottled grey-brown clay; at Stone Point this extends to 60cm below the surface, and at Pewit Island, to 110cm. Immediately beneath this layer, in both cores, there exists a grey/black herbaceous peat layer approximately 5cm thick, from which samples were extracted for ^{14}C dating. Beneath the layer of peat, both cores grade from mottled dark grey clay with plant fragments to blue-grey clay with occasional layers of shell fragments down to a depth below the surface of approximately 460cm.

- Radiocarbon dating of the peat layers and the shell bands indicates Hamford Water has experienced a relatively uninterrupted Holocene sequence of sedimentation for at least 4700 years at an approximate rate of 1 mm yr^{-1}.

- The peat layers are considered to represent undocumented periods of reclamation in the 14th century.

- Analysis of borehole records illustrates a picture of a shallow basin of Holocene alluvium overlying an undulating surface of London Clay sculptured by fluvial action during pre-Cromerian to early Anglian (c.650-450ka) Thames and Medway drainage. In places the London Clay protrudes through the alluvium to form the islands of Horsey and Skipper's, and in other places it is incised by deep channels cut by Holocene marine processes to form Walton, Hamford Water and Pye Channels.

9 Synthesis and Discussion

The aim of this chapter is two-fold, a synthesis of the foregoing research, and a discussion on the implications of the results for both coastal geomorphology and coastal management. Throughout this thesis, the target for study has been to test the hypothesis that given an apparent deterioration of saltmarsh, coupled with an ebb-dominated tidal cycle, the embayment is no longer a significant sediment sink for the southern North Sea. The reasoning behind the hypothesis was centred on two publications: McCave's paper (1987), suggesting that Hamford Water was a sediment sink for the East Anglian coast, and an NCC [English Nature] report by Burd (1992) detailing a significant loss of saltmarsh area between 1973 and 1988. It was also very apparent, simply by looking at Admiralty tidal prediction tables that the nature of the tidal cycle was predominantly ebb-dominant suggesting a possible net ebb transport of sediment. The need for research was emphasised because there was an increasing demand for measures to be taken to slow the apparent rate of loss of both Pye Sand and Stone Point which were exposing the interior of the embayment to ever-increasing wave action. The international importance of the site for nature conservation placed a high priority on immediate remedial action.

The research method centred on recording, observing and analysing various parameters applicable to estuarine geomorphology, sediment transport, and Holocene evolution. Sediment grain size data of surficial sediments were analysed and used to describe the spatial sediment distribution of the area. Hydrodynamic processes responsible for sediment erosion and deposition, particularly through the inlet throat, were also studied. An assessment of contemporary sediment accretion and/or erosion within the embayment were made and compared with the geological history of sedimentation assessed from down-core evidence and radiocarbon dating.

The major findings are summarised as follows:

- **Hydrodynamics**

  - **Waves** (*p.52*) – Hamford Water is affected by two different wave regimes: fully developed open sea waves, and depth-limited internally generated waves within

the embayment. The ability of waves to erode and transport sediment depends largely on the state of the tide and the age of the tidal cycle. Strong north-easterly winds and neap tides are considered the most erosive.

- **Tides** (*p.57*) – The tidal regime is diurnal and classified as mesotidal after Davies (1964) with an average tidal range of 3.8m on springs and 2.3m on neaps. There is a predicted tidal asymmetry: predicted duration (to the nearest 5 minutes) of the flood is 6 hours 40 minutes during springs and 6 hours 30 minutes during neaps. Predicted ebb times are 5 hours 40 during springs and 5 hours 50 minutes during neaps.

- **Currents** (*p.77*) – The tidal stage curve of Hamford Water is characterised by a short duration (≈ 10 minutes) high water stand and a slack low water of approximately 20 to 30 minutes. From slack high water, there is a rapid increase in ebb velocity, reaching a maximum about 1 hour after slack water. Thereafter, ebb velocities begin to reduce towards slack low water, which is of a much longer duration than that of slack high water. There is then a gradual flood, peak velocity not being reached until about 5 hours after slack low water (about 1.5 hours before slack high water). Flood velocity then quickly decreases towards high water. A significant feature of the flood tide is the 'spike' of flood current around Stone Point. The tidal flow within the embayment is complex: being affected by numerous islands, artificial breakwaters and a myriad of saltmarsh creeks. The existence of Horsey Island and other islands causes the flood tide to converge in zones where the tidal current is effectively zero; the same zone becomes a zone of divergence on the ebb tide. It was hypothesised that such zones of tidal convergence/divergence may have an effect on sedimentation rates and are identified as an area for future work.

- **Temperature and Salinity** (*p.83*) – Given the absence of any freshwater input and therefore no significant mixing, the importance of both temperature and salinity within the overall research scheme was considered low. Consequently further data collection was considered unnecessary. The effect of temperature

on sediment deposition was, however, highlighted as an important area of future research.

- **Sediment Grain Size** (*p.*147) – Hamford Water has two distinct sediment regimes: fine silts and clays in the embayment, and sands in the inlet. Most interior fine sediment falls within the relatively calm hydrodynamic stage II on a Pejrup (1988) triangular diagram whereas the inlet sandy sediments fall within the more violent hydrodynamic stage IV. The mean grain size of the inlet throat and ebb delta sands is 0.25mm (2ϕ, medium to fine sand) and the majority of the embayment mudflat and saltmarsh 0.011mm (6.5ϕ, medium to fine silt). The source of the majority of sediment in Hamford Water is considered to be allochthonous. The most striking feature of the surficial sediment distribution is a very sharp boundary (<1m) just inside the inlet throat between the coarse fraction and the fine fraction. This points to a marked change in the hydrodynamic conditions.

- **Sediment Transport** (*p.* 171) – Flux of SPM and the rate of suspended and bedload sediment transport during both a flood and ebb tide, and over a spring-neap cycle were assessed. SPM flux for a single spring and neap tidal cycle indicates that there is a net ebb transport of 670 tonnes on springs and 15 tonnes on neaps. However, the results were viewed as qualitative rather than quantitative due to the errors involved. The total load equation of Engelund and Hansen (1967) was seen as offering the most applicable net transport direction, and it was suggested that Hamford Water experiences a net flood transport on spring tides and a net ebb transport on neap tides. It was hypothesised that the change from ebb to flood transport is not linear; instead, a phase advance in peak transport is determined by tidal range, and by implication, peak velocities. It was also hypothesised that the morphology of Hamford Water contributes to the formation of a fluid mud reservoir that is incorporated into the overall sediment budget only after a critical shear stress is reached. The effect of a fluid mud layer on the sediment budget of Hamford Water is highlighted as an area for more research.

- **Contemporary Sedimentation Rates** (*p.*190) – From an assessment of discrete markers on both saltmarsh and mudflat, results indicate an overall net sediment accretion of 4.2 mm yr^{-1} but with a lesser accretion rate on saltmarsh than mudflat,

2.7 mm yr^{-1} and 5.9 mm yr^{-1} respectively. It was hypothesised that saltmarsh is being eroded and the eroded sediment is contributing to a greater mudflat accretion rate. This is supported by a study of the spatial extent of saltmarsh and the general changing morphology which indicates that there is a general loss of saltmarsh and a corresponding increase in the area of intertidal mudflat.

- **Holocene sedimentation** (*p.*210) – From an analysis of two vibrocores and radiocarbon dating of organic material within the cores, a number of key points were made: The stratigraphic sequence recorded from the two vibrocores are similar: both cores show a gradation from a shallow soil horizon marking the present-day saltmarsh surface, through an homogeneous layer of mottled grey-brown clay to a thin grey/black herbaceous peat layer approximately 5cm thick, beneath which the sediment is a mottled dark grey clay with plant fragments to blue-grey clay with occasional layers of shell fragments. Both cores are 4.5m deep. Radiocarbon dating indicates Hamford Water has experienced an apparently uninterrupted Holocene sequence of sedimentation for at least 4700 years at an approximate rate of 1 mm yr^{-1}. The peat layers are considered to represent undocumented periods of reclamation in the 14th century. Analysis of other borehole records illustrates a picture of a shallow basin of Holocene alluvium overlying an undulating surface of London Clay sculptured by fluvial action during pre-Cromerian to early Anglian (*c.*650-450*ka*) Thames and Medway drainage. In places the London Clay protrudes through the alluvium to form the islands of Horsey and Skipper's, and in other places it is incised by deep channels cut by Holocene marine processes to form Walton, Hamford Water and Pye Channels.

Ultimately, the overriding influence on the geomorphology and therefore, the future evolution of Hamford Water, is the movement of sediment. However, sediment transport in Hamford Water cannot be considered in isolation. In order to understand both fine and coarse sediment movement the sphere of influence has to be extended both offshore and to adjacent estuarine systems. This is an obvious consequence of assuming that sediment in Hamford Water is predominantly allochthonous. An immediate zone can be established which encompasses The Naze, the estuaries of the Stour and Orwell, the coastline from Bawdsey to Landguard Point, the coastline from The Naze to Clacton, and the offshore region as far as Cork Sand. It was discussed in

Section 3.2.7 and Figure 3-5, that IECS (1995) identified a complex series of sediment pathways that had a direct influence on Hamford Water. The complex sediment movements within the Harwich-Walton Bay area have maintained the offshore morphology of the bay in a dynamic equilibrium over a period of many centuries. The presence of features such as Landguard Point, the Cork Sand and Pye Sands are seen as essential in maintaining the morphodynamics of the Harwich-Walton Bay, the Stour-Orwell estuary and Hamford Water. Landguard Point deflects sand into the large-scale circulatory transport pathway in the Harwich-Walton Bay. Pye Sands acted as a conduit for sand moving north from the Naze; this sand flux enters the Stour-Orwell estuary but is then transported seaward along Landguard Point to re-enter the transport pathway. Cork Sand acts as an offshore wave break so that waves exceeding 4m in height do not propagate into the nearshore zone - thus reducing the coarse sediment transport into the estuary and maintaining the offshore system dynamics. Therefore, the morphology of the Harwich-Walton Bay and Hamford Water are inextricably linked to the processes of the Stour-Orwell estuary.

Although it is not the intention to criticize those pathways in any detail since it is outside the scope of the research site, modifications to the pathways in the inlet throat of Hamford Water are suggested based on the results of this research (Figure 9-1). Pye Sand is considered to be a critical feature in the circulation and movement of sand; it acts as both a conduit and a reservoir for sand moving north from the Naze:

A) Sand moves by wave action along the coast from the Naze towards Stone Point;

B) Strong flood currents move the sand anti-clockwise around Stone Point where it is stored in the lee of Stone Point;

C) Strong ebb currents move the sand out on to Pye Sand;

D) From Pye Sand it is either 1) stored, 2) removed offshore to join Pathway (6) of IECS (1995), or 3) returns in a clockwise circulation to Stone Point.

It is hypothesised that a similar circulation would exist on the northern bank of the inlet in the absence of the sea wall at Foulton Hall Point although the effect of the mouth of the Orwell and Stour and the breakwater at Blackman's Head are difficult to ascertain.

This circular pattern of sediment is typical of ebb-dominated tidal inlets. Smith and FitzGerald (1994) found that the channels and swash platform of the ebb delta are parts of clockwise and counter-clockwise sediment gyres that circulate sand within the ebb-tidal delta and account for the sand that bypasses the inlet.
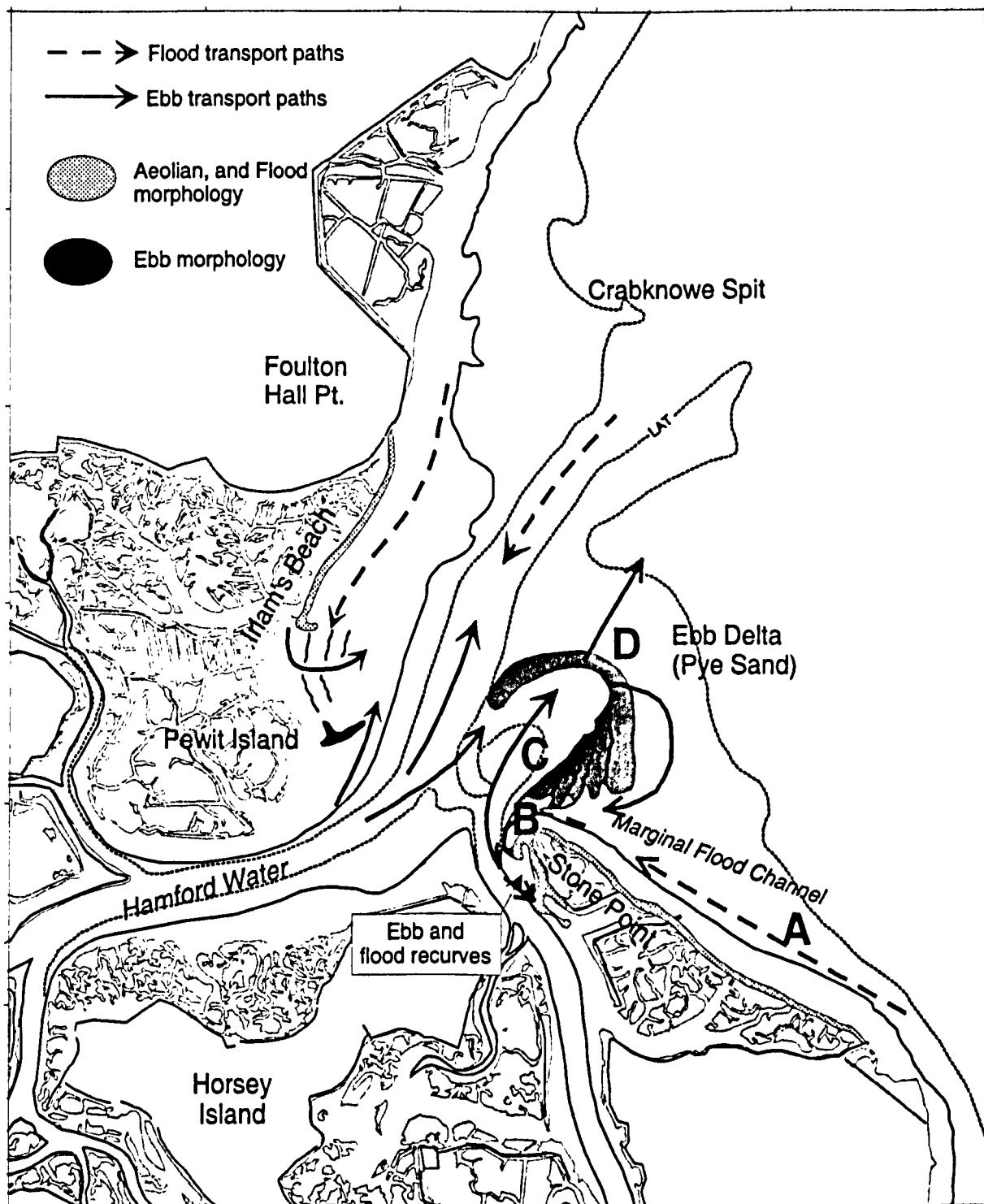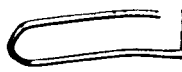
Figure 9-1 – Sediment movement in Hamford Water inlet (compare with Figure 3-1).

The movement of sand around Stone Point is considered to be of fundamental importance to the changing morphology of the entrance to Hamford Water. The morphology of Stone Point is essentially a recurved spit with a number of flood- and

ebb-orientated recurves superimposed (Figure 9-1). The coarse material that makes up Stone Point, and Irlam's Beach on the north shore, can only have a littoral drift or offshore origin. Any reduction in this supply will result in progressive erosion and widening of the inlet throat. Although there is no scientific evidence for a reduction in sediment supply to Hamford Water, Professor J.S. Pethick writes in (Toft and Maddrell, 1995) that:

Third Party material excluded from digitised copy. Please refer to original text to see this material.

IECS (1995) see the widening of the inlet and realignment of Stone Point as a response to increased wave action and a rising sea-level (*see above* Section 3.2.7). Although wave action and rising sea-level are not disputed, the alignment of Stone Point is more likely to be determined by the orientation of Walton Channel which is a semi-permanent morphological feature cut into the London Clay basement. Stone Point is therefore, unlikely to rotate any further west as long as the ebb tide flows out of Walton Channel. The existence of Stone Point as a protective barrier, however, is considered to be unstable. Essentially, Stone Point consists of Holocene alluvium lying on a 'bedrock' of London clay overlain and protected by a sand bank of both marine and aeolian origin. The London clay underneath slopes away from the Naze towards Hamford Water and is cut into by both Walton Channel, Hamford Water and Pye Channel. The saltmarsh at Stone Point is part of the entire Holocene alluvium that surrounds The Naze, to the north, west and south. The erosion of the Naze sediments (Red Crag and glacial) throughout the Holocene rise in sea-level created a spit on either side of the Naze and allowed the settlement of fine-grained, predominantly marine

sediment (there being a negligible fluvial input). Without the Naze, it is postulated that the coastline in this region would follow approximately the 5-metre contour line from Harwich, around the back of Beaumont Creek and back to Walton-on-the-Naze. The marshes that form the present-day Stone Point, i.e., those to the north-west of the current seawall, have rolled back 300m in 150 years and used to extend as far as the Mussel Scarfe. The predominant question that needs to be answered is why is Stone Point retreating?

If the O'Brien equation is considered, it is calculated that the cross-sectional area of the mouth is now too large for the tidal prism and therefore should continue to decrease. As outlined in Section 3.2.5, the O'Brien (1969) hypothesis suggest a linear relationship between tidal prism, P and cross-sectional area of the inlet, Ac in the form: $Ac = c.P$ where $c = 6.6 \times 10^{-5}$ (from Van Dongeren and de Vriend, 1994). If P is measured at mean high water springs as $17.7 \times 10^6 \, m^3$, Ac should equal $1168 \, m^2$. Now, the actual cross-sectional area is measured at $2975 \, m^2$, which is considerably greater than predicted. If the present-day Ac is compared with a measured value from the first Admiralty chart survey of 1847 (Ac (1847) = $3606 \, m^2$; Ac (1993) = $2975 \, m^2$), a reduction in Ac of 17.5% can be seen. Regarding the tidal prism, P, in the last 150 years there has been significant reclamation in Hamford Water which has led to a reduction P. It is not possible to measure accurately P for 1847, but given a measured Ac for 1847 of $3606m^2$, from the 1847 Admiralty chart, if O'Brien's relationship is to hold true, a prism of approximately 3 times greater should be expected ($P = c/Ac$, = $3606 / 6.6 \times 10^{-5} = 54.5 \times 10^6 \, m^3$). It is, however, possible to approximate the tidal prism by removing the seawalls from the calculation and measuring the volume of water up to the 4.5mOD contour; it measures at approximately $45 \times 10^6 \, m^3$. Therefore, using the 1993 Ac of $2975 \, m^2$, $P = Ac/c = 45 \times 10^6 \, m^3$. This would go some way to explaining what is happening. If the reduction in Ac since 1847 is considered: Ac 1847 = $3606 \, m^2$; Ac 1993 = $2974m^2$, i.e., $631m^2$ in 146 years, which equates to $4.3 \, m^2 \, yr^{-1}$. If the tidal prism remains constant, an Ac of $1168 \, m^2$ is required for equilibrium; $2975 - 1168 = 1807 \, m^2$, implying that equilibrium will be reached in 420 years. This assumes that the system was in equilibrium in 1847; but reclamation has been going on since the 1600's at least, and the Holocene core data would suggest even earlier than that. It also does not take into account sea-level rise and the effect on wave amplitude

of both sea and tidal waves. Therefore, it is considered that the *Ac* is too large for the tidal prism. However, it is not simply a case of adjusting to meet a new equilibrium: it is possible that the *Ac* has increased in size due to external sediment supply factors; and at the same time the prism has been reduced due to reclamation. The net result has manifest itself in a retreat of Stone Point and therefore a loss of protection for the embayment from the adverse affects of wave action. It may be that the whole of the embayment needs to be considered as two separate systems: Hamford Water and Walton Channel with a watershed across the Wade. It is suggested that in the absence of any preventative engineering works, a new channel would form around Stone Point and the confluence of Walton channel, Pye channel and Hamford Water would silt up.

The morphology and orientation of Stone Point used to be determined by the length of its extension towards the Mussle Scarfe and its attachment to the north-western edge of Pye Sand; the area from Stone Point to Pye Sand were part of the same spit. By eroding in a south-easterly direction and with the formation of a secondary channel (Outer Swatch), Stone Point has lost its seaward attachment. Its position is now determined by the orientation of Walton Channel which is cut into the London clay and therefore a fairly stable feature. Pye Sand is now an independent swash platform maintained by both wave and tidal action. The retreat of Stone Point is irreversible: once the Holocene, soft sediment erodes it cannot be replaced simply by sediment recharge techniques, the settlement of fine-grained sediment and its subsequent consolidation is measured in hundreds of years; erosion is measured in years.

It would be tempting to correlate dredging history of Harwich and Felixstowe with the rate of retreat of Stone Point as illustrated in Figure 9-2 (compare with Figure 7-13). Although there looks as if there is a correlation, in fact the first significant deepening occurred in 1906 when the lower harbour and approaches were deepened from 5.0 to 6.0 metres and remained that depth until 1968. The retreat of Stone Point appears to have continued regardless. Whether that is still the case is not sure.
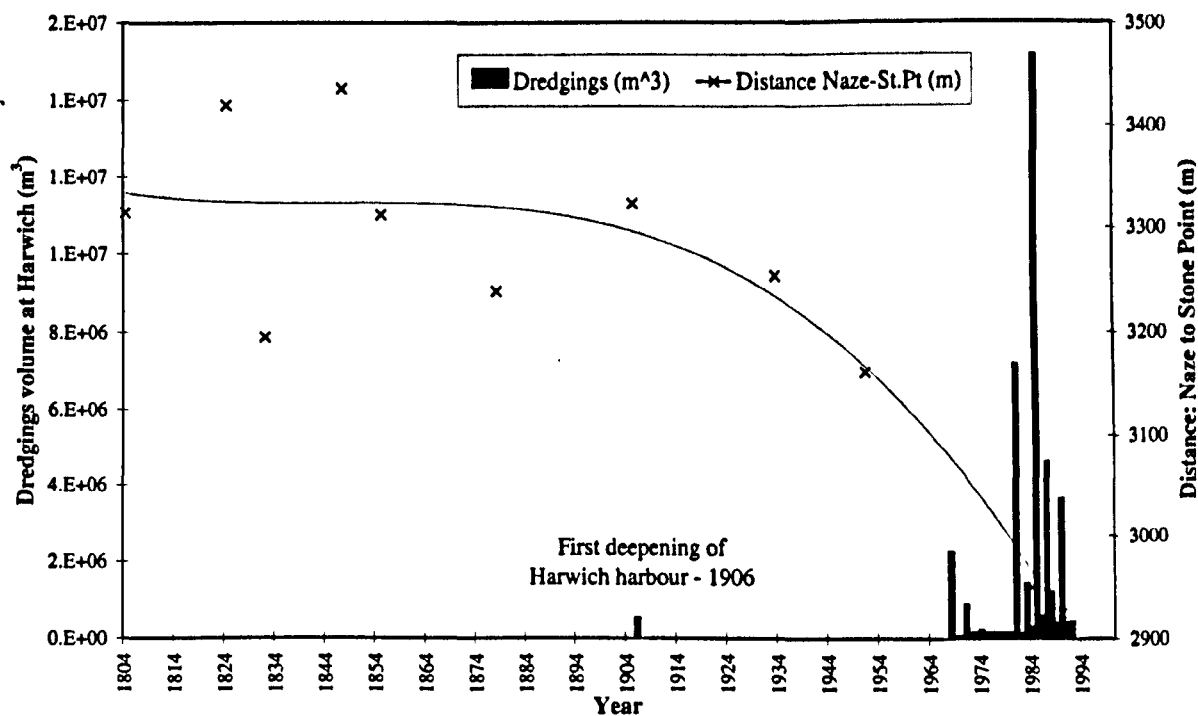
Figure 9-2 – Stone Point retreat and dredging history at Harwich

It is considered therefore, that Stone Point and Pye Sand are critical morphological features protecting the Hamford Water embayment. The question has to be asked that this research is unable to answer: is the observed erosion a sign of progressive change or cyclic change? If it is attributed to lack of sediment, is it directly related to nearby engineering works, or is there a general reduction in regional sediment supply in the Southern North Sea, or both?

9.1   Coastal Management

An important aim of this research has been to view the overall results from a coastal management perspective. In the United Kingdom (UK), the Government has a definitive policy towards management of the coastal zone (DoE, 1996):

'...*it is committed to protecting and preserving* [the coast] *whilst recognising and balancing this against the needs of the present.*'

The guiding principle is to:

'...*achieve sustainable development in the coastal environment through integrated management to achieve common goals.*'

The coastal zone is taken to be:

'...*the adjacent land, including developed and undeveloped areas; estuaries, tidal inlets; and the inter-tidal zone; and inshore marine zone.*'

Coastal Zone Management (CZM) is the:

'...*process which brings together all those involved in the development, management and use of the coast within a framework which facilitates the integration of their interests and responsibilities to achieve common objectives.*'

Research by Hydraulics Research, Wallingford (1993) has suggested that the coastline of England and Wales can be divided into 11 major sediment 'cells' in which

'... *the movement of coarse sediment (sand and shingle) is largely self contained. Interruptions to the movement of sand and shingle within one cell should not affect beaches in an adjacent sediment cell.*' (MAFF, 1995).

Each cell forms a discrete unit for the development of a Shoreline Management Plan (SMP) which is a document detailing a strategy for coastal defence for a specified length of coast. It takes into account all processes affecting the coastal zone. In practice, each cell is further divided into sub-cells or groups of sub-cells that can be further divided into Management Units. Management Units are lengths of shoreline with

'*coherent characteristics in terms both of natural coastal processes and land use.*'

In the UK the generic options available for each management unit are: do nothing; hold the existing defence line by maintaining or changing the standard of protection; advance the existing defence line; and, retreat the existing defence line. A further option is identified by Bennett and Doyle (1997) termed "*build-off*" which is the use of offshore breakwaters and islands to create areas of low wave energy to assist sedimentation and beach accretion. Each option is considered in relation to its most likely effect on adjacent management units and on the sediment cell as a whole.

Hamford Water falls within Sediment Cell No.3, which covers the Wash to the Thames (Figure 2-1); and forms Management Unit No.8 within Coastal Unit No.8 (Figure 9-3).
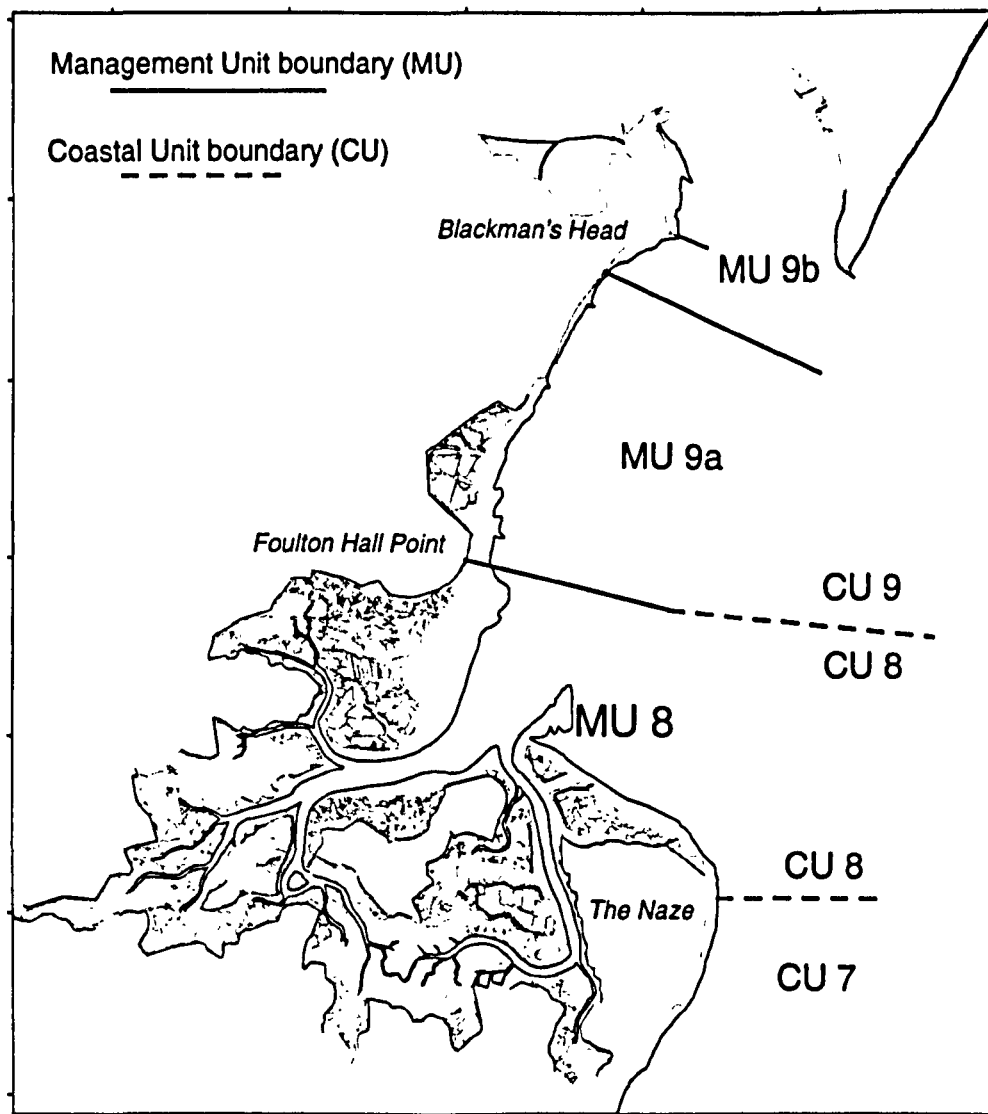
Figure 9-3 – Hamford Water Coastal Management Units.

The current Shoreline Management Plan (SMP) (Mouchel Associates Limited, 1996) adopts the following preferred policy for Management Unit 8:

1.   *In the short term (up to 10 years) – hold the existing defence line whilst initiating an extensive monitoring programme for the frontage to enable a hydraulic numerical model study to be undertaken. The model should investigate the various coastal defence options of do nothing, hold the line, advance the line and retreat the line. In addition, initiate a numerical study to investigate the sediment transport pathways between Felixstowe, Cork Sands, the Naze and Pye Sand to understand the effect the harbour dredging is having on this regime.*

2. *In the longer term – a) hold the line in defined areas; and b) implement the preferred option on the basis of the results of monitoring, modelling and economic evaluation. Managed set back will only be undertaken where it can be demonstrated that this is the only sustainable defence policy and that it produces more sustainable estuary morphology.*

The above SMP has been compiled from an informed assessment based on best available knowledge of the general processes that are affecting the coastal zone near Hamford Water. Obviously, more detailed research within sediment cells and sub-cells can contribute to a greater understanding of actual processes, with the ultimate aim of achieving sufficient knowledge definition that processes can be modelled to a high degree of accuracy. It is considered that research such as this project can offer a valuable contribution to knowledge of detailed sub-cell processes and therefore, attempt to fine-tune the relevant SMP.

It is apparent from this research and concurrent research (*see Section* 3.2.7) that the present boundary of Coastal Unit (CU) 8 and 9 should not be sited at Foulton Hall Point. CU 8 and 9 should be merged to reflect the increasing importance of Hamford Water in the overall circulation of the Stour, Orwell and Hamford Water. The current boundary between CU 8 and 9 could then remain as a Management Unit (MU) boundary if required.

In addition, although it has been assessed that there are two sedimentary regimes in Hamford Water, coarse sediment and fine sediment in suspension, and that the two are virtually independent of each other; the depositional juxtaposition of both fine and coarse sediment is complementary. For example, at Stone Point, the fine cohesive sediment provides a foundation for the coarse sediment to form a protective beach and in turn the coarse sediment protects the underlying cohesive sediment. Management plans that attempt to maintain existing morphological features or even extend, need to consider both the movement and fate of the different sediments.

Finally, this research would advocate a simple but radical alteration to the SMP: retreat the line at Foulton Hall point and hold the line in all other areas. The unyielding frontage at Foulton Hall point has re-aligning the entrance to Hamford Water inlet in a

southerly direction. The classical stable form of a tidal inlet, as illustrated in Figure 3-1, consists of a symmetrical shape involving both updrift and downdrift beaches with a central ebb channel and marginal flood channels. The seawall at Foulton Hall Point has the effect of causing an imbalance in the system. The main channel is now attempting to re-align itself, consequently depths in Pye Channel are decreasing, and a new channel is being cut in the Outer Swatch. This has had the effect of exposing Horsey Island to increased wave action. Stone Point has retreated and realigned itself clockwise to a more protective angle but is restricted be the semi-permanent nature of Walton Channel. Managed retreat of Foulton Hall Point would both balance the orientation of the inlet and increase the tidal prism and therefore move towards equilibrium as defined by the O'Brien relationship.

10 Conclusion

The mouth of Hamford Water has features of, and behaves much like a tidal pass or tidal inlet after Hubbard *et al.* (1979) and may be classed as transitional, as opposed to purely wave-dominated or tide-dominated. The tidal cycle is predominantly ebb-dominated but with a spring flood dominant marginal channel at Stone Point. The inlet system acts as an efficient sediment filter: coarse bedload sediment (D>0.2mm) and fine sediment in suspension is drawn in on the flood tide. Most coarse sediment enters via the marginal flood channel around Stone Point, having been transported by longshore drift from the Naze and offshore. The coarse fraction does not reach far into the embayment, most being deposited around Stone Point. The finer fraction (<63μm) in suspension may reach the innermost creeks and marsh but due to a very short high water stand, there is little time for deposition. The comparatively high ebb currents (peak ebb ≈1 m/s compared with peak flood ≈0.6 m/s), may return much of the fine fraction, still in suspension, to the open sea and flush the coarse fraction from Stone Point and deposit it on Pye Sand. Thus, the balance of the whole system relies on the supply of marine sediment and the nature of the tidal cycle. The coarse fraction is essential for maintaining Stone Point and Pye Sand and thus protecting the embayment from wave action. The fine fraction is essential for maintenance of the mudflats and salt marsh in the interior. The ultimate fate of Stone Point is determined by the supply of sand from the Naze as well as offshore sediment, albeit indirectly. Stone Point has retreated by about 300 metres in the last 150 years and the cross-sectional area of the entrance has reduced accordingly but not sufficiently enough to maintain equilibrium. The interior of the embayment is thus being exposed to more wave action and hence recent attempts to maintain Horsey Island.

It cannot be assumed that an ebb-dominant tidal cycle is a permanent feature. Many studies have been conducted on the morphological behaviour of tidal basins (for example, Van Dongeren & de Vriend, 1994), and Pethick's (1995) model of Holocene development of UK estuaries is applicable to Hamford Water. The essential feature is that the system oscillates between flood and ebb asymmetry. The present situation of ebb-dominance, and possible ebb-transport, may change to flood dominance and flood transport. However, what is more difficult to determine is the effect of a regional

reduction of marine sediment supply. The required quantity of sediment to replace that lost during ebb-dominance may not be available in the future.

Focussing on the overall coastal zone management context: the main conclusion regarding sediment transport and the fate of Hamford Water is that the position and extent of Pye Sand and Stone Point are crucial to the stability of the interior. The sediment that constitutes both these features can only come from outside Hamford Water. However, both Stone Point and Pye Sand are underlain by consolidated cohesive clay and silt, deposited under more sheltered conditions, that provides an anchor for the unconsolidated material. The erosion of this material, as the overlying unconsolidated sands are stripped off, is permanent. This is particularly evident at Stone Point where the old marsh surface is exposed as Stone Points rolls back. The addition of unconsolidated sediment can only be a temporary measure and will have to be repeated periodically.

The future evolution of the entrance points to a continued widening to a point where two channels may form with a central bank between them. Ironically, this may have the effect of protecting Horsey Island. However, for a second channel to form where the Inner Swatch is now would cause the current shoal area between Hamford Water and Walton Channel to dry at low water. This is unlikely to be allowed to happen if normal marine traffic is not to be disrupted; coastal management policy would preclude it.

In final conclusion, the original hypothesis that "given the evidence for an apparent deterioration of salt marsh, coupled with an ebb-dominated tidal cycle, the embayment is no longer a significant sediment sink for the southern North Sea" is considered to be unproven. Equally, however, the null hypothesis cannot be accepted conclusively; further work and more sophisticated data acquisition techniques are required in order to determine more accurately the annual balance of sediment flux and sediment transport for Hamford Water.

10.1   Further Work

The following areas of research are identified as requiring more work in order to contribute to a more complete understanding of the sediment dynamics and Holocene evolution of Hamford Water:

- Assess the significance of waves and tidal currents on the marginal channel around Stone Point and quantify the sediment transport.

- Conduct a tracer study to assess the movement of sediment around Stone Point into the Walton Channel and back out onto Pye Sand.

- More comprehensive coverage of sedimentation rates using artificial horizons with, say, Kestner cores as control. Silica flour in both cases.

- Assessment of volume and fate of sediment that would be released if all saltmarsh were to be eroded and the present line of seawall were to be maintained. If none of the released sediment left the system, to what level would the mudflat rise and would saltmarsh re-establish?

- Investigate the existence and possible influence of fluid mud reservoirs in the deeper areas of the main channels and their effect on SPM levels.

- Model the effect on the tidal prism and inlet hydraulics of two channels instead of one at the entrance.

- Investigate the effect on sedimentation rates of small-scale variations in temperature and salinity during the flooding of tidal mudflats.

- Investigate the existence of tidal convergence/divergence zones and their effects on sedimentation rates.

- Model the effect of a managed retreat at Foulton Hall Point versus a "Do Nothing" policy.

- Investigate the effects of local meteorological conditions on sedimentation and erosion within Hamford Water.

- Further lithological and biological analysis of the cores recovered from Stone Point and Pewit Island to build on the Holocene evolution of the site.

- Finally, continuous monitoring of the interaction of the physical processes at work within Hamford Water with overall sediment transport patterns of the Stour-Orwell and Southern North Sea is seen as essential.

"Science does not rest upon rock-bottom. The bold structure of theories rises, as it were, above a swamp, but not down to any natural or 'given' base; and when we cease our attempts to drive our piles into a deeper layer, it is not because we have reached firm ground. We simply stop when we are satisfied that they are firm enough to carry the structure, at least for the time being."

(Popper, 1959)

References

Note:

- *"Grey" literature references, i.e. Consultants reports etc., are indicated thus #, and a list of contact addresses is contained at Appendix A.*

Aaby, B. & Berglund, B.E. (1986) Characterisation of peat and lake deposits. In *Handbook of Holocene Palaeoecology and Palaeohydrology*, (ed. B.E. Berglund), Wiley, New York. Pp. 231–246.

ASCE (American Society of Civil Engineers) (1975) *Sedimentation Engineering.* Vanoni, V. A., (Ed.), New York, 745 p.

Ackers, P. and White, W. R. (1973) Sediment transport: new approach and analysis. *J. Hydraul. Div., Proc. ASCE*, **99**, 2041–2060.

Adam, P. (1990) *Saltmarsh Ecology.* Cambridge University Press.

Admiralty (1983) *HI 77 – Walton Backwaters – Report of Survey.* Admiralty Hydrographic Department. Taunton.

Aguire, E and Pasini, G. (1985) The Plio-Pleistocene boundary. *Episodes*, **8**, 116–120.

Allen, J.R.L. (1993) Muddy alluvial coasts of Britain: field criteria for shoreline position and movement in the recent past. *Proceedings of the Geologists' Association*, **104**, 241–262.

Allen, P. (1995) Walton-on-the-Naze. In *The Quaternary of the Lower Reaches of the Thames*. (ed. D.R. Bridgland, P.Allen, B.A. Haggart) 297-298. Quaternary Research Association.

Allen, J.R.L. and Pye, K. (1992) *Saltmarshes: Morphodynamics, Conservation and Engineering Significance.* Cambridge University Press.

Allsop, J.M. and Smith, N.J.P. (1988) The deep geology of Essex. *Proceedings of the Geologists' Association*, **99**, 249–260.

Amos, C.L. (1995) Siliclastic Tidal Flats. In: *Geomorphology and Sedimentology of Estuaries. Developments in Sedimentology 53.* (ed. G.M.E. Perillo), Elsevier Science, pp. 273–306.

Amos, C.L., Van Waggoner, N.A. and Daborn, G.R. (1988) The influence of sub-aerial exposure on the bulk properties of fine-grained intertidal sediment from the Minas Basin, Bay of Fundy. *Estuarine, Coastal and Shelf Science*, **27**, 1–13.

Anderson, F.E. (1983) The Northern muddy intertidal: seasonal factors controlling erosion and deposition – a review. *Can. J.Fish. Aquatic Sci.*, **40**, 143–159.

Anderson, F.E., Black, L., Watling, L.E., Mook, W. , and Mayer, L.M. (1981) A

temporal and spatial study of mudflat deposition and erosion. *Journal of Sedimentary Petrology*, **51**, 729–736.

Asghar Ali (1992) *Sedimentological, Geophysical and Oceanographic studies of postglacial and contemporary sedimentary processes of the NE Menai Strait and Conway Bay (Wales, UK)*. Unpublished Ph.D. thesis, University College of North Wales, Bangor.

Aubrey, D.G. and Speer, P.E. (1985) A study of non-linear tidal propagation in shallow inlet/estuarine systems. Part I: Observations. *Estuarine, Coastal and Shelf Science*, **21**, 185–205.

Bagnold, R.A. (1956) The flow of cohesionless grains in fluids. *Phil. Trans. R. Soc.*, **A249**, 235–297.

Bagnold, R.A. (1963) Mechanics of Marine Sedimentation. In *The Sea*, (ed. M.N. Hill), pp. 507–523. Wiley, New York.

Bagnold, R.A. (1966) An approach to the sediment transport problem from general physics. *US Geological Survey Professional Paper*, No. 422–I.

Bale, A.J., Morris, A.W. and Howland, R.J.M. (1985) Seasonal sediment movement in the Tamar estuary. *Oceanologica Acta*, **8**, 1–6.

Bennett, M.R. and Doyle, P. (1997) *Environmental Geology: Geology and the Human Environment*. Wiley.

Birks, H.J.B and Birks, H.H. (1980) *Quaternary Palaeoecology*. Edward Arnold, London.

Boon, J.D. and Byrne, R.J. (1981) On basin hypsometry and the morphodynamic response of coastal inlet systems. *Marine Geology*, **40**, 363–375.

Boothroyd, J.C. (1985) Tidal Inlets and Tidal Deltas. In *Coastal Sedimentary Environments*, (ed. R.A. Davis, Jr.), pp. 445–532. Springer-Verlag, New York.

Boothroyd, J.C. and Hubbard, D.K. (1975) Genesis of bedforms in mesotidal estuaries. In *Estuarine Research, 5, II. Geology and Engineering*. (ed.) L.E. Cronin. pp. 129–149. Academic Press, New York.

\# **Boyden, P.B.** (1979) *The First 124,999,061 Years of Walton: A short account of the town to AD 939*. Frinton and Walton Library.

Brampton, A.H. (1992) *Engineering significance of British saltmarshes. In Saltmarshes: Morphodynamics, Conservation and Engineering Significance*, (ed. J.R.L. Allen & K. Pye), pp. 115–122. Cambridge University Press.

Brew, D. S. (1990). *Sedimentary environments and Holocene evolution of the Suffolk estuaries*. Ph.D., Univ. East Anglia,

Brew, D.S., Funnell, B.M. and Kreiser, A. (1992) Sedimentary environments and Holocene evolution of the lower Blyth estuary, Suffolk (England), and a comparison with other East Anglian coastal sequences. *Proceedings of the Geologists' Association*, **103**, 57–74.

Bridgland, D.R. (1988) The Pleistocene fluvial stratigraphy and palaeogeography of Essex. *Proceedings of the Geologists' Association*, **99**, 291–314.

Bridgland, D.R., Allen, P. and Haggart, B.A. (ed.) (1995) *The Quaternary of the Lower Reaches of the Thames: Field Guide*. Quaternary Research Association.

Bridgland, D.R., D'Olier, B., Gibbard, P.L. and Roe, H.M. (1993) Correlation of Thames terrace deposits between the Lower Thames, eastern Essex and the submerged offshore continuation of the Thames-Medway valley. *Proceedings of the Geologists' Association*, **104**, 51–57.

Bridgland, D.R., Gibbard, P.L. and Preece, R.C. (1990) The Geology and Significance of the Interglacial Sediments at Little Oakley, Essex. *Philosophical Transactions of the Royal Society of London*, **B328**, 307–339.

Bruun, P. (1978) *Stability of Tidal Inlets. Theory and Engineering*. Elsevier, Amsterdam.

Burd, F. H. (1992). *Erosion and vegetation change on the saltmarshes of Essex and north Kent between 1973 and 1988*. (Research and survey in nature conservation. No 42). Peterborough, Nature Conservancy Council.

Carlyon-Hughes, B. (1939) *The History of Harwich Harbour*. The Harwich Harbour Conservancy Board, Harwich.

Carter, R. B. G. (1988). *Coastal Environments: An Introduction to the Physical, Ecological and Cultural Systems of Coastlines*. Academic Press, London.

Catt, J.A. (1978) Loess and coversands. In *British Quaternary Studies: Recent Advances*, (ed. F.W. Shotton), pp. 221–230. Clarendon Press, Oxford.

Chatfield, C. (1996) *The Analysis of Time Series*. Fifth Edition. Chapman & Hall, London. 283 pp.

Clayton, K.M., McCave, I.N. and Vincent, C.E. (1982) *The establishment of a sand budget for the East Anglian coast and its implications for coastal stability. In Shoreline Protection*, (ed. Institute of Civil Engineers), pp. 91–96. Thomas Telford, London.

Coakley, J.P and Syvitski, J.P.M. (1991) SediGraph Technique. In *Principles, Methods and Applications of Particle Size Analysis*. (ed. J.P.M. Syvitski), pp 129–142. CUP.

Cobbold, D.L. (1995) *A palaeoenvironmental reconstruction from the Holocene sediments of the Walton Backwaters (Hamford Water), Essex.* Unpublished BSc dissertation, University of Wales, Bangor.

Curtin, W. and Lane, R.F. (1970) *Concise Practical Surveying.* Edward Arnold.

Daborn, G.R. and 10 others. (1993) An ecological cascade effect: Migratory birds affect stability of intertidal sediments. *Limnology and Oceanogrpahy*, 38, 225–231.

Davidson, N.C., Laffoley, D. d'A., Doody, J.P., Way, L.S., Gordon, J., Key, R., Drake, C.M., Pienkowski, M.W., Mitchell and Duff, K.L. (1991) *Nature Conservation and estuaries in Great Britain.* Nature Conservancy Council, Peterborough.

Davis, R.A. (1994) *The Evolving Coast.* Scientific American Library, New York.

Davies, J.L. (1964) A morphogenic approach to world shorelines. *Z. Geomorphol.*, 8, 27–42.

Department of the Environment (1996) *Coastal Zone Management: Towards Best Practice.* DoE, London.

Dixon, R.G. (1979) Sedimentary facies in the Red Crag (Lower Pleistocene, East Anglia). *Proceedings of the Geologists' Association*, 90, 117-132.

Dixon, A.M. (1989) *Man's Effect on the coast of Essex.* Report to The National Rivers Authority, Anglian Region (unpublished).

Dixon, A.M. (1990) *Sea Defence Instability due to Salting and Foreshore Loss: Foreshore Recharging.* Report to National Rivers Authority, Anglian Region (unpublished).

Dixon, A.M. (1992) *Trial Foreshore Recharge.* Report to National Rivers Authority, Anglian Region (unpublished).

Dobereiner, C. and McManus, J. (1983) Turbidity maximum migration and harbour siltation in the Tay Estuary. *Can. J. Fish. Aquat. Sci.*, 40, suppl. 1, 117-129.

Dronkers, J. (1986) Tidal asymmetry and estuarine morphology. *Netherlands Journal of Sea Research*, 20(2/3), 117–131.

Dyer, K.R. (1973) *Estuaries: A Physical Introduction.* John Wiley & Sons.

Dyer, K.R. (1979) *Estuarine hydrography and sedimentation.* Cambridge University Press.

Dyer, K.R. (1986) *Coastal and Estuarine Sediment Dynamics.* Wiley-Interscience.

Dyer, K.R. (1996) Sediment Transport Processes in Estuaries. In *Geomorphology and Sedimentology of Estuaries. Developments in Sedimentology 53.* (ed. G.M.E. Perillo), pp. 423-447. Elsevier Science B.V.

Dyer, K.R. (1997) *Estuaries: A Physical Introduction.* 2nd edition. John Wiley & Sons.

EC MAST-I (1993) *G6-M Coastal Morphodynamics: On the methodology and accuracy of measuring physico-chemical properties to characterize cohesive sediments.* Commission of the European Communities.

Einstein, H.A. (1950) The bed load function for sediment transportation in open channels. US Dept. of Agriculture, Soil Conservation Serv., Tech. Bull. 1026.

Eisma, D. and Kalf, J. (1987) Dispersal, concentration and deposition of suspended matter in the North Sea. *Journal of the Geological Society, London,* 144, 161–178.

Engelund, F. and Hansen, E. (1967) A Monograph on Sediment Transport in Alluvial Streams. Technisk Vorlag, Copenhagen.

English Nature (1992) *Hamford Water Site of Special Scientific Interest.* (SSSI citation and description).

Escoffier, E.F. (1940) The Stability of Tidal Inlets. *Shore and Beach,* 1, 114–115.

Evans, G. (1965) Intertidal flat sediments and their environments of deposition in the Wash. *Journal of the Geological Society, London,* 121, 209–245.

Fawn, A.J., Evans, K.A., McMaster, I. and Davies, G.M.R. (1990) *The Red Hills of Essex.* Colchester Archaeological Group.

Finley, R.J. (1978) Ebb-tidal delta morphology and sediment supply in relation to seasonal wave energy flux, North Inlet, South Carolina. *Journal of Sedimentary Petrology,* 48, 227–238.

FitzGerald, D.M. (1984) Interactions between the ebb-tidal delta and landward shoreline: Price Inlet, South Carolina. *Journal of Sedimentary Petrology,* 54(4), 1303–1318.

Fitzgerald, D.M. and Nummedal, D. (1983) Response characteristics of an ebb-dominated tidal inlet channel. *Journal of Sedimentary Petrology,* 53, 833–845.

FitzGerald, D.M., Penland, S., and Nummedal, D. (1976) Sand circulation patterns at Price Inlet, South California. *Proceedings of the 15th Coastal Engineering Conference,* pp. 1886–1880.

FitzGerald, D.M., Penland, S., and Nummedal, D. (1976) Sand circulation patterns at Price Inlet, South California. Proceedings of the 15th Coastal Engineering Conference, pp. 1886–1880.

Friedrichs, C.T. (1995) Stability shear stress and equilibrium cross-sectional geometry of sheltered tidal channels. *Journal of Coastal Research*, **11(4)**, 1062–1074.

Frostick, L.E. and McCave, I.N. (1979) Seasonal shifts of sediment within an estuary mediated by algal growth. *Estuarine, Coastal and Marine Science*, **9**, 569–576.

Frey, R.W. and Basan, P.B. (1985) Coastal Salt Marshes. In *Coastal Sedimentary Environments*, (ed. R.A. Davis, Jr.), pp. 225–301. Springer-Verlag, New York.

Fry, V.A. and Aubrey, D.G. (1990) Tidal velocity asymmetries and bedload transport in shallow embayments. *Estuarine, Coastal and Shelf Science*, **30**, 453–473.

Funnel, B.M. (1972) The histroy of the North Sea. *Bull. Geol. Soc. Norfolk*, **21**, 2–10.

Funnell, B.M. and Wilkes, D.F. (1976) Engineering characteristics of the East Anglian Quaternary deposits. *Quarterly Journal of Engineering Geology*, **9**, 145–158.

Gadd, P.E., Lavelle, J.W. and Swift, D.J.P. (1978) Estimate of sand transport on the New York shelf using near-bottom current meter observations. *Journal of Sedimentary Petrology*, **48**, 239–252.

Gao, S. (1993) *Sediment Dynamics and stability of tidal inlets*. Unpublished PhD thesis, University of Southampton.

Gao, S. and Collins, M. (1992) Net sediment transport patterns inferred from grain-size trends, based upon definition of "transport vectors". *Sedimentary Geology*, **80**, 47–60.

Gao, S. and Collins, M. (1995) Net sand transport direction in a tidal inlet, using foraminiferal tests as natural tracers. *Estuarine, Coastal and Shelf Science*, **40**, 681–698.

Goudie, A. (ed.) (1985) *The Encyclopaedic Dictionary of Physical Geography*. Blackwell Reference.

Goudie, A. (1990) *The Landforms of England and Wales*. Basil Blackwell, Oxford.

Graf, W.H. (1971) *Hydraulics of Sediment Transport*. McGraw-Hill, N.Y.

Graham, A. (1988) *Molluscs: Prosobranch and Pyramidellid Gastrapods*. The Linnean Society of London.

Gramolt, D.W. (1960) *The coastal marshlands of East Essex between the seventeenth and mid-nineteenth centuries*. Unpublished MA thesis, University of London.

Grieve, H. (1959) *The Great Tide: The story of the 1953 flood disaster*. Essex County Council, Chelmsford.

Guy, H.P., Simmons, D.B. and Richardson, E.V. (1966) Summary of alluvial channel data from flume experiments, 1956–1961. *US Geological Survey Professional Paper*, **462–I**, 96pp.

Hardisty, J. (1983) An assessment and calibration of formulations for Bagnold's bedload equation. *Journal of Sedimentary Petrology*, **53**, 1007–1010.

Harkness, D.D. (1983) The extent of natural ^{14}C deficiency in the coastal environment of the United Kingdom. *Proceedings of the First International Symposium on C–14 and Archaeology*, **PACT 8**, 351–364.

Harland, M.G. and Harland, H.J. (1980) *The Flooding of Eastern England*. Minimax Books Limited, Peterborough. 64pp.

Harris, P.T. (1988) Large-scale bedforms as indicators of mutually evasive sand transport and the sequential infilling of wide-mouthed estuaries. *Sedimentary Geology*, **57**, 273–298.

Hayes, M.O. (ed.) (1969) *Coastal Environments: NE Massachusetts and New Hampshire. Guidebook*. Fieldtrip for Eastern Section of SEPM, May 9–11, 1969, 462 pp.

Hayes, M.O. (1975) Morphology of sand accumulation in estuaries. In *Estuarine Research Vol.II*, (ed. L.E. Cronin) 3–22. Academic Press, New York.

Hayes, M.O. (1979) Barrier island morphology as a function of tidal and wave regime. In: *Barrier Islands: From the Gulf of St/ Lawrence to the Gulf of Mexico*. (ed.) S.P. Leatherman pp. 1–28. New York: Academic,

Hayes, M.O. (1980) General morphology and sediment patterns in tidal inlets. *Sedimentary Geology*, **26**, 139–156.

Heathershaw, A. D. (1981) Comparison of measured and predicted sediment transport rates in tidal currents. *Marine Geology*, **42**, 75-104.

Heathershaw, A.D. and Langhorne, D.N. (1988) Observations of near-bed velocity profiles and seabed roughness in tidal currents flowing over sandy gravels. *Estuarine, Coastal and Shelf Science*, **26**, 459–482.

Heyworth, A. and Kidson, C. (1982) Sea-level changes in south-west England and Wales. *Proceedings of the Geologists Association*, **93**, 91–111.

Hilgen, F.J. (1991) Astronomical calibration of Gauss to Matuyama sapropels in the Mediterranean and implication for the Geomagnetic Polarity Time Scale. *Earth and Planetary Science Letters*, **104**, 226–244.

Hine, A.C. (1975) Bedform distribution and migration patterns on tidal deltas in the Chatham Harbor Estuary, Cape Cod, Massachusetts. In: *Estuarine Research, Vol.2: Geology and Engineering*. (ed. L.E. Cronin), pp. 235–252. Academic

Press, New York.

Hine, A.C. (1975) Bedform distribution and migration patterns on tidal deltas ib the Chatham Harbor Estuary, Cape Cod, Massachusetts. In: *Estuarine Research, Vol.2: Geology and Engineering.* (ed. L.E. Cronin), pp. 235–252. Academic Press, New York.

Howarth, M.J. and 10 others. (1994) Seasonal cycles and their spatial variability. In *Understanding the North Sea System.* (ed. H. Charnock *et al.*) pp. 5–26. Chapman & Hall for the Royal Society, London.

HR Wallingford (1990) *Walton Backwater: An assessment of a trial replenishment scheme.* Report EX2191, HR Wallingford.

HR Wallingford (1992a) *Development of Harwich Deep Water Channel.* Report EX2651. HR Wallingford Ltd.

HR Wallingford (1992b) *Computer modelling Studies of Wave Effects.* Report EX2651, HR Wallingford.

HR Wallingford (1997) *Harwich Harbour Approach Channel Deepening: Summary of hydraulic impact studies.* Report EX3746, HR Wallingford.

Hubbard, D.K. (1977) Variations in Tidal Inlet Processes and Morphology in the Georgia Embayment. Technical Report 14–CRD Department of Geology, University of South Carolina, Columbia, South Carolina.

Hubbard, D.K., Barwis, J.H. and Nummedal, D. (1977) Sediment transport in four South Carolina Inlets. Coastal Sediments, '77, 582–601.

Hubbard, D.K., Oertel, G and Nummedal, D. (1979) The role of waves and tidal currents in the development of tidal-inlet sedimentary structures and sand body geometry: examples from North Carolina, South Carolina and Georgia. *Journal of Sedimentary Petrology,* **49**, 1073–1092.

Hunt, C.O. (1989) The palynology and correlation of the Walton Crag (Red Crag Formation, Pliocene). *Journal of the Geological Society,* **146**, 743–745.

IECS (1994) *Sites of historical sea defence failure. Phase II Study.* Report to English Nature (No. Z038-94-F) Institute of Estuarine and Coastal Studies, University of Hull.

IECS (1995) *Essex estuaries – geomorphology.* Institute of Estuarine and Coastal Studies, University of Hull.

Jago, C.F. and Mahamod, Y. (1999) A total load algorithim for sand transport by fast steady currents. *Estuarine, Coastal and Shelf Science,* **48**, 93–99.

Jermyn, Stanley T. (1974) *Flora of Essex.* Essex Naturalists' Trust Limited.

Jones, R.L. and Keen, D.H. (1993) *Pleistocene Environments in the British Isles.* Chapman and Hall, London.

Kandiah, A. (1974) *Fundamental aspects of surface erosion of cohesive soils.* Unpublished PhD, University of California, Davis.

Kestner, F.J.T. (1961) Short-term changes in the distribution of fine sediments in estuaries. *Proceedings of the Institute of Civil Engineers,* 9, 193–216.

King, S.E. and Lester, J.N. (1995) The value of salt marsh as a sea defence. *Marine Pollution Bulletin,* 30, 180–189.

Kirby, R., Bleakley, R.J., Weatherup, S.T.C., Raven, P.J. and Donaldson, N.D. (1993) Effect of episodic events on tidal mud flat stability, Ardmillan Bay, Strangford Lough, Northern Ireland. In *Nearshore and Estuarine Cohesive Sediment Transport,* (ed. A.J. Mehta), pp. 378–392. American Geophysical Union, Coastal and Estuarine Studies, Vol. 42.

Kjerfve, B. (1975) Velocity averaging in estuaries characterized by a large tidal range to depth ratio. *Estuarine, Coastal and Marine Science,* 3, 311–323.

Kodz, D. (1994) *Managed Retreat: An Alternative to Hard Engineered Sea Defences in Saltmarsh Environments. Case Study: Hamford Water, Essex.* Unpublished BSc dissertation, University of Portsmouth.

Land, J.M., Kirby, R. and Massey, J.B. (1997) Developments in the combined use of acoustic doppler current profilers and profiling siltmeters for suspended solids monitoring. In *Cohesive Sediments: 4th Nearshore and Estuarine Cohesive Sediment Transport Conference,* INTERCOH '94, (ed. N. Burt, R. Parker, J. Watts). Pp. 187–196 Wiley.

Langhorne, D.N. (1981) An evaluation of Bagnold's dimensionless coefficient of proportionality using measurements of sandwave movement. *Marine Geology,* 43, 49–64.

Lee, A.J. and Ramster, J.W. (1981) *Atlas of the seas around the British Isles.* Ministry of Agriculture, Fisheries and Food. Directorate of Fisheries Research, HMSO, London.

Leeks, G.J.L. (1975) *The morphology of Hamford Marshes, Essex.* Unpublished B.Sc. dissertation, University of London, Queen Mary College.

Leeks, G.J.L. (1979) Mudlarks in the Essex marshes. *Geographical Journal,* 51, 665–669.

Lindholm, R. (1987) *A Practical Approach to Sedimentology.* Allen & Unwin, London.

Long, S. P., & Mason, C. F. (1983). *Saltmarsh ecology.* Glasgow: Blackie.

Lowe, J.J. and Walker, M.J.C. (1984) *Reconstructing Quaternary Environments.* Longman Scientific.

Ludwick, J.C. (1989) Bed load transport of sand mixtures in estuaries: A review. *Journal of Geophysical Research*, **94**, 14315–14326.

Maddock, T. Jr. (1969) The behaviour of straight open channels with moveable beds. *United States geological Survey Professional Paper 622–A*, Washington, D.C., 70p.

Madsen, O.S. (1989) Transport determinations by tracer. A: Tracer theory. In *Nearshore Sediment Transport*, (ed. R. J. Seymour), pp. 103–114. Plenum Press, New York.

MAFF (1995) *Shoreline Management Plans: A guide for coastal authorities.* Ministry of Agriculture, Fisheries and Food. 24 pp.

Mahamod, Y. (1989) *Sedimentary processes in the Dwyryd Estuary.* Unpublished PhD thesis, University of Wales, Bangor.

Markham, R. (1973) Suffolk and East Essex. In *The Estuarine Region of Suffolk and Essex*, (ed. J.G. Capewell), pp. 2–11. The Geologist's Association.

Mathers, S.J. and Zalasiewicz, J.A. (1988) The Red Crag and Norwich Crag of southern East Anglia. *Proceedings of the Geologists' Association*, **99**, 261–278.

McCave, I.N. (1979) Suspended Sediment. In *Estuarine hydrography and sedimentation*, (ed. K.R. Dyer), pp. 131–185. Cambridge University Press.

McCave, I.N. (1987) Fine sediment sources and sinks around the East Anglian coast. *Journal of the Geological Society*, **144**, 149–152.

McCave, I.N. and Geiser, A.C. (1979) Megaripples, ripples and runnels on intertidal flats of the Wash, England. *Sedimentology*, **26**, 353–369.

McCave, I.N. and Syvitski, J.P.M. (1991) Principles and methods of geological particle size analysis. In *Principles methods, and application of particle size analysis*. (ed. J.P.M. Syvitski), pp. 3–21. Cambridge University Press.

McLaren, P. and Bowles, D. (1985) The effects of sediment transport on grain-size distributions. *Journal of Sedimentary Petrology*, **55**, 457–470.

McManus, J. (1988) Grain size determination and interpretation. In *Techniques in Sedimentology*. (ed. M.E. Tucker), pp. 63–85. Blackwell, Oxford.

Mehta, A.J. (1978) Bed friction characteristics of three tidal entrances. *Coastal Engineering*, **2**, 69–83.

Miller, M.C., McCave, I.N., and Komar, P.D. (1977) Threshold of sediment motion under unidirectional currents. *Sedimentology*, 24, 507–527.

Mitchell, G.F., Penny, L.F., Shotton, F.W. and West, R.G. (1973) *A Correlation of Quaternary Deposits in the British Isles*. Geological Society of London, Special Report No.4, 99 pp.

Mouchel (1996) *Essex Shoreline Management Plan*. Mouchel (Mouchel Essex) Associates Limited.

Nichols, MM and Briggs, R.B (1985) Estuaries. In *Coastal Sedimentary Environments*, (ed. R.A. Davis, Jr.), pp. 77–186. Springer-Verlag, New York.

NRA (1992) *East Anglia Saltmarshes*. NRA, Peterborough.

NRA (1993) *Essex Saltings Research 1986–1992*. Report prepared by the Institute of Estuarine and Coastal Studies, University of Hull.

O'Brien, M.P. (1969) Equilibrium flow areas of inlets on sandy coasts. *J. Waterways, Harbour Coast. Eng. Div. ASCE* 95, 43-52.

Oertel, G.F. (1975) Ebb-tidal deltas in Georgia estuaries. In *Estuarine Research vol 2: Geology and Engineering*. (ed.) L.E. Cronin pp. 267–276. New York: Academic

Oertel, G.F. (1988) Processes of Sediment Exchange Between Tidal Inlets, Ebb Deltas, and Barrier Islands, Lecture Notes on Coastal and Estuarine Studies, 29. Springer-Verlag.

Open University (1989) *Waves, Tides and Shallow-Water Processes*. The Open University, Pergammon Press.

Parker, W.R. (1994) On the characterisation of cohesive sediment for transport modelling. In *Proceedings of the 4th Nearshore and Estuarine Cohesive Sediment Transport Conference, INTERCOH '94* (ed. N. Burt, R Parker and J. Watts), pp. 3–14. Wiley and Sons.

Pejrup, M. (1988) The triangular diagram used for classification of estuarine sediments: a new approach. In *Tide-Influenced Sedimentary Environments and Facies*, (ed. P.L. de Boer, A. van Gelder and S.D. Nio), pp. 289–300. D.Reidel Publishing, Dordrecht.

Pethick, J. S. (1984). *An introduction to Coastal Geomorphology*. London: Edward Arnold

Pethick, J. S. (1992) Saltmarsh geomorphology. In *Saltmarshes: Morphodynamics, Conservation and Engineering Significance*, (ed. J.R.L. Allen & K. Pye), pp. 41–62. Cambridge University Press.

Pethick, J. S. (1993) Shoreline adjustments and coastal management: physical and

biological processes under accelerated sea-level rise. *Geographical Journal*, 159(2), 162–168.

Pethick, J.S. (1995) Estuarine Processes. In *A Guide to the Understanding and Management of Saltmarshes*. (ed. A.R. Toft and R.J. Maddrell). Pp. 33–72. National Rivers Authority [Environment Agency], Bristol.

Pethick, J.S. (1996) The geomorphology of mudflats. In *Estuarine Shores: Evolution, Environments and Human Alterations*. (ed. K.F. Nordstrom and C. T. Roman), pp. 185–221. Wiley.

Pethick, J. S., & Leggett, D. (1993). The geomorphology of the Anglian Coast. In *Coasts of the southern North Sea*. (ed. R. Hillard). ASCE.

Popper, K.R. (1959) *The Logic of Scientific Discovery*. Routledge, London.

Posford Duvivier. (1993). *Harwich approach channel deepening: environmental statement*. (7567). Posford Duvivier Environment.

Pritchard, D.W. (1955) Estuarine circulation patterns. *Proceedings of the American Society of Civil Engineers Separates*, 81(717), 473–517.

Pugh, D.T. (1987) *Tides, Surges and Mean Sea-Level. A Handbook for Engineers and Scientists*. John Wiley & Sons.

Rawson, K.J. and Tupper, E.C. (1994) *Basic Ship Theory Volume 2*. Longman Scientific, Harlow, Essex. 702 pp.

Ratcliffe, D.A. (1977) *A Nature Conservation Review*. Cambridge University Press, Cambridge.

Raudkivi, A. J. (1976) *Loose Boundary Hydraulics*. Pergamon Press, Oxford. 331p.

Reynolds, W.J. (1988) Ebb-tidal delta dynamics for a tide-dominated barrier island. In *Hydrodynamics and Sediment Dynamics of Tidal Inlets*, (ed. D.G. Aubrey and L. Weishar), 348–363. Springer-Verlag.

Richard, G.A. (1978) Seasonal and environmental variations in sediment accretion in a Long Island salt-marsh. *Estuaries*, 1, 29–35.

Robinson, A.H.W. (1952) The changing coastline of Essex. *Essex Naturalist*, 29, 79–93.

Roberts, N. (1998) *The Holocene: An Environmental History*. Second Edition. Blackwell, Oxford.

Rouse, H. (1938) Experiments on the mechanics of sediment suspension. Fifth International Congress for Applied Mechanics. pp. 550–554.

Scourse, J.D. (1992) Quaternary sea-level change and coastal management. *Geoscientist*, 2, 13–16.

Shepard, F.P. (1954) Nomenclature based on sand-silt-clay ratios. *Journal of Sedimentary Petrology*, 24, 151–158.

Sherlock, R.L. (1935) *British Regional Geology: London and Thames Valley.* HMSO

Smith, J.B. and FitzGerald, D.M. (1994) Sediment transport patterns at the Essex River inlet ebb-tidal delta Massachusetts, USA. *Journal of Coastal Research*, 10(3), 752–774.

Spiegel, M.R. (1992) *Theory and Problems of Statistics.* Schaum's Outline Series. McGraw-Hill, New York.

Steers, J.A. (1964) *The Coastline of England and Wales.* Cambridge: Cambridge University Press.

Sternberg, R.W. (1972) Predicting initial motion and bedload transport of sediment particles in the shallow marine environment. In *Shelf Sediment Transport: Process and Pattern.* (ed. D.J.P. Swift, D.B. Duane and O.H. Pilkey). pp. 61–82. Dowden, Hutchinson and Ross, Stroudsberg.

Sumbler, M.G. (1996) *British Regional Geology: London and the Thames Valley.* (4th Edition), HMSO for BGS. 173pp.

Swan, A.R.H. and Sandilands, M. (1995) *Introduction to Geological Data Analysis.* Blackwell Science.

Syvitski, J.P.M. (ed) (1991) *Principles, Methods and Applications of Particle Size Analysis.* CUP, Cambridge.

Thorne, P.D. (1986) An intercomparison between visual and acoustic detection of seabed gravel movement. *Marine Geology*, 72, 11–31.

Thorne, P.D., Williams, J.J. and Heathershaw, A.D. (1989) In situ acoustic measurements of marine gravel threshold and transport. *Sedimentology*, 36 61–74.

Toft, A.R. and Maddrell, R.J. (ed.) (1995) *A Guide to the Understanding and Management of Saltmarshes.* National Rivers Authority, Bristol.

Trebble, N. (1976) *British Bivalve Seashells.* 2nd edition. London: HMSO.

Toels-Smith, J. (1955) Karakterisering af løse jordater. Characterisation of unconsolidated sediments. *Danm. Geol. Unders.* Ser. IV, 3 (10), 73 pp.

\# UKAE, Harwell. Binnie and Partners. (1984) Preliminary study of small scale tidal energy. Phase 2 – Camel estuary (Padstow) and Hamford Water (The Naze). United Kingdom Atomic Energy Authority, Harwell.

\# Unicomarine Ltd. (1992) Essex Intertidal Study: Survey 2 – July 1991. Unicomarine Limited, Letchworth.

Van de Kreeke, J. (1985) Stability of tidal inlets – Pass Cavallo, Texas. *Estuarine, Coastal and Shelf Science*, **21**, 33–43.

Van de Kreeke, J. (1990) Stability analysis of a two-inlet bay system. *Coastal Engineering*, **14**, 481–497.

Van Dongeren, A.R. and de Vriend, H.J. (1994) A model of morphological behaviour of tidal basins. *Coastal Engineering*, **22**, 287–310.

Van Rijn, L. C., 1986. Evaluation of measuring instruments for suspended sediment. In: *International Conference of Measuring Techniques of Hydraulic Phenomena in Offshore, Coastal and Inland Waters*. (London, England, 9–14 April, 1986), 401–423.

Viles, H. and Spencer, T. (1995) *Coastal Problems: Geomorphology, Ecology and Society at the Coast*. Edward Arnold, London.

Wang, P.X. and Murray, J.W. (1983) The use of foraminifera as indicators of tidal effects in estuarine deposits. *Marine Geology*, **51**, 239–250.

Warren, S.H. (1912) A prehistoric internment in north-east Essex. *Essex Naturalist*, **16**, 198–208.

Warren, S.H., Piggott, S., Clark, J.G.D., Burkitt, M.C., Godwin, H. and M.E. (1936) Archaeology of the submerged land-surface of the Essex coast. *Proceedings of the Prehistorical Society, London*, **2**, 178–210.

Whitaker, W. (1877) *The geology of the eastern end of Essex (Walton Naze and Harwich)*. (Explanation of Quarter Sheet 48SE with adjoining part of 48NE.) HMSO.

Whitaker, W. and Thresh, J.C. (1916) *The water supply of Essex from underground sources*. Memoirs of the Geological Survey of England and Wales, HMSO.

White, S.J. (1970) Plane bed thresholds of fine-grained sediments. *Nature*, **228**, 152-153.

Whitehouse, R. (1995) Observations of the boundary layer characteristics and the suspension of sand at a tidal site. *Continental Shelf Research*, **15**, 1549–1567.

Whiteman, C.A. (1992) The palaeogeography and correlation of pre-Anglian-Glaciation terraces of the River Thames in Essex and the London Basin. *Proceedings of the Geologists' Association*, **103**, 37–56.

Whiteman, C.A. and Rose, J. (1992) Thames River sediments of the British Early and Middle Pleistocene. *Quaternary Science Reviews*, **11**, 363–375.

Wilkinson, R.H. (1984) A method for evaluating statistical errors associated with logarithmic velocity profiles. *Geo-Marine Letters*, **3**, 49–52.

Wilkinson, T.J. (1988) Archaeology and environment in south Essex: rescue archaeology along the Grays By-pass, 1979/80. *East Anglian Archaeology 42*, Essex County Council, Chelmsford. 136pp.

Wilkes, M. (1989) *Operational Research: Analysis and Applications*. McGraw-Hill, London. 502 pp.

Williams, G.P. (1967) Flume experiments on the transport of a coarse sand. *US Geological Society Professional Paper* **562-B**, 31p.

\# WS Atkins Limited (1993) *Harwich Dredge Disposal: Numerical modelling of sediment transport. Final report.* WS Atkins Limited, Surrey.

Yalin, M.S. (1963) An expression for bedload transportation. *Journal of Hydraulics Division ASCE*, **89**, 221–250.

Zeuner, F.R. (1958) *Dating the Past: An Introduction to Geochronology*. Methuen, London.

Appendix A – Contact addresses for "grey" literature cited.

APB Research and Consultancy, Pathfinder House, Maritime Way, Southampton SO14 3EA.

CCRU – Cambridge Coastal Research Unit, University of Cambridge Department of Geography, Sidney Street, Cambridge.

EC MAST-I, co-sponsored report by Commission of the European Communities Directorate General XII, prepared as part of EC MAST-I research programme. *Contact the European Union, Brussels.*

English Nature, Northminster House, Peterborough. PE1 1UA.

Environment Agency, River House, Waterside Drive, Aztec West, Bristol.

Frinton and Walton Library, Old Road, Frinton-on-Sea, Essex. CO13.

HR Wallingford, Wallingford, Oxon OX10 8BA

Institute of Estuarine and Coastal Studies (IECS), University of Hull, Hull. HU6 7RX.

Mouchel (Mouchell Essex), Waterloo Chambers, Waterloo Lane, Chelmsford, Essex. CM1 1BD

NRA *see Environment Agency*

Posford Duvivier, Rightwell House, Bretton Centre, Peterborough. PE3 8DW.

UKAE, United Kingdom Atomic Energy Authority. *Reports held at the British Library, Boston Spa, Wetherby, West Yorkshire LS23 7BQ.*

UnicoMarine, 7 Diamond Centre, Works Road, Letchworth, Hertfordshire.

WS Atkins, Woodcote Grove, Ashley Road, Epsom, Surrey KT18 5BW.

Appendix B – Grain Size Data

(See Section 5.3, page 123)

Sample No.	Ellipse No.	Geographical Location	Mean (mm)	Mode	Sorting	Skewness	Kurtosis	%Gravel	%Sand	%Silt	%Clay
1	5	Beaumont Quay	0.00779	0.00779	0.01311	2.97	12.10	0.0	3.7	43.3	52.9
2	5	Beaumont	0.00729	0.00729	0.01309	3.02	12.24	0.0	3.6	39.5	56.9
3	5	Beaumont Cut entrance	0.00913	0.00913	0.01547	2.56	8.81	0.0	6.0	41.4	52.6
4	5	Landermere Quay	0.00969	0.00969	0.01613	2.43	8.02	0.0	6.7	42.9	50.4
5	5	Landermere Ch	0.00530	0.00530	0.01092	3.71	17.63	0.0	2.0	32.3	65.6
6	5	Moze Ck	0.00535	0.00535	0.01081	3.50	15.85	0.0	1.5	33.5	65.0
7	5	Landermere buoys	0.00680	0.00680	0.01236	3.13	13.32	0.0	2.9	37.9	59.2
8	5	Landermere core	0.00799	0.00799	0.01502	2.78	9.92	0.0	5.5	37.8	56.7
9	5	Landermere outer 2	0.00511	0.00511	0.01076	4.04	20.27	0.0	2.3	32.3	65.5
10	5	Garnham Outer	0.00755	0.00755	0.01344	2.87	11.07	0.0	3.5	41.5	55.0
11	5	Honey Pot	0.01292	0.01292	0.02076	1.71	4.34	0.0	13.0	33.9	53.1
12	5	Garnham Inner	0.00792	0.00792	0.01424	2.87	10.83	0.0	4.8	39.0	56.2
13	5	Kirby Ck North	0.00779	0.00779	0.01398	2.90	11.14	0.0	4.5	38.2	57.3
14	5	Horsey Is West	0.00867	0.00867	0.01567	2.65	9.11	0.0	6.3	39.3	54.3
15	5	Kirby Ck Entrance	0.00802	0.00802	0.01403	2.72	10.08	0.0	4.0	39.4	56.7
16	5	Bramble Is jetty	0.00895	0.00895	0.01490	2.52	8.90	0.0	5.0	41.8	53.2
17	5	Oakley Ck	0.00783	0.00783	0.01256	2.81	11.36	0.0	2.7	42.8	54.5
18	5	Kirby Ck west Ch	0.00875	0.00875	0.01483	2.70	9.77	0.0	5.4	42.6	52.0
19	4	Hamford West 1	0.14087	0.14087	0.28760	4.58	27.13	1.3	46.7	21.3	30.7
20	5	Horsey Is North	0.00778	0.00778	0.01426	2.85	10.58	0.0	4.5	41.1	54.5
21	5	Kirby Quay 1	0.00825	0.00825	0.01523	2.76	9.76	0.0	5.8	37.7	56.5
22	5	East Cardinal	0.00736	0.00736	0.01289	3.06	12.69	0.0	3.5	40.5	55.9
23	5	Kirby Quay 2	0.00718	0.00718	0.01342	3.06	12.10	0.0	3.8	38.5	57.7
24	5	Boat Ck	0.00783	0.00783	0.01336	2.77	10.70	0.0	3.4	41.6	55.1
25	5	Wade West	0.05426	0.05426	0.17201	7.71	73.76	0.0	28.3	31.5	40.1
26	5	Peter's Point	0.00870	0.00870	0.01619	2.64	8.84	0.0	7.1	38.1	54.8
27	4	Hamford East 2	0.11605	0.11605	0.17334	5.85	56.44	0.3	53.1	18.2	28.4
28	5	New Is	0.00810	0.00810	0.01500	2.79	10.02	0.0	5.6	39.7	54.8
29	5	Pewet Is 3	0.01110	0.01110	0.01896	2.10	5.90	0.0	10.8	39.3	50.0
30	1	Pewit Is 1	0.37487	0.37487	0.34099	2.77	11.80	0.0	97.2	2.8	0.0
31	5	Wade Centre	0.01665	0.01665	0.02342	1.24	2.81	0.0	18.2	33.6	48.3
32	1	Pewet Is Marginal Bank	0.22954	0.22954	0.10431	10.33	165.48	0.0	98.5	1.5	0.0
33	5	Wade South	0.00775	0.00775	0.01406	2.92	11.19	0.0	4.6	40.1	55.3
34	1	Irlam's Beach	0.27231	0.27231	0.11226	5.13	68.27	0.0	99.4	0.6	0.0
35	1	Pewit	0.22837	0.22837	0.10479	10.89	175.87	0.0	99.8	0.2	0.0
36	5	Hamford Water Centre	0.01133	0.01133	0.01908	1.98	5.52	0.0	10.4	34.9	54.7
37	5	Wade East	0.01364	0.01364	0.02046	1.62	4.14	0.0	12.1	38.7	49.2
38	5	Dugmore VGU	0.05548	0.05548	0.17246	7.58	71.87	0.0	28.3	31.6	40.2
39	2	Horsey VGU	7.81108	7.81108	5.62223	-0.18	1.30	46.3	50.8	1.4	1.4
40	5	Island Point Buoy	0.00856	0.00856	0.01452	2.73	9.97	0.0	4.9	42.8	52.3
41	5	Island Point 2	0.00878	0.00878	0.01467	2.67	9.67	0.0	5.1	42.7	52.2
42	5	Pye Ch 1	0.00790	0.00790	0.01365	2.95	11.55	0.0	4.3	42.1	53.6

Sample No.	Ellipse No.	Geographical Location	Mean (mm)	Mode	Sorting	Skewness	Kurtosis	%Gravel	%Sand	%Silt	%Clay
43	2	Pye Sand VGU	7.27279	7.27279	5.57621	-0.04	1.35	40.4	57.0	1.2	1.3
44	2	Mussel Scarfe	7.19728	7.19728	5.82889	-0.03	1.23	43.1	53.2	1.8	1.9
45	4	Pye Ch 2	0.16685	0.16685	0.26500	3.88	23.15	0.0	56.6	19.1	24.3
46	5	Twizzle	0.00930	0.00930	0.01501	2.34	8.01	0.0	4.6	42.0	53.4
47	5	Titchmarsh Inner	0.01051	0.01051	0.01754	2.22	6.73	0.0	8.5	40.3	51.2
48	3	Walton Ch 1	0.38190	0.38190	0.69334	3.40	15.10	1.4	71.5	14.4	12.8
49	1	Outer Swatch 1	0.17430	0.17430	0.06464	8.91	184.12	0.0	99.9	0.1	0.0
50	5	Standcreek Salts	0.00757	0.00757	0.01426	2.86	10.63	0.0	4.5	38.2	57.3
51	5	Pye Ch 4	0.01672	0.01672	0.02227	1.28	3.07	0.0	16.4	40.1	43.5
52	1	Outer Swatch 2	0.27818	0.27818	0.10660	5.28	70.29	0.0	100.0	0.0	0.0
53	1	Stone Pt 12	0.32915	0.32915	0.21613	4.99	34.04	0.0	100.0	0.0	0.0
54	2	Stone Point VGU	7.89806	7.89806	5.56098	-0.22	1.36	46.1	50.7	1.6	1.6
55	1	Stone Pt 2	0.40087	0.40087	0.33086	3.39	15.49	0.0	99.9	0.1	0.0
56	5	Dardanelles	0.00970	0.00970	0.01620	2.44	8.08	0.0	7.0	41.9	51.2
57	1	Stone Pt 3	0.23758	0.23758	0.12540	6.42	71.83	0.0	100.0	0.0	0.0
58	1	Swatch VGU	0.22782	0.22782	0.09307	10.02	170.19	0.0	99.8	0.2	0.0
59	1	Stone Pt 4	0.34992	0.34992	0.27877	2.80	13.48	0.0	99.4	0.6	0.0
60	5	Titchmarsh Outer	0.01122	0.01122	0.01771	1.98	5.82	0.0	7.8	42.4	49.8
61	5	Walton Ch 3	0.00727	0.00727	0.01209	3.18	13.91	0.0	2.9	45.6	51.4
62	1	Stone Pt 5	0.18683	0.18683	0.11737	11.24	157.64	0.0	100.0	0.0	0.0
63	1	Stone Pt 6	0.28788	0.28788	0.21974	4.99	33.86	0.0	99.7	0.3	0.0
64	1	Stone Pt 7	0.21539	0.21539	0.07151	3.82	40.53	0.0	100.0	0.0	0.0
65	1	Stone Point Dune	0.27257	0.27257	0.10962	5.01	65.17	0.0	99.6	0.4	0.0
66	1	Stone Pt 8	0.17643	0.17643	0.06978	10.72	231.64	0.0	99.9	0.1	0.0
67	1	Stone Pt 9	0.28020	0.28020	0.10537	4.09	49.50	0.0	100.0	0.0	0.0
68	5	Stone Pt 10	0.00936	0.00936	0.01702	2.44	7.69	0.0	7.9	36.8	55.3
69	1	Stone Pt 11	0.25882	0.25882	0.07750	6.23	109.64	0.0	100.0	0.0	0.0
70	1	Inner Swatch 2	0.27262	0.27262	0.14682	2.99	27.17	0.0	97.8	2.2	0.0
71	5	Pye Ch 6	0.00653	0.00653	0.01171	3.11	13.30	0.0	2.0	40.2	57.8
72	2	Walton Ch 4	6.52885	6.52885	5.83697	0.16	1.27	37.9	58.1	1.9	2.1
73	3	Stone Marsh	0.14885	0.14885	0.15816	7.04	79.27	0.0	76.2	12.4	11.4
74	5	Hedge End Is	0.00655	0.00655	0.01208	3.43	15.35	0.0	3.1	40.7	56.2
75	1	Pye Sand Marginal bank	0.21898	0.21898	0.08662	7.92	123.89	0.0	99.4	0.6	0.0
76	4	Walton Ch 5	0.21793	0.21793	0.32149	2.29	9.58	0.0	52.7	20.4	27.0
77	5	Salt Fleet	0.01011	0.01011	0.01744	2.23	6.80	0.0	8.1	36.8	55.1
78	4	Pye Sand Ebb Lobe	0.17514	0.17514	0.27817	3.93	23.43	0.0	57.6	19.1	23.3
79	5	Pye Ch 7	0.01544	0.01544	0.02006	1.43	3.72	0.0	11.4	47.9	40.8
80	5	Foundary Reach	0.00754	0.00754	0.01288	2.93	12.00	0.0	3.3	40.6	56.1
81	3	Pye Ch 10	0.14114	0.14114	0.12626	2.86	25.07	0.0	74.3	13.6	12.1
82	5	Pennyhole Bay North	0.00961	0.00961	0.01607	2.44	8.09	0.0	6.7	42.0	51.3
83	5	Pennyhole Bay Centre	0.01070	0.01070	0.01734	2.06	6.17	0.0	7.1	40.9	52.0
84	5	Pennyhole Bay South	0.01509	0.01509	0.02213	1.42	3.38	0.0	15.4	34.7	49.9

Grain size data from other workers

Sample	Location	Mean Phi	Mean (mm)	Sorting	Type
HR01	Foulton Hall North	-3.069	8.40	0.0030	Inter-tidal
HR02	Foulton Hall Centre	-3.119	8.70	0.0024	Inter-tidal
HR03	Foulton Hall South	-2.980	7.90	0.0042	Inter-tidal
HR04	Foulton Hall Low Water	0.152	0.90	0.5357	Inter-tidal
HR05	Horsey Island South	-2.764	6.80	0.0089	Inter-tidal
HR06	Horsey Island Inshore	-2.785	6.90	0.0084	Inter-tidal
HR07	Horsey Island North	-2.924	7.60	0.0051	Inter-tidal
HR08	Pye Sand North	-1.070	2.10	0.2331	Inter-tidal
HR09	Pye Sand Low Water	1.321	0.40	0.7577	Inter-tidal
HR10	Pye Sand Centre	-2.321	5.00	0.0312	Inter-tidal
HR11	Pye Sand South	-2.826	7.10	0.0073	Inter-tidal
IECS01	Foulton Hall North	-2.966	7.82	0.0044	Saltmarsh
IECS02	Foulton Hall South	-2.990	7.95	0.0040	Saltmarsh
IECS03	Stone Marsh	-2.817	7.05	0.0075	Saltmarsh
IECS04	Walton Central Marsh	-2.887	7.41	0.0059	Saltmarsh
IECS05	Horsey Island	-2.819	7.06	0.0075	Saltmarsh
IECS06	Skipper's Island	-2.824	7.09	0.0073	Saltmarsh
CCRU1	Kirby Quay	-2.574	5.96	0.0160	Inter-tidal
CCRU2	Kirby Quay	-2.745	6.71	0.0095	Saltmarsh

HR = Hydraulics Research Wallingford (HR, 1990)

IECS = Institute of Estuarine and Coastal Studies (IECS, 1994)

CCRU = Cambridge Coastal Research Unit, University of Cambridge (*pers. comm.*)

Appendix C – Errors associated with Eulerian measurement of tidal current speed and direction in estuaries.

(See Section 4.4.1.1, page 59)

The motions affecting any small (<10m in waterline length) anchored survey boat conducting Eulerian measurement of estuarine parameters are rarely considered. It is quite often assumed that the boat remains at a fixed station throughout a survey and all subsequent data are attributed to that station. In reality a boat riding to a single anchor is far from steady and with positional accuracy's of ± 1m achievable with current dGPS systems, it is prudent to consider whether any such positional errors may influence data quality.

Any vessel on the surface of the sea is affected by six degrees of freedom (Rawson and Tupper, 1994) (Figure): three rotational (roll, pitch and yaw) and three translational (surge, heave and sway). Any small disturbance can be resolved into components of these six motions. For a ship riding to a single anchor, however, the most significant motions affecting instruments suspended over the side are pitch, roll and yaw. The translational motions of surge, heave and sway are more applicable to a vessel underway and are therefore considered negligible in the following discussion.
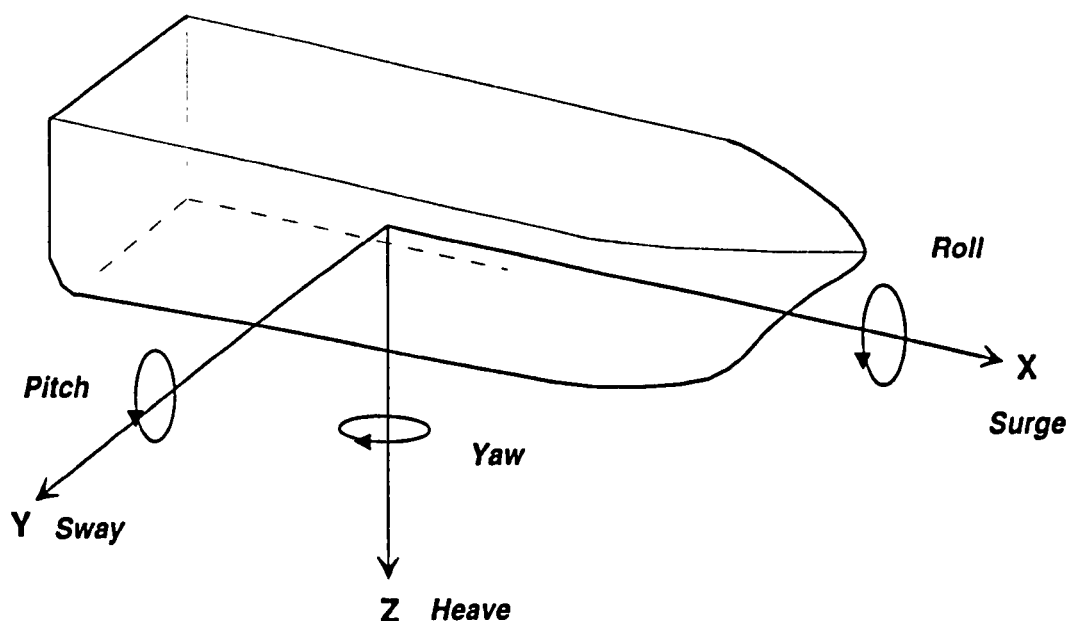
Figure C-1 – Principal motions acting on a ship.

Consider a derrick secured at a central position, *A*, and extending outward at right angles to the fore and aft line of the vessel a distance *x*, from which an oceanographic instrument may be suspended (Figure). The main effect of pitch and roll is to cause a vertical displacement of the instrument resulting in an error in recorded depth. This is therefore applicable to all instruments if depth is a relevant variable. Yaw is only applicable to current meters in that a positive or negative velocity is recorded as the current meter is dragged through the water. The limits of each can be measured or estimated for an assessment of random errors.

Whilst surveying in Hamford Water, it was determined that any pitch was negligible. Wave action was minimal: significant wave height, h_s was estimated, by observation to be 0.2m and consequently the wavelength, *l* was much less than the waterline length of the survey vessel. Roll, however, was felt particularly at high water and from the wake of passing boats. It frequently reached 15° but averaged ±5°. An estimation of roll error, L_e can be calculated by taking the sine of the roll angle, θ (recorded from the horizontal), multiplied by the distance, *x* from the end of the jib boom (from which the instrument is suspended) to the centre-line of the vessel (Figure):
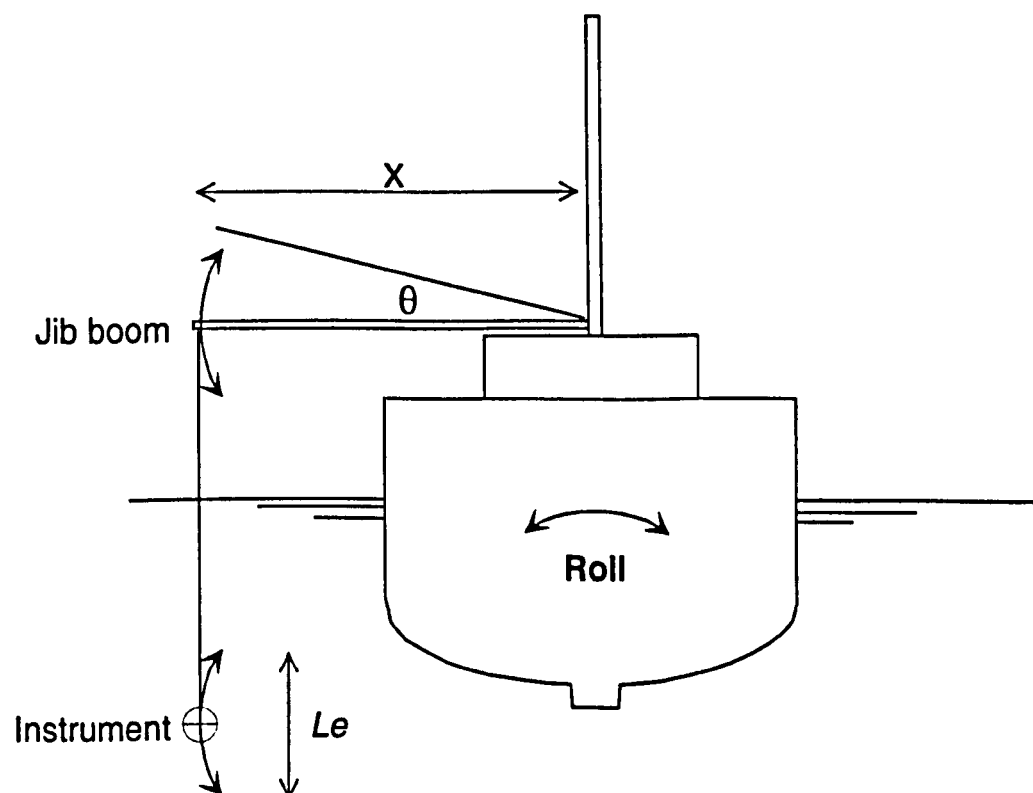
Figure C-2 – Estimation of roll error.

$$L_e = \sin\theta x \qquad\qquad (C:1$$

For example, for a roll angle, θ of 10°, and a jib-centreline length, x of 3.5m, the resulting rise and fall of the instruments, the roll error, L_e is ±0.6m.

Yaw was only found to have a significant effect on velocity recordings during periods of near-slack water. The speed of the vessel as it traverses through the arc of a yaw causes a current meter to record unrealistic velocities according the following equation:.

$$V_e = \frac{\theta^o}{360}(2\pi r) = \frac{r\theta}{t} \; (\theta \; in \; radians) \qquad\qquad (C:2$$

where, V_e is the velocity error; r is the distance, in metres, from the anchor position to the instrument; θ is the yaw angle, in radians; and t is the time taken, in seconds, to complete the full arc of the yaw (Figure).
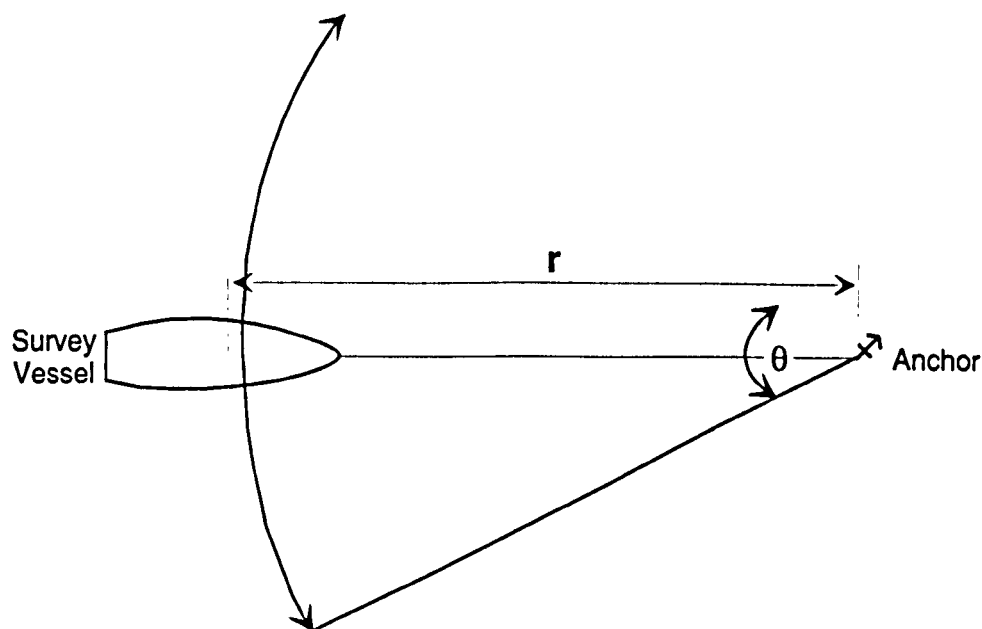
Figure C-3 – Yaw error

For example, a yaw angle, θ of 60° on an anchored vessel with an anchor to current meter distance, r of 22m, yawing over a period, t of 60s caused a velocity reading of 0.38m s^{-1} at slack water. This effect is most noticeable at slack water when the current speed is less than the speed of the yaw and the current meter reverses its orientation depending on the direction of yaw. It is assumed at this point that the current meter in use has a directional component. If the current speed is greater than the speed of the yaw, the increase in

recorded velocity on the upward swing of a yaw is negated by the returning downward swing because the current meter remains pointing into the current, assuming, of course, that the current velocity remains relatively constant throughout the duration of yaw. Yaw is also less pronounced as current speed increases because the anchored vessel achieves directional stability from the hydrodynamic flow around the hull and is less likely to yaw.

Yaw also causes variation in the actual charted position of an anchor station. With accuracy's of ±1.0m achievable with current differential Global Positioning Systems (dGPS) the swing of an anchored survey vessel is certainly measurable. In the research vessel used in this work, the anchor-to-instrument distance of ≈22m combined with a yaw of 60° produced a variation in position of ±10.0m.

The effects of yaw can be reduced by mooring the survey vessel fore and aft in the direction of tidal flow. However, extreme caution is needed when the vessel is stern-to the current flow: small vessels with wide, flat transoms can be broached by strong current flow. It is recommended that the vessel is always bows-to the current.

Appendix D – Velocity Gradient Unit (VGU)
(See Section 4.4.1.2, p.60)

The VGU consists of a vertical array of five pairs of Type C31 10.001 A.OTT current meters attached to a steel mast: 5 facing the flood tide and 5 the ebb (Figure). It is deployed as near as possible to the low water mark and aligned with the dominant ebb-flood direction as determined by observation prior to deployment. Each pair of current meters is positioned on the mast to gain as much information from the logarithmic flow profile as possible. Current-meter heights above the bed for all surveys conducted in this research were 0.10, 0.25, 0.50, 1.00 and 1.50 metres.
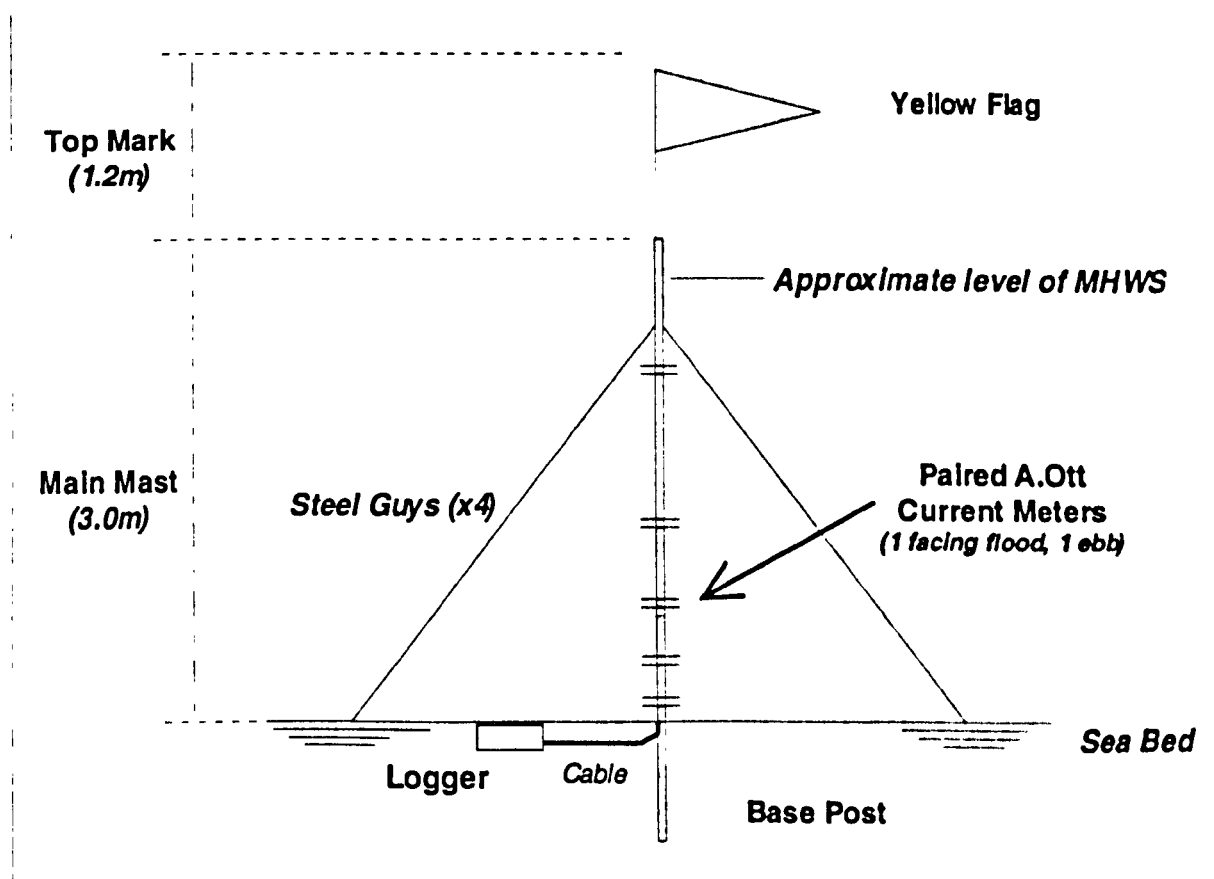
Figure D-1 – Velocity Gradient Unit (VGU)

Operation of the VGU is straightforward: each current meter triggers, via a reed switch, one pulse per impeller revolution that is fed by cable to a data logger (University of Wales, School of Ocean Sciences VGU Logger MKII, Software version 1.02 September 1994). The logger is pre-programmed to count for a predetermined period (logging period) for each sample (cycle period). The data values thus obtained are a time-averaged count over the logging interval and can be easily downloaded from the logger

via RS232C interface to a laptop PC in the field. Conversion to velocity in metres per second is via a calibration equation supplied by A.OTT for this class of current meter. No further calibration was performed for this survey.

For Ott calibration for rotation speeds, n (revs s^{-1}) ≤ 0.91,

$$u(ms^{-1}) = 0.2416n + 0.016 \qquad\qquad (D:1$$

For Ott calibration for rotation speeds, n (revs s^{-1}) ≥ 0.91,

$$u(ms^{-1}) = 0.2578n + 0.001 \qquad\qquad (D:2$$

When operating to design specification, the VGU is an efficient data collector: it is theoretically possible to record a continuous lunar tidal cycle (14.75 days). In practice, however, a number of problems can beset the equipment and cause data loss. The most common cause being fouling of the impellers by algae or drift litter. Other causes include faulty connectors between current meter and logger cable, broken impellers from drift litter, operator error during download of data, and occasionally, vandalism. For these reasons, it was considered prudent to check the VGU and download the data logger as often as possible, normally every day and certainly no more than every three days.

Data downloaded from the VGU logger was in seven columns of ASCII text format giving date, time and count for each current meter. These were imported to Microsoft Excel, separated into individual tidal cycles and de-spiked by visual observation to remove the in-air values (values are logged regardless of whether the current meters are submerged or not). On completion of de-spiking, the form of the velocity profiles, depth average velocity, shear velocity, shear stress, roughness length, drag coefficient and sediment transport calculations were computed using an Excel spreadsheet macro.

Use of data obtained from the VGU is subject to certain assumptions that highlight some limitations of the VGU. Primarily, the VGU is restricted by a lack of ability to accurately record both the directional component of the tidal current, the existence of any vertical current shear, and any turbulent fluctuations. As already discussed, when the VGU is set-up it is aligned with the ebb-flood current direction as determined by prior reconnaissance survey. It is therefore assumed that the horizontal motion of the tidal current near the VGU follows a simple to-and-fro motion. Vertical current shear at high water cannot reliably be detected from analysis of the raw data simply because each pair

of current meters are recording at the same time. It has to be assumed that the entire column of water reverses flow direction at the same time.

The VGU also lacks any method of recording the depth of water above each current meter and any change in the height of each current meter above the bed due to, for example, migrating bedforms. It was necessary to check the heights of the current meters above the bed and therefore record the changing nature of the bed around the VGU mast for reasons discussed later in Section 4.6.7. A summary of the limitations of the VGU and possible remedial action is presented in Table below.

Table D-1 – VGU limitations

Limitations	Possible remedy
Deployment elevation	None, deploy as low as possible
Impeller fouling	Daily checks
Directional component	Simultaneous profiling
Vertical shear	Simultaneous profiling
Turbulent fluctuations	N/A with impeller-type current meters
Bed Height and bed forms	Daily checks
Depth of water	Pressure sensor

Appendix E – VGU Reliability

(See Section 4.6.3, *p.*87)

Table E-1 – Summary of velocity profiles at Dugmore Creek.

Total Profiles Recorded, n =	756		%	Complete+Partial
Complete	411		54.4	69%
Partial	110		14.6	
Unreliable	235		31.1	
Flood Profiles, n =	405			
Complete	238		58.8	73%
Partial	58		14.3	
Unreliable	109		26.9	
Ebb Profiles, n =	351			
Complete	173		49.3	64%
Partial	52		14.8	
Unreliable	126		35.9	

Table E-2 – Percentage r-squared values for Dugmore Creek

Cycle	Coverage	n=	R^2 values >= 0.8		
			Flood+Ebb	Flood	Ebb
Dug9501	Complete	35	91%	95%	87%
	Partial	8	75%	75%	75%
Dug9502	Complete	31	94%	100%	85%
	Partial	8	88%	80%	100%
Dug9503	Complete	31	97%	100%	92%
	Partial	7	100%	100%	75%
Dug9504	Complete	31	90%	89%	92%
	Partial	10	60%	50%	75%
Dug9505	Complete	33	94%	95%	93%
	Partial	7	71%	50%	80%
Dug9506	Complete	36	75%	83%	62%
	Partial	9	78%	80%	75%
Dug9507	Complete	32	76%	75%	76%
	Partial	4	100%	100%	0%
Dug9508	Complete	30	93%	95%	91%
	Partial	8	88%	100%	75%
Dug9509	Complete	29	93%	94%	92%
	Partial	10	80%	60%	100%
Dug9510	Complete	31	88%	94%	79%
	Partial	11	55%	100%	0%
Dug9511	Complete	29	59%	87%	37%
	Partial	10	40%	100%	0%
Dug9512	Complete	33	91%	100%	75%
	Partial	10	70%	100%	25%
Dug9513	Complete	30	80%	89%	67%
	Partial	8	50%	100%	20%
	Mean Complete		86%	92%	79%
	Mean Partial		73%	84%	54%
	Total mean		80%	88%	66%

Table E-3 – Summary of velocity profiles on Pye Sand.

Total Profiles Recorded, n =	795	%	Complete+Partial
Complete	456	57.4	74.3
Partial	135	17.0	
Unreliable	204	25.7	
Flood Profiles, n =	426		
Complete	250	58.7	76.5
Partial	76	17.8	
Unreliable	100	23.5	
Ebb Profiles, n =	369		
Complete	206	55.8	71.8
Partial	59	16.0	
Unreliable	104	28.2	

Table E-4 – Percentage r-squared values for Pye Sand.

			R^2 values >= 0.8		
Cycle	Coverage	n =	Flood+Ebb	Flood	Ebb
Pye9501	Complete	36	94%	100%	88%
	Partial	12	58%	43%	80%
Pye9502	Complete	37	89%	100%	73%
	Partial	8	75%	75%	75%
Pye9503	Complete	33	88%	89%	87%
	Partial	10	80%	80%	60%
Pye9504	Complete	36	83%	81%	87%
	Partial	8	75%	60%	100%
Pye9505	Complete	35	86%	89%	82%
	Partial	10	80%	100%	60%
Pye9506	Complete	38	89%	100%	73%
	Partial	12	50%	57%	40%
Pye9507	Complete	35	83%	82%	83%
	Partial	10	50%	60%	40%
Pye9508	Complete	33	88%	90%	85%
	Partial	11	64%	67%	60%
Pye9509	Complete	33	94%	88%	100%
	Partial	9	89%	80%	100%
Pye9510	Complete	37	95%	95%	94%
	Partial	12	58%	50%	75%
Pye9511	Complete	34	82%	94%	72%
	Partial	10	80%	80%	80%
Pye9512	Complete	39	72%	61%	88%
	Partial	11	80%	86%	67%
Pye9513	Complete	30	87%	87%	87%
	Partial	12	67%	83%	50%
	Mean Complete		87%	89%	84%
	Mean Partial		70%	71%	68%
	Total mean		78%	80%	76%

Table E-5 – Spring profile coverage and r-squared values for the Inner Swatch.

Swatch 94422 Total Profiles Recorded, n =	46	%	Complete+ Partial (%)
Complete	22	47.8	60.9
Partial	6	13.0	
Unreliable	18	39.1	
Flood Profiles, n =	23		
Complete	12	52.2	69.6
Partial	4	17.4	
Unreliable	7	30.4	
Ebb Profiles, n =	23		
Complete	10	43.5	52.2
Partial	2	8.7	
Unreliable	11	47.8	

	$R^2 >= 0.8$		
	Ebb+Flood	Flood	Ebb
Swatch 9422			
Complete	64%	75%	50%
Partial	33%	25%	50%
Complete+Partial	57%	65%	45%

Table E-6 – Neap profile coverage and r-squared values for the Inner Swatch

Swatch 9401 Total Profiles Recorded, n =	49	%	Complete+ Partial (%)
Complete	27	55.1	67.3
Partial	6	12.2	
Unreliable	16	32.7	
Flood Profiles, n =	27		
Complete	6	22.2	59.3
Partial	10	37.0	
Unreliable	11	40.7	
Ebb Profiles, n =	7		
Complete	6	85.7	85.7
Partial	0	0.0	
Unreliable	1	14.3	

	$R^2 >= 0.8$		
	Ebb+Flood	Flood	Ebb
Swatch 9401			
Complete	63%	75%	45%
Partial	17%	17%	0%
Complete+Partial	56%	62%	45%

Appendix F – Suspended Sediment Calibration Curves
(See Section 5.5.2, p.133)

Hamford Water - Transmissometer Calibration
Spring Ebb Tide

Hamford Water - Transmissometer Calibration
Neap Flood Tide
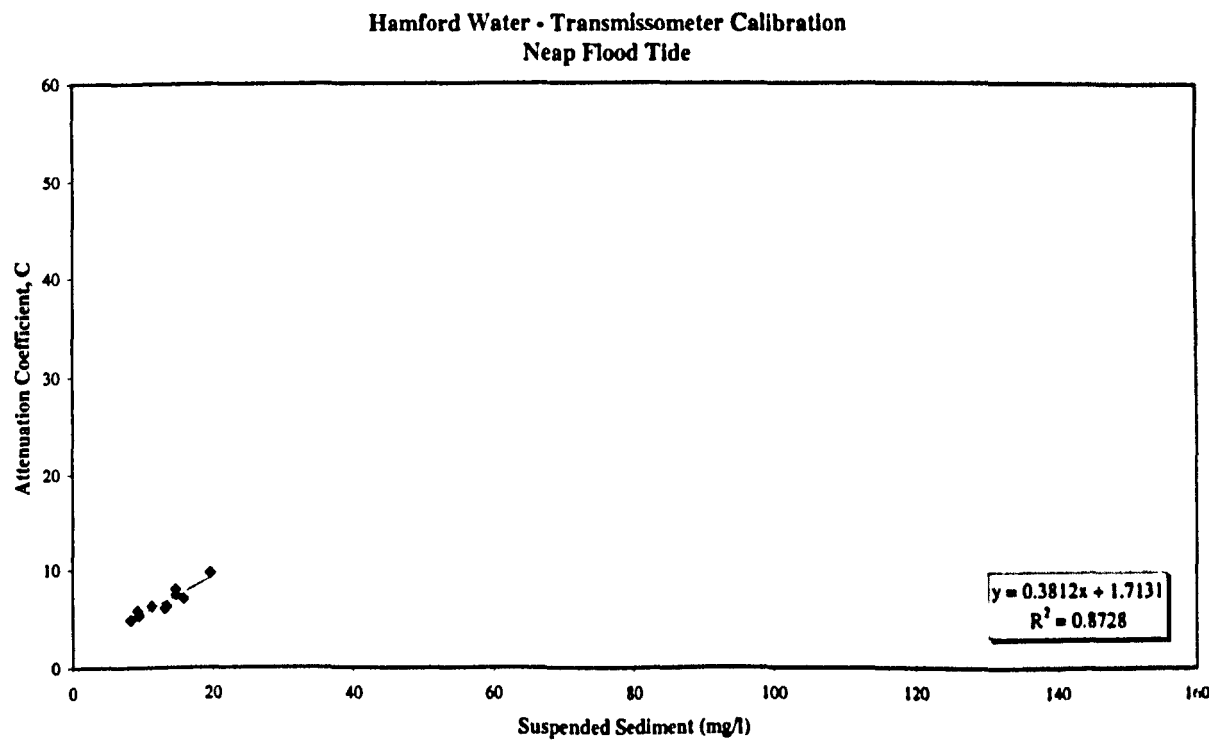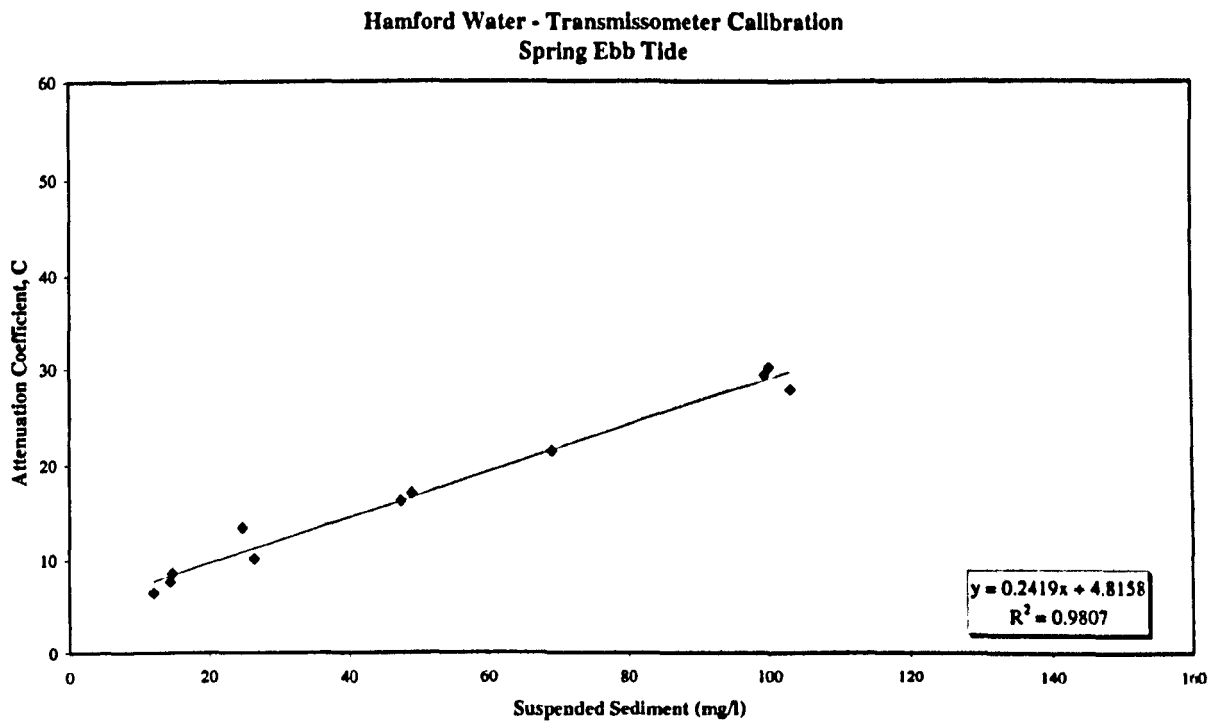
Hamford Water - Transmissometer Calibration
Neap Ebb Tide

$y = 0.3014x + 3.2185$
$R^2 = 0.7536$
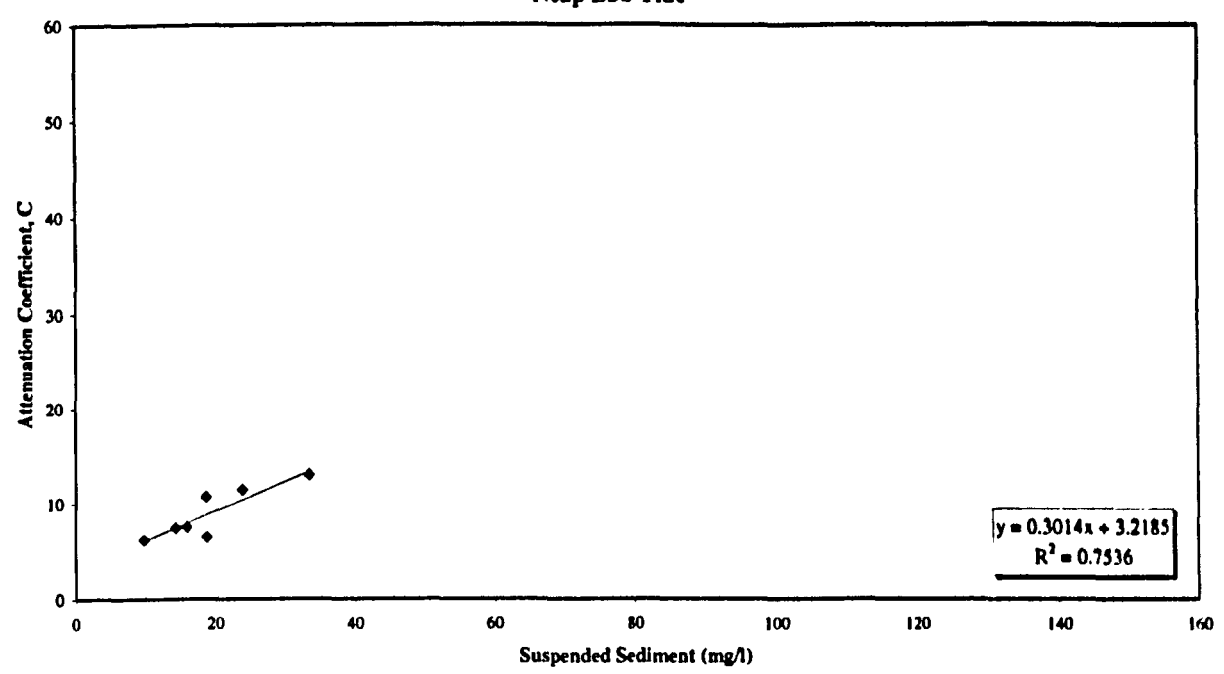
Hamford Water - Transmissometer Calibration
Spatial Spring High Water (Summer)

$y = 0.2565x + 11.228$
$R^2 = 0.935$
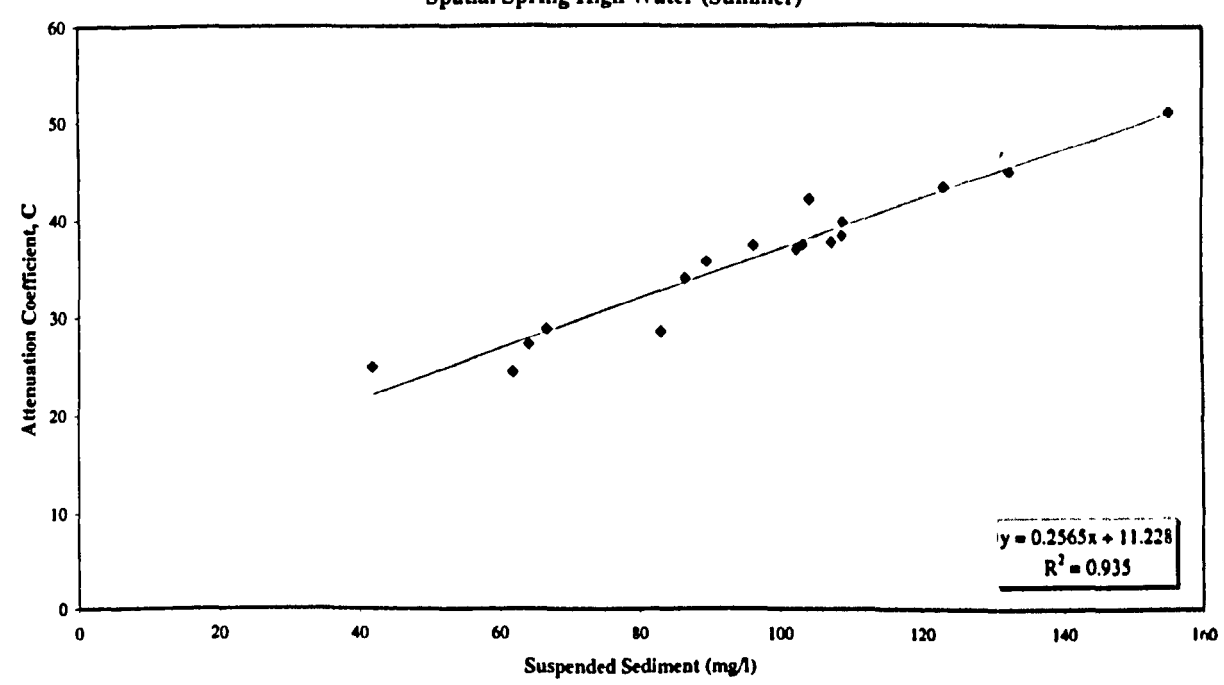
Hamford Water - Transmissometer Calibration
Spatial Neap High Water (Summer)

$y = 0.3741x + 2.3627$
$R^2 = 0.5627$
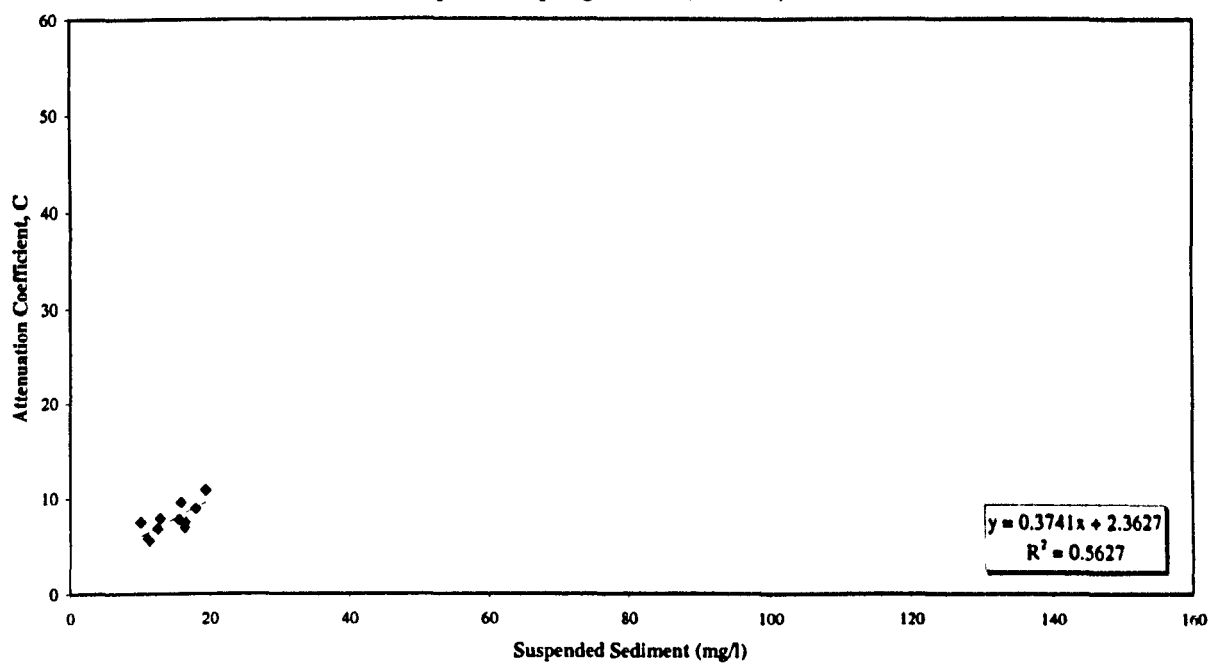
Hamford Water - Transmissometer Calibration
Spring Flood Tide

$y = 0.455x + 0.0009$
$R^2 = 0.9571$
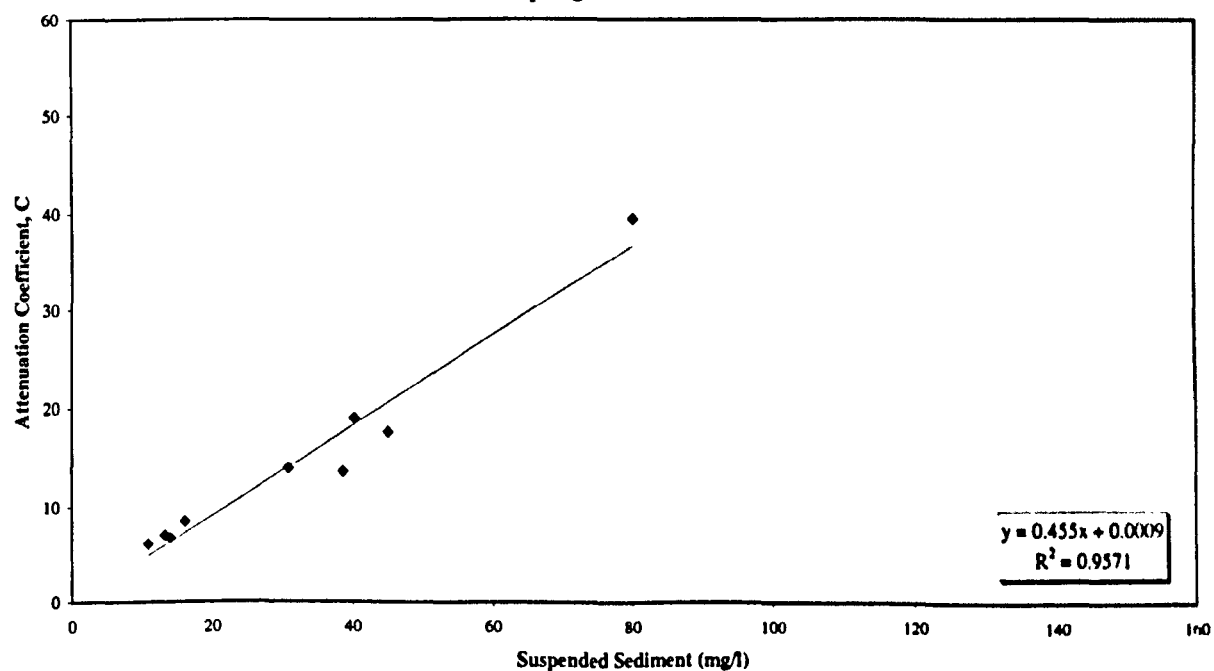
Appendix G – Depth averaged velocity versus U_{100}

(See Section 6.3.1, p.153)
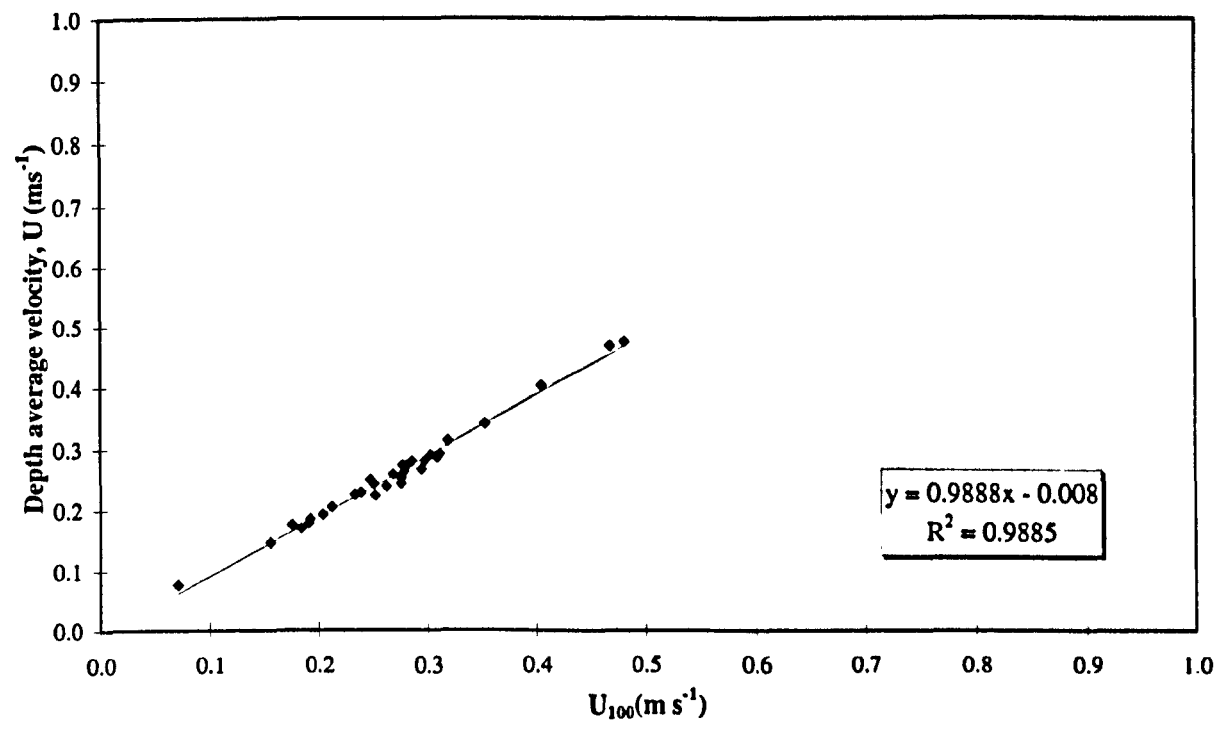
Figure G-1 – $\overline{u}$ versus u_{100} at Station 1, Springs.
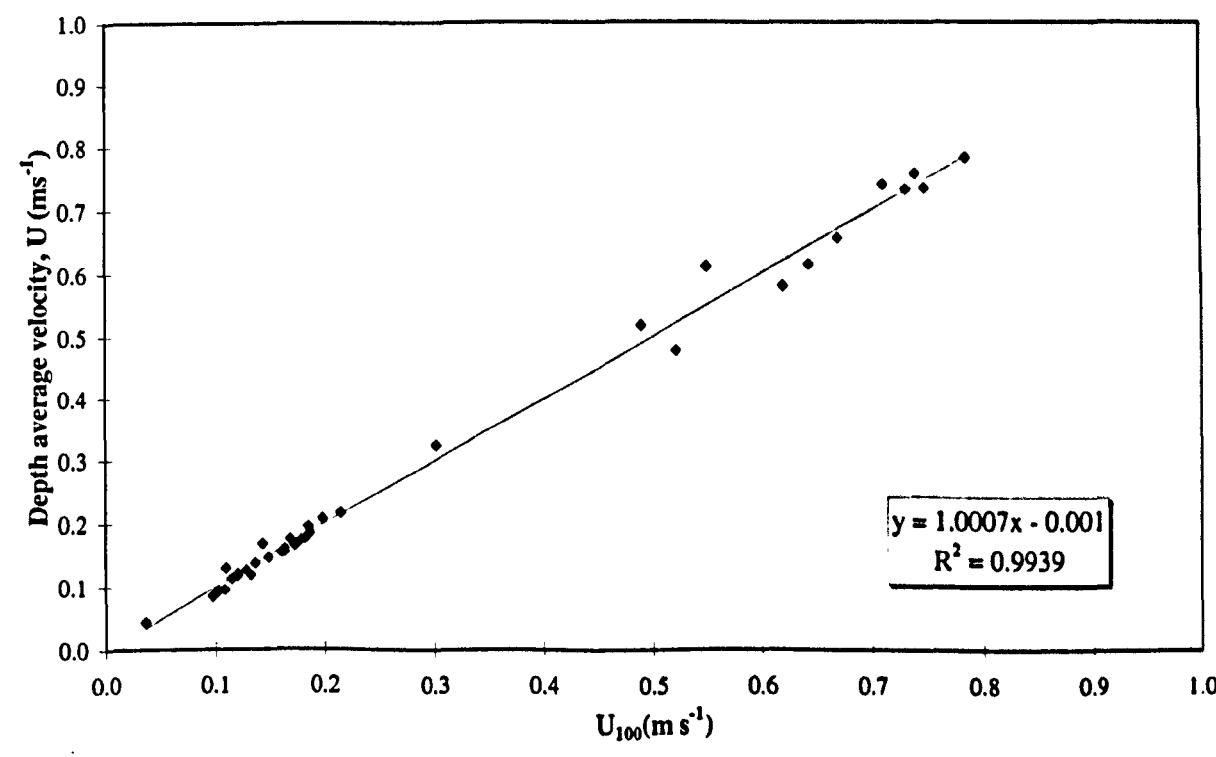
Figure G-2 – $\overline{u}$ versus u_{100} at Station 3, Springs.
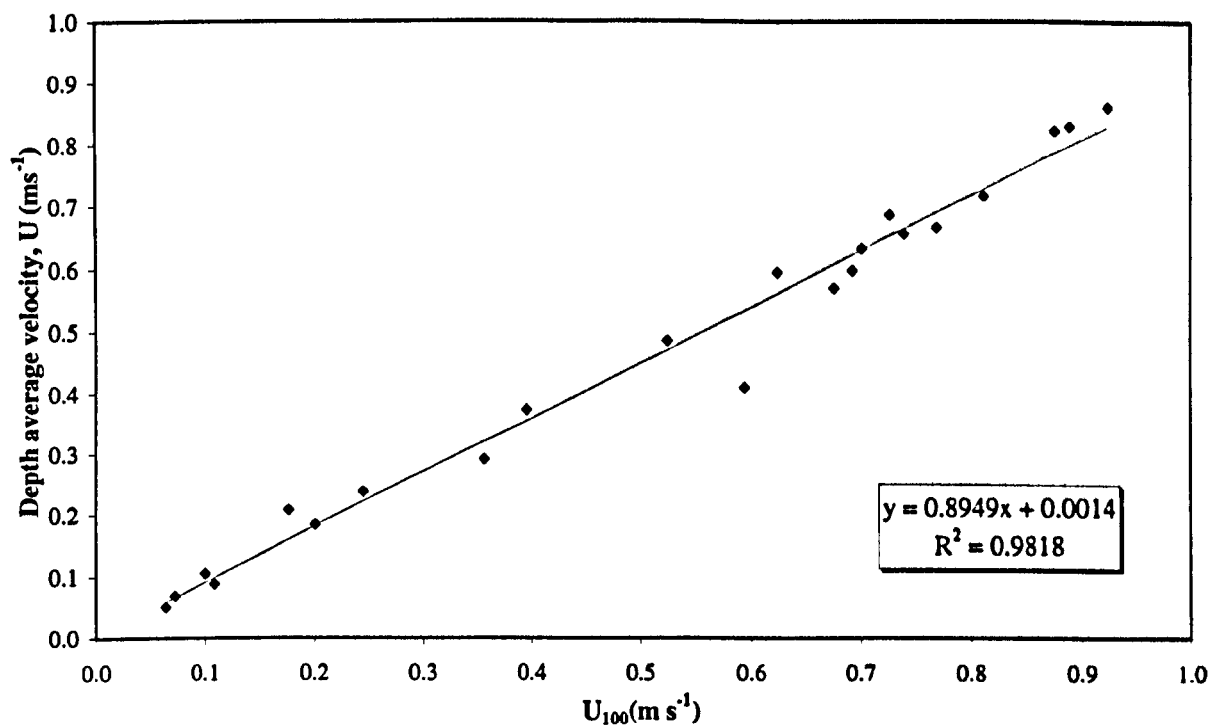
Figure G-3 – $\bar{\bar{u}}$ **versus** u_{100} **at Station 5, Springs.**
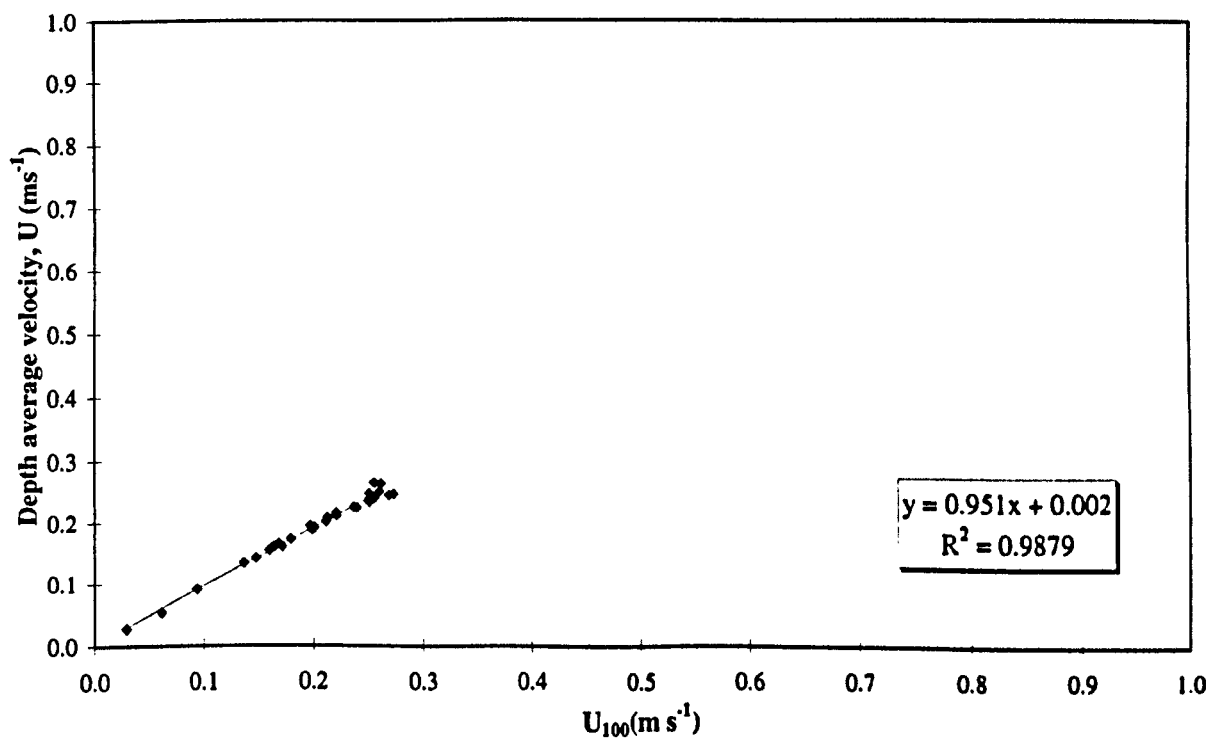
Figure G-4 – $\bar{\bar{u}}$ **versus** u_{100} **at Station 1, Neaps.**
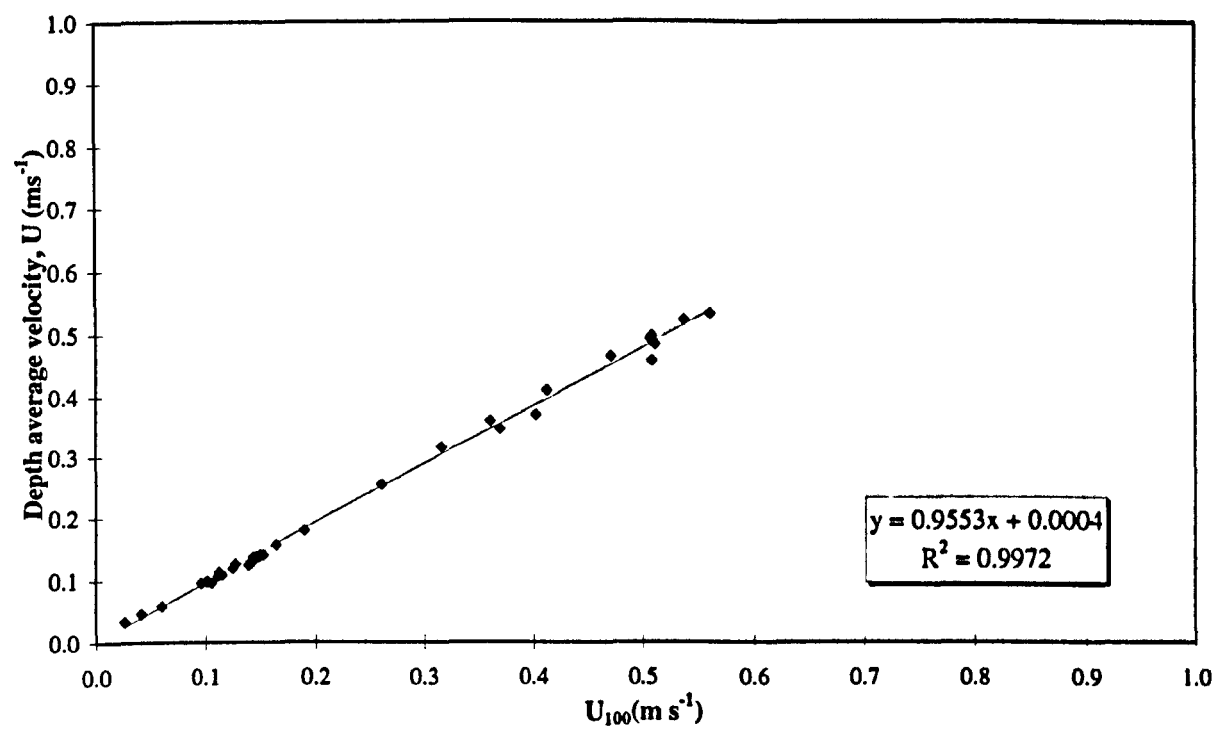
Figure G-5 – $\bar{\bar{u}}$ versus u_{100} at Station 3, Neaps.

The chart shows the regression equation:

$$y = 0.9553x + 0.0004$$
$$R^2 = 0.9972$$
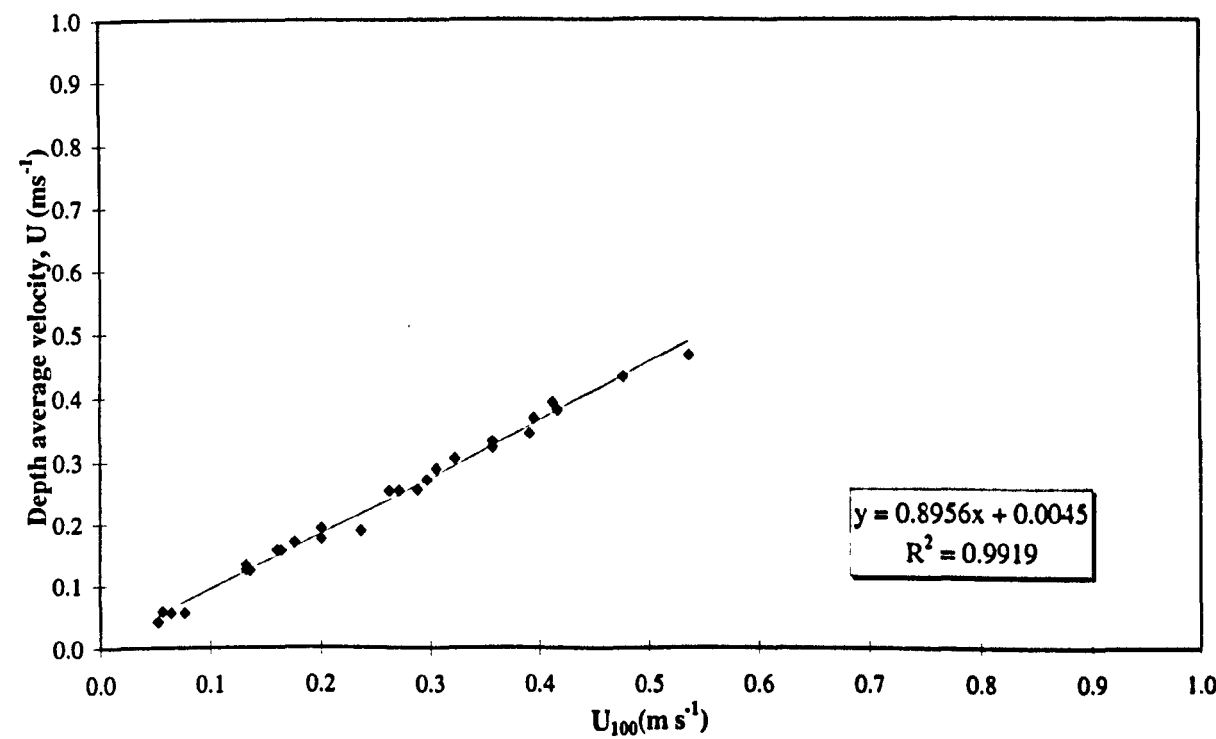
Figure G-6 – $\bar{\bar{u}}$ versus u_{100} at Station 5, Neaps.

The chart shows the regression equation:

$$y = 0.8956x + 0.0045$$
$$R^2 = 0.9919$$

Appendix H – Water and Sediment Flux Data

(See Section 6.2, p.148)

Date:Time	t=	Stn. No.	Tide (m)	Predicted Volume (m³)	Vol diff. (m³)	Inlet Area (m²)	U (ms⁻¹)	Water Vol (m³ s⁻¹)	Susp. Sed. conc. (g l⁻¹)	Susp. Sed. Flux (kg)	Water Flux (kg)
16/06/96 08:30	0	1	0.58	3838989		8.5	0	0.0	0.00	0	0
		2				741.5	0.06175	82417.7	0.00	0	82417725
		3				55	0	0.0	0.00	0	0
		4				152	0.049	13406.4	0.00	0	13406400
16/06/96 09:00	1	1	0.72	4065920	226931.8	8.5	0	0.0	0.00	0	0
		2				741.5	0.40375	538885.1	6.85	3691	538885125
		3				55	0	0.0	0.00	0	0
		4				152	0.073	19972.8	1.21	24	19972800
16/06/96 09:30	2	1	1.01	4656022	590101.6	21	0.00875	330.8	0.00	0	330750
		2				786.5	0.55813	790144.6	12.99	10264	790144641
		3				103	0.25	46350.0	0.00	0	46350000
		4				190	0.115	39330.0	1.61	63	39330000
16/06/96 10:00	3	1	1.41	5566911	910888.8	51	0.1518	13935.2	0.01	0	13935240
		2				854	0.58164	894097.0	18.59	16621	894097008
		3				173.5	0.179	55901.7	0.89	50	55901700
		4				247	0.153	68023.8	5.04	343	68023800
16/06/96 10:30	4	1	1.81	6854058	1287147.0	125.5	0.2153	48636.3	0.22	11	48636270
		2				944	0.4955	841953.6	26.85	22606	841953600
		3				267.5	0.0744	35823.6	2.04	73	35823600
		4				323	0.116	67442.4	3.73	252	67442400
16/06/96 11:00	5	1	2.15	8323350	1469292.3	238	0.2077	88978.7	10.01	891	88978680
		2				1034	0.47683	887476.0	21.62	19187	887475996
		3				361.5	0.0842	54788.9	1.51	83	54788940
		4				399	0.181	129994.2	7.76	1009	129994200
16/06/96 11:30	6	1	2.42	9774169	1450818.5	352.5	0.1987	126075.2	7.37	929	126075150
		2				1102	0.38181	757358.3	18.56	14057	757358316
		3				432	0.0939	73016.6	1.48	108	73016640
		4				456	0.215	176472.0	10.02	1768	176472000
16/06/96 12:00	7	1	2.66	11231263	1457094.2	444.5	0.2577	206185.8	13.00	2680	206185770
		2				1169	0.44331	932812.9	25.90	24160	932812902
		3				502.5	0.1674	151413.3	5.19	786	151413300
		4				513	0.303	279790.2	15.54	4348	279790200
16/06/96 12:30	8	1	2.93	12964700	1733437.3	659	0.3034	359893.1	15.11	5438	359893080
		2				1259	0.46675	1057748.9	22.98	24307	1057748850
		3				596.5	0.1758	188756.5	9.64	1820	188756460
		4				589	0.328	347745.6	15.54	5404	347745600
16/06/96 13:00	9	1	3.25	15149910	2185210.2	909.5	0.2662	435796.0	13.17	5739	435796020
		2				1349	0.42739	1037788.4	17.57	18234	1037788398
		3				690.5	0.1615	200728.4	10.43	2094	200728350
		4				665	0.295	353115.0	11.19	3951	353115000
16/06/96 13:30	10	1	3.63	17852325	2702415.2	1178	0.2084	441891.4	9.31	4114	441891360
		2				1439	0.32167	833189.6	11.10	9248	833189634
		3				784.5	0.1371	193598.9	7.13	1380	193598910
		4				741	0.269	358792.2	9.21	3304	358792200
16/06/96 14:00	11	1	3.97	20380395	2528069.3	1527	0.1723	473583.8	9.31	4409	473583780
		2				1552	0.23228	648897.4	6.60	4283	648897408
		3				902	0.1125	182655.0	5.23	955	182655000
		4				836	0.229	344599.2	8.40	2895	344599200
16/06/96 14:30	12	1	4.18	21408000	1027605.1	1743	0.276	865922.4	9.37	8114	865922400
		2				1619	0.26278	765793.5	7.19	5506	765793476
		3				972.5	0.2069	362178.5	7.88	2854	362178450
		4				893	0.319	512760.6	8.40	4307	512760000

Hamford Water Tidal Flux Calculations - Spring Ebb											
Date:Time	t=	Stn. No.	Tide (m)	Predicted Volume (m³)	Vol diff. (m³)	Inlet Area (m²)	U (ms⁻¹)	Water Vol (m³ s⁻¹)	Susp. Sed conc. (g l⁻¹)	Susp. Sed. Flux (kg)	Water Flux (kg)
16/06/96 15:00	13	1	4.18	21408000	0.0	1816	-0.1783	-582827.0	5.66	-3299	-582827040
		2				1642	-0.2174	-642547.4	5.27	-3386	-642547440
		3				996	-0.11	-197208.0	5.42	-1069	-197208000
		4				912	-0.216	-354585.6	7.37	-2613	-354585600
16/06/96 15:30	14	1	3.94	20157330	-1250670.1	1670	-0.3441	-1034364.6	13.48	-13943	-1034364600
		2				1597	-0.26655	-766224.6	4.83	-3701	-766224630
		3				949	-0.2887	-493157.3	11.80	-5819	-493157340
		4				874	-0.361	-567925.2	9.68	-5498	-567925200
16/06/96 16:00	15	1	3.51	16960066	-3197264.1	1317	-0.4063	-963174.8	67.97	-65467	-963174780
		2				1484	-0.760778	-2032190.2	87.32	-177451	-2032190194
		3				831.5	-0.7451	-1115191.2	34.48	-38452	-1115191170
		4				779	-0.711	-996964.2	29.13	-29042	-996964200
16/06/96 16:30	16	1	3	13414110	-3545956.0	909.5	-0.2469	-404200.0	24.62	-9951	-404199990
		2				1349	-0.825889	-2005423.7	111.19	-222983	-2005423670
		3				690.5	-0.7382	-917508.8	45.61	-41848	-917508780
		4				665	-0.726	-869022.0	67.63	-58772	-869022000
16/06/96 17:00	17	1	2.49	10150307	-3263803.0	547	-0.2329	-229313.3	8.40	-1926	-229313340
		2				1214	-0.7385	-1613770.2	70.25	-113367	-1613770200
		3				549.5	-0.6213	-614527.8	10.22	-6280	-614527830
		4				551	-0.594	-589129.2	40.19	-23677	-589129200
16/06/96 17:30	18	1	2.07	7893478	-2256828.8	352.5	-0.1101	-69858.5	7.58	-530	-69858450
		2				1102	-0.556563	-1103998.4	34.73	-38342	-1103998367
		3				432	-0.3277	-254819.5	15.00	-3822	-254819520
		4				456	-0.396	-325036.8	18.49	-6010	-325036800
16/06/96 18:00	19	1	1.73	6574781	-1318696.8	205.5	-0.0599	-22157.0	3.46	-77	-22157010
		2				1012	-0.394571	-718750.5	13.18	-9473	-718750534
		3				338	-0.148	-90043.2	2.51	-226	-90043200
		4				380	-0.264	-180576.0	5.37	-970	-180576000
16/06/96 18:30	20	1	1.45	5658000	-916781.4	125.5	-0.0498	-11249.8	1.21	-14	-11249820
		2				944	-0.340143	-577971.0	11.14	-6439	-577970986
		3				267.5	-0.1491	-71791.7	3.79	-272	-71791650
		4				323	-0.25	-145350.0	3.18	-462	-145350000
16/06/96 19:00	21	1	1.19	5065922	-592077.7	83.5	-0.00535	-804.1	0.00	0	-804105
		2				899	-0.444143	-718712.2	9.73	-6993	-718712203
		3				220.5	-0.0853	-33855.6	0.00	0	-33855570
		4				285	-0.193	-99009.0	2.66	-263	-99009000
16/06/96 19:30	22	1	0.91	4463051	-602871.0	66	0	0.0	0.00	0	0
		2				876.5	-0.450583	-710884.8	9.13	-6490	-710884799
		3				197	0	0.0	0.00	0	0
		4				266	-0.072	-34473.6	0.65	-22	-34473600
16/06/96 20:00	23	1	0.65	3971365	-491685.5	14	0	0.0	0.00	0	0
		2				764	-0.457083	-628580.5	5.22	-3281	-628580542
		3				79.5	0	0.0	0.00	0	0
		4				171	-0.057	-17544.6	0.32	-6	-17544600
16/06/96 20:30	24	1	0.48	3657921	-313444.3	2	0	0.0	0.00	0	0
		2				696.5	-0.367917	-461257.5	0.00	0	-461257543
		3				36	0	0.0	0.00	0	0
		4				114	-0.368	-75513.6	0.00	0	-75513600

Hamford Water Tidal Flux Calculations - Neap Flood

Date:Time	t=	Stn. No.	Tide (m)	Predicted Volume (m³)	Vol diff. (m³)	Inlet Area (m²)	U (ms⁻¹)	Water Vol (m³ s⁻¹)	Susp. Sed conc. (g l⁻¹)	Susp. Sed. Flux (kg)	Water Flux (kg)
20/06/95 12:00	0	1	1.46	2737562		83.5	0	0	0	0	0
		2				899	0.061	98710.2	0.63	62.187426	98710200
		3				220.5	0	0	0	0	0
		4				285	0.07375	37833.75	0.67	25.3486125	37833750
20/06/95 12:30	1	1	1.57	3073018	335455.94	103	0	0	1.23	0	0
		2				921.5	0.16083	266768.721	1.66	442.836077	266768721
		3				244	0.08	35136	1.56	54.81216	35136000
		4				304	0.1275	69768	1.24	86.51232	69768000
20/06/95 13:00	2	1	1.77	3771210	698191.6	125.5	0.05	11295	6.77	76.46715	11295000
		2				944	0.29293	497746.656	4.21	2095.51342	497746656
		3				267.5	0.1429	68806.35	2.06	141.741081	68806350
		4				323	0.16625	96657.75	1.48	143.05347	96657750
20/06/95 13:30	3	1	2.02	4681598	910388.38	150.5	0.12	32508	4.78	155.38824	32508000
		2				966.5	0.35958	625561.326	7.53	4710.47678	625561326
		3				291	0.1257	65841.66	2.24	147.485318	65841660
		4				342	0.16	98496	1.85	182.2176	98496000
20/06/95 14:00	4	1	2.27	6024949	1343350.5	205.5	0.1214	44905.86	4.61	207.016015	44905860
		2				1011.5	0.37883	689735.781	7.14	4924.71348	689735781
		3				338	0.0454	27621.36	0.22	6.0766992	27621360
		4				380	0.202	138168	2.5	345.42	138168000
20/06/95 14:30	5	1	2.51	7325032	1300083.8	396.5	0.0178	12703.86	2.97	37.7304642	12703860
		2				1124	0.31717	641698.344	4.99	3202.07474	641698344
		3				455.5	0.0622	50997.78	1.1	56.097558	50997780
		4				475	0.23167	198077.85	4.18	827.965413	198077850
20/06/95 15:00	6	1	2.73	8737463	1412430.4	441.5	0.1934	153694.98	3.91	600.947372	153694980
		2				1146.5	0.30208	623402.496	4.6	2867.65148	623402496
		3				479	0.0952	82081.44	1.84	151.02985	82081440
		4				494	0.23583	209700.036	3.79	794.763136	209700036
20/06/95 15:30	7	1	2.95	10149893	1412430.4	494.5	0.2421	215493.21	5.81	1252.01555	215493210
		2				1191.5	0.32808	703633.176	4.98	3504.09322	703633176
		3				526	0.141	133498.8	1.68	224.277984	133498800
		4				532	0.27667	264939.192	3.68	974.976227	264939192
20/06/95 16:00	8	1	3.19	11790108	1640215.3	601.5	0.2374	257032.98	5.91	1519.06491	257032980
		2				1236.5	0.33558	746900.406	5.47	4085.54522	746900406
		3				573	0.1405	144911.7	1.69	244.900773	144911700
		4				570	0.30167	309513.42	3.72	1151.38992	309513420
20/06/95 16:30	9	1	3.43	13456477	1666368.5	722	0.1991	258750.36	7.85	2031.19033	258750360
		2				1304	0.29733	697892.976	5	3489.46488	697892976
		3				643.5	0.2165	250771.95	2.13	534.144254	250771950
		4				627	0.275	310365	3.83	1188.69795	310365000
20/06/95 17:00	10	1	3.67	15206536	1750058.8	909.5	0.1722	281908.62	4.07	1147.36808	281908620
		2				1349	0.26957	654569.874	4.53	2965.20153	654569874
		3				690.5	0.1086	134978.94	1.35	182.221569	134978940
		4				665	0.25143	300961.71	3.94	1185.78914	300961710
20/06/95 17:30	11	1	3.87	16693635	1487099.6	1108	0.1608	320699.52	2.81	901.165651	320699520
		2				1394	0.1735	435346.2	2.5	1088.3655	435346200
		3				737.5	0.1085	144033.75	1.47	211.729613	144033750
		4				703	0.22286	282007.044	3.05	860.121484	282007044
20/06/95 18:00	12	1	3.97	17437185	743549.8	1176.5	0.1338	283348.26	2.26	640.367068	283348260
		2				1416.5	0.17342	442168.974	2.27	1003.72357	442168974
		3				761	0.0589	80681.22	0.7	56.476854	80681220
		4				722	0.21286	276632.856	2.45	677.750497	276632856

Date:Time	t=	Stn. No.	Tide (m)	Predicted Volume (m³)	Vol diff. (m³)	Inlet Area (m²)	U (ms⁻¹)	Water Vol (m³ s⁻¹)	Susp. Sed conc. (g l⁻¹)	Susp. Sed. Flux (kg)	Water Flux (kg)

Hamford Water Tidal Flux Calculations - Neap Ebb

Date:Time	t=	Stn. No.	Tide (m)	Predicted Volume (m³)	Vol diff. (m³)	Inlet Area (m²)	U (ms⁻¹)	Water Vol (m³ s⁻¹)	Susp. Sed conc. (g l⁻¹)	Susp. Sed. Flux (kg)	Water Flux (kg)
21/06/95 07:00	13	1	3.92	17065410	-371774.9	1108	-0.375	-747900	0.86	-643.194	-747900000
		2				1394	-0.120917	-303404.94	2.29	-694.7973	-303404936
		3				737.5	-0.0409	-54294.75	0.8	-43.4358	-54294750
		4				703	-0.106875	-135239.63	1.65	-223.14538	-135239625
21/06/95 07:30	14	1	3.85	16544925	-520484.86	975.5	-0.2045	-359081.55	4.91	-1763.0904	-359081550
		2				1371.5	-0.109667	-270734.92	5.21	-1410.5289	-270734923
		3				714	-0.0881	-113226.12	4.39	-497.06267	-113226120
		4				684	-0.336875	-414760.5	4.87	-2019.8836	-414760500
21/06/95 08:00	15	1	3.66	15132181	-1412744.6	844.5	-0.1697	-257960.97	4.67	-1204.6777	-257960970
		2				1326.5	-0.290429	-693457.32	6.89	-4777.921	-693457323
		3				667	-0.2654	-318639.24	5.64	-1797.1253	-318639240
		4				646	-0.395714	-460136.24	7.19	-3308.3796	-460136239
21/06/95 08:30	16	1	3.38	13109317	-2022863.9	719	-0.119	-154009.8	4.17	-642.22087	-154009800
		2				1281.5	-0.303333	-699698.23	11.02	-7710.6745	-699698231
		3				620	-0.3217	-359017.2	6.14	-2204.3656	-359017200
		4				608	-0.369286	-404146.6	6.42	-2594.6212	-404146598
21/06/95 09:00	17	1	3.06	10887492	-2221824.6	601.5	-0.1413	-152985.51	4.17	-637.94958	-152985510
		2				1236.5	-0.3675	-817944.75	13.11	-10723.256	-817944750
		3				573	-0.3453	-356142.42	5.59	-1990.8361	-356142420
		4				570	-0.410714	-421392.56	9.3	-3918.9508	-421392564
21/06/95 09:30	18	1	2.74	8801664	-2085828	444.5	-0.0556	-44485.56	2.96	-131.67726	-44485560
		2				1169	-0.313417	-659492.05	7.56	-4985.7599	-659492051
		3				502.5	-0.3785	-342353.25	2.48	-849.03606	-342353250
		4				513	-0.375	-346275	6.89	-2385.8348	-346275000
21/06/95 10:00	19	1	2.45	6992161	-1809503.2	396.5	-0.055	-39253.5	3.16	-124.04106	-39253500
		2				1124	-0.187583	-379517.93	7.76	-2945.0591	-379517926
		3				455.5	-0.2495	-204565.05	2.24	-458.22571	-204565050
		4				475	-0.347143	-296807.27	6.89	-2045.0021	-296807265
21/06/95 10:30	20	1	2.2	5648810	-1343350.5	310	-0.0267	-14898.6	2.11	-31.436046	-14898600
		2				1079	-0.118	-229179.6	3.89	-891.50864	-229179600
		3				408.5	-0.153	-112500.9	2.87	-322.87758	-112500900
		4				437	-0.304167	-239257.76	3.75	-897.21661	-239257762
21/06/95 11:00	21	1	1.98	4504311	-1144499.6	238	-0.0463	-19834.92	0.27	-5.3554284	-19834920
		2				1034	-0.140375	-261265.95	4.79	-1251.4639	-261265950
		3				361.5	-0.2313	-150506.91	1.7	-255.86175	-150506910
		4				399	-0.234	-168058.8	2.95	-495.77346	-168058800
21/06/95 11:30	22	1	1.8	3875938	-628372.44	176	-0.05	-15840	6.38	-101.0592	-15840000
		2				989	-0.1065	-189591.3	2.98	-564.98207	-189591300
		3				314.5	-0.0988	-55930.68	1.54	-86.133247	-55930680
		4				361	-0.16375	-106404.75	1.92	-204.29712	-106404750
21/06/95 12:00	23	1	1.67	3422114	-453824.54	150.5	0	0	0.36	0	0
		2				966.5	-0.131875	-229422.94	2.77	-635.50154	-229422938
		3				291	-0.0579	-30328.02	0.85	-25.778817	-30328020
		4				342	-0.1	-61560	0.71	-43.7076	-61560000

Appendix I – Sediment Transport Data

(See Section 0)

Tidal Cycle	Sediment transport rates (kg m⁻¹) using method of Engelhund and Hansen (1967)												Tidal Range (m)
	Station 1			Station 3			Station 5			Totals			
	Flood	Ebb	Net	Flood	Ebb	Net	Flood	Ebb	Net	Flood	Ebb	Net Total	
1							-242.46	24.94	-217.52	-242.46	24.94	-435.04	2.3
2							-39.17	50.03	10.86	-39.17	50.03	21.72	2.6
3							-312.68	38.32	-274.36	-312.68	38.32	-548.72	2.3
4		No Data					-24.65	339.91	315.26	-24.65	339.91	630.52	2.7
5							-348.41	58.15	-290.27	-348.41	58.15	-580.53	2.5
6							-18.94	144.80	125.86	-18.94	144.80	251.71	3.0
7							-460.18	438.56	-21.62	-460.18	438.56	-43.24	2.8
8							-168.73	248.43	79.70	-168.73	248.43	159.40	3.3
9							-1041.74	187.85	-853.88	-1041.74	187.85	-1707.77	3.2
10							-525.74	485.67	-40.08	-525.74	485.67	-80.16	3.6
11							-4932.05	7995.39	3063.34	-4932.05	7995.39	6126.69	3.5
12	-2941.25	1745.74	-1195.52	-309.41	23824.93	23515.52	-1438.85	310.95	-1127.90	-1748.25	24135.88	43579.73	3.9
13	-842.57	884.28	41.71	-89.65	13663.49	13573.84	-3503.34	250.25	-3253.09	-3592.99	13913.74	20683.21	3.9
14	-3313.14	534.63	-2778.51	-243.45	13747.79	13504.35	-6253.85	183.14	-6070.71	-6497.30	13930.94	12088.76	3.8
15	-934.35	367.24	-567.12	-38.55	15491.97	15453.42	-8990.15	428.02	-8562.14	-9028.71	15919.99	13215.44	3.8
16	-2526.35	470.14	-2056.22	-255.69	9969.78	9714.09	-17026.43	1035.90	-15990.53	-17282.12	11005.68	-14609.10	3.7
17	-527.28	200.34	-326.94	-45.20	11291.79	11246.59	-6108.58	5584.13	-524.45	-6153.78	16875.92	21117.33	3.7
18	-1275.55	127.49	-1148.06	-103.43	3435.35	3331.92	-21934.99	2860.82	-19074.18	-22038.43	6296.17	-32632.57	3.5
19	-456.64	167.75	-288.89	-20.36	3502.99	3482.63	-7589.48	749.93	-6839.56	-7609.85	4252.92	-7002.74	3.6
20	-987.58	88.26	-899.32	-66.18	1466.95	1400.77	-47095.60	878.56	-46217.04	-47161.78	2345.51	-90531.86	3.2
21	-167.58	108.37	-59.21	-9.78	3355.79	3346.01	-1122.42	400.92	-721.51	-1132.20	3756.70	5189.79	3.3
22	-320.14	18.38	-301.76	-69.62	1285.43	1215.81	-19302.99	379.69	-18923.30	-19372.61	1665.13	-35716.73	2.9
23	-113.51	42.87	-70.64	-8.35	2569.32	2560.97	-4223.68	431.14	-3792.54	-4232.02	3000.46	-2533.78	3.2
24	-385.68	60.26	-325.42	-92.20	825.12	732.92	-3152.45	417.94	-2734.52	-3244.65	1243.06	-4328.61	2.8

Tidal Cycle	Sediment transport rates (kg m⁻¹) using method of Hardisty (1983)												Tidal Range (m)
	Station 1			Station 3			Station 5			Totals			
	Flood	Ebb	Net	Flood	Ebb	Net	Flood	Ebb	Net	Flood	Ebb	Net Total	
1							0.00	42.63	42.63	0.00	42.63	85.26	2.3
2							0.00	0.00	0.00	0.00	0.00	0.00	2.6
3							0.00	0.00	0.00	0.00	0.00	0.00	2.3
4		No Data					0.00	13.25	13.25	0.00	13.25	26.49	2.7
5							0.00	9.20	9.20	0.00	9.20	18.39	2.5
6							0.00	18.41	18.41	0.00	18.41	36.83	3.0
7							-5.37	59.84	54.47	-5.37	59.84	108.94	2.8
8							0.00	187.62	187.62	0.00	187.62	375.24	3.3
9							-41.57	164.79	123.22	-41.57	164.79	246.44	3.2
10							-9.20	176.26	167.06	-9.20	176.26	334.12	3.6
11							-46.33	255.31	208.97	-46.33	255.31	417.95	3.5
12	0.00	22.82	22.82	0.00	1463.33	1463.33	-47.57	327.71	280.14	-47.57	1813.86	3532.58	3.9
13	0.00	22.89	22.89	0.00	1024.88	1024.88	-92.91	445.58	352.68	-92.91	1493.35	2800.89	3.9
14	0.00	2.67	2.67	0.00	919.38	919.38	-728.92	158.70	-570.22	-728.92	1080.76	703.67	3.8
15	0.00	2.67	2.67	0.00	629.45	629.45	-516.79	374.79	-142.00	-516.79	1006.91	980.25	3.8
16	0.00	0.00	0.00	0.00	688.79	688.79	-1029.17	307.54	-721.63	-1029.17	996.33	-65.68	3.7
17	0.00	0.00	0.00	0.00	739.36	739.36	-254.24	738.31	484.07	-254.24	1477.67	2446.87	3.7
18	0.00	0.00	0.00	0.00	229.63	229.63	-873.25	100.29	-772.96	-873.25	329.92	-1086.66	3.5
19	0.00	0.00	0.00	0.00	246.33	246.33	-390.36	639.78	249.42	-390.36	886.11	991.49	3.6
20	0.00	0.00	0.00	0.00	3.43	3.43	-1909.93	278.86	-1631.07	-1909.93	282.29	-3255.28	3.2
21	0.00	0.00	0.00	0.00	164.52	164.52	-5.63	254.61	248.97	-5.63	419.13	826.99	3.3
22	0.00	0.00	0.00	0.00	0.00	0.00	-1429.12	496.25	-932.87	-1429.12	496.25	-1865.74	2.9
23	0.00	0.00	0.00	0.00	4.11	4.11	-186.59	89.43	-97.16	-186.59	93.55	-186.09	3.2
24	0.00	0.00	0.00	0.00	0.00	0.00	-334.88	3.72	-331.16	-334.88	3.72	-662.32	2.8

Tidal Cycle	Sediment transport rates (kg m⁻¹) using method of Jago and Mahammod (1999)												Tidal Range (m)
	Station 1			Station 3			Station 5			Totals			
	Flood	Ebb	Net	Flood	Ebb	Net	Flood	Ebb	Net	Flood	Ebb	Net Total	
1							-9.67	34.26	24.60	-9.67	34.26	49.19	2.3
2							-0.08	11.22	11.15	-0.08	11.22	22.29	2.6
3							-8.14	4.80	-3.33	-8.14	4.80	-6.67	2.3
4							0.00	27.42	27.42	0.00	27.42	54.84	2.7
5				No Data			-9.51	18.01	8.50	-9.51	18.01	17.00	2.5
6							-0.32	28.36	28.04	-0.32	28.36	56.09	3.0
7							-22.07	45.79	23.72	-22.07	45.79	47.43	2.8
8							-5.19	129.17	123.97	-5.19	129.17	247.95	3.3
9							-50.66	111.21	60.55	-50.66	111.21	121.10	3.2
10							-24.40	118.80	94.40	-24.40	118.80	188.80	3.6
11							-61.59	171.14	109.55	-61.59	171.14	219.10	3.5
12	-13.73	23.40	9.67	-0.33	1165.90	1165.57	-55.56	244.53	188.97	-69.62	1433.83	2742.15	3.9
13	-1.95	22.57	20.62	0.00	774.56	774.56	-90.12	352.87	262.76	-92.07	1150.00	2117.81	3.9
14	-23.19	11.90	-11.29	-0.34	670.83	670.49	-519.67	119.73	-399.94	-543.21	802.46	541.71	3.8
15	-4.99	10.87	5.88	0.00	440.33	440.33	-337.77	283.44	-54.33	-342.76	734.64	788.74	3.8
16	-25.53	8.47	-17.06	-0.73	479.26	478.53	-705.78	229.15	-476.64	-732.04	716.87	-4.81	3.7
17	-0.76	7.49	6.73	0.00	513.33	513.33	-182.87	650.61	467.74	-183.63	1171.42	1976.34	3.7
18	-7.78	1.21	-6.57	-0.05	157.82	157.77	-576.26	64.78	-511.48	-584.09	223.80	-712.79	3.5
19	-1.72	1.57	-0.15	0.00	161.91	161.91	-255.65	577.89	322.24	-257.37	741.37	969.72	3.6
20	-7.03	0.17	-6.86	-0.05	32.83	32.78	-1564.90	200.39	-1364.51	-1571.97	233.38	-2670.15	3.2
21	-0.30	0.18	-0.12	0.00	116.22	116.22	-32.08	171.97	139.89	-32.38	288.38	512.29	3.3
22	-1.72	0.00	-1.71	-0.04	13.69	13.65	-1301.03	371.24	-929.79	-1302.79	384.93	-1833.99	2.9
23	-0.02	0.07	0.05	0.00	32.23	32.23	-140.65	61.65	-79.00	-140.67	93.95	-93.41	3.2
24	-0.42	0.05	-0.37	0.00	8.75	8.75	-219.29	16.07	-203.23	-219.71	24.87	-389.26	2.8

Appendix J – Erosion and Accretion Data
(See Section 7.3, p.175)

n=	Sample	Aspect	Type	Rate (dz)		0	1	2	5	8	11	14	17	20	23	26
79	ID	E/W	M/C	/yr (mm)	RSQ	Aug-93	Sep-93	Oct-93	Jan-94	Apr-94	Jul-94	Oct-94	Jan-95	Apr-95	Jul-95	Oct-95
1	MA-T1-02	East	Marsh	1.39	0.33	10.0	10.2	10.4	10.7	10.6	10.7	10.5	10.8	10.5	10.7	10.7
2	MA-T1-03	East	Creek	-0.24	0.00	43.9	44.8	45.3	44.3	45.2	44.8	45.4	45.2	44.9	45.0	44.8
3	MA-T1-04	East	Creek	4.53	0.49	53.1	51.9	51.6	52.6	52.0	51.8	51.5	52.0	51.1	51.4	51.0
4	MA-T1-05	East	Marsh	6.52	0.73	11.0	10.7	10.9	11.3	11.5	11.1	11.3	11.6	11.4	12.0	12.7
5	MA-T1-07	East	Creek	2.92	0.05	43.6	44.3	43.6	45.6	44.7	44.2	45.5	44.8	45.7	43.6	42.9
6	MA-T1-08	East	Marsh	1.84	0.03	33.0	32.5	33.0	31.3	32.5	31.3	33.1	32.6	31.4	32.3	33.5
7	MA-T1-10	East	Creek	8.37	0.53	33.3	32.8	33.3	31.1	32.5	31.6	31.0	31.2	31.2	30.8	31.4
8	MA-T1-11	East	Marsh	2.00	0.62	10.2	10.5	10.2	10.7	10.5	10.6	10.6	10.7	10.8	10.7	10.9
9	MA-T1-14	East	Marsh	13.72	0.83	10.2	9.7	10.2	11.5	11.0	11.5	11.5	12.1	11.6	12.6	13.6
10	MA-T2-02	East	Marsh	7.11	0.92	10.4	10.3	10.3	10.6	10.6	11.1	11.4	11.2	11.4	11.5	11.8
11	MA-T2-04	East	Creek	-3.73	0.13	66.4	66.5	66.4	65.2	66.1	65.8	68.1	66.6	67.1	66.6	66.5
12	MA-T2-05	East	Marsh	1.99	0.64	12.9	13.0	12.7	13.2	13.1	13.2	13.2	13.3	13.2	13.3	13.3
13	MA-T2-07	East	Creek	10.82	0.86	59.8	60.1	60.0	60.1	58.9	59.5	59.2	58.5	58.2	58.6	57.6
14	MA-T2-08	East	Marsh	2.29	0.68	9.3	9.4	9.6	9.9	9.8	9.9	9.9	9.9	9.9	10.0	10.1
15	MA-T2-10	East	Marsh	1.29	0.59	11.9	12.1	12.2	12.3	12.2	12.4	12.4	12.3	12.4	12.5	12.4
16	MA-T2-12	East	Creek	8.26	0.38	59.1	59.4	59.6	60.1	58.5	58.0	59.5	60.0	57.9	57.5	58.0
17	MA-T2-14	East	Marsh	5.44	0.77	10.2	10.5	10.1	10.4	10.2	10.3	10.7	10.5	11.2	11.1	11.4
18	MA-T3-02	East	Marsh	0.86	0.07	8.9	9.0	8.8	8.3	8.6	8.5	8.5	8.8	9.1	8.8	8.8
19	MA-T3-03	East	Marsh	1.69	0.53	12.3	12.5	12.5	12.9	12.7	12.8	12.7	12.9	12.9	12.7	13.0
20	MA-T3-05	East	Creek	9.97	0.87	61.2	62.2	62.1	61.9	61.2	61.6	61.5	60.9	61.0	60.5	59.7
21	MA-T3-06	East	Marsh	2.72	0.52	11.4	11.7	11.6	11.2	11.6	11.5	11.6	11.9	12.1	12.1	11.9
22	MA-T3-08	East	Creek	13.34	0.84	51.7	52.3	52.3	51.2	51.7	50.4	51.4	50.6	50.5	49.6	49.1
23	MA-T3-09	East	Marsh	1.63	0.31	12.1	12.2	12.4	12.9	12.6	12.7	12.6	12.9	12.7	12.6	12.9
24	MA-T3-11	East	Creek	6.36	0.80	63.1	63.3	63.1	63.7	63.3	63.1	62.9	62.8	62.2	62.4	62.0
25	MA-T3-12	East	Marsh	2.85	0.85	11.4	11.4	11.4	11.6	11.8	11.7	11.7	11.7	11.9	12.1	12.0
26	MA-T3-14	East	Creek	11.99	0.78	41.7	42.6	42.2	41.7	42.3	42.0	42.1	41.5	41.0	40.1	39.6
27	MA-T3-16	East	Marsh	1.16	0.42	8.7	9.0	9.0	9.3	9.1	9.2	9.2	9.2	9.3	9.4	9.2
28	MA-T4-02	East	Marsh	0.39	0.08	14.3	14.3	14.2	14.6	14.4	14.5	14.4	14.4	14.3	14.4	14.5
29	MA-T4-03	East	Marsh	1.27	0.16	11.0	11.2	10.9	11.7	11.3	11.6	11.5	11.6	11.3	11.5	11.4
30	MA-T4-05	East	Creek	10.57	0.30	69.7	69.7	70.0	72.1	71.2	71.7	71.5	70.4	68.0	69.2	68.5
31	MA-T4-06	East	Marsh	-0.98	0.13	10.3	10.5	10.4	10.9	10.7	10.7	10.7	10.7	10.3	10.5	10.3
32	MA-T4-08	East	Creek	10.90	0.92	60.4	60.7	60.9	60.9	60.1	60.0	59.6	59.8	59.0	59.2	58.4
33	MA-T4-09	East	Marsh	5.65	0.90	13.1	13.0	13.0	13.6	13.4	13.7	13.7	13.6	13.9	14.2	14.4
34	MA-T4-11	East	Creek	11.21	0.80	59.8	60.2	60.2	59.1	59.5	59.4	59.5	58.2	58.5	58.6	57.3
35	MA-T4-12	East	Marsh	5.11	0.66	13.6	13.0	13.6	12.9	13.2	13.2	13.3	13.8	13.9	13.7	14.4
36	MA-T5-02	West	Marsh	5.08	0.74	11.3	11.1	11.3	11.9	11.8	12.1	12.2	12.1	11.9	12.3	12.5
37	MA-T5-04	West	Creek	-0.39	0.01	37.0	37.7	38.3	37.4	38.2	38.0	38.2	38.1	38.4	38.0	37.5
38	MA-T5-05	West	Marsh	4.44	0.85	12.1	12.2	12.2	12.6	12.9	12.8	12.9	12.8	13.1	13.1	13.2
39	MA-T5-07	West	Creek	2.65	0.32	33.2	34.2	34.1	33.9	33.7	34.0	34.1	33.9	34.2	33.7	33.1

n= 39	Sample ID	Aspect E/W	Type M/C	Rate (dz) /yr (mm)	RSQ	0 Aug-93	1 Sep-93	2 Oct-93	5 Jan-94	8 Apr-94	11 Jul-94	14 Oct-94	17 Jan-95	20 Apr-95	23 Jul-95	26 Oct-95
40	MA-T5-08	West	Marsh	4.47	0.58	11.2	10.7	11.0	11.7	11.2	11.3	11.1	11.7	11.3	11.8	12.1
41	MA-T5-10	West	Creek	4.55	0.59	31.9	32.6	32.5	31.9	32.4	32.2	32.3	32.1	32.1	31.7	31.1
42	MA-T5-11	West	Marsh	0.60	0.21	13.4	13.3	13.2	13.6	13.4	13.5	13.4	13.5	13.4	13.5	13.5
43	MA-T5-13	West	Marsh	-0.70	0.13	10.5	10.2	10.6	10.3	10.2	10.2	10.2	10.3	10.1	10.2	10.3
44	MA-T5-16	West	Creek	-2.53	0.09	45.2	44.6	43.0	44.1	45.1	44.6	44.8	44.5	45.0	44.6	44.1
45	MA-T5-17	West	Creek	14.13	0.83	41.2	40.9	42.2	41.7	40.3	40.6	40.1	40.1	39.0	39.2	38.7
46	MA-T6-02	West	Creek	-58.15	0.99	39.0	40.3	41.0	42.3	Abandoned	-	-	-	-	-	-
47	MA-T6-03	West	Creek	62.77	1.00	40.5	40.4	39.9	38.3	Abandoned	-	-	-	-	-	-
48	MA-T6-04	West	Creek	-13.20	0.82	56.2	56.3	56.6	56.8	Abandoned	-	-	-	-	-	-
49	MA-T6-05	West	Creek	11.03	0.97	39.3	39.1	39.1	38.8	Abandoned	-	-	-	-	-	-
50	MA-T6-06	West	Creek	17.08	0.97	45.3	45.0	44.7	44.4	Abandoned	-	-	-	-	-	-
51	MA-T6-07	West	Creek	-6.78	0.94	46.3	47.2	47.2	47.4	Abandoned	-	-	-	-	-	-
52	MA-T6-08	West	Creek	0.78	0.00	55.3	55.0	55.5	55.1	Abandoned	-	-	-	-	-	-
53	MA-T6-09	West	Creek	-9.78	0.27	37.1	37.1	37.7	37.6	Abandoned	-	-	-	-	-	-
54	QY-T1-02	East	Marsh	1.90	0.25	11.0	11.0	10.7	10.2	10.6	10.6	10.7	10.8	11.1	11.1	10.9
55	QY-T1-04	East	Marsh	11.40	0.93	12.4	12.5	12.7	12.9	Abandoned	-	-	-	-	-	-
56	QY-T1-06	East	Creek	-2.19	0.80	83.9	83.6	83.6	83.8	83.7	83.8	83.8	83.9	83.8	84.0	84.2
57	QY-T1-08	East	Marsh	7.62	1.00	8.4	8.6	8.7	8.9	Abandoned	-	-	-	-	-	-
58	QY-T1-10	East	Creek	-1.75	0.02	56.1	56.2	55.8	56.1	Abandoned	-	-	-	-	-	-
59	QY-T1-11	East	Marsh	1.76	0.79	10.5	10.7	10.7	10.8	10.9	10.9	10.9	10.9	11.0	11.1	11.0
60	QY-T1-13	East	Creek	11.63	0.93	34.0	34.6	35.1	34.8	34.0	34.2	33.9	33.5	33.2	33.0	32.3
61	QY-T2-01	West	Marsh	0.24	0.85	7.7	7.7	7.7	7.7	7.7	7.7	7.7	7.7	7.7	7.7	7.7
62	QY-T2-03	West	Marsh	5.76	0.82	11.4	11.0	10.6	10.7	11.2	11.0	11.2	11.2	11.6	11.6	12.1
63	QY-T2-05	West	Creek	3.40	0.54	36.8	37.3	37.4	37.8	37.4	37.5	37.3	37.0	37.0	37.2	36.6
64	QY-T2-06	West	Marsh	1.53	0.55	14.1	14.1	13.9	13.7	13.9	13.9	14.0	14.0	14.2	14.1	14.2
65	QY-T2-08	West	Creek	17.92	0.89	44.9	45.5	45.6	45.0	44.0	44.0	43.5	44.1	42.6	42.7	41.1
66	QY-T2-09	West	Marsh	-0.51	0.63	12.7	12.7	12.7	12.8	12.7	12.7	12.7	12.7	12.6	12.7	12.6
67	QY-T2-11	West	Creek	5.17	0.83	34.0	34.5	34.5	34.7	34.3	34.4	34.2	34.2	33.9	33.8	33.3
68	QY-T2-12	West	Marsh	-0.93	0.20	9.5	9.8	9.5	9.9	9.8	9.8	9.7	9.6	9.6	9.7	9.5
69	QY-T3-02	West	Marsh	-8.49	0.79	9.8	10.0	10.6	10.8	10.1	10.1	9.7	9.9	9.0	8.9	8.7
70	QY-T3-03	West	Creek	7.19	0.90	35.7	35.8	35.2	35.1	34.8	34.7	34.6	34.6	34.2	34.3	33.8
71	QY-T3-04	West	Creek	27.13	0.78	55.7	56.9	56.8	55.8	58.0	56.0	53.5	55.0	52.5	53.0	51.0
72	QY-T3-05	West	Marsh	0.98	0.19	6.3	6.2	5.9	6.1	6.4	6.3	6.0	6.2	6.3	6.2	6.4
73	QY-T3-07	West	Creek	13.26	0.92	47.2	47.9	48.4	48.4	47.5	47.6	47.1	47.0	46.3	46.0	45.3
74	QY-T3-08	West	Marsh	4.60	0.88	10.7	10.5	10.6	10.4	10.8	10.7	10.9	10.9	11.2	11.2	11.5
75	QY-T3-10	West	Marsh	4.00	0.92	7.9	7.6	7.6	7.7	7.9	7.9	8.0	8.0	8.2	8.2	8.6
76	QY-T3-12	West	Marsh	1.51	0.88	9.3	9.2	9.3	9.4	9.3	9.4	9.4	9.5	9.4	9.5	9.6
77	QY-T3-14	West	Creek	9.81	0.42	48.8	49.7	49.7	49.5	50.5	50.0	47.5	49.5	48.8	49.0	47.0
78	QY-T3-16	West	Marsh	-0.07	0.00	12.8	12.8	12.8	12.8	12.9	12.9	12.7	12.8	12.8	12.9	12.7

Appendix K – List of Map and Charts consulted.

(See Section 7.3.2)

#	Date	Title of map or chart
1	c.1530	*Title unknown* - Henry VIII's reign
2	1575	J. Saxton
3	1610	J.Speed
4	1667	John Thornton
5	1675	John Seller (see p.61 of Tooley)
6	1682	John Thornton
7	1686	Greenvil Collins
8	1693	Levee et Grayee par ordre du Roy
9	1774	Chapman and Andre
10	1788	James Luttrell
11	1789	Hamilton Moore
12	1794	William Heather
13	1804	Harwich Harbour and Neighbouring Waters by Graeme Spence
14	1824	Admiralty Odi 66 Shelf DK
15	1832	G+J Cary Sheet No. 28
16	1838	1st edition OS map
17	1847	Admiralty (Naze to Orfordness)
18	1855	Admiralty (North Foreland to Orfordness)
19	1878	Admiralty (North Foreland to Orfordness)
20	1898	OS Essex Sheet XXX. N.W. (based on 1874 survey with revisions)
21	1905	Admiralty
22	1933	Admiralty (North Foreland to Orfordness)
23	1940	Admiralty
24	1951	Admiralty (North Foreland to Orfordness)
25	1959	Admiralty
26	1964	Admiralty
27	1971	Admiralty
28	1974	Admiralty
29	1981	Admiralty
30	1984	Admiralty
31	1989	Admiralty
32	1993	Admiralty 2695 Plans on the East Coast of England
33	1993	Ordnance Survey Latest?

Where a chart or map, used to assess the rate of retreat of Stone Point, was without a scale, or the scale was not readily discernible, a method of measuring distance was required. In most cases the scale was not visible because the map or chart being used

was a facsimile. The following method was used to measure distances and determine the accuracy of such measurements:

- At least three known landmarks were selected that appeared on both the map to be measured and on the latest Ordnance Survey map or Admiralty chart. The landmarks were selected so that the area of interest fell within the triangle formed by the three points.

- Next, the distance (in mm) was measured between selected points on the map to be assessed.

- By dividing the actual distance, obtained from latest published source, by the measured distance, a factor was obtained. The mean of at least three factors was used.

- Next, the unknown distance was measured (to 0.5mm using a standard millimetre rule), and multiplied by the factor.

- Finally, by multiplying the measurement accuracy by the factor, the error bounds were calculated.

The method is also useful if only a photocopy of a section of map or chart is available. It has the added advantage of reducing errors due to some photocopy distortion.

Appendix L – Bore hole records

(See Section 8.2.1 and Figure 8-1)

Northing	Easting	Map Ref	Grid Ref.	Max depth(m)	Reference
625500.0	223100.0	X01	TM25502310	3.32	ERA372-5
625450.0	223400.0	X02	TM25452340	3.20	ERA372-10
625300.0	223950.0	X03	TM25302395	3.30	ERA372-14
625250.0	224250.0	X04	TM25252425	3.15	ERA372-18
625200.0	224400.0	X05	TM25202440	3.10	ERA372-22
622450.0	224650.0	X06	TM25502465	3.60	ERA372-26
622450.0	223300.0	X07	TM22452330	2.00	ERA407-1
622500.0	223100.0	X08	TM22502310	2.00	ERA407-2
622600.0	222500.0	X09	TM22602250	4.00	ERA407-7
622700.0	222450.0	X10	TM22702245	4.00	ERA407-8
622800.0	222600.0	X11	TM22802260	4.00	ERA407-14
622700.0	222450.0	X12	TM22702245	4.15	ERA407-15
624300.0	223300.0	S1	TM24302330	12.00	ESS-J1198-1
622500.0	227700.0	L1	TM22502770	3.50	Lk-1
622950.0	227550.0	L2	TM22952755	3.10	Lk-2
623300.0	227500.0	L3	TM23302750	2.80	Lk-3
623850.0	227500.0	L4	TM23852750	3.80	Lk-4
623700.0	227400.0	L5	TM23702740	3.80	Lk-5
623550.0	227300.0	L6	TM23552730	3.60	Lk-6
623450.0	227100.0	L7	TM23452710	3.60	Lk-7
623100.0	227150.0	L8	TM23102715	3.10	Lk-8
623950.0	225450.0	B1	TM23952545	53.34	BGS-1
621300.0	226600.0	B2	TM21302660	56.39	BGS-2
622250.0	223100.0	B3	TM22252310	68.58	BGS-3
622150.0	221450.0	B4	TM22152145	68.58	BGS-4
624850.0	225500.0	A1	TM24852550	5.00	HW-A-1
624700.0	225800.0		TM24702580	4.50	HW-A-2
624700.0	225800.0	V1/A2	TM24702580	4.50	HW-V-1
623200.0	225900.0	V2	TM23202590	5.00	HW-V-2
623350.0	226000.0	A3	TM23352600	2.30	HW-A-3
623400.0	226050.0	A4	TM23402605	4.45	HW-A-4
621250.0	224900.0	A5	TM21252490	5.00	HW-A-5
624500.0	224850.0	A6	TM24502485	5.50	HW-A-6
622900.0	223054.0	A7	TM22902305	2.00	HW-A-7

Reference Key:

ERA - Essex River Authority

ESS - Eastern Soil Survey

Lk - Leeks (1975)

BGS - British Geological Survey

HW - This research

Appendix M – List of Samples for Radiocarbon Dating
(see Section, 8.3.2, p.200)

Samples submitted for dating:

WBSPT1	**Peat**	**46g**
WBSPT2	**Shell**	**10.4g**
WBPWT1	**Peat**	**58g**
WBPWT2	**Shell**	**10.8g**

Sample	Species/Material	Depth (m)	Wt. (g)
WBSPT1			
SPT01P	Peat	0.66 - 0.67	19.54
SPT02P	Peat	0.67 - 0.68	13.42
SPT03P	Peat	0.68 - 0.69	13.19
WBSPT2			
SPT14F	Shell fragments	3.68 - 3.70	1.57
SPT18C	*Cerastoderma edule*	3.91 - 3.93	0.06
SPT19C	*Cerastoderma edule*	3.93 - 3.95	0.97
SPT26C	*Cerastoderma edule*	4.27 - 4.29	1.12
SPT27C	*Cerastoderma edule*	4.29 - 4.31	0.72
SPT29C	*Cerastoderma edule*	4.33 - 4.35	1.45
SPT29L	*Littorina littorea*	4.33 - 4.35	2.72
SPT30C	*Cerastoderma edule*	4.35 - 4.37	0.68
SPT31C	*Cerastoderma edule*	4.37 - 4.39	0.47
SPT32C	*Cerastoderma edule*	4.39 - 4.41	0.62
SPT32R	*Rossoidae*	4.39 - 4.41	0.01
WBPWT1			
PWT01P	Peat	1.06 - 1.07	22.31
PWT02P	Peat	1.07 - 1.08	17.42
PWT03P	Peat	1.08 - 1.09	17.61
WBPWT2			
PWT04L	*Littorina saxitilus*	2.82 - 2.84	0.29
PWT09C	*Cerastoderma edule*	3.22 - 3.24	0.27
PWT09L	*Littorina littorea*	3.22 - 3.24	0.19
PWT09M	*Mytilus edulus*	3.22 - 3.24	2.48
PWT09R	*Rossoidae*	3.22 - 3.24	0.01
PWT10S	Shell fragments	3.24 - 3.26	1.07
PWT14C	*Cerastoderma edule*	3.47 - 3.49	0.73
PWT14L	*Littorina littorea*	3.47 - 3.49	1.97
PWT14M	*Mytilus edulus*	3.47 - 3.49	4.04
PWT14R	*Rossoidae*	3.47 - 3.49	0.02

Appendix N – Core Photographs

(See Section 8.3, p.194)

Plate 1

STONE POINT CORE PHOTOGRAPH

Photograph shows both halves of the full length of the core retrieved from the Stone Point site. The "wavy" pattern down the sides of some of the sections was caused by the spatula used to dissect the core. A Munsell soil colour chart is included in the frame.

Plate 2

STONE POINT CORE PHOTOGRAPH - DETAIL

Photograph shows an enlarged view of the "peat" horizon at 0.68m. A Munsell soil colour chart is included in the frame.

Plate 3

PEWIT ISLAND CORE PHOTOGRAPH

Photograph shows both halves of the full length of the core retrieved from the Pewit Island. The "wavy" pattern down the sides of some of the sections was caused by the spatula used to dissect the core. A Munsell soil colour chart is included in the frame.
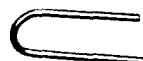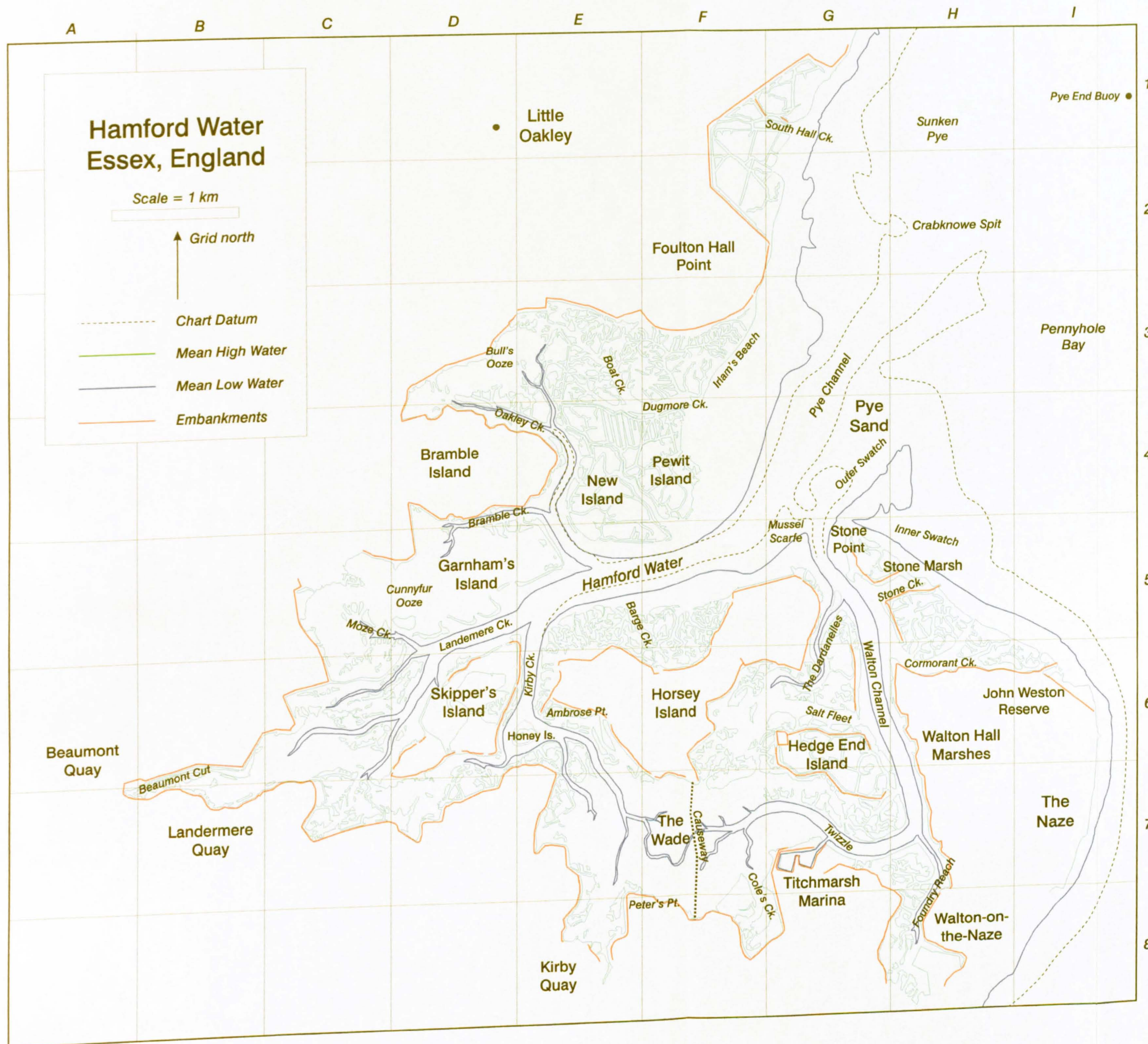
ANNEX A

<u>ANNEX B</u>

Third Party Material excluded from digitised copy.
Please refer to original text to see this material.

Hamford Water
Essex, England

Scale = 1 km

↑ Grid north

- - - - - Chart Datum
———— Mean High Water
———— Mean Low Water
———— Embankments

Hamford Water Map Index:

Map labels:

Little Oakley · Pye End Buoy · South Hall Ck. · Sunken Pye · Crabknowe Spit · Foulton Hall Point · Pennyhole Bay · Bull's Ooze · Boat Ck. · Irlam's Beach · Dugmore Ck. · Pye Channel · Pye Sand · Oakley Ck. · Bramble Island · Pewit Island · New Island · Outer Swatch · Bramble Ck. · Mussel Scarfe · Stone Point · Inner Swatch · Stone Marsh · Garnham's Island · Hamford Water · Stone Ck. · Cunnyfur Ooze · Moze Ck. · Barge Ck. · Landermere Ck. · Kirby Ck. · The Dardanelles · Walton Channel · Cormorant Ck. · Beaumont Quay · Skipper's Island · Horsey Island · John Weston Reserve · Ambrose Pt. · Salt Fleet · Walton Hall Marshes · Honey Is. · Hedge End Island · Beaumont Cut · The Naze · Landermere Quay · The Wade · Causeway · Twizzle · Titchmarsh Marina · Cole's Ck. · Peter's Pt. · Foundry Reach · Walton-on-the-Naze · Kirby Quay